
**INHIBITION OF MAMMALIAN NICOTINIC ACETYLCHOLINE
RECEPTORS BY PHILANTHOTOXIN ANALOGUES IS
STRONGLY INFLUENCED BY SUBUNIT COMPOSITION**

By

Hamid Saeid Kachel

Thesis submitted to the University of Nottingham as requirement
for the Degree of Doctor of Philosophy

October 2014

School of Life Sciences
University of Nottingham
Nottingham
U.K

Contents

Abstract.....	vi
Abbreviations.....	viii
Acknowledgment.....	x
CHAPTER ONE.....	1
GENERAL INTRODUCTION.....	1
Summary.....	1
1.1. Overview.....	2
1.2. Nicotinic acetylcholine receptors.....	4
1.2.1. Molecular structure and diversity.....	4
1.2.2. Architecture and functional state.....	12
1.2.3. Role and distribution.....	20
1.3. Pharmacology.....	25
1.4. Polyamines and Philanthotoxin.....	30
1.5. <i>Xenopus</i> oocytes as a system for investigating ion channels....	37
1.6. Aims of the project.....	39
CHAPTER TWO.....	41
MATERIAL AND METHODS.....	41
Summary.....	41
2.1. Molecular biology.....	42
2.1.1. Chemicals and Plasmids.....	42
2.1.2. DNA manipulation.....	43
2.1.3. In vitro RNA transcription.....	45
2.2. Electrophysiology procedure.....	46
2.2.1. Oocyte preparation.....	46
2.2.2. Selection of oocytes for microinjection.....	47
2.2.3. Assaying oocytes for gene expression.....	47
2.3. Data analysis.....	50
CHAPTER THREE.....	52
ELECTROPHYSIOLOGICAL CHARACTERIZATION OF THE RESPONSE OF nAChRs TO ACh.....	52
Summary.....	52

3.1. Pharmacological characterization of the ACh response of mammalian nAChRs expressed in <i>Xenopus</i> oocytes	53
3.2. Current-voltage characteristics of $\alpha 4\beta 2$ nAChRs.....	59
3.3. Recovery of $\alpha 4\beta 2$ nAChRs from desensitization by 10 μ M ACh.....	59
CHAPTER FOUR	61
PHARMACOLOGICAL CHARACTERIZATION OF nAChR INHIBITION BY PhTX-343	61
Summary	61
4.1. Effects of PhTX-343 on ACh-induced responses of wild-type and mutant nAChRs	62
4.2. Voltage-dependent and -independent inhibition of nAChRs by PhTX-343.....	71
4.3. Recovery from inhibition by PhTX-343	80
4.4. Competition of PhTX-343 with ACh on nAChRs	84
CHAPTER FIVE	87
PHARMACOLOGICAL CHARACTERIZATION OF nAChR INHIBITION BY PhTX-12	87
Summary	87
5.1. PhTX-12 inhibits the ACh-induced response of wild-type and mutated nAChRs.....	88
5.2. Voltage effects on the inhibition of nAChRs by PhTX-12.....	92
5.3. Recovery from inhibition by PhTX-12	99
5.4. Non-competitive action of PhTX-12.....	102
CHAPTER SIX	105
STRUCTURE ACTIVITY RELATIONSHIP OF PhTX-343 ON $\alpha 4\beta 2$ AND $\alpha 3\beta 4$	105
Summary	105
6.1. Structure activity relationship (SAR)	106
6.1.1. Single region modification (SRM)	107
6.1.2. Double region modification (DRM)	116
6.3. Comparison of PhTX-343 potency with two LGIC antagonists.....	122
CHAPTER SEVEN	125
GENERAL DISCUSSION.....	125
Summary	125

7.1. Characterization of the ACh response of the nAChRs expressed in <i>Xenopus</i> oocytes.....	126
7.2. Screening PhTX-343 and PhTX-12 for nAChR subtype selectivity	129
7.4. Structure-Activity Study.....	145
CONCLUSIONS	153
REFEFRENCES.....	154
APPENDIX.....	166

Abstract

Philanthotoxin-433 (PhTX-433) is an active component of the Egyptian solitary digger wasp, *Philanthus triangulum*, venom which non-selectively inhibits several excitatory ion channels. With the aim of improving potency and selectivity, several synthetic analogues were developed based on the single or multiple modifications in the hydrophilic polyamine tail and hydrophobic aromatic head group of the PhTX.

In the first part of this study, we investigated the pharmacological actions of two synthetic analogues, Philanthotoxin-343 (PhTX-343) and Philanthotoxin-12 (PhTX-12), on mammalian hetero- and homooligomeric nicotinic acetylcholine receptor (nAChR) subunit combinations expressed in *Xenopus* oocytes. Whole-cell currents in response to application of acetylcholine alone or co-applied with PhTX-analogue were studied electrophysiologically using two-electrode voltage-clamp at three different membrane holding potentials ($V_H = -60$ mV, -80 mV and -100 mV). Concentration-inhibition curves were constructed and IC_{50} values estimated for each holding potential. The IC_{50} (95% CI, n=oocytes) values for PhTX-343 inhibition of $\alpha 3\beta 4$, $\alpha 3\beta 2$, $\alpha 4\beta 2$, $\alpha 4\beta 4$, $\alpha 7$, $\alpha 3\beta 4_{(F255V)}$, $\alpha 4\beta 2_{(V253F)}$ and $\alpha 1\beta 1\delta\gamma$ peak currents at -100 mV were 0.07 μ M (0.05 - 0.10 μ M, n=9), 3.20 μ M (1.69 - 6.26 μ M, n=8), 0.14 μ M (0.09 - 0.21 μ M, n=7), 0.28 μ M (0.17 - 0.46 μ M, n=6), 8.7 μ M (6.9 - 11.0 μ M, n =9), 0.01 μ M (0.01 - 0.02 μ M, n=8), 0.10 μ M (0.06 - 0.16 μ M, n=8) and 3.2 μ M (2.5 - 4.1 μ M, n=9) respectively; for PhTX-12 they were 2.03 μ M (1.22 - 3.26 μ M, n=8), 74.0 μ M (21 - 259 μ M, n=10), 1.6 μ M (0.7 - 3.6 μ M, n=11), 1.82 μ M (0.81 - 4.11 μ M, n=9), 12.1 μ M (9.0 - 16.0 μ M, n =10), 1.0 μ M (0.5 - 2.0 μ M, n=5), 3.4 μ M (1.3 - 8.7 μ M, n=9) and 5.0 μ M (2.8 - 8.8 μ M, n=8) respectively; i.e. in contrast to M-nAChR, PhTX-343 was more potent than PhTX-12 in all cases. All IC_{50} s were lower when inhibition was measured after 1 minute of application indicating use dependence. For inhibition of heteromeric nAChRs, the peak potency of PhTX-343 was strongly augmented by

holding the cell at more negative V_H while this was not the case for PhTX-12 where only weak voltage-dependence was observed. The inhibition of homomeric $\alpha 7$ receptors by PhTX-343 was voltage-independent, whereas the block by PhTX-12 was voltage-dependent. In addition, these two synthetic analogues were different in their recovery rates (PhTX-12 was generally faster than PhTX-343) but they were similar in their mechanism of action, non-competitive inhibition.

In the second part of the project, I explored the structure-activity relations of twenty one synthetic analogues, with a view to improving their activity and selectivity on rat neuronal $\alpha 4\beta 2$ and $\alpha 3\beta 4$ nAChRs at $V_H = -100$ mV. We showed that the presence of positive charge in the polyamine tail of PhTX compounds is essential for nAChR subtype selectivity and its removal made the molecule lose its selectivity. Also, it appears that adding a bulky group to the terminal ammonium drastically reduced activity whereas a similar addition to the head region it increased their potency. In addition, we identified the key regions and substitutions responsible for increasing PhTX activity, cyclohexylalanine in place of tyrosine, and selectivity, phenyl group. Analogues having cyclohexylalanine and a phenolic group in the head region showed IC_{50} values in the low nano-molar and pico-molar (160-400 pM) range. These data suggest that PhTXs could serve as lead compounds for highly potent and selective inhibitors of N-nAChRs.

Abbreviations

α -BGT	α -Bungarotoxin
ACh	Acetylcholine
AMPA	α -amino-3-hydroxy-5-methyl-4-isoxazolepropionic acid receptor
CCh	Carbachol
Ch-A-Tr	Choline-Acetyl-Transferase
CI	Confidence interval
CNS	Central nervous system
CPZ	Chlorpromazine
DDF	<i>p</i> -N,N-(dimethylamino)phenyldiazonium Fluoroborate
DMPP	Dimethylphenylpiperazinium
d-TC	d-tubocurarine
EC ₅₀	Half maximal effective concentration
FDA	Food and Drug Administration
H	Human
IC ₅₀	Half maximal inhibitory concentration
iGluR	Ionotropic glutamate receptor
I-V	Current-Voltage
LGIC	Ligand gated ion channel
M	Mouse
mAChR	Muscarinic acetylcholine receptor
MBTA	4-(<i>N</i> -maleimido) benzyltrimethylammonium iodide
M-nAChRs	Muscle type nicotinic acetylcholine receptor
MTSEA	2-aminoethyl methanethiosulfonate
nAChRs	Nicotinic acetylcholine receptor
NCI	Non-competitive inhibitor

NMDAR	<i>N</i> -methyl-D-aspartate receptor
NMJ	Neuromuscular junction
N-nAChRs	Neuronal type nicotinic acetylcholine receptor
pcDNA	plasmid Cytomegalovirus promoter Deoxyribonucleic acid
PhTX	Philanthotoxin
PNS	Peripheral nervous system
R	Rat
SAR	Structure-Activity Relationships
SCAM	Substituted cysteine accessibility method
SPS	Solid-Phase Synthesis
SubCh	Suberycholine
TEVC	Two-electrode voltage-clamp
M	Transmembrane segments
TDF	Trimethylammonium diazonium fluoroborate
VACht	Vesicle acetylcholine transporter
VAMP	Vesicle-associated membrane protein
V_H	Holding potential

Acknowledgment

I would like to express my deep gratitude to my research supervisor Dr. Ian R. Mellor, for his patient guidance, enthusiastic encouragement and useful critiques for this research work. I would like also extend my grateful thanks to Dr. Ian Duce and Prof. Paul O'Shea for providing support, advice and useful feedback on the project. Also thanks to Mr. Declan Brady for his expert advice and assistance with molecular biology.

I would like also extend my thanks to everyone in A70 Electrophysiology laboratory for their help (Dr. Mark Burton, David Richards, Rohit Patel, John Grzeskowiak and Izuddin Abu).

I am very grateful for the help of our collaborators Dr. Henrik Franzyk and Prof. Kristian Strømgaard from the University of Copenhagen for supplying philanthotoxin analogues and Dr. Denis Tikhonov for useful information on the 3-dimensional structures of philanthotoxin analogues and the nicotinic acetylcholine receptor pore.

Special thanks for Prof. Dlawer Ala'Aldeen, University of Nottingham, for his endless help and support.

Also thanks for University of Zaxo, specially Dr. Lazgin A. Jamil, Pro. Omar A. M. Al-Habib, Pro. Wijdan M. S. Mero, Dr. Yousif M. Fattah, Dr. Intisar N. Waheed, Dr. Dizar A. Kheder and Dr. Abbas B. Qadiir.

Finally, I wish to thank my family for their support and encouragement throughout my study.

This work was funded by the Ministry of Higher Education in Kurdistan Government.

CHAPTER ONE

GENERAL INTRODUCTION

Summary

Members of the neuronal nicotinic acetylcholine receptor (N-nAChR) family are oligomeric ligand gated ion channel proteins and belong to the "Cys-loop" receptor superfamily, which also includes 5-HT₃ receptors, GABA_A, glutamate-gated chloride channels and glycine receptors. Five subunits of the receptor are organized in a circular manner around a central 'water-filled ion conducting pore'. Each subunit is composed of four membrane-spanning segments named M1-M4. The pore lumen is determined by the second of these membrane segments, M2. Binding sites for non-competitive inhibitors (NCIs) are located on the M2 trans-membrane segment of the pore. The nAChRs play a critical role in many physiological and pathophysiological processes.

The venom of the Egyptian digger wasp, *Philanthus triangulum*, contains a toxin, philanthotoxin-433 (PhTX-433), that interacts with ionotropic glutamate receptors and nAChRs in their target prey. PhTX-433 or PhTX-343 has a polyamine tail and aromatic head group that works as a strong non-competitive inhibitor of cation selective ionotropic receptors.

This project aimed to investigate the action of several philanthotoxin analogues such as PhTX-343 and PhTX-12 on the major wild-type and mutant N-nAChRs in CNS and PNS, $\alpha 4\beta 2$, $\alpha 4\beta 4$, $\alpha 3\beta 4$, $\alpha 3\beta 2$, $\alpha 7$, and M-nAChRs, $\alpha 1\beta 1\gamma\delta$, by their expression in *Xenopus* oocytes.

1.1. Overview

Ionotropic-receptor protein interactions with neurotransmitters, results in activation or inhibition of cellular events. Modulation of this important signalling event has become an important research area for the development of drugs and understanding pharmacological properties of particular receptor proteins in the cell. The origin of receptor theory goes back to Langley in 1905, who reported the presence of a "receptive substance" in the end-plate of frog neuromuscular junction (NMJ), which binds with nicotine and is stimulated by the chemical-transmitter released from the presynaptic neuron. Research by scientists like Dale and Otto Loewi showed that acetylcholine (ACh) was a chemical neurotransmitter used for communication in autonomic ganglia and at the neuromuscular junction (NMJ). ACh is synthesized in presynaptic nerve cytosol by Choline-Acetyl-Transferase (Ch-A-Tr) from choline and acetyl-Co-enzyme-A (**Figure 1.1**) and packaged into individual vesicles. ACh is released and exerts its impacts on the peripheral and central nervous system (PNS, CNS) via two separate groups of receptors: Metabotropic muscarinic ACh receptors (mAChRs), respond slowly to ACh application due to their interaction with the second messenger cascades, while ionotropic nicotinic ACh receptors (nAChRs) mediate fast synaptic transmission and are the focus point of this work.

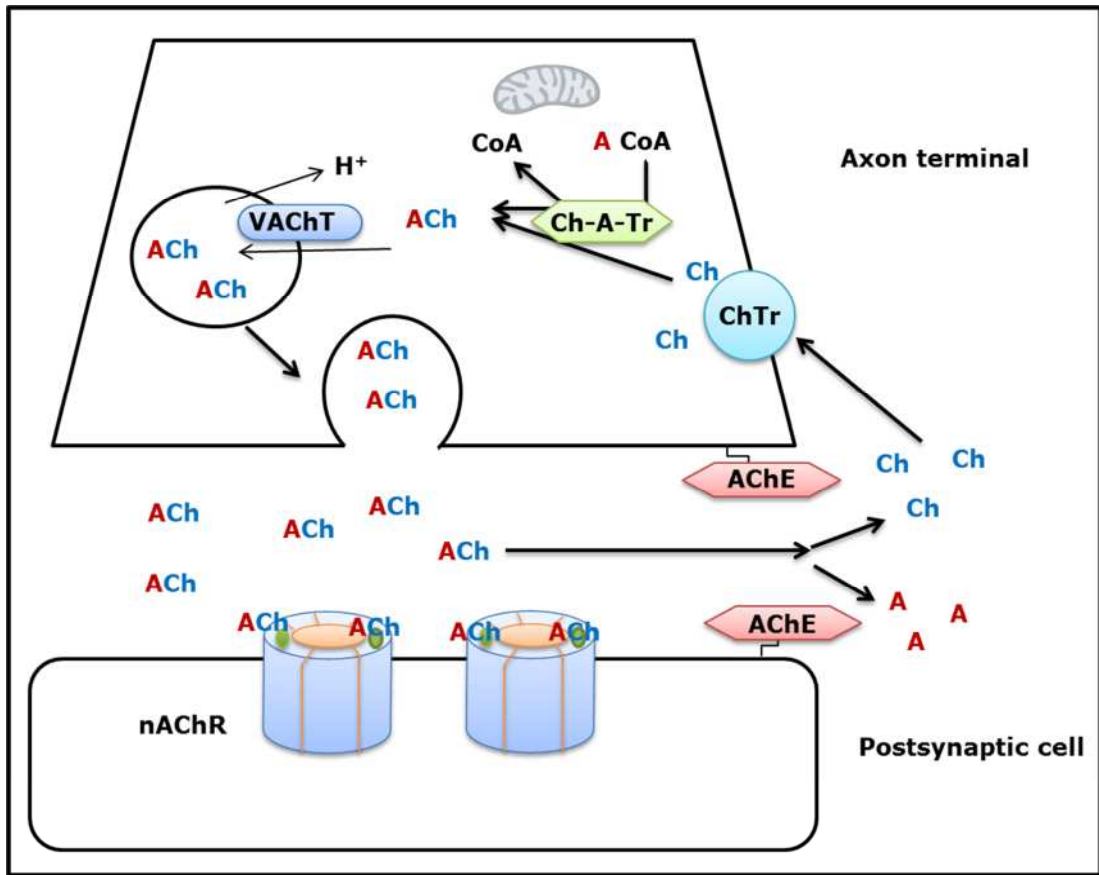


Figure 1.1. Mechanisms of synthesis, degradation and synaptic transmission of acetylcholine (ACh). ACoA = acetyl-Co-enzyme-A, Ch = choline, AChE = acetylcholine esterase, ChTr = choline transporter, Ch-A-Tr = choline acetyl transferase, VAcHT = vesicle acetylcholine transporter.

Based on their major location of expression in the body, nAChRs can be classified into two subtypes: Muscle-type nAChRs (M-nAChRs) are located on the skeletal muscles where they mediate excitatory neuromuscular transmission, while the neuronal-type nAChRs (N-nAChRs) generate fast electrical transmission in the brain and autonomic ganglia. The N-nAChRs in the CNS form one of the major excitatory group of receptors, which play critical roles in several brain activities such as learning, consciousness, attention, reward and memory (Steinlein and Bertrand, 2008; Taly et al., 2009). Also, their role in non-pathological nociceptive pain has been well studied, for instance knockout of $\alpha 4$ and $\beta 2$ in a mouse model led to a reduction in the antinociceptive response of

nicotine on the hot plate test (Marubio et al., 1999). Alteration in the expression level and function of this group of receptors might lead to the development of many pathophysiological disorders; for example epilepsy, Tourette's syndrome, Parkinson's disease, Alzheimer's disease, anxiety, depression and schizophrenia (Gotti and Clementi, 2004; Romanelli et al., 2007; Unwin, 2013).

As mentioned above, nAChRs participate in the control of signaling of much of the CNS, PNS and skeletal muscle (Romanelli and Gualtieri, 2003). They have become promising targets for several therapies such as drugs being developed for smoking cessation, memory enhancement, pain relief and the treatment for Parkinson's disease (Li et al., 2001). Thus, the study of N-nAChRs and the development of selective agonists and antagonists could further our current understanding of the functioning profile of different nAChR subtypes (Romanelli and Gualtieri, 2003). Several useful ligands (agonists and antagonists) that have been investigated on nAChRs have a natural source such as those obtained from plants and animals, which include nicotine, conotoxins and philanthotoxin-433 (Romanelli and Gualtieri, 2003). For these reasons N-nAChRs have become a novel therapeutic target for drug discovery and research.

1.2. Nicotinic acetylcholine receptors

1.2.1. Molecular structure and diversity

nAChRs are oligomeric excitatory ion channels, which have wide subtype diversity due to the various possible subunit combinations (**Figure 1.2**). Each subtype has particular pharmacological and functional characteristics and may be confined to a specific region of the CNS or PNS (Millar and Gotti, 2009). This family and other phylogenetically associated receptors including 5-HT₃ serotonin receptors, GABA_A and GABA_C gamma aminobutyric acid receptors, glutamate-gated chloride channels and glycine receptors, are all members of a large superfamily called the ligand gated ion channel (LGIC) superfamily and often referred to as the 'Cys-loop receptors' because of a highly conserved loop

constrained by a disulphide bridge in the N-terminal part of the protein. In the last decade, scientists identified homologues of LGIC in prokaryotic cells and suggested that these may be the ancestral source of animal Cys-loop receptors (Duret et al., 2011; Tasneem et al., 2005).

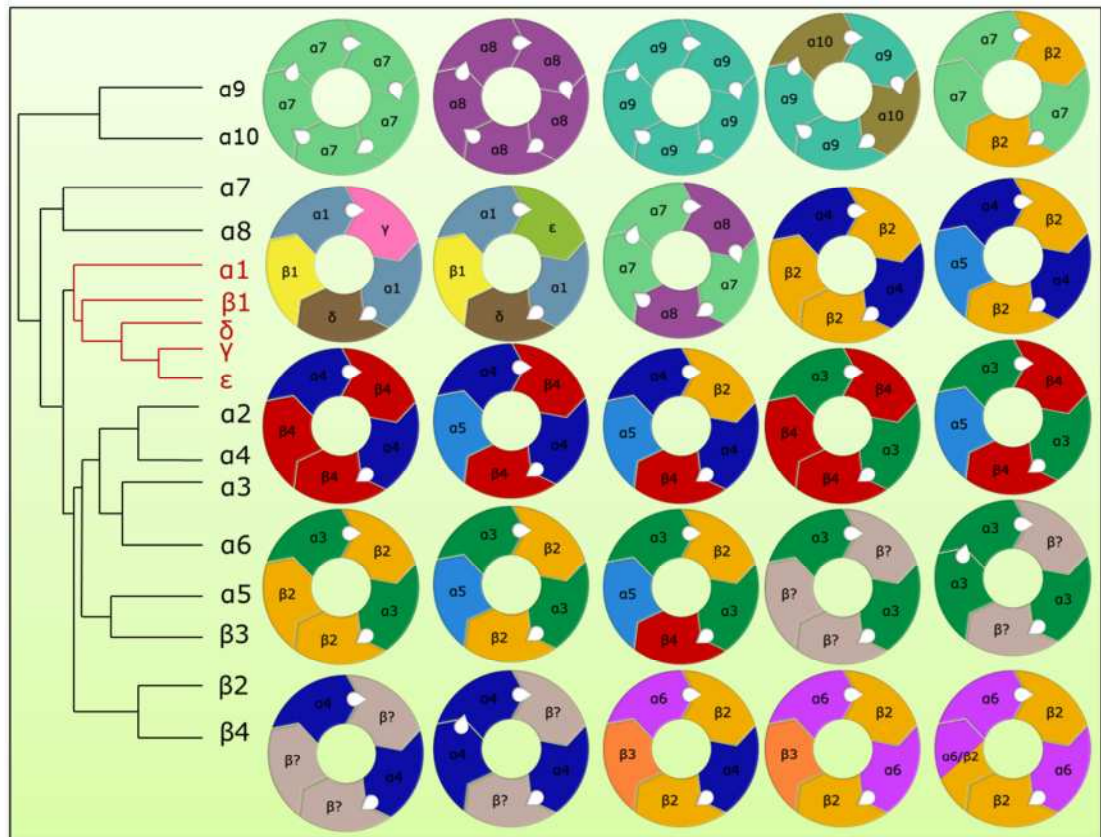


Figure 1.2. Schematic representation of the vertebrate nAChR phylogenetic tree and subtype diversity as a result of various subunit combinations. The $\alpha 8$ -subunit is only present in avian vertebrates. The ACh binding site is shown as a white dot positioned at the interface of the principal subunit (α) and complementary subunit (α or β in neuronal; δ , γ and ϵ of muscle). Idea derived from Le Novere (2002).

All nAChR subunits share numerous homologous characteristics composed of the following parts: (i) a large hydrophilic amino terminal region consisting roughly of 200 amino acids and containing more than three glycosylation sites; (ii) three hydrophobic transmembrane segments (M1-M3) of approximately 20 amino acids each connected together via small loops; (iii) an intracellular

hydrophilic link, 110-270 residues long, between M3 and M4 and containing phosphorylation sites; (iv) another hydrophobic transmembrane segment (M4); (v) a small hydrophilic extracellular C-terminal region (**Figure 1.3**) (Albuquerque et al., 2009; Bouzat, 2012; Paterson and Nordberg, 2000).

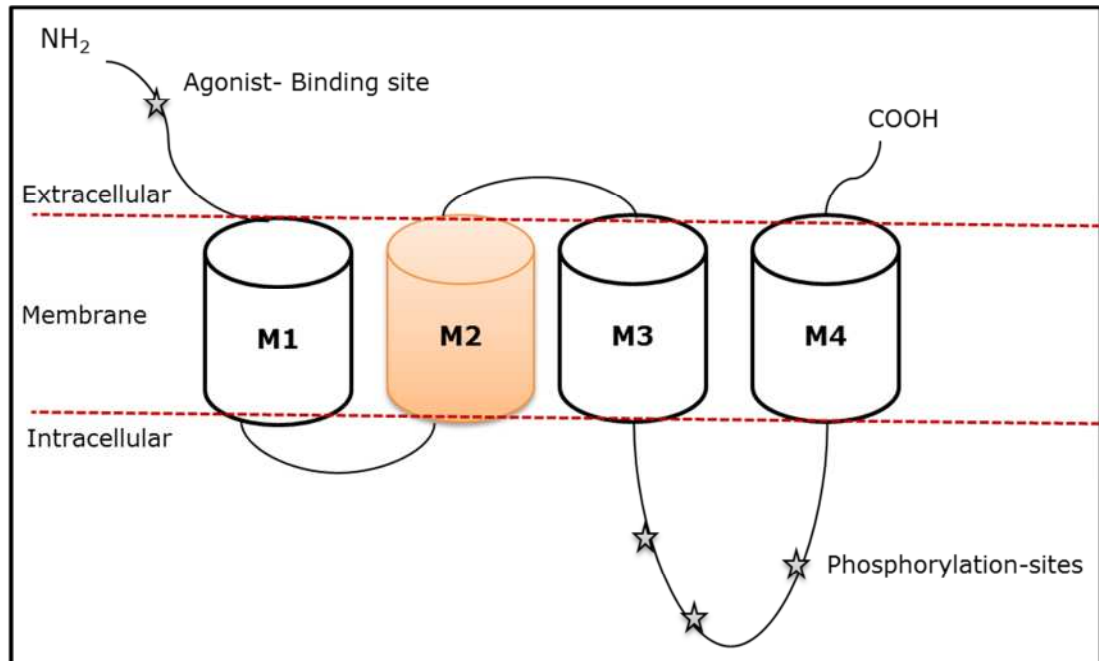


Figure 1.3 The topology of a single nAChR subunit. M1, M2, M3 and M4 represent transmembrane domains. The M2 domain (brown) forms the pore region of the receptors. Both the long N-terminal, which contains the agonist binding site, and the shorter C-terminal are projected towards the extracellular space.

In total, seventeen subunits of nAChR have so far been described and cloned in vertebrates; five non-neuronal ($\alpha 1$, δ , $\beta 1$, γ and ϵ) and twelve neuronal ($\alpha 2-10$ and $\beta 2-4$) (Millar and Gotti, 2009). The multiple sequence alignment of nAChR subunits obtained from the Uniprot databank (<http://www.uniprot.org/>) using the ClustalW software shows a vast subunit similarity across the three species, rat, mouse and human; models that have been used in this project (**Table 1.1**). Changeux and colleagues for the first time purified and described $\alpha 1$, $\beta 1$, δ , γ subunits in the muscle-like electric organ of the fish, *Torpedo californica* (Changeux et al., 1970). These subunits have

stoichiometry of 2($\alpha 1$) and 1($\beta 1, \delta, \gamma$) in foetal tissue and fish electric organ (Reynolds and Karlin, 1978), while in mature skeletal muscle γ is substituted by ϵ leading to increased open time and ion conductance through the channel (Imoto et al., 1991). Cloning of these subunits at the beginning of the 1980s developed a new era of molecular analysis of nAChRs (Changeux, 2012). In contrast, subunits of N-nAChRs have been divided in two distinct subfamilies: α -neuronal subunits ($\alpha 2$ - $\alpha 10$) which carry pairs of adjacent cysteines that are similar in location to C192 and C193 of their analogue subunit in muscle-nAChRs ($\alpha 1$), whereas β -neuronal subunits ($\beta 2$ to $\beta 4$) lack these pairs of important residues, like in the non-neuronal $\beta 1, \gamma, \delta$ and ϵ subunits (Gaimarri et al., 2007; Gotti and Clementi, 2004; Lindstrom, 2000). It has been suggested that both types of neuronal subunits (α and β) participate in determination of pharmacological characteristics of diverse subtypes of N-nAChRs (Chavez-Noriega et al., 1997; Luetje and Patrick, 1991).

Two subtypes of nAChR have been identified in brain, heteromeric (α -Bgtx-insensitive) and homomeric (α -Bgtx-sensitive) (Lindstrom, 2000). The heteromeric subtype might be composed of as few as two homologous subunits including α subunits ($\alpha 2$ - $\alpha 4$ or $\alpha 6$) and β subunits ($\beta 2$ or $\beta 4$) (Dani and Bertrand, 2007). Two different stoichiometries, $2(\alpha)3(\beta)$ and $3(\alpha)2(\beta)$, have been found for $\alpha 4\beta 2$ (probably same for $\alpha 3\beta 4$ nAChRs) in endogenous cells (Grady et al., 2010) and heterologous expression systems (Moroni and Bermudez, 2006). The stoichiometry containing 3- β -subunits has higher agonist sensitivity and lower Ca^{2+} permeability compared to the 2- β -subunit stoichiometry (Arias, 2012). In human, $(\alpha 4\beta 2)_2 \beta 2$ is the most common type in the CNS, while in the PNS it is $(\alpha 3\beta 4)_2 \beta 4$. In homomeric receptors the whole receptor structure is formed by identical subunits. The most abundant homomeric receptor has been found in mammals composed of five $\alpha 7$ subunits, while $\alpha 8$ in avian species is also able to produce an all-alpha heteromeric receptor with $\alpha 7$ (Couturier et al., 1990; Gotti et al., 1994). Furthermore, $\alpha 7$ has the ability to produce functional heteromeric receptors by combination with $\beta 2$ (Khiroug et al., 2002) and non-functional type with $\beta 3$ (Broadbent et al., 2006) by using a heterologous expression system. Similarly, $\alpha 9$, which is mainly found in cochlear hair cells, has the capability to construct a homomeric protein complex when expressed in *Xenopus* oocytes (Elgoyhen et al., 1994). Co-expression of $\alpha 9$ with $\alpha 10$ will generate a heteromeric receptor, which shows faster and stronger agonist desensitization and roughly 100-fold increase in current response compared to homomeric $\alpha 9$. According to these findings the native receptor of $\alpha 9$ is a heteromeric complex with $\alpha 10$ (Elgoyhen et al., 2001; Vetter et al., 2007). Plazas and co-workers have demonstrated that the stoichiometry of these two subunits is $(\alpha 9)_2(\alpha 10)_3$ by their expression in *Xenopus* oocytes (Plazas et al., 2005).

Heterologous expression of 'orphan' subunits ($\alpha 5$ and $\beta 3$) alone or in pairs with another α or β subunit does not produce any functional channels. They

can only generate active receptor channels when they participate as a third subunit, so this group of receptors is more complex in their pharmacological function compared to the previous ones due to the subunit variety (Conroy and Berg, 1995; Lindstrom, 2000; Wang et al., 1996). These subunits cannot contribute directly to the agonist-binding sites, so they possibly occupy the position as auxiliary subunit like their analogue $\beta 1$ subunit in muscle type nAChR. They may play a role in other activity like agonist sensitivity, conductance, receptor localisation and desensitization (Kuryatov et al., 2008). The expression pattern of nAChR subunits may be highly restricted to certain regions in the brain, for example the $\alpha 5$ -subunit is mainly present in hippocampus, striatum, cerebral cortex, thalamus and superior colliculus (Mao et al., 2008; Wada et al., 1990), while the $\alpha 6$ -subunit is found in substantia nigra and ventral tegmental area (Rasmussen et al., 2014). In addition, receptors containing these subunits have unique pharmacological properties, for example $\alpha 5$ -containing receptors have been strongly connected to drug addiction (Gao et al., 2014) and $\alpha 6$ -containing to reward behaviour and motor control (Drenan et al., 2008). Thus this class of receptor becomes an attractive target for pharmaceutical treatment for various CNS disorders such as smoking cessation and Parkinson's disease.

N-nAChRs are found presynaptically and postsynaptically, while M-nAChRs are only found postsynaptically. Pre-synaptic-types are involved in the release of several neurotransmitters such as ACh, noradrenaline, 5-HT, dopamine, glutamate and GABA, whereas postsynaptic types rapidly convert the chemical signal into membrane depolarization of the postsynaptic neuron or muscle (Arias, 2012; Jones et al., 1999; MacDermott et al., 1999). N-nAChRs allow the inward passage of cations at hyperpolarized membrane potentials more than outward current at positive potentials, otherwise known as inward rectification; this is not the case in muscle (Francis and Papke, 1996). This

phenomenon might be caused by inhibition of the channel by interacellular Mg^{2+} and spermine when there is a force pushing the outward passage of cations (Haghighi and Cooper, 1998; Neuhaus and Cachelin, 1990). The phenomenon of outward and inward current inhibition by Mg^{2+} has been observed and confirmed previously for other ionotropic receptors such as NMDAR (Li-Smerin et al., 2001).

In addition, the permeability of Ca^{2+} in brain nAChRs is higher compared to their analogue in muscle. Roughly 2% of the whole current generated by ion exchange through M-nAChRs is carried by Ca^{2+} . This percentage approximately increased 2.5-fold and 5-fold in heteromeric $\alpha+\beta$ combinations and homomeric $\alpha7$ N-nAChRs, respectively (Vernino et al., 1994). Lipovsek et al (2014) showed that mammalian heteromeric $\alpha9\alpha10$ are also highly Ca^{2+} permeable combinations of nAChRs. This suggests the importance of homomeric $\alpha7$ nAChRs in neurons and heteromeric $\alpha9\alpha10$ in cochlear hair cells for the control of intracellular concentration of Ca^{2+} due to their role as one of the main pathways of Ca^{2+} entry at holding potentials the same as or more negative than resting potential (Lindstrom et al., 1995; Lipovsek et al., 2014).

Desensitization of nAChRs is strongly dependent on subunit combination (Giniatullin et al., 2005). Vertebrate nAChRs can be divided into either: non- β -containing nAChRs (homomeric) which have a rapid desensitization (milliseconds) or β -containing nAChRs (heteromeric) that have lower desensitization rates (seconds) compared to homomeric (Corringer et al., 2000; McGehee and Role, 1995; Quick and Lester, 2002).

1.2.2. Architecture and functional state

Members of the nAChR family are complex integral membrane proteins of roughly 290 kDa. Electron microscopic studies (EMS) show that the *Torpedo* electric organ nAChR is approximately 80 Å in width and 120 Å in length, with 15 Å and 65 Å extending to the cytoplasmic and extracellular space, respectively, and 40 Å embedded in the lipid bi-layer. This heteromeric receptor has two ACh-orthosteric sites which are located at a distance of 40 Å above the cell membrane surface (Unwin, 2005) (**Figure 1.5**). The pore has a tapering shape for cation flow when viewed from the extracellular side of the receptor (Miyazawa et al., 2003), with a diameter of 20 Å at the cytoplasmic side, 25 Å at synaptic cleft and it is narrower in the membrane spanning region (Hucho et al., 1996).

On the cytoplasmic side there is an interacting protein called rapsyn, which has a 43 kDa molecular weight and was first purified with NMJ nAChRs. This complex has a role in connecting the receptor with the cytoskeleton as well as clustering them in the end plate of nerve-muscle synapses, which is essential for active transmission (Gotti and Clementi, 2004; Millar and Harkness, 2008). It has been revealed that a lack of this complex in neuronal nAChRs such as $\alpha 3\beta 2$ and $\alpha 4\beta 2$ will not affect their packaging on the plasma membrane of the cell (Millar and Harkness, 2008). However, Osman and co-workers (2008) have reported the presence of rapsyn with $\alpha 9$ and $\alpha 10$ of rodent internal ear. Thus, rapsyn is possibly associated with certain subtypes of neuronal nAChR and participates in particular functions.

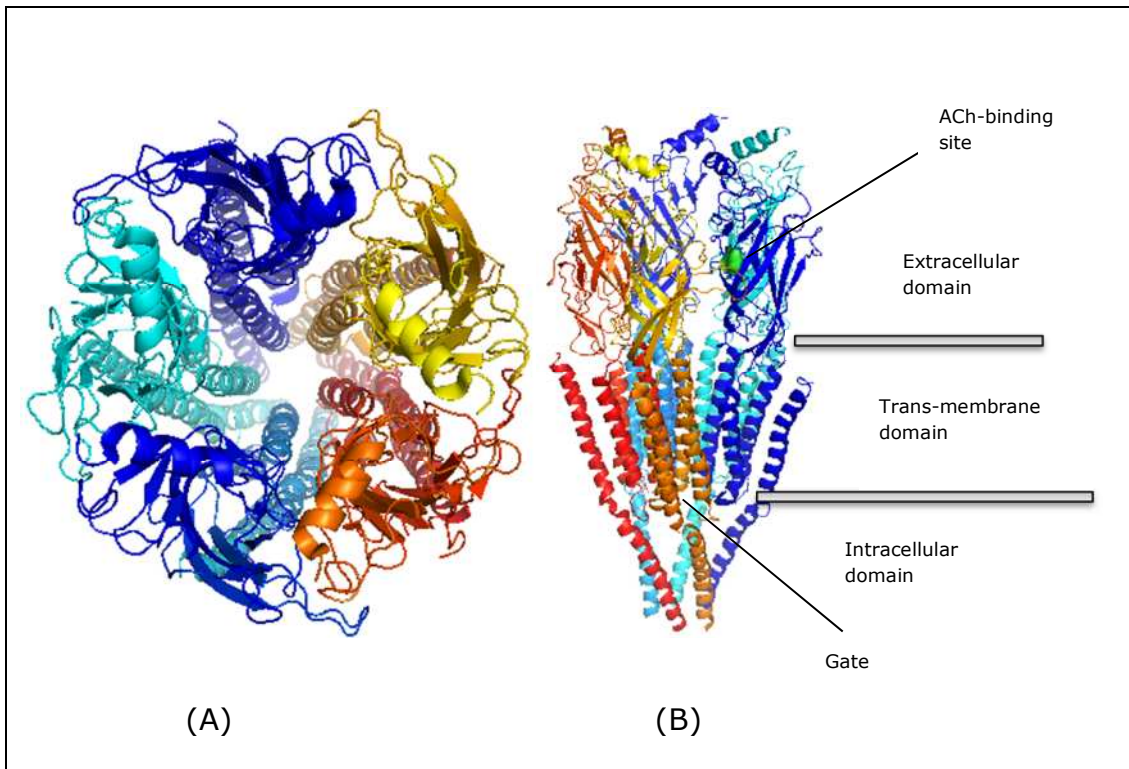


Figure 1.5. Folding and construction of closed channel M-nAChRs (2BG9) viewed from the synaptic cleft (A) and in the plane of the lipid bilayer (B). The green colour shown in figure B represents the agonist binding site and grey horizontal lines represent the position of the lipid bi-layer. Idea derived from Unwin (2013) by using Pymol software.

Improvement in the understanding of the ACh orthosteric site stems from the discovery and crystallization of the homologous acetylcholine binding protein (AChBP) from *Lymnaea stagnalis*, *Aplysia californica* and *Bulinus truncatus* snails. AChBP is synthesized and saved in glial nerve cells and modulates synaptic transmission where it is released into the synapse (Brejc et al., 2001). The nAChR ligand-binding sites are located at the interface between an α -subunit and a neighbouring subunit. Changeux and collaborators (1984) have demonstrated that each muscle-type nAChR carries two allosteric ligand binding sites. Similarly, heteromeric neuronal types are thought to carry two ligand binding sites, whereas five sites per homomeric neuronal nAChR are proposed, one at each subunit interface. Initially, it was expected that only the α -subunit

was responsible for the construction of ligand-binding sites due to a high affinity for the competitive antagonist, 4-(N-maleimido)benzyltrimethylammonium iodide (MBTA), to residues in the α -subunits just near to α Cys-192 and α Cys-193, and a ratio of two α -subunits to two agonist-binding sites (Kao et al., 1984). Further evidence supporting the interface position of the ligand binding site in nAChRs includes paired expression of α/γ or α/δ subunits leading to the formation of active ACh-binding sites, whereas other combinations do not (Blount and Merlie, 1989), and the α/γ interface binding site displays pharmacological characteristics markedly different to that between α/δ ; the latter combination having higher affinity for α -conotoxin MI compared to the former in muscular nAChR in mouse, but the other way round for d-tubocurarine (dTC) (Sine, 1993; Sine et al., 1995). Also, they are different in their affinity for ACh (Sine et al., 1990). So, the ligand-activating site has two components: principal and complementary. In heteromeric receptors the α -subunits carry the principal component and the δ , γ and ϵ in muscle and β subunit in neuronal hold the complementary component, whereas, each subunit of homomeric receptors participate in both components.

The polypeptide chains of the receptor's ligand binding domain are arranged around pairs of β -sheets which combine into β -loops via a disulphide bridge and forming the Cys-loop (Unwin, 2005). Identification of aromatic residues important for ACh binding led to the proposal of a binding pocket consisting of six loops named A-F (**Figure 1.6**). The key photolabelled residues from *Torpedo marmorata* principal subunit (α -subunit) that participate in ACh binding are Tyr93 (Loop A), Trp149 (Loop B) and Tyr190, Cys192 and Cys193 (Loop C) and three less labelled residues Trp86, Tyr151 and Tyr198 (Dennis et al., 1988; Galzi et al., 1990). The main amino acids from the complementary subunits (δ or γ -subunit) that contribute to ACh binding are γ Trp55 and δ Asp75 (Loop D), γ Tyr111 and δ Arg117 (Loop E) (Chiara et al., 1998; Chiara et al.,

1999) and δ Asp165, δ Asp180 and δ Glu182 (Loop F) (Czajkowski and Karlin, 1995).

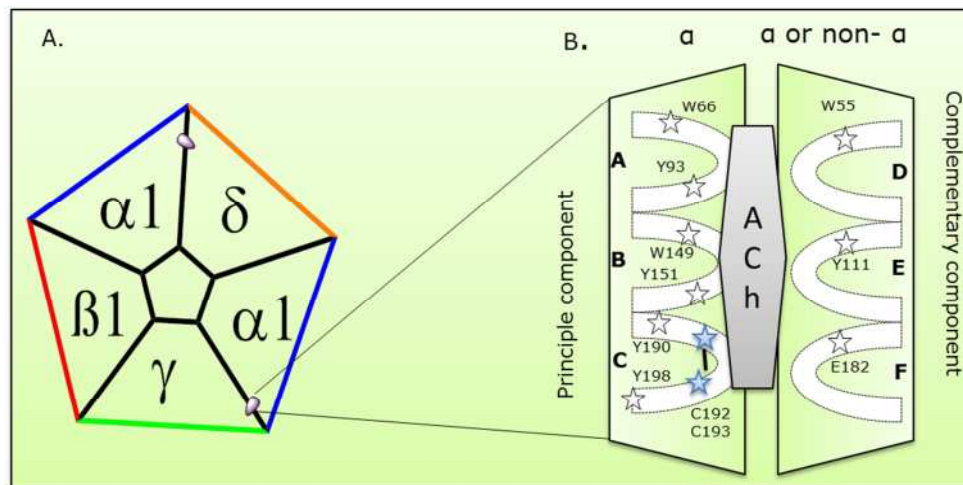


Figure 1.6. Schematic representation of the orthosteric ligand binding domain in Torpedo nAChRs, (A) The location of the ACh binding site (B) Represents the principle and complementary component with their loops, and the cysteine pair in loop C of the principal subunit, found only in α -subunits.

The agonist-binding pocket is measured to be 33 Å from the ion channel; binding of ligand to this site leads to a global conformational change (Herz et al., 1989; Unwin, 2005). These changes are dependent on time of exposure to and concentration of the ligand, and will lead to ion channel activation and desensitization. According to the Monod-Wyman-Changeux (MWC) theory, nAChR has the ability to change spontaneously between four functional states: Resting state (B) in the absence of agonist, Active state (A) by short exposure to agonist and low and high affinity desensitized states (I and D) from prolonged exposure to agonist (Karlin, 1967). Unwin (2005) reported that the ligand-binding site is the principle mediator for receptor conformation after binding with agonist. This eventually will follow by reorganization of hydrophobic domains inside the pore and opening the gate to allow penetration of small cations (**Figure 1.7**), which can pass through the narrowest part of the ion channel with diameter of 6.5 Å (Huang et al., 1978). A recent model has been published based on the crystal structure of human GABA_AR β 3 homopentamer at 3 Å

resolution. This model suggests that the binding of benzamidine to the agonist binding pocket and placed the channel into desensitized closed state (Miller and Aricescu, 2014).

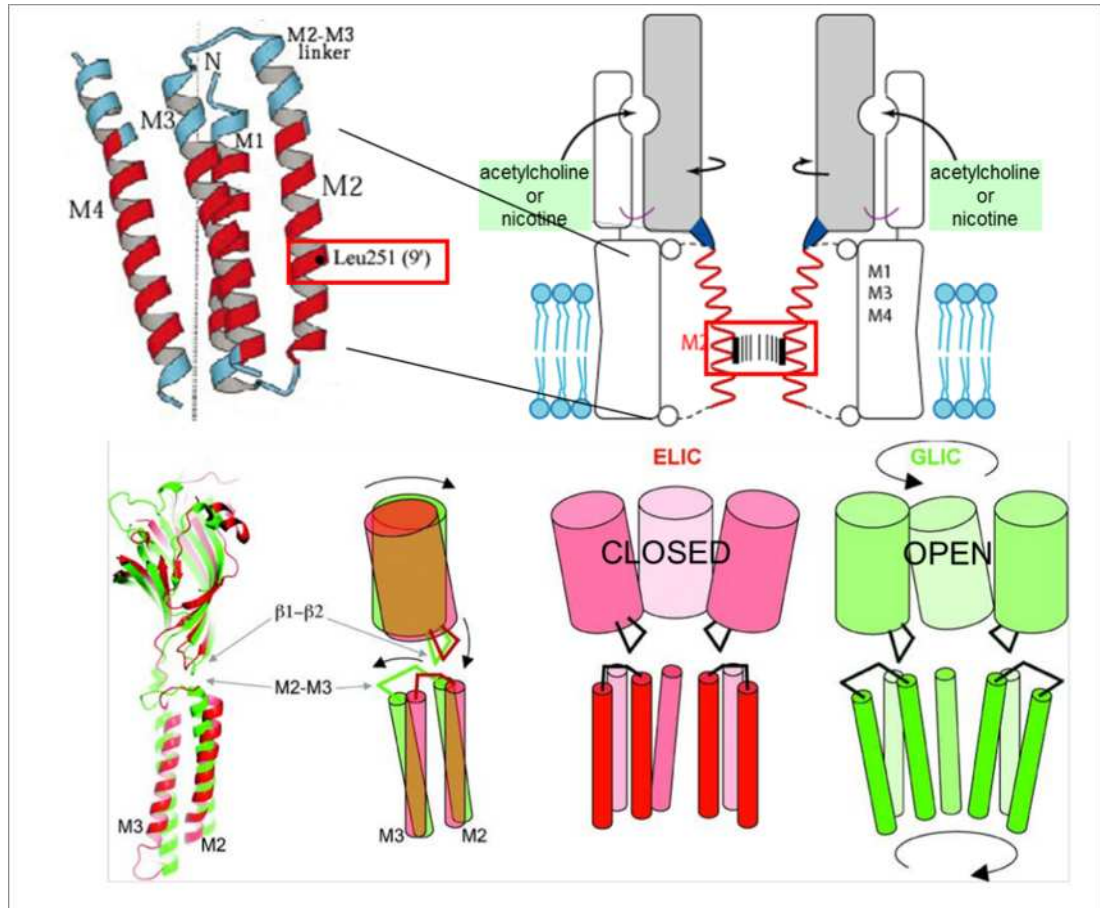


Figure 1.7. Illustrating the transduction mechanism of nAChR agonist binding to channel gating. Top is swivel (Miyazawa et al., 2003) and bottom is twist model (Corringer et al., 2010).

The location of the non-conducting gate in the channel of nAChRs has been debated. Work by Unwin using high resolution electron microscopy assumed that α -helices and β -sheet from transmembrane M2 and the ammonium terminal of M1 from all subunits contribute in the construction of the pore region of the receptor, while other transmembrane domains shield the pore from the lipid bilayer (Unwin, 2005). Tikhonov and collaborators showed that in human muscle-type nAChRs the channel lumen is formed by eight rings of

residues with different chemical properties; each one is formed from participation of identical or homologous residues from various subunits. The rings arranged from extracellular to intracellular are outer glutamate, leucine, valine, equatorial leucine, serine, threonine, intermediate glutamate and internal aspartate ring, respectively (Tikhonov et al., 2004) (**Figure 1.8**). In the case of neuronal receptors these rings have pretty similar properties to those of M-nAChRs. The residues from M2 from each subunit that participate in the ion channel pore are presented in **Table 1.2**. Unwin (2005) demonstrated that the leucine ring at position 247 functions as a gate (position **11** in **Table 1.2**). In contrast, Karlin and Wilson, using substituted-cysteine-accessibility-method (SCAM), showed that 2-aminoethyl methanethiosulfonate (MTSEA) has accessibility to bind amino acids in the intermediate ring at position 240 in the closed state of the channel, which indicated that the location of the resting gate was deeper in the channel pore and close to the selectivity filter (Wilson and Karlin, 2001; 1998). According to Tikhonov et al. (2004) the closed channel is the result of a hydrophobic ring (equatorial leucine) barrier to ions carrying water in their stable shell, while MTSEA does not have these properties, so it can penetrate the channel gate even when it is closed but hydrated cations cannot pass through it.

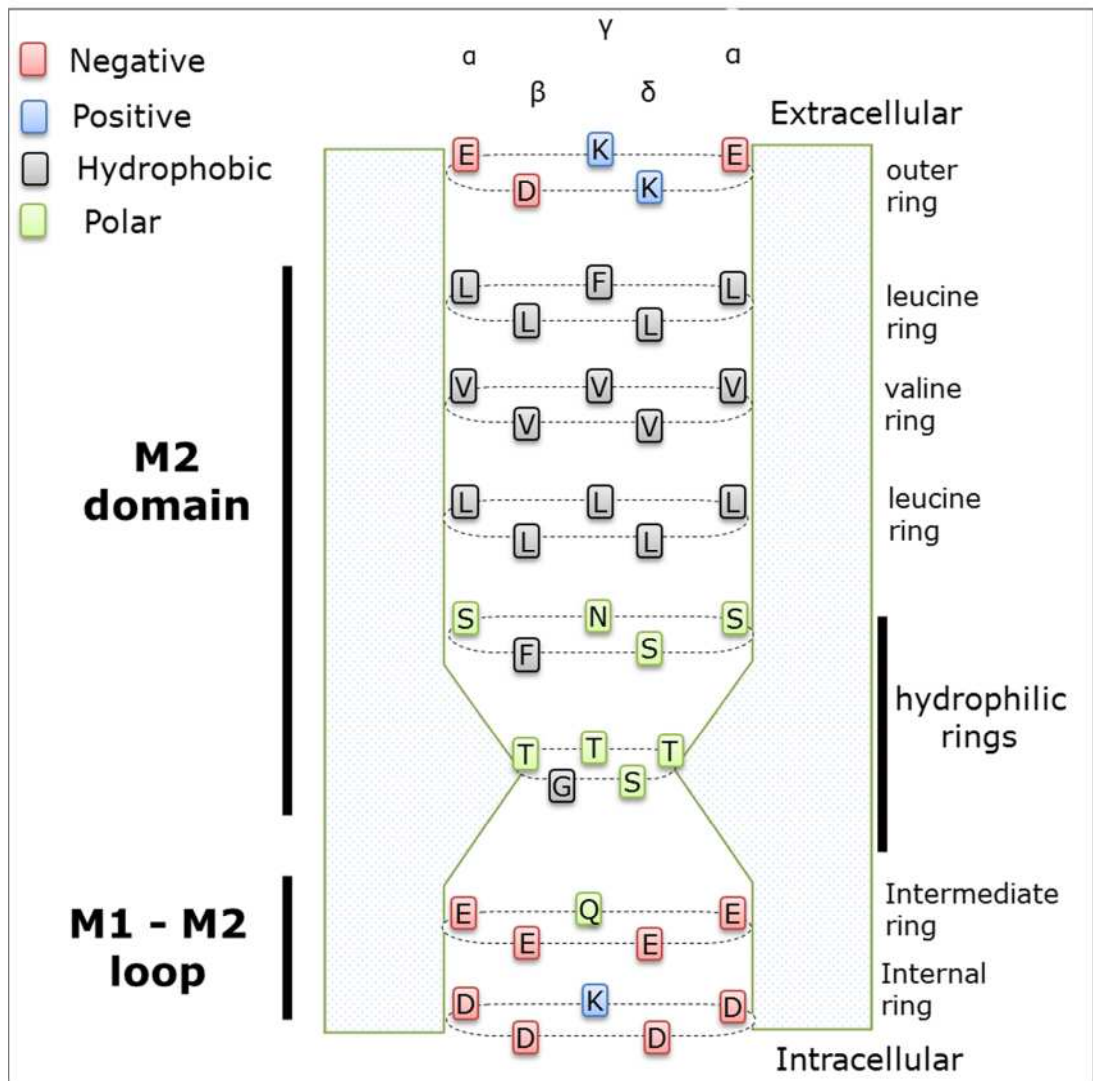


Figure 1.8. The ion channel of embryonic human M-nAChRs. The pore region is generated by eight rings of homologous amino acids from the M2 domain and M1-M2 loop of different subunits. The α -helical M2 transmembrane region mainly participates in the formation of the upper part of the pore which functions as a water filled pathway, while the loop component is responsible for the pore selectivity filter.

Table 1.2. Aligned sequences for the nAChR second transmembrane domain, M2, across three mammalian species. **Blue** and **red** amino acids are the single difference between M2 domains of $\beta 2$ and $\beta 4$ -subunits. The bold residues participate in the ion channel pore lining rings.

	Position																			
M2 Segment	1	2	3	4	5	6	7	8	9	10	11	12	13	14	15	16	17	18	19	20
Rat																				
$\alpha 3$	E	K	V	T	L	C	I	S	V	L	L	S	L	T	V	F	L	L	V	I
$\alpha 4$	E	K	V	T	L	C	I	S	V	L	L	S	L	T	V	F	L	L	L	I
$\alpha 7$	E	K	I	S	L	G	I	T	V	L	L	S	L	T	V	F	M	L	L	V
$\beta 2$	E	K	M	T	L	C	I	S	V	L	L	A	L	T	V	F	L	L	L	I
$\beta 4$	E	K	M	T	L	C	I	S	V	L	L	A	L	T	F	F	L	L	L	I
Mouse																				
$\alpha 1$	E	K	M	T	L	S	I	S	V	L	L	S	L	T	V	F	L	L	V	I
$\beta 1$	E	K	M	G	L	S	I	F	A	L	L	T	L	T	V	F	L	L	L	L
δ	E	K	T	S	V	A	I	S	V	L	L	A	Q	S	V	F	L	L	L	L
γ	Q	K	C	T	V	A	T	N	V	L	L	A	Q	T	V	F	L	F	L	V
ϵ	Q	K	C	T	V	S	I	N	V	L	L	A	Q	T	V	F	L	F	L	I
Human																				
$\alpha 1$	E	K	M	T	L	S	I	S	V	L	L	S	L	T	V	F	L	L	V	I
$\alpha 2$	E	K	I	T	L	C	I	S	V	L	L	S	L	T	V	F	L	L	L	I
$\alpha 3$	E	K	V	T	L	C	I	S	V	L	L	S	L	T	V	F	L	L	V	I
$\alpha 4$	E	K	I	T	L	C	I	S	V	L	L	S	L	T	V	F	L	L	L	I
$\alpha 5$	E	K	I	C	L	C	T	S	V	L	V	S	L	T	V	F	L	L	V	I
$\alpha 6$	E	K	V	T	L	C	I	S	V	L	L	S	L	T	V	F	L	L	V	I
$\alpha 7$	E	K	I	S	L	G	I	T	V	L	L	S	L	T	V	F	M	L	L	V
$\alpha 9$	E	K	V	S	L	G	V	T	I	L	L	A	M	T	V	F	Q	L	M	V
$\alpha 10$	E	K	V	S	L	G	V	T	V	L	L	A	L	T	V	F	Q	L	L	L
$\beta 1$	E	K	M	G	L	S	I	F	A	L	L	T	L	T	V	F	L	L	L	L
$\beta 2$	E	K	M	T	L	C	I	S	V	L	L	A	L	T	V	F	L	L	L	L
$\beta 3$	E	K	L	S	L	S	T	S	V	L	V	S	L	T	V	F	L	L	V	I
$\beta 4$	E	K	M	T	L	C	I	S	V	L	L	A	L	T	F	F	L	L	L	I
δ	E	K	T	S	V	A	I	S	V	L	L	A	Q	S	V	F	L	L	L	I
γ	Q	K	C	T	V	A	I	N	V	L	L	A	Q	T	V	F	L	F	L	V
ϵ	Q	K	C	T	V	S	I	N	V	L	L	A	Q	T	V	F	L	F	L	I

Experimental data from site directed mutagenesis techniques shows the contribution of particular amino acid rings in determining Permeability characteristics of the nAChR. For instance, the intermediate negatively charged ring, glutamate, is mainly responsible for the permeability of divalent cations, so mutation of $\alpha 7E237$ to A eliminates Ca^{2+} permeability of the channel, while it does not affect sodium or potassium permeability (Bertrand et al., 1993). Furthermore, the mutations $\alpha 7V251D$ and $\alpha 7E237A$ in the hydrophobic ring and intermediate ring of M1-M2 loop with an insertion of alanine or proline at the intracellular end of M2 shows their role in charge selectivity by creating a channel with anion selectivity (Corringer et al., 1999; Galzi et al., 1992).

1.2.3. Role and distribution

nAChRs are found in various regions of organisms due to their important function in many activities. To confirm the distribution pattern of these receptors in CNS and PNS, different groups of probes including fluorescent and radiolabelled ligands and antibodies have been used. These studies provide a wealth of knowledge about the density and region specificity of nAChR gene expression (Sargent, 1993). Understanding the role of particular nAChR subunits in physiological and pathophysiological processes has been improved markedly after using new knockout (Ko) and knockin (Kin) genetic techniques.

Peripheral nervous system

Muscle type nAChRs at neuromuscular junctions between motor neurons and skeletal muscle are mainly localized postsynaptically, where they convert the chemical signal from their binding with ACh to an electrical signal ultimately generating muscle contraction (Jensen et al., 2005). Abnormality in the function of this type of receptors will lead to pathological disorders such as myasthenia gravis (Lindstrom, 2000). Therefore, it becomes a novel target for drug discovery such as muscle relaxants (Lee, 2003).

The neuronal nAChRs in mammalian autonomic pathways that mediate fast synaptic transmission mainly form varying subtypes from α (3, 4, 5, 7) and β (3, 4) subunits which are significantly different in their localization and modulatory functions (Skok et al., 2001). The ratio of cells containing α 3, α 4, α 5 and α 7 in sympathetic pathways of the guinea pig is roughly three fold higher than in the parasympathetic pathway (Glushakov et al., 2004), therefore, the pharmacology of both pathways are markedly different. The most predominant α subunits in autonomic ganglia are α 3 forming heteromeric receptors such as α 3 β 4, "ganglionic-type nAChRs" (Papke and Heinemann, 1991), and α 7 as homomeric receptors in rat (Herrero et al., 1999). Knockout of the α 3 subunit in mice has led to wide failure in autonomic pathways mainly causing intestinal,

bladder and pupillary of eye disorders (Xu et al., 1999). Also, it has a major role in autoimmune autonomic ganglionopathy (Vernino et al., 2009).

Central nervous system

To further understand nAChRs and map their expression in the CNS, researchers have used various techniques such as ligand binding and gene expression.

Clarke et al. (Clarke et al., 1985) used three radioligands; ^{125}I - α -Bgtx (antagonistic), ^3H -nicotine and ^3H -ACh (agonistic) on rat brain tissue to identify the distribution of high-affinity binding sites. This study shows identical regional distribution of both agonist's binding sites which are distinct from that of the antagonist. Binding sites of ^{125}I - α -Bgtx are observed mainly in the hippocampus, hypothalamus, inferior colliculus and particularly layers I and IV of the cerebral cortex. Binding sites of ^3H -nicotine and ^3H -ACh were seen in high density in interpeduncular nucleus, numerous thalamic nuclei, medial habenula and superior colliculus. Moderate density was seen in ventral tegmental, cerebral cortex (especially in layer III and IV), presubiculum and substantia nigra pars compact. Low density was noticed in the cerebellum and no labelling was seen in either the hippocampus or the hypothalamus region.

Given that N-nAChR genes differ in their expression patterns in different areas of the brain (**Table 1.3**); it is likely that unique neuronal subsets express different nAChRs genes. To assess the gene expression of N-nAChRs in the CNS, different methods have been used such as in situ hybridization, RNase protection and Northern blots (Sargent, 1993). In situ hybridization studies show that several areas of rat brain express at least a single gene of N-nAChR with a unique pattern in each region (Wada et al., 1989). For example, $\alpha 4$ subunits are widely expressed in a high concentration in many areas of the rat brain, whereas $\alpha 2$ subunit expression is highly limited in its regional distribution. The $\alpha 3$ expression pattern was intermediate between $\alpha 4$ and $\alpha 2$. In the case of β

subunits, $\beta 2$ expression is observed in the majority of the rat brain parts, whereas $\beta 3$ expression was restricted to particular regions (Deneris et al., 1989). $\beta 4$ expression was observed strongly only in medial habenula (Duvoisin et al., 1989) but a later study noticed more broad expression of $\beta 4$ in rat CNS (Dineley-Miller and Patrick, 1992).

The native subtypes of nAChRs expressed in CNS have been suggested to participate in many brain activities and behaviour. For example, it has been proposed that probably both $\alpha 4\beta 2$ and $\alpha 4\beta 4$ are involved in neurodegeneration, cognition, anxiety, depression and pain, whereas $\alpha 3\beta 2$ nAChRs are linked to addiction and release of dopamine, and $\alpha 7$ connected to the release of GABA (Lloyd and Williams, 2000).

There are several lines of evidence that propose a role for nAChRs in neuroprotection (Arneric and Brioni, 1999). Firstly, a reduction in the nAChR population was observed in the cortex and hippocampus of Alzheimer's disease patients. Secondly, Smokers appear to be less likely to develop early onset Alzheimer's disease (van Duijn et al., 1995), suggesting that nAChRs could play a potential role for finding a pharmaceutical treatment for this disease. Thirdly, a few subtypes of mammalian nAChRs such as $\alpha 7$ and $\alpha 9\alpha 10$ are highly permeable to Ca^{2+} , indicating a critical role in controlling intracellular signaling, synaptic transmission and modulation of nerve growth factor (Albuquerque et al., 1997; Lipovsek et al., 2014; Role and Berg, 1996). Finally, some nAChR modulators are neuroprotective in both *in vitro* and *in vivo* studies. A few of these ligands have a huge side effect due to non-selective action over different subtypes of nAChRs. This problem could be solved by identifying ligands that interact selectively with one particular subtype over other combinations of nAChR subunits.

Table 1.3. The regional distribution of the various subunit combinations of nAChRs in the CNS. Modified from (Taly et al., 2009)

CNS regions	Expressed combinations of N-nAChRs
Spinal cord	$\alpha 4\beta 2$, $\alpha 3\beta 2$, $\alpha 7$.
Raphe nuclei	$\alpha 4\beta 2$.
Oculus aeruleus	$\alpha 3\beta 4$, $\alpha 6\beta 2\beta 3$,
Interpeduncular nucleus	$\alpha 4\beta 2$, $\alpha 2\beta 2$, $\alpha 3\beta 3\beta 4$, $\alpha 7$.
Substantia nigra	$\alpha 4\beta 2$, $\alpha 4\alpha 5\beta 2$, $\alpha 3\beta 4$, $\alpha 6\beta 2\beta 3$, $\alpha 7$.
Ventral tegmental area	
Thalamus	$\alpha 4\beta 2$.
Hypothalamus	$\alpha 4\beta 2$, $\alpha 7$.
Amygdala	$\alpha 4\beta 2$, $\alpha 7$.
Striatum	$\alpha 4\beta 2$, $\alpha 4\alpha 5\beta 2$, $\alpha 6\beta 2\beta 3$, $\alpha 6\alpha 4\beta 2\beta 3$.
Olfactory bulb	$\alpha 4\beta 2$, $\alpha 7$.
Cortex	$\alpha 4\beta 2$, $\alpha 4\alpha 5\beta 2$, $\alpha 7$.
Hippocampus	$\alpha 4\beta 2$, $\alpha 4\alpha 5\beta 2$, $\alpha 3\beta 4$, $\alpha 7$.
Medial habenule	$\alpha 4\beta 2$, $\alpha 3\beta 4$, $\alpha 3\beta 3\beta 4$, $\alpha 7$.
Pineal gland	$\alpha 7$, $\alpha 3\beta 4$.
Cerebellum	$\alpha 4\beta 2$, $\alpha 3\beta 4$, $\alpha 7$, $\alpha 3\beta 2$.

Non-neuronal location of neuronal nAChRs

In the immune system, three- α (3, 4, 7) and two- β (2, 4) subunits are found on T-cells (Kuo et al., 2002); also functional nicotinic receptors containing α (4 or 7) subunits are found on B-lymphocytes, where they decrease antibody production and stimulate growth (Skok et al., 2003). Moreover, both human macrophage and brain microglia have $\alpha 7$ nAChRs (Gotti and Clementi, 2004). The $\alpha 7$ nAChR also has a critical role in the immune system and has become a potential therapeutic target for anti-inflammatory drugs (Pohanka, 2012).

In the human skin, epidermal keratinocytes synthesize ACh (Lindstrom, 2010) and express receptors which have pharmacological and biophysical characteristics of the ganglionic $\alpha 3$ subunit (Grando et al., 1995). These receptors perform numerous skin functions such as proliferation, differentiation, adhesion, motility and apoptosis, via controlling Ca^{2+} influx into keratinocytes (Gotti and Clementi, 2004; Grando et al., 1995). The vascular system endothelial cells and smooth muscle express different types of nicotinic subunits, also some subunits have been found in bronchial cells of lung (Lindstrom, 2010).

Invertebrate and insect nAChRs

The complete genomic sequence of the nematode worm *Caenorhabditis elegans* was a great achievement; it gives researchers the opportunity to use this animal as a model for the investigation of many human diseases which might lead to the development of new treatments. One important target for drug discovery is nAChRs; it appears from analysis of this small worm's genome sequence that it has at least 27 distinct nAChR subunits (Jones and Sattelle, 2003). So far, Levamisole, which acts as an agonist of invertebrate nAChRs, has been used in humans and other animals as a drug to control the intestinal disease cause by helminthes such as tapeworms, roundworm and blood flukes (Fleming et al., 1997; Martin, 1997; Millar and Denholm, 2007).

Insect nAChRs are the major excitatory neurotransmitter gated ion channels, which are present in huge abundance in excitatory post-synaptic membrane (Sattelle, 1980). Therefore, due to the critical role of these receptors as fast excitatory channels, they present an effective target for the development of selective insecticides (Matsuda et al., 2001). So far, the presence of seven α -subunits (D- $\alpha 1$ to $\alpha 7$) and three β -subunits (D- $\beta 1$ to $\beta 3$) of nAChRs have been confirmed by molecular cloning studies in the fruit fly *Drosophila melanogaster* (Millar, 2003; Tomizawa and Casida, 2001). The data reported from insect genomic sequence projects suggested a comparable level of nAChR subunit

diversity found in the fruit fly to other insect species (Jones et al., 2006). Insect nAChRs are difficult to express alone to investigate their characteristics, therefore to understand the pharmacological properties of each insect subunit and their possibility to co-assemble with others to generate functional channels, researchers have used native tissue and heterologous expression systems (Millar, 1999; 2003). Several techniques and approaches have been used to investigate the profile of insect nAChRs such as their expression with the vertebrate auxiliary subunit, $\beta 2$ (Bertrand et al., 1994; Lansdell et al., 1997), developing a chimeric subunit (Lansdell and Millar, 2004) and using insect cells as a native source of receptors (Lansdell et al., 1997).

1.3. Pharmacology

Pharmacologically various groups of synthetic and natural compounds have been examined and their effects on the activity of nAChRs explained (**Figure 1.9**). These drugs can be divided into three main categories based on binding sites and consequent events after interacting with receptors (**Figure 1.10**): agonists (stimulation), antagonists (inhibition), and allosteric ligands (molecules that stimulate or inhibit agonist activity by binding to allosteric sites other than the agonist binding-site).

Agonists are drugs that lack subtype selectivity between different combinations of nAChR subunits (Gotti et al., 1997), with few exceptions. A diverse range of agonists has been tested; some of them are full agonists with strong potency such as ACh and carbacol (CCh), while others are partial agonists with weak potency like suberylcholine (SubCh). However, a few agonists have been identified as selective for N-nAChRs such as dimethylphenylpiperazine (DMPP) for $\alpha 3\beta 4$ (Prado and Segalla, 2004) and varenicline as a full agonist on $\alpha 7$ and partial agonist on $\alpha 4\beta 2$ has been permitted recently by FDA (Food and Drug Administration) to use as an aid drug for smoking cessation (Mihalak et al., 2006).

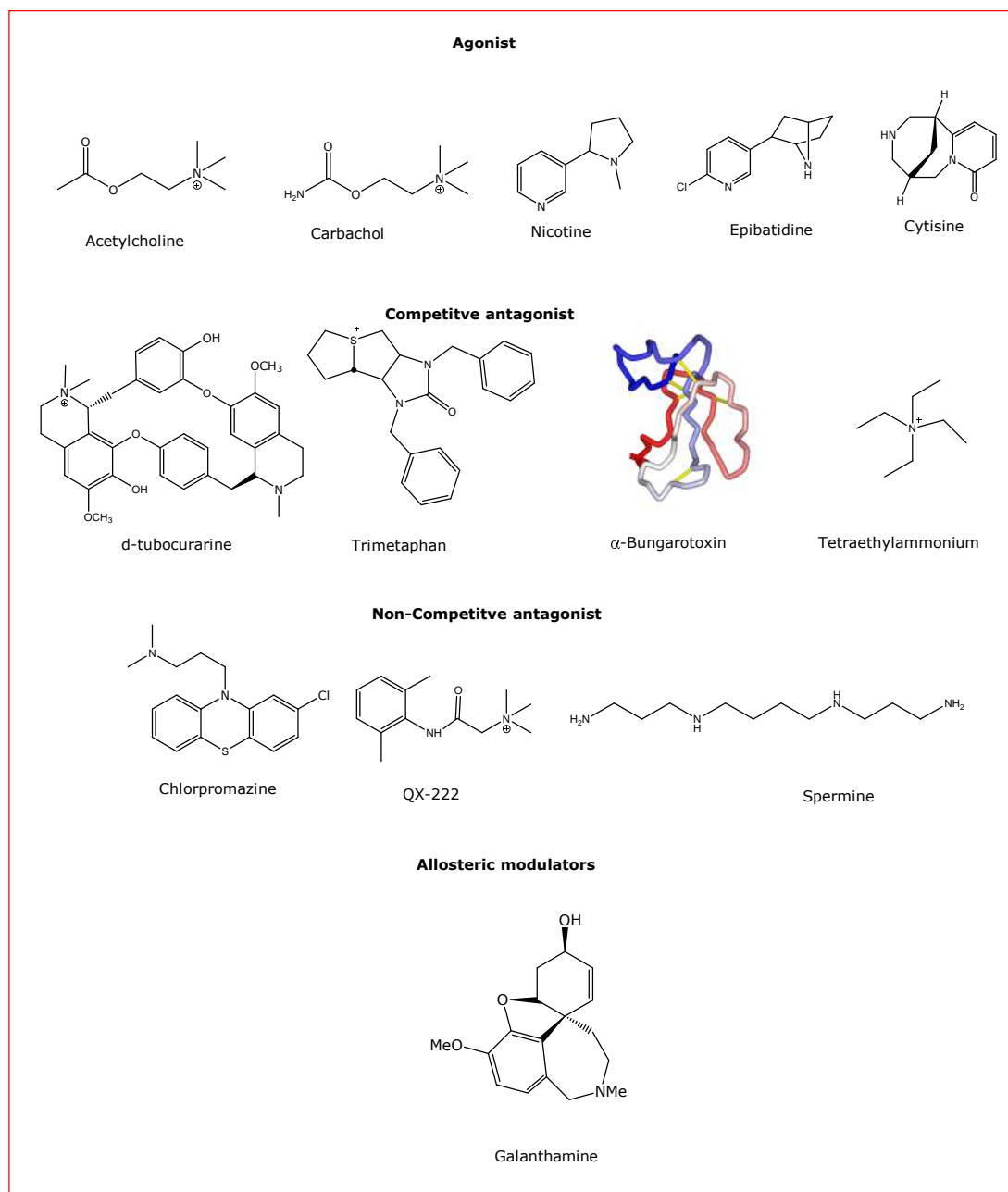


Figure 1.9. Structures of established nAChR ligands.

Antagonists are compounds that diminish the action of any agonist. These drugs have shown a high subtype specificity among nAChRs and can be divided into classes based on their site of action: Competitive antagonists compete with agonist for their binding sites, whereas non-competitive antagonists have two possible sites of action, some at the subunit-lipid interface and others in the pore lumen of nAChRs. Changeux et al. (1984) called the substances with binding

sites in the lumen as non-competitive inhibitors (NCIs), which classically have been identified as blockers of the open ion channel, inhibiting passage of ions (Neher and Steinbach, 1978). It seems to be that open channel blockers are mostly cationic and interact within the membrane electrical field so their activity is usually voltage-dependent (i.e. their effect increases at more hyperpolarizing membrane potentials).

A well-studied example of a competitive muscle-type nAChR selective antagonist is the snake toxin derived from *Bungarus multicinctus*, Malayan Banded (Formosan) Krait, called α -bungarotoxin (α -Bgtx), which was used via various types of experiments to determine the pharmacological properties of muscle-type nAChRs. Also it was used in the original affinity purification of nAChRs from electric organ (Lindstrom and Patrick, 1974) that led to the first nAChR protein partially sequenced (Raftery et al., 1980) from which the whole cDNA sequence was obtained (Ballivet et al., 1982). Further works show that neuronal ($\alpha 7$ to $\alpha 9$) homomeric receptors are also inhibited by α -Bgtx, whereas heteromeric neuronal receptors are not blocked by the toxin. Research on this toxin has lead scientists to understand the properties and distribution of homomeric receptors like $\alpha 7$, and their possible role in neurotransmission (Itier and Bertrand, 2001). d-Tubocurarine (d-TC), the active chemical compound of curare, also acts as a specific M-nAChR selective competitive antagonist. Competitive antagonists of N-nAChRs include κ -bungarotoxins (κ -BgTX), tetraethylammonium and trimetaphan; the latter one is used during surgery causing local hypotension. Other competitive antagonists of nAChRs include trimethylammonium diazonium fluoroborate (TDF), p-N,N-(dimethylamino)phenyldiazonium fluoroborate (DDF) and maleimidobenzyltrimethylammonium (MBTA) that all interact with agonist-binding sites through covalent binding and are widely used in nAChR labelling studies (Arias, 2000).

Non-competitive nAChR antagonists such as chlorpromazine (CPZ) and QX-222 were used to characterize the ion channel/M2 domain. Works by Giraudat et al. (1989) and Revah et al. (1990) show the ability of CPZ to label residues in the α -helical portion of the M2 region. This blocker has a high affinity for its binding sites in the ion channel; therefore a number of homologous residues (Ser240, Thr244 and Leu247) in different nAChR subunits were identified. Its antagonistic action on nAChRs as an open-channel blocker is voltage-dependent, while its effect as closed channel blocker by reducing frequency of channel opening and role in enhanced desensitization is voltage-independent (Benoit and Changeux, 1993; Wang and Sun, 2005).

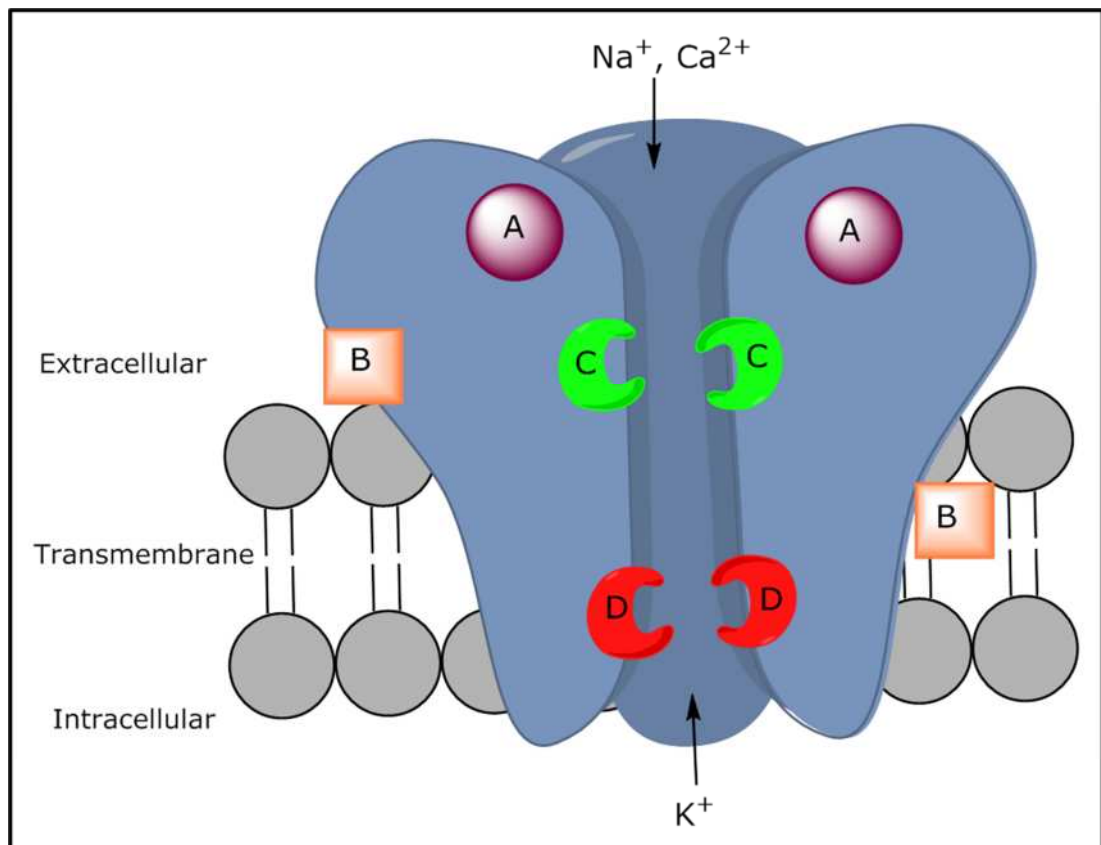


Figure1.10. schematic drawing of nAChRs showing various binding sites: (A) Agonist and competitive antagonist (B) Allosteric modulators (C) non-luminal (D) luminal binding sites of non-competitive antagonist.

Further work characterizing different residues of the pore region was done by using a wide range of compounds which have binding sites in the channel such as QX-222, the local anaesthetic, found to mostly interact with the same rings that CPZ binds to (serine, threonine and leucine) (Arias, 1998).

Spermine is a ubiquitous polyamine that participates in cellular metabolism in all eukaryotic cells. Its non-competitive action on $\alpha 3\beta 4$ and $\alpha 4\beta 2$ neuronal nAChRs was investigated by Haghghi and Cooper (1998). They showed that this compound displayed a high affinity to block neuronal nAChRs at depolarized potential when applied from the cytoplasmic side of the pore. The spermine concentration in a neurone such as rat superior cervical ganglion (SCG) cells, is high and their voltage-dependent mode of blocking explains the inward neuronal rectification of nAChRs. As explained by the Woodhull model of voltage-dependent block (Woodhull, 1973), the mode of channel blocking by spermine occurs after entering the open channel and interacting with its binding sites in the membrane electrical field where it can impede the penetration of small cations through the channel. In contrast it acts as a voltage-independent inhibitor of muscle TE671 cell line nAChRs in the presence of 100 μM arcaïne (a potent antagonist at the polyamine site of the NMDA receptor) and can potentiate the receptors in the absence of arcaïne when applied extracellularly (Shao et al., 1998).

Also a number of natural active antagonists for nAChRs have been identified, for instance α -conotoxin and philanthotoxin-433 (PhTX-433). Synthetic derivatives of the latter form the basis of this project. α -Conotoxin is a small neurotoxic peptide of 12-20 amino acids, which is derived from the venom of cone snails (genus *Conus*) (Jensen et al., 2005). In addition, different types of conotoxin act on the NMJ type of nAChRs. The family of α -conotoxins can be further divided into four subfamilies: $\alpha 3/5$, $\alpha 4/3$, $\alpha 4/6$ and $\alpha 4/7$, depending on the number of amino acid residues separating the cysteine residues in loop I and

II (Dutton and Craik, 2001). The last three types of conotoxin are selective inhibitors of N-nAChRs, while $\alpha 3/5$ are selective for M-nAChRs (Nicke et al., 2004).

Ethidium is an irreversible non-competitive nAChR antagonist with higher affinity for the open channel state. It has a deep binding site in the ion channel (Bixel et al., 2000). Ethidium has been used as a tool in a number of experiments to describe the activity of compounds as antagonists or agonists as well as receptor characterization.

Extensive studies show that a diverse group of structurally related molecules can modulate signalling pathways of nAChRs via allosteric binding sites at the receptor complex. Zinc as an endogenous ligand mainly impacts on heteromeric neuronal nAChRs. Zn^{2+} enhances the strength of the agonist response at concentrations up to 100 μM and higher concentrations impede the nAChRs functional state (Jensen et al., 2005).

1.4. Polyamines and Philanthotoxin

Polyamines are compounds carrying more than one amino group in their structure and are synthesized in all eukaryotic cells. Putrescine, spermine and spermidine are the main biological polyamines that have so far been found in living cells which play a critical role in many physiological activities such as modulation of ion channel function, including nAChR. These organic compounds have also been found and identified in the venom of predatory spiders and wasps. Eldefrawi and his colleagues (1988) for the first time characterized the active component of the Egyptian solitary digger wasp, *Philanthus triangulum*, venom, which causes paralysis to honeybees, and named it philanthotoxin-433 (PhTX-433). It has molecular weight of 435 (**Figure 1.11**) and 4-3-3 denotes the methylene groups separating nitrogens in the tail region (Nakanishi et al., 1997).

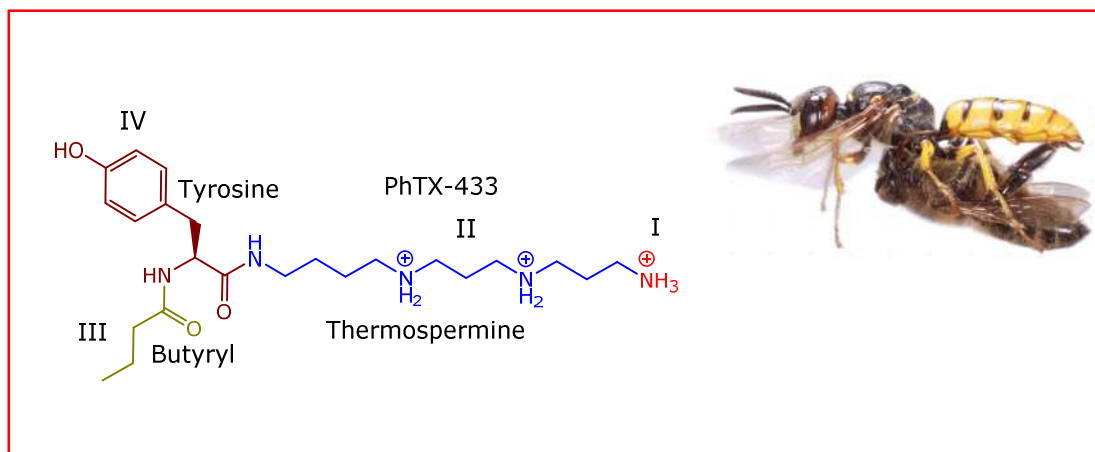


Figure 1.11. *Philanthus triangulum* with paralysed honeybee and chemical structure of the venom active component, PhTX-433. (Red) region I= ammonium group, (blue) region II= thermospermine, (green) region III= butyryl and (brown) region IV= tyrosine. (Photograph courtesy of Warren Photographic).

The structure of natural PhTX-433 is composed of a long polyamine (thermospermine 4-3-3) chain, which carries a primary amino group at the terminal end, and a head-group containing an aliphatic butyryl group and an aromatic tyrosyl group at the other end. These moieties are linked together via amide bonds (Stromgaard et al., 2005) and form a molecule with hydrophobic properties at the head and hydrophilic at the tail region. It acts as a non-competitive antagonist targeting several important cation-permeable ion channels such as ionotropic glutamate receptors and nAChRs (Stromgaard et al., 2000A). The inhibitory potency of PhTX-433 has been reported previously on qGluR naturally expressed in locust leg muscle, where its IC_{50} was 18 μ M (Bruce et al., 1990). This potency was in agreement also with binding assay studies on rat NMDA receptors but was higher ($IC_{50} = 1 \mu$ M) in nAChRs (Anis et al., 1990). The antagonistic actions of PhTX-433 and the many analogues that have been synthesized is mainly related to the number of nitrogen atoms in the polyamine chain and their probable interactions with negatively charged or polar amino acids of the channel's cation-selective lumen (Mellor et al., 2003; Stromgaard et

al., 2002) and to a lesser extent on the head group which anchors the toxin to the extracellular entrance of the channel (Stromgaard et al., 2005).

The main obstacle facing use of the natural toxin (PhTX-433) as a candidate for drug development and understanding pharmacological characteristics of ionotropic receptors is the lack of subtype selectivity. Therefore, modifying the toxin's structural moieties by adding, removing or substituting groups of atoms might lead to changes in their inhibitory potency toward particular categories of targeted receptors. This selectivity makes the philanthoxins important tools for examining functional activity of specific ionotropic receptors (Stromgaard et al., 2005).

The existence of four different sections in the structure of PhTX-433 makes it suitable for developing a wide range of analogues by using solid-phase synthesis (SPS). The action of these analogues has been investigated on different types of receptors, and it appears that some analogues have specific inhibitory properties on particular receptor categories. The pharmacologically standard analogue that mostly has similar properties to PhTX-433 is PhTX-343 where the polyamine chain is spermine rather than thermospermine. Replacing one or both secondary amino groups in the long-polyamine tail of PhTX-343 with a methylene group will lead to PhTX-83 and PhTX-12, respectively (**Figure 1.12**).

Converting PhTX-343 to PhTX-12 markedly altered the inhibitory potency of the toxin on different receptors. PhTX-343 non-selectively antagonizes different types of ionotropic receptor including nAChRs and iGluRs and their potency level is mostly similar on all of them. However, PhTX-12 exhibits strong inhibitory activity on M-nAChRs in *Torpedo* electric organ and human, whilst it does not affect several types of iGluRs (Stromgaard et al., 2000B). A further modification of the PhTX-12 polyamine tail led to the development of a series of analogues, PhTX-7 to PhTX-11. PhTX-11 was found to be the only synthesized

compound to have a considerable increase in potency compared to PhTX-12, whereas, all others did not (Stromgaard et al., 2002). Moreover, PhTX-83 has been known to have strong antagonism selectivity toward α -amino-3-hydroxy-5-methyl-4-isoxazolepropionic acid receptors (AMPA) (Mellor et al., 2003).

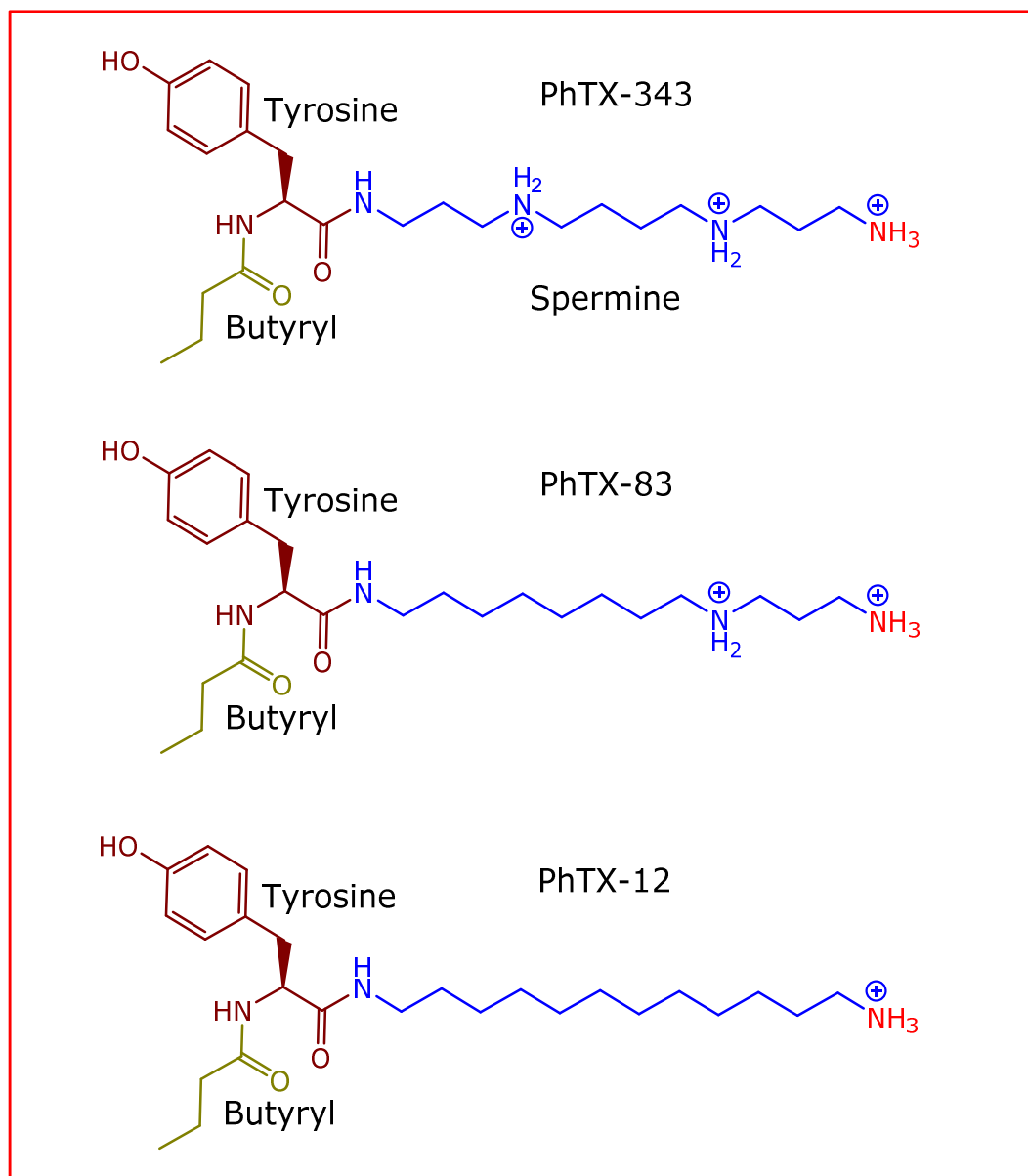


Figure 1.12. Shows the structure of philantotoxin-343 and its basic analogues PhTX-83 and PhTX-12.

However, ambiguous effects have been reported from the modification of the aromatic head group of philanthotoxins with few exceptions that lead to strong subtype selectivity. For instance, replacing the amino acid moiety (tyrosyl group) in PhTX-343 derivatives with N-cyclohexyl-L-alanine (Cha) led to the

synthesis of six analogues. All these analogues show selectivity towards human muscle nAChRs and their potency at negative holding potential was significantly higher than PhTX-343, while mostly similar potencies were recorded on AMPA receptors (Olsen et al., 2006). In contrast to this, the antagonism potency of PhTX-343 derivatives on both NMDAR and nAChR was increased markedly by substituting the butyryl group with 2-phenylacetyl (Stromgaard et al., 2000B).

Philanthotoxin head-group modification has proposed the orientation mode of this toxin inside the receptor channel. In a photo-labelling study, Choi et al (1995) found that in *Torpedo* electric organ nAChRs the α -subunit is probably the main subunit responsible for the action of philanthotoxins due to their high crosslinking to approximately 20,000 Dalton between Ser173 to Glu338 and 12,000 Dalton from Asn339 to Gly437, with N₃-Ph-¹²⁵I₂-PhTX-343-Lys. They suggested a "head-down" orientation mode for philanthotoxin in the lumen of nAChR channel. However, a "tail-down" interaction mode for N₃-Ph-¹²⁵I₂-PhTX-343-Lys has been suggested in the channel pore by Bixel et al (2000) when N₃-Ph-¹²⁵I₂-PhTX-343-Lys was applied from the extracellular side, while intracellular application of this compound and PhTX-343 did not show any effect on nAChRs of the BC(3)HI muscle cell line (Jayaraman et al., 1999). In addition, the latter mode of philanthotoxin receptor interaction has been supported by structure-activity relationships (SAR) using toxin analogues having a huge aromatic head group (Bixel et al., 2000; Nakanishi et al., 1997).

Interestingly, modification of the terminal amino group in philanthotoxin structures, which is mainly responsible for toxin inhibition activity (Jaroszewski et al., 1996), dramatically affects their potency. It has been shown by previous studies that the polyamine tail might bind to residues near the serine ring (Tikhonov et al., 2004). Therefore, adding positive charge to this region such as arginine or lysine will decrease half maximal inhibitory concentration, IC₅₀,

whereas adding a bulky group or neutralizing the charge will increase philanthotoxin IC₅₀ value.

Most investigations on the action of philanthotoxins on nAChRs have used muscle-type receptors. An early patch clamp study by Rozental and colleagues suggested that PhTX-433, at micro-molar concentrations (1-20 μ M), inhibited frog muscle responses and reduced channel opening rate and channel open and burst time. Binding of [¹²⁵I]- α -Bgtx to honeybee brain membrane was inhibited by PhTX-433, as was [³H]-perhydrohistrionicotoxin a synthetic derivative of a natural alkaloid NCI extracted from the skin of the Colombian frog, *Dendrobates histrionicus*. Moreover, low and high concentrations of PhTX-433 caused potentiation and inhibition of the binding affinity of [³H]-ACh to *Torpedo* electric organ, respectively (Rozental et al., 1989). Brackley et al (1990) showed that the ACh response of *Xenopus* oocytes injected with rat brain RNA was potentiated at low concentration of PhTX-343. Therefore, Rozental and co-workers concluded that the main inhibitory action of natural philanthotoxin on nAChRs is due to a non-competitive mode of antagonism, open-channel block, but also it has a competitive mode of inhibition at high concentrations (Rozental et al., 1989).

Initially, a closed channel mode of inhibition was suggested for PhTX-343 due to its higher affinity for the closed channel state of nAChRs than the open channel conformation in BC(3)H1 cell line by using a laser pulse photolysis method. This work concluded that the rate constant of channel opening was decreased by PhTX-343, while channel closing was not affected; also channel opening was affected by using PhTX-343 at different holding potentials indicating voltage-dependence of toxin action (Jayaraman et al., 1999).

Data from electrophysiological studies proved the idea of voltage-dependent and independent inhibition of muscle (Mellor et al., 2003; Shao et al., 1998) and neuronal (Liu et al., 1997) nAChRs by philanthotoxins. The antagonist

action of PhTX-343 is time-dependent, which indicates that its inhibition mode is slow and requires gate opening following receptor activation (Brier et al., 2003). Mellor et al (2003) found that nAChRs in the TE671 cell line were antagonized by PhTX-12 even at depolarized membrane potential, while this was not the case for analogues like PhTX-343 and 9-oxa-PhTX-38. Furthermore, the impacts of PhTX-343 on neuronal nAChRs in rat phaeochromocytoma, PC12, cells using whole cell patch-clamp measurements was investigated. It appeared that the 100 μ M ACh evoked inward current was inhibited by 0.1 and 1 μ M of PhTX-343 at -60 holding potential. Also, the inward current of 100 μ M ACh and 0.1 μ M of PhTX-343 was gradually reduced during membrane hyperpolarization pulse application starting from -40 mV to -120 mV; such reduction was not found with application of ACh alone (Liu et al., 1997).

The position and organization of both shallow and deep non-competitive binding sites in the pore region of nAChRs was suggested by Tikhonov and his co-workers. The inhibition mode of blockers such as PhTX-343 results in binding to the deep site in a mostly voltage- and state-dependent manner in the open channel conformation, because this site is located beyond the gate (at the equatorial leucine ring). In contrast, compounds like PhTX-12 antagonize via shallow sites with a voltage-independent or weak voltage-dependent action because they do not have to penetrate through the narrowest portion of channel (Tikhonov et al., 2004).

The likely reason behind these two different modes of inhibition by PhTX-343 and PhTX-12 is their shape (**Figure 1.13**). PhTX-12 has a distance of twelve methylene groups between the single ammonium in the tail region and the aromatic head, so the molecule can adopt a folded shape in vacuo due to H-bond formation, whereas in the case of PhTX-343 these bonds form between two carbonyl groups of the head region and hydrogen atoms of the nearest ammonium group in the polyamine tail, which give a distinct head and tail

conformation to PhTX-343 (Tikhonov et al., 2004). Consequently, the diameter of PhTX-12 is roughly 12 Å, which prevents their penetration in the deep pore region of nAChRs and binds to the outer pore region, while the roughly 5 Å diameter of PhTX-343 gives it the ability to penetrate deep in the pore and interact with the hydrophilic and charged rings.

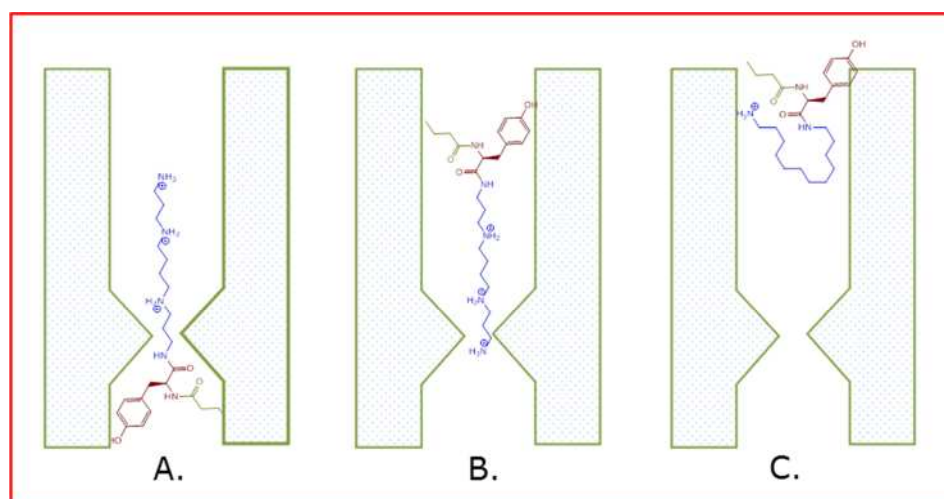


Figure 1.13. Schematic representation of the proposed mode of orientation and interaction for PhTX-343 A. head-down B. head-up C. PhTX-12.

1.5. *Xenopus oocytes* as a system for investigating ion channels

Xenopus laevis oocytes from the South African clawed frog have so far been used as a versatile expression system for various biological studies. This system is widely used to express functional ion transport proteins (Sigel, 2010) due to the low numbers of endogenous transport proteins in their surface membrane (Dascal, 1987); functional nAChRs have not been detected (Sumikawa et al., 1981). Gurdon and his colleagues for the first time confirmed that injection of *Xenopus laevis* oocyte nuclei with deoxyribonucleic acid (DNA) or of cytoplasm with ribonucleic acid (RNA) (**Figure 1.15**) will allow its processing to produce functional protein (Gurdon et al., 1971; Mertz and Gurdon, 1977). The electrical properties of newly synthesised ion channels can

be measured by two-electrode voltage clamp (TEVC) or patch clamp recording techniques such as inside-out or outside-out (Stuhmer, 1998).

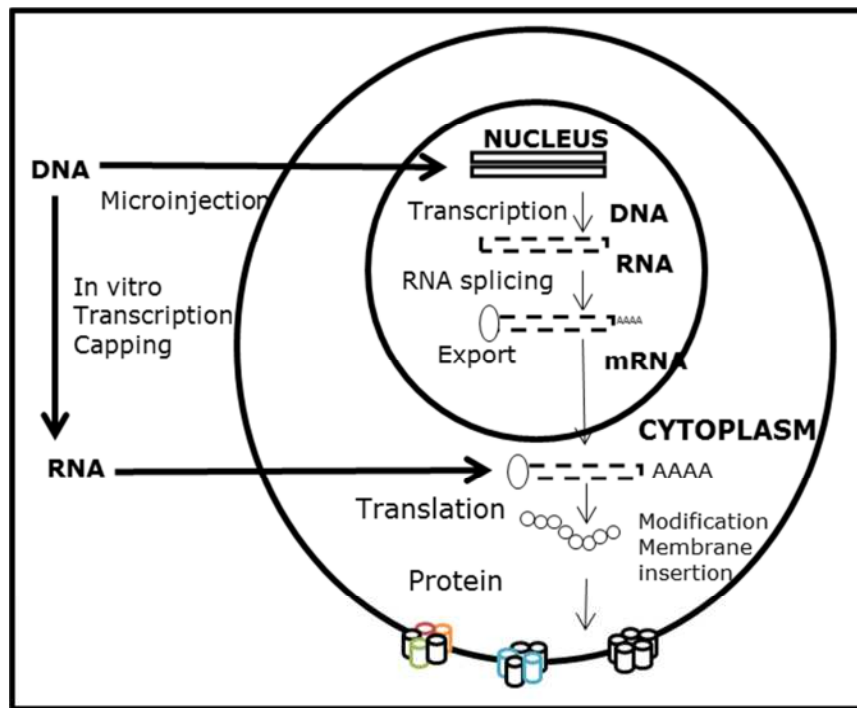


Figure 1.14. Genetic processing of foreign nAChR subunit encoding DNA or RNA in a *Xenopus* oocyte.

The first transmembrane ionotropic receptor expressed in *Xenopus* oocytes was the nAChR. It appeared that pharmacological properties of expressed nAChR was mostly similar to the native subtypes, which indicate the efficiency of this artificial system in assembling different receptor subunits and their localization in membrane (Sumikawa et al., 1981). Further investigation about the functional activity of the receptor was done by Barnard's group. They showed that nAChR subunit messenger-RNA injected into the oocyte could translate and post-translate then insert into their correct location in the membrane, where they function as a receptor (Barnard et al., 1982).

Xenopus oocytes have many advantages as an experimental tool in the biology laboratory. They are large, roughly 1 mm in diameter, and easily obtained (Moeller and Fenton, 2010). An oocyte has the ability to be injected

with more than 50nl of diluted nucleic acid. Moreover, the hard oocyte plasma membrane gives more benefits to cells such as surviving during defolliculation, removal of connective tissues, and easier penetration of the microinjection pipette (Sigel, 2010). The main advantage of using this artificial system in terms of nAChR studies is that most of the electrophysiological techniques can be simply performed on the oocyte. So, after membrane clamping, the effects of a wide range of natural and synthetic substances (agonist and antagonist) can be measured on the cell response. These data will help the further understanding of the receptor-chemical characterization.

1.6. Aims of the project

While philanthotoxin analogues have been well studied at ionotropic glutamate receptors and M-nAChRs the information of their actions on N-nAChRs is sparse, restricted mainly to a single study on PC12 cells (Liu et al., 1997). This suggests that they may be selective for certain neuronal subtypes and this may reveal more about the binding requirements for philanthotoxins. To address this gap in our knowledge, we aimed to characterise the effects of PhTX-343 and numerous analogues on a range of N-nAChR subtypes found in the mammalian nervous system and compared them to the muscle type receptor.

The first objective was to investigate the action PhTX-343 and PhTX-12 on the major wild-type and mutant N-nAChRs in CNS and PNS, $\alpha 4\beta 2$, $\alpha 4\beta 4$, $\alpha 3\beta 4$, $\alpha 3\beta 2$, $\alpha 7$, and M-nAChRs, $\alpha 1\beta 1\gamma\delta$, by their expression in *Xenopus* oocytes. The peak and decay current IC_{50} values for both analogues obtained at -80 mV by using the two-electrode voltage-clamp technique to generate concentration-inhibition relationships. Their IC_{50} values on different investigated subtypes of nAChRs were compared to evaluate whether there is any subunit-specific sensitivity difference for inhibition by PhTX-343 or PhTX-12.

The second objective was to examine the mode of inhibitory action of PhTX-343 and PhTX-12 on the various nAChR subtypes. Again two-electrode voltage-clamp was employed to evaluate whether the action of PhTX-343 and PhTX-12 is dependent or independent on the membrane holding potential. Furthermore, I investigated whether PhTX-343 or PhTX-12 competed with ACh for its binding site or not.

The final objective was to conduct a structure-activity study of twenty one synthetic analogues of PhTX-343, to investigate whether their potency and selectivity could be improved on rat neuronal $\alpha 4\beta 2$ and $\alpha 3\beta 4$ nAChRs.

CHAPTER TWO

MATERIAL AND METHODS

Summary

We used several molecular biology techniques for nAChR DNA manipulation and RNA transcription. The heat shock technique was used to insert the plasmid into *E. coli* strain XL-1 or X10-gold. DNA was extracted by using a maxi prep kit from sigma. Agarose gel electrophoresis and DNA sequencing were used to confirm each subunit. RNA transcription was achieved through two main steps: linearization and transcription.

Electrophysiological recordings were taken from microinjected oocytes by using two-electrode voltage clamp using a Geneclamp 500 voltage and patch clamp amplifier (Axon instrument). A range of experimental protocols were applied such as ACh concentration-response relationships, PhTX concentration-inhibition relationships and voltage-dependence of inhibition.

Data were recorded by using WinEDR computer software and analysed by using Graphpad prism 6 to calculate different variables such as IC_{50} , EC_{50} and δ value.

2.1. Molecular biology

2.1.1. Chemicals and Plasmids

Restriction enzymes were obtained from New England Biolabs and Promega. Markers for determination of DNA band size were obtained from Bio-Rad. *E. coli* bacteria strain XL-1 and X10-gold were used for DNA manipulation. All other chemicals were purchased from Sigma. Kits for RNA synthesis were obtained from Ambion.

Each nAChR subunit gene from rat, mouse and human was provided in a particular plasmid. The characteristics of all subunits and plasmids are shown in **(Table 2.1)**. All plasmids have resistance to ampicillin. All plasmids were obtained from the Salk Research Institute, except human $\alpha 7$ that was kindly provided by Prof. David B. Sattelle formerly at the University of Manchester now at University College London, and mutated rat $\beta 2_{(V253F)}$ and $\beta 4_{(F255V)}$ from Dr. Cecilia Borghese at the University of Texas at Austin.

Table 2.1. Characteristics of different plasmids used for DNA manipulation.

Subunit	Subunit size (bp)	Plasmid	Plasmid size (bp)	Restriction enzyme	Linearization enzyme	Promoter
Rat						
$\alpha 4$	2094	pSP64	2999	<i>HindIII</i>	<i>EcoRI</i>	SP6
$\alpha 3$	1858	pSP64	2999	<i>SmaI</i> (5'-) <i>EcoRI</i> (3'-)	<i>EcoRI</i>	SP6
$\beta 4$	2522	pBSSK(+)	2958	<i>EcoRI</i> (5'-) <i>XhoI</i> (3'-)	<i>XhoI</i>	T3
$\beta 2$	2197	pSP65	3005	<i>EcoRI</i>	<i>HindIII</i>	SP6
Mouse						
$\alpha 1$	1860	pSP65	3005	<i>EcoRI</i>	<i>SmaI</i>	SP6
$\beta 1$	2100	pSP65	3005	<i>EcoRI</i>	<i>HindIII</i>	SP6
γ	1844	pSP64	2999	<i>BamHI</i> (5'-) <i>EcoRI</i> (3')	<i>EcoRI</i>	SP6
δ	1961	pSP65	3005	<i>EcoRI</i>	<i>SmaI</i>	SP6
Human						
$\alpha 7$					<i>XbaI</i>	T7

2.1.2. DNA manipulation

Transformation

The processes of transformation was started by adding 1 μ l of 1:10 diluted pcDNA (\sim 40 ng/ μ l) to an Eppendorf containing 30 μ l of competent cells and incubated for 20 minutes on ice. The heat shock technique was then used to insert the plasmid into E. coli strain XL-1 or X10-gold. This was achieved by putting the sample in a water bath at 42 °C for one minute then placing it on ice for another 2 minutes. After this time, 200 μ l of LB broth (10 g Tryptone, 5 g yeast extract, and 10 g NaCl in one litre of deionized water) was added to the sample and left at 37 °C for half an hour. Then cells were gently spread on a petri dish that contained agar and 50 μ g/ml ampicillin (the antibiotic important for the selection step) and left for 24 hours, after which, colonies had developed. A single colony was then selected under sterile conditions and transferred to a tube containing 5 ml of LB broth with 50 μ g/ml ampicillin. The sample was incubated in a shaking bath at 37 °C at 221 rpm, overnight.

Crude DNA extraction

1.5 ml from the above culture was added to a fresh tube and the cells were centrifuged using an Eppendorf 5417R centrifuge at maximum speed, 14000 rpm, for 1 minute. The supernatant was removed and the pellet was re-suspended in 100 μ l of solution I (50 mM glucose, 25 mM Tris-Cl, 10 mM EDTA, pH=8). 200 μ l of solution II (0.2 M NaOH, freshly diluted from a 10 M stock, and 1% SDS) and 150 μ l of solution III (60 ml of 5 M potassium acetate, 11.5 ml of glacial acetic acid, 28.5 ml water; the resulting solution was 3 M with respect to potassium and 5 M with respect to acetate) were then added. The samples were mixed gently by inverting the tubes 6 times after adding each of the solutions. The mixture was next centrifuged for 10 minutes at 14000 rpm, and the supernatant was transferred into a new tube. Next, 350 μ l of isopropanol was added to the supernatant and the mixture was again spun at maximum speed,

14000 rpm, for 10 minutes. The liquid was removed and 175 μ l of 70% ethanol was added to the pellet without vortexing and the tube was centrifuged, at 14000 rpm, for 1 minute. The supernatant was removed and 30 μ l of distilled water was added to the remaining DNA pellet. To start DNA analysis, 3 μ l of each pcDNA (the sample) was added to 3 μ l of restriction enzyme (10% total reaction volume), and 3 μ l of each specific enzyme buffer and BSA (1 mg/ml), and the volume was made up to 30 μ l by adding distilled water.

Agarose gel electrophoresis and sequencing

Agar gels were prepared by adding 50 ml of 1x Tris-acetate-EDTA (TAE) buffer to 0.5 g of agarose and mixing them gently. The mixture was melted in a microwave for 2 minutes and then left to cool down to 60 °C. After that, 1 μ l of ethidium bromide (0.5-1 μ g/ml) was added to visualize pcDNA bands under UV light. The gel was cast by pouring the agar into the gel holder after the comb had been placed in the appropriate position. The gel was then left to set and then put in the electrophoresis tank. 3 μ l loading buffer (methylene blue 0.2 mg/ml) and 3 μ l pcDNA was mixed on clean parafilm and loaded into the wells with the first well loaded with 10 μ l 1kb ladder only. The cover was gently placed on and the voltage adjusted to 100 V. This was left to run for 45 minutes. Upon completion, the bands were visualised using UV light. For further confirmation, the samples were sent for sequencing by using primers directed at the specific promoters as shown in **Table 2.1** and the result was in a full agreement with published sequence of each subunit.

DNA maxi preparation

The process of DNA maxi preparation began by adding 1 μ l of competent cells that contained plasmids to a conical flask containing 400 ml of LB broth solution and 400 μ l of 50 μ g/ml ampicillin. The mixture was left shaking overnight. Following this, the solution was centrifuged at 13,000 rpm for 30 minutes. The supernatant was removed and the bacterial pellet was re-

suspended homogenously in 10 ml of buffer P1. 10 ml of buffer 2 was then added and the solution was mixed by inverting the tube 4 to 6 times. This was left to incubate at room temperature for 5 minutes. Then 10 ml of buffer P3 was added to the solution and mixed thoroughly by inverting the tube 4 to 6 times. This was left to incubate on ice for 20 minutes. The mixture was then centrifuged at 13,000 rpm, for 30 minutes.

A QIAGEN-tip was equilibrated by adding 10 ml Buffer QBT and allowing the column to empty by gravitational flow. After this, the supernatant from the centrifuge step was added to the QIAGEN-tip and washed twice by adding 30 ml Buffer QC. DNA was eluted using 15 ml Buffer QF into a clean vessel and precipitated by adding 10.5 ml isopropanol at room temperature, 25 °C, and centrifuging at 11,000 rpm, for 30 minutes, at 4 °C. The supernatant was removed and the DNA pellet was washed with 5 ml of 70% ethanol and centrifuged again at 11,000 rpm for 10 minutes. Finally, the supernatant was once again removed and the pellet left to air-dry for 5-10 minutes. The pellet was then re-suspended in a suitable volume of buffer or distilled water. Following this, the concentration could be determined by using the nano-drop technique.

2.1.3. In vitro RNA transcription

Linearization of pcDNA

Linearization of pcDNA was achieved by using different restriction enzymes depending on the plasmid; for more details about plasmids and enzymes see **Table 2.1**. 5 µg of pcDNA and 5 µl each of restriction enzyme, buffer (according to type of plasmid) and BSA (0.1 mg/ml) were combined and the total volume was made up to 50 µl by adding nuclease free water. This was mixed gently and left to incubate for 1 hour in a 37 °C water bath. The enzymatic action was terminated by adding 2.5 µl of 0.5 M EDTA, 5 µl of 5 M

ammonium acetate and 100 µl of 100% ethanol and freezing at -20 °C for 1 hour. The mixture was then centrifuged at 14000 rpm, for 15 minutes at 4 °C and the pellets left to dry for 5 to 10 minutes. 4 µl of distilled water was added to the DNA pellet and their concentration was determined using a nano-drop.

Transcription

To synthesise mRNA in vitro 0.1 to 1 µg of linearized DNA with 10 µl of NTP/CAP and 2 µl each of enzyme SP6, T7 or T3, depending on the plasmid, and its reaction buffer were combined. The tube was flicked gently to collect the mixture in the bottom and then placed in a water bath at 37 °C for 2 hours. The reaction was terminated by adding 30 µl of nuclease free water and lithium chloride to precipitate the RNA and placed in the freezer for 1 hour. The mixture was centrifuged at maximum speed for 15 minutes at 4 °C. The supernatant was removed and the pellets were washed with 1 ml of 70% ethanol. Finally, these were centrifuged again at 14000 rpm for 15 minutes at 4 °C. The supernatant was once again removed and the pellet was re-suspended using 15 µl of nuclease free water. The sample concentrations were determined by nano-drop. All RNA was stored at -80 °C.

2.2. Electrophysiology procedure

2.2.1. Oocyte preparation

Oocytes isolated from mature female *Xenopus laevis* were supplied by the European Xenopus Resource Centre, University of Portsmouth, UK. Oocytes were treated with collagenase (0.5 mg/ml, Sigma type 1A) in Ca²⁺-free solution (96 mM NaCl, 2 mM KCl, 1 mM MgCl₂, 5 mM HEPES, 2.5 mM Na-pyruvate, 100 U/ml penicillin, 0.1 mg/ml streptomycin, pH 7.5) with shaking at 19 °C to defolliculate and remove the connective tissue surrounding the cells. A spherical shape of the cells remains because it is still surrounded by the vitelline layer. After the separation of oocytes, they were washed 4-7 times with modified Barth's solution (96 mM NaCl, 2 mM KCl, 1.8 mM CaCl₂, 1 mM MgCl₂, 5 mM HEPES, 2.5

mM Na-pyruvate, 0.5 mM theophylline, 50 mg/ml gentamicin, pH 7.5) and kept at 19 °C in the same solution.

2.2.2. Selection of oocytes for microinjection

Oocytes were examined under the microscope to select those cells which looked healthy and had reached stage VI of development. Healthy oocytes should not damage easily when injected. The selected oocytes were kept in clean modified Barth's solution (MBS) in the 19 °C incubator.

Injection pipettes were prepared from glass capillaries (model 4878, World Precision Instruments Inc, USA) by using a vertical pipette puller (model 700C, David Kopf Instruments, USA). The end of the capillary was broken roughly to 15 μm gently under the microscope, filled with paraffin and mounted onto the nano-liter injector (World Precision Instruments Inc, USA). A mixture of nAChR subunit RNAs was loaded into the pipette to be ready for injection; for heteromeric neuronal receptors a 1:1 ratio of $\alpha:\beta$ RNA at 200 ng/ μl ; for mouse embryonic muscle a 1:1:1:1 ratio of $\alpha:\beta:\lambda:\delta$ at 25 ng/ μl ; human $\alpha 7$ at 100 ng/ μl was mixed with RIC-3 at 30 ng/ μl . Each oocyte was injected with 50 nl of RNA solution. Injected oocytes were saved in Barth's solution at 19 °C for two to three days until mRNA expressed and gave the target protein. During this time oocytes were regularly checked to remove unhealthy oocytes from the solution.

2.2.3. Assaying oocytes for gene expression

Electrophysiological recordings were taken from injected oocytes by using two-electrode voltage clamp using a Geneclamp 500 voltage and patch clamp amplifier (Axon instrument) (**Figure 2**).

Microelectrodes were prepared from borosilicate glass capillaries (Harvard model 1.5 mm O.D. and 1.17mm I.D.) using a programmable micropipette puller (model p-97, Sutter instrument company, USA) and had resistances of 0.5-2.5 M Ω when filled with 3 M KCl (which works as a good conductor to minimize the series resistance).

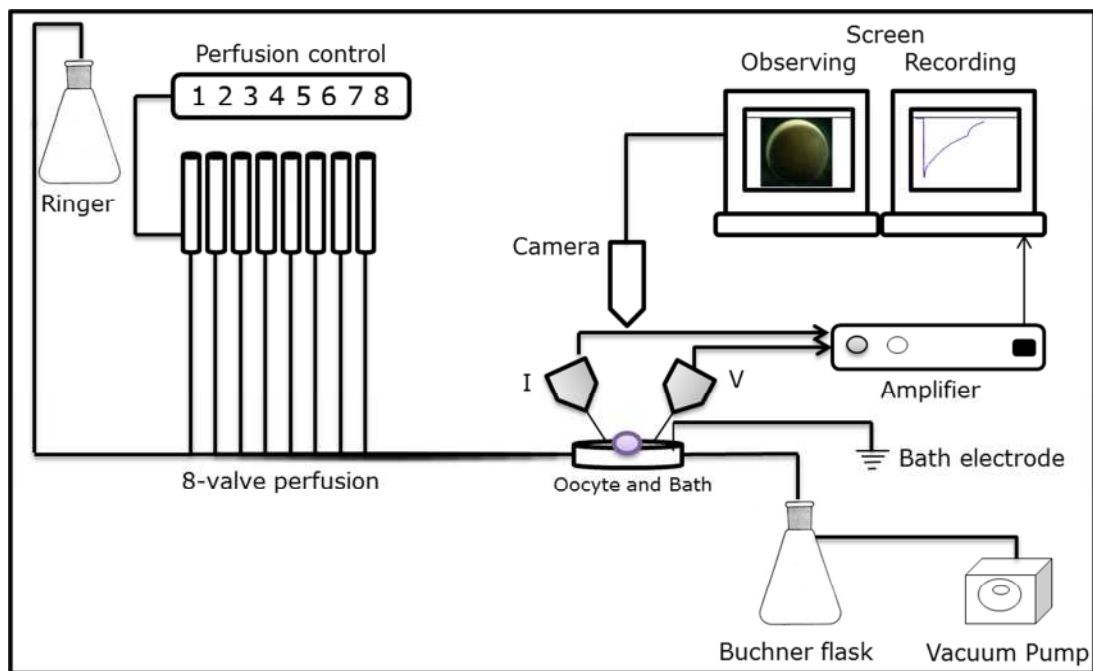


Figure 2. Diagrammatic representation of the main equipment set up used for current recording in this project. I = current electrode and V= voltage electrode. Oocytes were placed in the perfusion bath and voltage-clamped with a Gene clamp 500 amplifier. Perfusion of either ACh alone or co-applied with PhTX analogue was controlled by an automate 8-valve perfusion system. Data were recorded to a PC with WinEDR software.

An injected oocyte was put in the perfusion chamber by using a plastic pasture pipette. The bath was perfused with fresh Frog Ringer solution (96 mM NaCl, 2 mM KCl, 1.8 mM CaCl₂ and 5 mM HEPES, pH 7.5). After lowering the electrode carefully into the bath, the junction potentials were zeroed and the electrode resistance was checked. The resistance should be between 0.5 to 2.5 MΩ; if it was not the electrode was changed. Voltage and current electrodes were inserted into the cell. The resting membrane potential was observed on the Geneclamp 500; there should be agreement between both electrodes and normally it should be between -20 and -50 mV. The oocyte was voltage clamped and the holding potential (V_H) was altered to the required voltage depending on the experiment. Agonists and antagonists were applied by an 8-channel perfusion system (Automate) and agonist evoked currents were recorded to a PC

via a digidata 1200 analog-to-digital converter (Axon Instruments) using WinEDR v3.2.6 Software (John Dempster, University of Strathclyde).

A wide range of experiments and solutions were used on the oocyte:

ACh concentration-response relationships – Each nAChR combination was activated repeatedly by applying a range of ACh concentration (from 10 nM to 1 mM) with one minute application and 6 minutes washing interval depending on the receptor's sensitivity. EC₅₀ values were calculated for the peak current, decay current and net charge by normalizing all responses as a percentage of the maximum response.

PhTX-343 concentration-inhibition relationships – A constant concentration of 10 μM to 100 μM ACh was used in the experiments depending on the subunit combination and their sensitivity to ACh (EC₅₀). These ACh concentrations were prepared from a 10 mM stock solution with Frog Ringer. Experiments examining the impacts of philanthotoxins used PhTX-343 at (10⁻⁹ M - 10⁻⁵ M). A 1 mM concentration of PhTX-343 was prepared by adding 0.64 ml of Frog Ringer to a 0.5 mg aliquot of toxin. Serial dilutions were then carried out in ACh test solution to create the different concentrations required for testing, i.e. PhTX-343 was co-applied with a fixed concentration of ACh. The same protocol was used for all other analogues but adjusting the PhTX concentration range for increased or decreased potency.

Voltage-dependence of inhibition – The above concentration-inhibition relationship procedure was repeated for PhTX-343 and PhTX-12 at three different holding potentials: -60 mV, -80 mV and -100 mV. The IC₅₀ value on each combination was compared statically at different V_H by using student *t*-test. The *p* value was used as an indicator for voltage dependence level of each PhTX analogue.

Recovery from inhibition – approximately EC₅₀ ACh concentration was repeatedly applied at six minute intervals after co-application of the highest toxin concentration with ACh at V_H = -80 mV.

2.3. Data analysis

WinEDR, electrophysiology computer software from the University of Strathclyde, was used to measure the current amplitude of responses to ACh at the peak and the decay at the point after one minute application of the response. In addition, net charge movement, ion exchange, were calculated via area under curve for the period of a single minute. Also WinWCP from the same software source was used for estimating time constants. Graphpad prism 6 was used for data analysis, graph plotting and curve fitting. Concentration-inhibition and concentration-response curves were used to estimate IC₅₀ and EC₅₀ values for philanthotoxin analogues and ACh respectively using the following equations:

$$\% \text{ Control} = \frac{100}{1 + ([\text{PhTX}]/\text{IC}_{50})^{nH}} \quad (\text{Eq. 1})$$

$$\% \text{ Maximum response} = \frac{M}{1 + (\text{EC}_{50}/[\text{ACh}])^{nH}} \quad (\text{Eq. 2})$$

Where M is the maximum response and nH is the Hill slope.

All plotted points are the mean and standard error of the mean from 3-15 oocytes. IC₅₀s and EC₅₀s were compared using an unpaired *t*-test.

An adapted version of the Woodhull (1973) equation, that describes the action of single site ion channel blockers, was used to obtain further knowledge about PhTX-343 and PhTX-12 binding sites in relation to the nAChR pore. The IC₅₀ (95% CI) data was plotted against V_H and fitted with Eq. 3 to determine the

penetration distance (δ) of each blocking compound in the membrane electrical field.

$$IC_{50}(V_H) = IC_{50}(0 \text{ mV}) * \exp\left(\frac{Z\delta V_{HF}}{RT}\right) \quad (\text{Eq. 3})$$

To calculate the time constant (τ) value for the desensitization rate of wild type nAChR current decay, we used a two exponential equation to calculate fast (τ_1) and slow (τ_2) time constants for each combination.

$$y(t) = A_1 * \exp(-t/\tau_1) + A_2 * \exp(-t/\tau_2) + S_s \quad (\text{Eq. 4})$$

Where A_1 and A_2 are amplitudes of the fast and slow components at $t = 0$, τ_1 and τ_2 are the fast and slow time constants, and S_s is the steady state current.

CHAPTER THREE

ELECTROPHYSIOLOGICAL CHARACTERIZATION OF THE RESPONSE OF nAChRs TO ACh

Summary

The whole-cell response of eight different combinations of nAChRs expressed in *Xenopus* oocytes was extensively characterized. The peak current, decay current and net charge movement criteria were estimated from 1 minute ACh applications. It appears from our data that these three criteria are subunit dependent. For instance, the results from our study show that the peak current EC_{50} values of nAChRs calculated from concentration response curves were mostly dependent on the α -subunit with a rank order from high to low of $\alpha 7 > \alpha 3 > \alpha 1 > \alpha 4$. In addition the response desensitization rate was mostly dependent on the β -subunit with rank order from faster to slower of non- β -containing $> \beta 2 > \beta 4 > \beta 1$ -containing receptors. Also we showed that exchange of a single amino acid difference between the M2 domain of $\beta 2$ -subunit and $\beta 4$ -subunit significantly reduced the peak current EC_{50} value of $\alpha 4\beta 2$ nAChRs, while it increased it for $\alpha 3\beta 4$ nAChRs. This led us to conclude that replacing valine 253 by phenylalanine in the rat $\beta 2$ -subunit increased sensitivity to ACh, while substitutions of phenylalanine 255 by valine in the $\beta 4$ -subunit reduced sensitivity to ACh.

3.1. Pharmacological characterization of the ACh response of mammalian nAChRs expressed in *Xenopus* oocytes

To confirm that *Xenopus* oocytes originally did not express any functional subtype of nAChRs, the highest ACh concentration used in this work, 1mM, was applied to un-injected clamped ($V_H = -80$ mV) oocytes. This did not cause any detectable response (data not shown). However, application of 1 mM ACh to oocytes injected with transcribed mRNA from cDNA encoding subunits of neuronal homomeric $\alpha 7$ or heteromeric 1:1 ($\alpha 3$ or 4 : $\beta 2$ or 4) or muscle-embryonic type ($\alpha 1\beta 1\delta\gamma$), showed strong receptor activation, which indicates that *Xenopus* oocytes express the target receptor and can be used as an expression system for this group of receptors.

A single injected oocyte was placed in a perfusion chamber (0.5 ml) and constantly perfused with *Xenopus* ringer during the recording. The oocytes were clamped at -80 mV and perfused with a range of increasing ACh concentrations depending on the sensitivity of expressed combination in oocytes, with 6 minute intervals between each application. The EC_{50} values for the peak response, decay response and net charge transfer were calculated from concentration-response curves (**Figure 3.1.**) and presented as mean (95% CI) in **Table 3.1.** Based on the peak current EC_{50} value the sensitivity order of nAChRs to ACh based on their α -subunit, from lower to higher, was $\alpha 7 < \alpha 3 < \alpha 1 < \alpha 4$; homomeric $\alpha 7$ had roughly the same ACh sensitivity as heteromeric $\alpha 3\beta 4$ and 6-fold, 12-fold, 15-fold and 20-fold lower than $\alpha 3\beta 2$, $\alpha 1\beta 1\delta\gamma$, $\alpha 4\beta 2$ and $\alpha 4\beta 4$ nAChRs, respectively. On the other hand, the decay current EC_{50} value was mostly dependent on the β -subunit in each subtype. For example, expression of $\beta 4$ with $\alpha 4$ or $\alpha 3$ subunits showed 3-fold and 12-fold reduction in ACh sensitivity compared to $\beta 2$ -containing nAChRs, respectively.

The shape of the response generated by 100 μ M ACh was considerably different in desensitization rate and hence net charge movement among

investigated combinations of nAChRs. The most rapid desensitization was observed for receptors containing $\alpha 7$ -subunit alone followed by $\beta 2$ -containing, $\beta 4$ -containing and finally the muscle subtype nAChRs (**Figure 3.1. Trace**). The highest EC_{50} value based on net charge movement was recorded for $\alpha 3\beta 4$ and was 76 μM . The data points for the decay response to ACh at concentrations higher than 100 μM do not fit to the sigmoidal curve because the responses became smaller, which suggests an antagonist action for ACh. This inhibition activity of ACh was higher in $\beta 4$ -containing nAChRs compared to other subtypes.

To further investigate whether substitution of aromatic phenylalanine at position 255 of $\beta 4$ -subunit M2 domain by aliphatic valine or vice versa in the $\beta 2$ -subunit at position 253 had any effect on signal transduction from receptor activation to gate opening or not, we compared the EC_{50} values calculated from concentration-response curves of $\alpha 4\beta 2_{(V253F)}$ and $\alpha 3\beta 4_{(F255V)}$ with wild type nAChRs. It appears that the peak current EC_{50} value of $\alpha 4\beta 2_{(V253F)}$ was significantly lower than for $\alpha 4\beta 2$ ($p = 0.0031$), while in the case of $\alpha 3\beta 4_{(F255V)}$ the peak current EC_{50} value was significantly higher than for $\alpha 3\beta 4$ ($p < 0.0001$). In both cases the decay current EC_{50} values were not significantly different between mutant and wild-type.

Also time constants for desensitization of nAChRs (fast, tau 1 and slow, tau 2) were calculated by using Eq. 4. There was no significant difference between tau 1 or tau 2 values of wild-type and mutated $\alpha 4\beta 2$ and $\alpha 3\beta 4$ nAChRs as shown in **Table 3.2**, which indicates no critical role of this single amino acid modification on the desensitization rate. It appears that $\beta 4$ -containing receptors have higher tau values than $\beta 2$ -containing which further support the slow desensitization rate proposed for receptors containing $\beta 4$ -subunits over $\beta 2$ -subunits. On the other hand, $\alpha 7$ has lowest tau 2 values and M-nAChRs has the highest value.

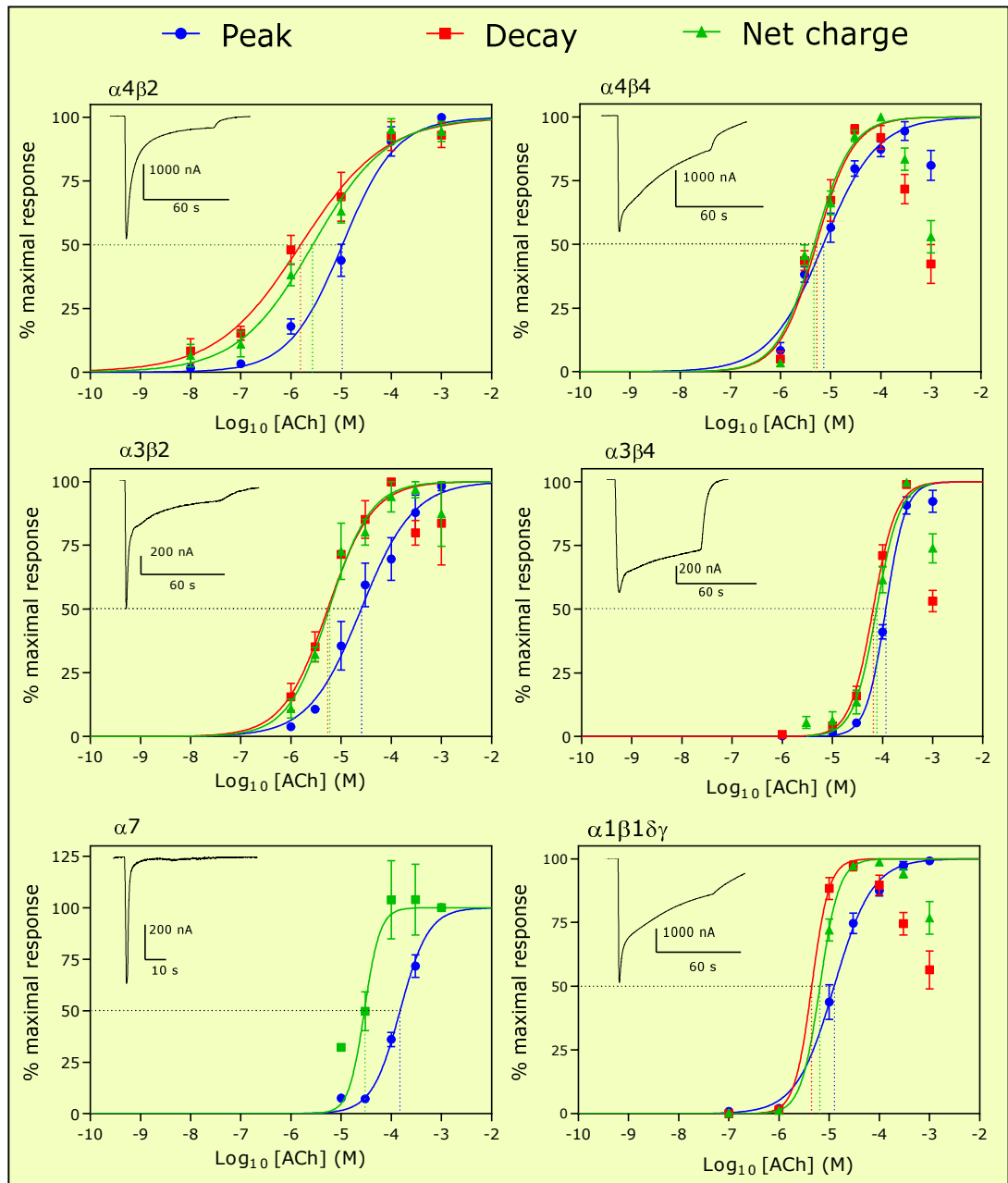


Figure 3.1. Characterization of ACh response across six different subunit combinations of nAChRs. Traces shown are whole-cell current recorded at a holding potential of -80 mV elicited by a one minute pulse of 100 μ M ACh in oocytes injected with α 4 β 2, α 4 β 4, α 3 β 2, α 3 β 4, α 7, α 1 β 1 δ γ nAChRs. Concentration-response curves for peak current, decay current and net charge of each nAChR subtype were constructed. The data points for each curve were normalized to the maximal response and plotted as mean \pm S.E.M. The curves are fits of Eq. 2. Calculated EC₅₀ for each receptor subtype are shown in **Table 3.1**.

Table 3.1. Estimated ACh EC₅₀ (μM) values for **peak**, **decay** and **net charge** response of oocytes injected with mRNA encoding the rat α3 or α4 subunits either with β2 or β4 subunits, mouse embryonic muscle type nAChRs and human homomeric α7 at a holding potential of -80 mV. Values are average of n, number of tested oocytes. Receptors containing α7 or α3-subunits showed a lower sensitivity to ACh compared to those containing α4 or α1-subunits.

nAChRs	n	EC ₅₀ μM (95% CI)		
		Peak	Decay	Net charge
α4β2	5	10 (7.4-15)	1.5 (0.8-2.9)	2.7 (1.7-4.2)
α4β2 _(V253F)	5	4.8 (3.3-7.0)	1 (0.6-1.7)	1.6 (1.0-2.3)
α4β4	12	7.2 (5.4-9.5)	5.2 (2.4-11.3)	4.7 (3.0-7.3)
α3β2	5	25 (17-36)	5.4 (3.2-8.9)	5.8 (4.1-8.1)
α3β4	8	116 (105-129)	65 (46-91)	76 (53-109)
α3β4 _(F255V)	5	209 (183-238)	57 (30-106)	104 (91-120)
α7	6	150 (129-175)		29 (18-46)
α1β1γδ	6	12 (10-15)	4.5 (1.3-15)	6.5 (4-10)

Table 3.2. Comparison of current decay tau values of wild-type and mutated N-nAChRs for responses to 100 μ M ACh for β 4-containing receptors or 10 μ M ACh for other combinations. Both α 4 β 2_(V253F) and α 3 β 4_(F255V) did not show any significant change in their tau 1 and tau 2 values compared to their wild-types. β 4-containing receptors showed higher tau values compared to β 2-containing nAChRs. The lowest tau values were recorded for α 7 and the highest for α 3 β 4 (tau 1) or embryonic M-nAChRs (tau 2).

	Tau 1 (s) (S.E.M)	Tau 2 (s) (S.E.M)	n
α 4 β 2	3.19 (0.93)	23.14 (2.92)	5
α 4 β 2 _(V253F)	2.42 (0.59)	15.12 (1.72)	5
P value	0.2131	0.453	
α 3 β 4	12.63 (5.53)	331.13 (111.71)	5
α 3 β 4 _(F255V)	5.84 (1.1)	73.1 (8.7)	4
P value	0.32	0.0815	
α 4 β 4	4.12 (3.48)	44.37 (12.42)	4
α 3 β 2	2.1 (0.72)	27.42 (8.44)	3
α 7	0.79 (0.31)	17.98 (10.1)	5
α 1 β 1 δ γ	1.45 (213)	401.95 (352.54)	2

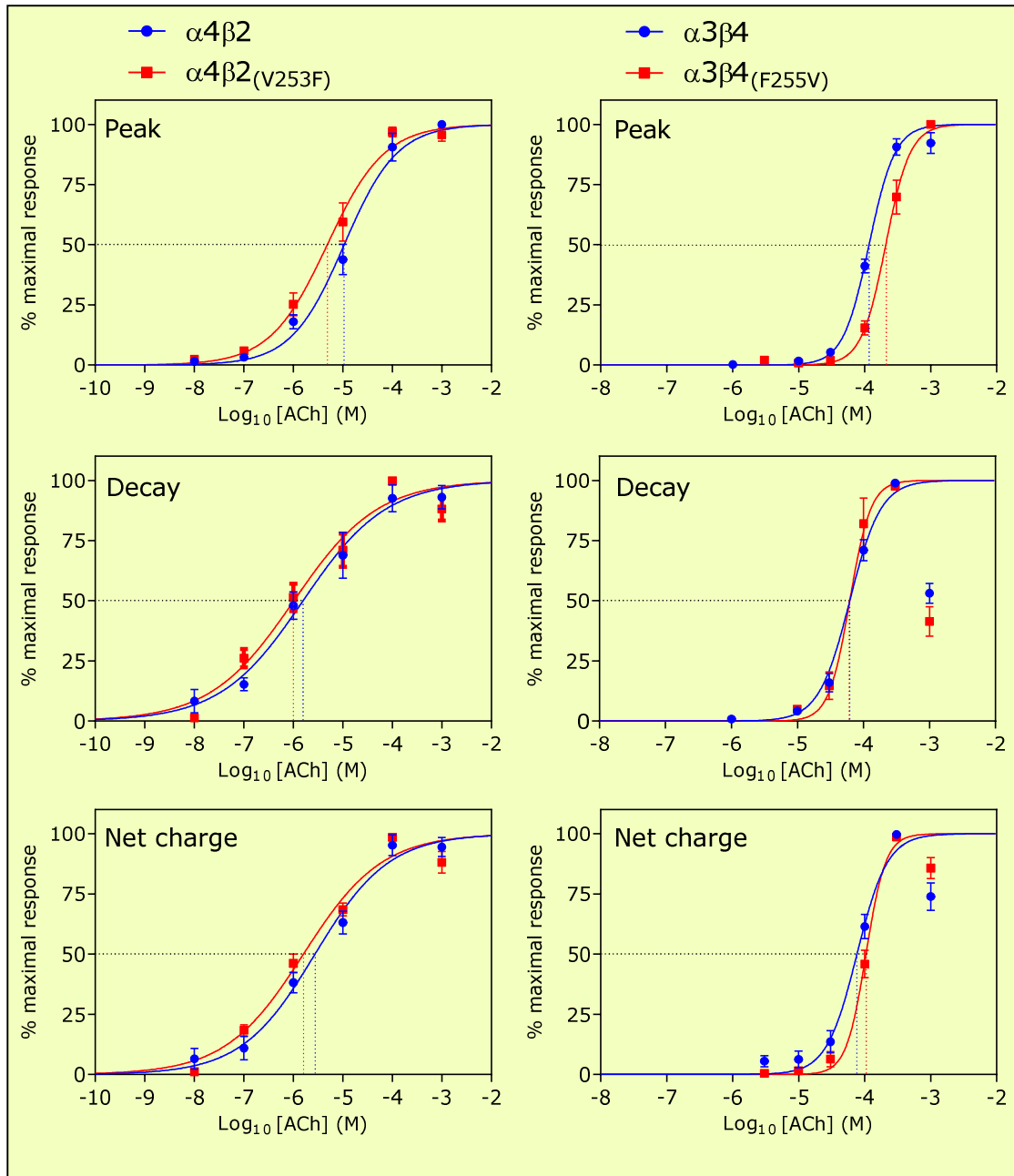


Figure 3.2. Combined rat $\alpha 4\beta 2$, $\alpha 4\beta 2_{(V253F)}$, $\alpha 3\beta 4$ and $\alpha 3\beta 4_{(F255V)}$ N-nAChR concentration-response curves for peak current, decay current and net charge transfer at holding potentials of -80 mV. The points are mean \pm S.E.M. of n oocytes normalized data to the maximum ACh response from same cells and fits are to Eq. 2.

3.2. Current-voltage characteristics of $\alpha 4\beta 2$ nAChRs

The current-voltage (I-V) characteristics of ACh responses of neuronal $\alpha 4\beta 2$ nAChRs was examined by applying 10 μM ACh for 1 minute at six minute intervals at different holding potentials beginning with +40 mV and changing by -20 mV gradually for each application up to -140 mV. Whole-cell currents were normalized to the maximum response (at -140 mV) and mean values are plotted against voltage in **Figure 3.3**. The current was inwardly rectifying.

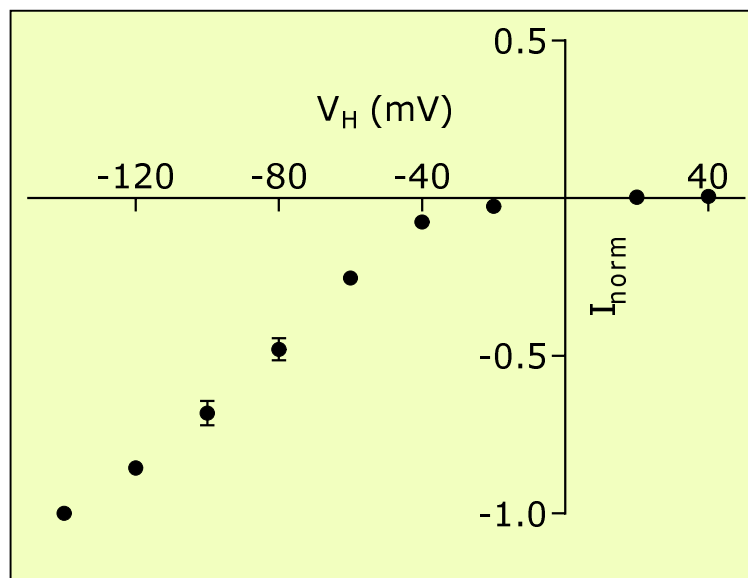


Figure 3.3. Current-voltage relationship of $\alpha 4\beta 2$ N-nAChR responses to 10 μM ACh. Points are mean normalized response \pm S.E.M. for 2-6 oocytes plotted against V_H . Some error bars are smaller than the symbol size and are not shown.

3.3. Recovery of $\alpha 4\beta 2$ nAChRs from desensitization by 10 μM ACh

The recovery rate of $\alpha 4\beta 2$ nAChRs from ACh desensitization was investigated by using 10 μM applications separated by variable time periods from 1 to 8 minutes at a holding potential of -80 mV. Each ACh response was normalized as % of the initial ACh response and plotted against the time period separating it from the previous response (**Figure 3.4.A**). Full recovery to the first ACh peak value was not obtained during the experimental time period but a time interval between 5 to 7 minutes showed the best recoveries of control

response. Further investigation showed that 6 minutes is the best time interval between different applications of ACh to ensure a stable response to 10 μ M ACh.

Figure 3.4.B shows the stability of ACh peak current and decay current responses to a series of 10 μ M ACh applications, each separated by 6 minutes. Therefore, this interval was used as control between each application of ACh throughout the whole study.

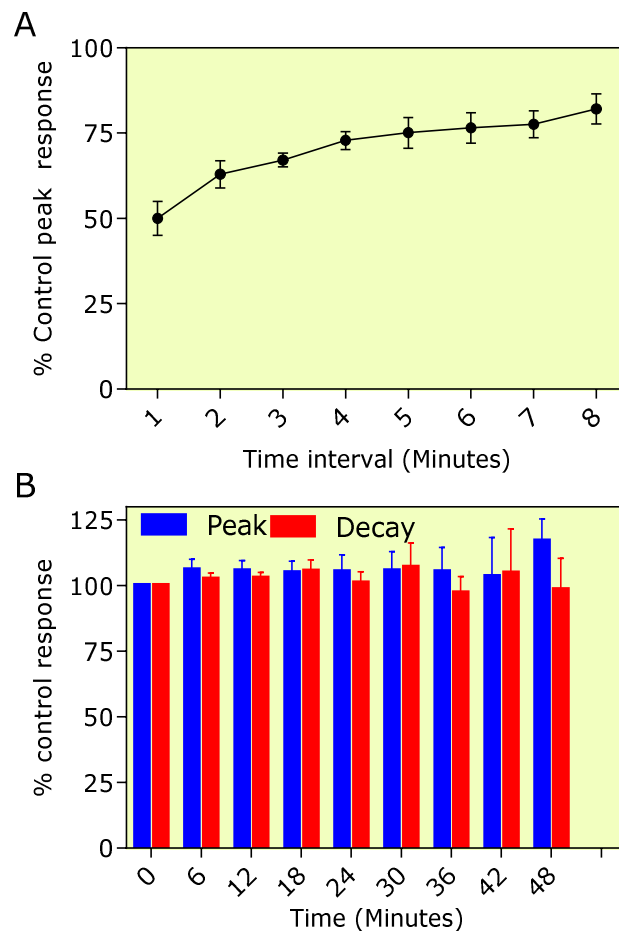


Figure 3.4. Recovery of wild type rat α 4 β 2 ACh responses from 10 μ M desensitization, (A) recovery of peak amplitude currents from desensitization at different interval time, (B) show recovery percentage of a series of 10 μ M ACh applications separated by constant 6 minute intervals for peak and decay current, respectively. The data points for tested ACh peak and decay response current were normalized with control response and plotted against application interval time as mean \pm S.E.M. (n = 7 oocytes).

CHAPTER FOUR

PHARMACOLOGICAL CHARACTERIZATION OF nAChR INHIBITION BY PhTX-343

Summary

The pharmacological actions of PhTX-343 on recombinant nAChRs expressed in *Xenopus* oocytes after micro-injection with mRNA was investigated by using TEVC. Concentration-inhibition curves for PhTX-343 were constructed for each combination of nAChR subunits at -60 mV, -80 mV and -100 mV. ACh EC₅₀ concentration was used as a control and applied for 1 minute with 6 minutes interval either alone or co-applied with PhTX-343 at various concentrations ranging between 0.1 nM to 100 μ M depending on subtype sensitivity. A four-parameter logistic equation was used to calculate peak and decay current IC₅₀ values by plotting PhTX-343 concentration against the mean of normalised current as % of control response. It appears that the β -subunit was more critical for PhTX-343 inhibition than the α -subunit. PhTX-343 had selectivity for β 4-containing over β 2-containing nAChRs. β 2-containing receptors appeared to be more affected by alteration of the membrane potential than β 4-containing receptors by comparing the peak current IC₅₀s at -60 mV and -100 mV, and the absence of a β -subunit changed PhTX-343 inhibition to voltage-independent. The IC₅₀ values were used in an adapted Woodhull equation to predict the interaction site of PhTX-343 in the channel by calculating the δ value. PhTX-343 inhibition was non-competitive because it did not shift the ACh EC₅₀ value significantly.

4.1. Effects of PhTX-343 on ACh-induced responses of wild-type and mutant nAChRs

The *Xenopus* oocytes expressing functional homomeric or heteromeric N-nAChRs ($\alpha 7$, $\alpha 4\beta 2$, $\alpha 4\beta 2_{(V253F)}$, $\alpha 4\beta 4$, $\alpha 3\beta 4$, $\alpha 3\beta 4_{(F255V)}$, $\alpha 3\beta 2$ and $\alpha 1\beta 1\delta\gamma$) were used to investigate the pharmacological action of PhTX-343 on receptor function. The highest concentration of PhTX-343 used in this study, 100 μM , was applied alone (at $V_H = -80$ mV) to oocytes expressing nAChRs. This did not produce any response. In contrast co-application of PhTX-343 with roughly EC_{50} concentration of ACh inhibited the peak and decay current of each subtype of nAChRs in a concentration-dependent manner (**Figure 4.1., 4.2. and 4.5.**). Stronger inhibition was observed for the decay current in comparison to the peak current. At concentrations lower than 10 nM, PhTX-343 slightly potentiated the ACh control response currents induced by $\alpha 4\beta 4$, $\alpha 7$ and $\alpha 1\beta 1\delta\gamma$. The IC_{50} s were calculated for peak and decay currents from a plot of percentage current inhibition by PhTX-343 and presented as mean values (95% CI) in **Table 4.1.**

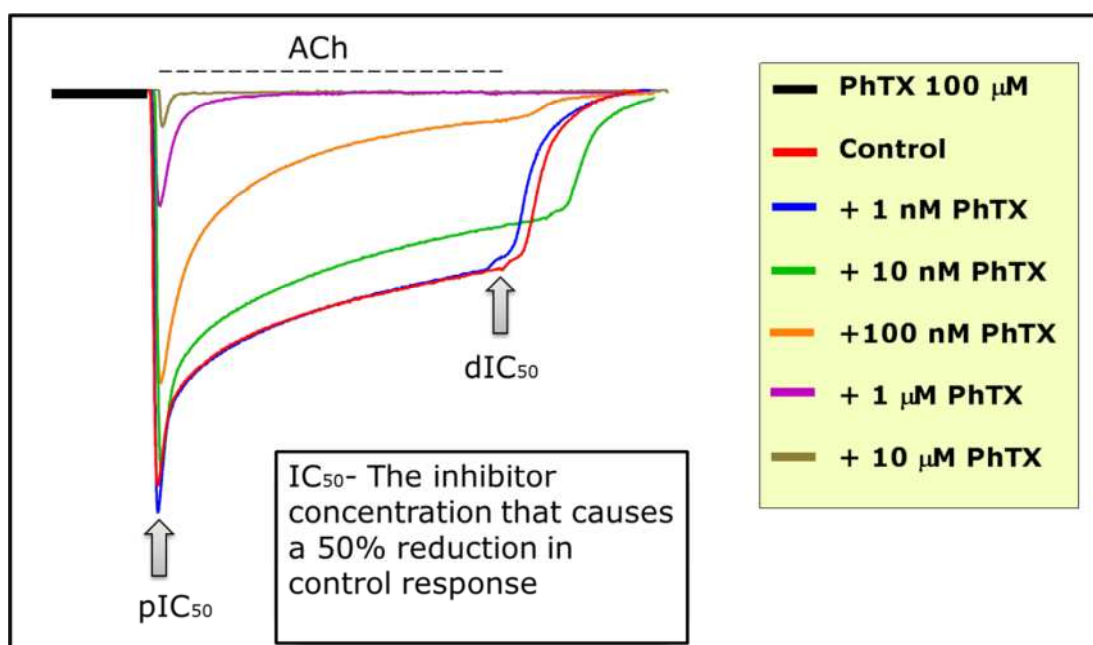


Figure 4.1. Example trace from two-electrode voltage clamp recording protocol used in this study and showing amplitude and 1 minute position on the response used to calculate peak and decay current IC_{50} values.

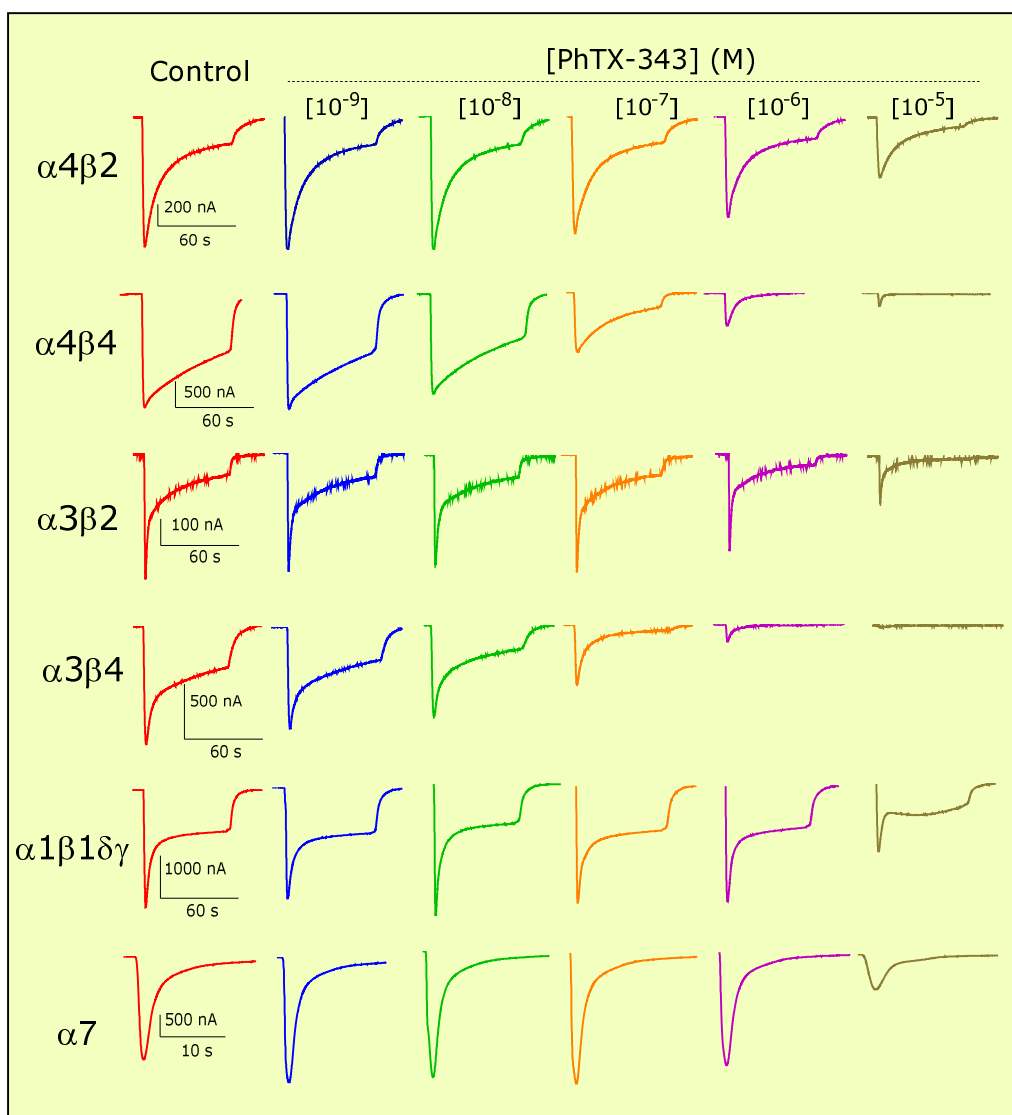


Figure 4.2. Example traces showing the sensitivity of nAChR subtypes to inhibition by PhTX-343. Approximately EC_{50} ACh concentration ($10 \mu\text{M}$ for $\alpha 4\beta 2$, $\alpha 4\beta 4$ and $\alpha 1\beta 1\delta\gamma$, $30 \mu\text{M}$ for $\alpha 3\beta 2$ and $100 \mu\text{M}$ for $\alpha 3\beta 4$ and $\alpha 7$ nAChRs) was perfused to oocytes clamped at -80 mV to generate control (Red). Then, increasing concentrations of PhTX-343 (other colours) was co-perfused with ACh at six minute intervals. Stronger current inhibition was observed by PhTX-343 on the $\beta 4$ -containing nAChRs over $\alpha 7$, $\alpha 1\beta 1\delta\gamma$ and $\beta 2$ -containing combinations.

First, the inhibitory effect of PhTX-343 was evaluated on the nAChRs with the major brain α -subunit, $\alpha 4$, in combination with either $\beta 2$ or $\beta 4$ at a holding potential of -80 mV (**Table 4.1**). The PhTX-343 IC_{50} value for peak and decay inhibition of $\alpha 4\beta 4$ was roughly 3-fold ($0.35 \mu\text{M}$) and 5-fold ($0.06 \mu\text{M}$) lower than calculated for $\alpha 4\beta 2$ nAChRs, respectively. These results suggest that PhTX-343 potency in nAChRs containing $\alpha 4$ -subunits depends on the β -subunit. It seems that PhTX-343 has a relatively lower affinity for binding sites on $\alpha 4\beta 2$ in comparison to the $\alpha 4\beta 4$ combination.

Secondly, the pharmacological effects of PhTX-343 were investigated on the main ganglionic nAChR α -subunit, $\alpha 3$, expressed in *Xenopus* oocytes either with $\beta 4$ or $\beta 2$ subunits at -80 mV (**Table 4.1**). IC_{50} values obtained from peak and decay current inhibition of $\alpha 3\beta 4$ by PhTX-343 were 80 nM and 10 nM, respectively. The IC_{50} value for $\beta 2$ containing receptors was considerably higher than $\beta 4$ containing subtypes when combined with the $\alpha 3$ subunit. The potency of PhTX-343 on $\alpha 3\beta 2$ nAChRs was reduced by 115-fold on peak current and 137-fold on decay current compared to the major ganglionic subtype of nAChRs, $\alpha 3\beta 4$. These results further strongly support the previous notion that PhTX-343 has a higher affinity for $\beta 4$ -containing receptors with $\alpha 3$ -subunit rather than $\beta 2$ -containing.

The data from both previous experiments was further analysed to investigate the role of the α -subunit. The IC_{50} value of $\beta 4$ -subunit in combination with $\alpha 4$ was approximately 4-times and 6-times higher on peak current and decay current than of $\alpha 3\beta 4$ nAChRs; whereas the IC_{50} value of $\beta 2$ expression with $\alpha 4$ was 10-fold and 4-fold lower than that of $\alpha 3\beta 2$ peak and decay current respectively. The high affinity of PhTX-343 to $\alpha 3$ -subunit in $\beta 4$ -containing and $\alpha 4$ -subunit in $\beta 2$ -containing nAChRs is in agreement with the previous suggestion that affinity of PhTX-343 is dependent mostly on the type of β -subunit rather

than the α -subunit. The highest IC_{50} values were recorded for $\beta 2$ -containing nAChRs, while the lowest were observed for $\beta 4$ -containing nAChRs.

To further highlight the possible reason behind a high affinity of PhTX-343 for $\beta 4$ -containing over $\beta 2$ -containing nAChRs, we compared the amino acid sequence of both β -subunits. Identical membrane topology has been proposed for all subunits of nAChRs. Comparison of data from the amino acid sequence alignment shows over 61% similarity between $\beta 4$ and $\beta 2$ subunits with less than 10% variation in some regions (**Figure 4.3**). This analysis shows several changes in various parts of both subunits, particularly in N-terminals with only a single amino acid variation in the M2 domain ($\beta 2_{(V253)}$, $\beta 4_{(F255)}$). The impact of this single variation and several chimeric subunits constructed from $\beta 2+\beta 4$ has been investigated previously on the potency of other inhibitors of nAChRs such as cocaine (Francis et al., 2000) and substance P (Stafford et al., 1998). To evaluate the role of these single amino acids in this position of the pore, the effects of PhTX-343 were investigated on mutated receptors $\alpha 4\beta 2_{(V253F)}$ and $\alpha 3\beta 4_{(F255V)}$.

Inhibition of $\alpha 4\beta 2_{(V253F)}$ and $\alpha 3\beta 4_{(F255V)}$ by PhTX-343 was concentration dependent (**Figure 4.4**). The peak current IC_{50} value of $\alpha 3\beta 4_{(F255V)}$ was reduced by about 3-fold with no noticeable change in the decay current value compared to $\alpha 3\beta 4$ nAChRs, while in the case of $\alpha 4\beta 2_{(V253F)}$ an approximately 3-fold reduction was calculated for decay current IC_{50} with no change for the peak current value compared to $\alpha 4\beta 2$ nAChRs. These data, although suggesting some involvement in PhTX-343 interaction, did not support the idea that a single amino acid difference in the M2 domain is responsible for the high affinity of PhTX-343 for $\beta 4$ -containing over $\beta 2$ -containing nAChRs which has been proposed for other open channel blockers. This mutation is explained in more detail in the voltage- dependence section.

To further highlight these conflicting results obtained with $\alpha 4\beta 2_{(V253F)}$ and $\alpha 3\beta 4_{(F255V)}$ combinations of nAChRs with PhTX-343, we decided to substitute the α -subunit between both combinations and generate $\alpha 4\beta 4_{(F255V)}$ and $\alpha 3\beta 2_{(V253F)}$ N-nAChRs (**Figure 4.6**). IC_{50} values for PhTX-343 inhibition at -100 mV were 0.5 μ M (0.3-0.7 μ M) for peak current and 17 nM (10-27 nM) for decay current for $\alpha 4\beta 4_{(F255V)}$ receptors. These values are not significantly different from that obtained from wild-type rat $\alpha 4\beta 4$ nAChRs. Based on these results it seems that phenylalanine at position 255 of $\beta 4$ is not responsible for the difference in the PhTX-343 sensitivity. On the other hand, the sensitivity of $\alpha 3\beta 2_{(V253F)}$ for PhTX-343 inhibition was increased by 2-fold (IC_{50} 1.5 μ M) on the peak current and by 3-fold (112 nM) on the decay current compared with the $\alpha 3\beta 2$ nAChRs. The results obtained from this point mutation in the $\beta 2$ -subunit, valine at position 253 by phenylalanine, show a role of this position in PhTX-343 sensitivity but this might not be through direct contact with the toxin at a binding site but through changing receptor properties such as desensitization.

Finally, to further improve knowledge on the profile of PhTX-343 across nAChRs and their relationship with auxiliary subunits, their action was investigated in homomeric $\alpha 7$ nAChRs with no auxiliary subunits and muscle-type nAChRs which contain more than one secondary subunit, $\alpha 1\beta 1\delta\gamma$ (**Table 4.1**). The latter combination showed a roughly 2-fold increase in peak and decay current IC_{50} value compare to the homomeric $\alpha 7$. The potency of PhTX-343 on decay current of both M-nAChRs and homomeric N-nAChRs was lower compared to all other tested heteromeric N-nAChRs. These data suggest that the absence of secondary subunits or having more than one type reduces the activity of PhTX-343 on nAChRs.

rβ4	RLANAEEKLMDDLLNKTRYNNLIRPATSSSQSLISIRLELSLSQLISVNEREQIMTTSIWL	60
hβ4	RVANAEEKLMDDLLNKTRYNNLIRPATSSSQSLISIKLQLSLAQLISVNEREQIMTTNVWL	60
rβ2	--TDTEERLVEHLLDPSRYNKLIRPATNGSELVTVQLMVSQAQLISVHEREQIMTTNVWL	58
hβ2	--TDTEERLVEHLLDPSRYNKLIRPATNGSELVTVQLMVSQAQLISVHEREQIMTTNVWL	58
rβ4	KQEWTDYRLAWNSSCYEGVNIILRIPAKRVWLDPDIVLYNNADGTYEVSVYTNVIVRNSGSI	120
hβ4	KQEWTDYRLTWNSSRYEGVNIILRIPAKRIWLPDIVLYNNADGTYEVSVYTNLIVRNSGSI	120
rβ2	TQEWEDYRLTWKPEDFDNMKKVRLPSKHIWLPDVVLYNNADGMYEVSFYSNAVVSVDGSI	118
hβ2	TQEWEDYRLTWKPEEFDNMKKVRLPSKHIWLPDVVLYNNADGMYEVSFYSNAVVSVDGSI	118
rβ4	QWLPPAIYKSACKIEVKHFPPFDQQNCTLKFRSWTYDHTEIDMVLKSPTAIMDDFTPSGEW	180
hβ4	LWLPPAIYKSACKIEVKYFPPFDQQNCTLKFRSWTYDHTEIDMVLMTPTASMDFTPSGEW	180
rβ2	FWLPPAIYKSACKIEVKHFPPFDQQNCTMKFRSWTYDRTEIDLVLKSDVASLDDFTPSGEW	178
hβ2	FWLPPAIYKSACKIEVKHFPPFDQQNCTMKFRSWTYDRTEIDLVLKSEVASLDDFTPSGEW	178
rβ4	DIVALPGRRTVNPQDPSYVDVITYDFI IKRKPLFYTIINLI IPCVLITSLAILVFYLPSCDG	240
hβ4	DIVALPGRRTVNPQDPSYVDVITYDFI IKRKPLFYTIINLI IPCVLITSLAILVFYLPSCDG	240
rβ2	DI IALPGRRNENPDDSTYVDITYDFI IRRKPLFYTIINLI IPCVLITSLAILVFYLPSCDG	238
hβ2	DIVALPGRRNENPDDSTYVDITYDFI IRRKPLFYTIINLI IPCVLITSLAILVFYLPSCDG	238
rβ4	EKMTLCISVLLALTF ²⁵⁵ FLLLLISKIYPPTSLDIPLIGKYL ²⁵⁵ LFTMVLVTF ²⁵⁵ SIVT ²⁵⁵ SVCVLNVHH	300
hβ4	EKMTLCISVLLALTF ²⁵⁵ FLLLLISKIYPPTSLDVPLIGKYL ²⁵⁵ LMFTMVLVTF ²⁵⁵ SIVT ²⁵⁵ SVCVLNVHH	300
rβ2	EKMTLCISVLLALTV ²⁵⁵ FLLLLISKIYPPTSLDVPLIGKYL ²⁵⁵ LMFTMVLVTF ²⁵⁵ SIVT ²⁵⁵ SVCVLNVHH	298
hβ2	EKMTLCISVLLALTV ²⁵⁵ FLLLLISKIYPPTSLDVPLIGKYL ²⁵⁵ LMFTMVLVTF ²⁵⁵ SIVT ²⁵⁵ SVCVLNVHH	298
rβ4	RSPSTHTMASWVKECF ²⁵³ LHKLPTFLFMKRPGLVSLVRVPHPSQLHLATADTAATSALGPT	360
hβ4	RSPSTHTMAPWVKRCFLHKLPTFLFMKRPGLDSSPARAFPPSKSCVTKPEATATS----T	356
rβ2	RSPTTHTMAPWVKVVFLEKLPTLLFLOQPRHRCARQLRLRRRQREREGAGALFFR----	354
hβ2	RSPTTHTMAPWVKVVFLEKLPALEFMQQRHRCARQLRLRRRQREREGAGALFFR----	354
rβ4	SPSNLYGSSMYFVNPVPAAPKSAVSSHTAGLPRDARLRSSGRFREDLQEALEGVSFIAQH	420
hβ4	SPSNFYGNSSMYFVNPASAASKSPAGSTPVAIPRDFWLRSGRFRQDVQEALEGVSFIAQH	416
rβ2	-EGPAADPCTCFVNPASVQG-LAGAFRAEPT-AAGPGRSVGPCSCGLREAVDGVRFIADH	411
hβ2	-EAPGADSTCFVNRASVQG-LAGAFGAEPAVPVAGPGRSGEPCGCGLREAVDGVRFIADH	412
rβ4	LESDDRDQSVIEDWKFVAMVVDRLFLWVVFVVCILGTMGLFLPPLFQIHAPSKDS-----	475
hβ4	MKNDDQSVVEDWKYVAMVVDRLFLWVFMFVCVLGTVGLFLPPLFQTHAASEGPYAAQR	476
rβ2	MRSEDDQSVREDWKYVAMVIDRLFLWIFVFCVFGTVGMFLQPLFQNYTATTFLHPDHS	471
hβ2	MRSEDDQSVSEWYVAMVIDRLFLWIFVFCVFGTIGMFLQPLFQNYTTTTFLHSDHS	472
rβ4	-----	
hβ4	D----- 477	
rβ2	APSSK 476	
hβ2	APSSK 477	

Figure 4.3. Multiple sequence alignments of the rat (r) and human (h) neuronal β2 and β4 amino acid sequences by using Clustal-W software. The four transmembrane domains are shown in boxes and the single amino acid difference in the M2 domain and linker region between M2 and M3 are highlighted in colour.

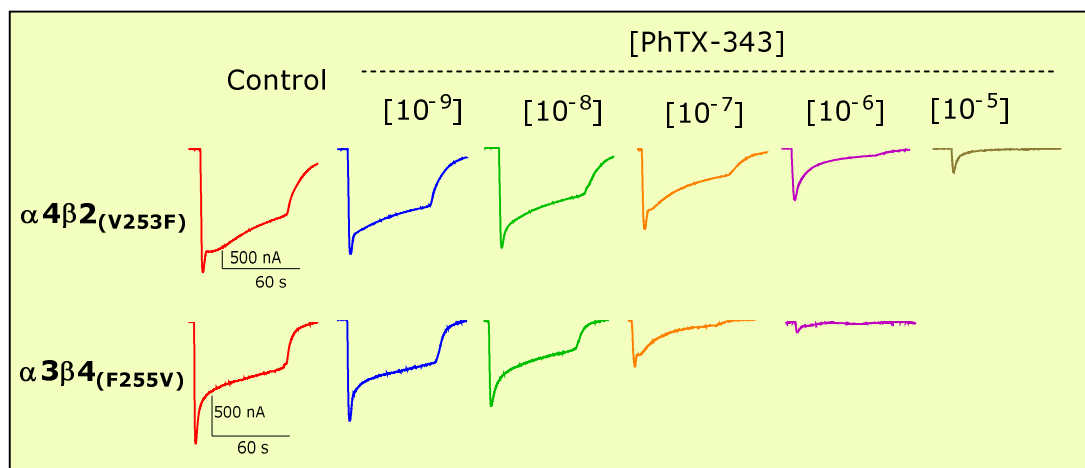


Figure 4.4. Example traces showing the sensitivity of inhibition of mutated nAChR subtypes to PhTX-343. Approximately EC_{50} ACh concentration ($10\ \mu\text{M}$ for $\alpha 4\beta 2_{(V253F)}$ and $100\ \mu\text{M}$ for $\alpha 3\beta 4_{(F255V)}$) was perfused over oocytes clamped at $-80\ \text{mV}$ to generate a control (Red), then increasing concentrations of PhTX-343 (other colours) were co-perfused with ACh at 6 minute intervals.

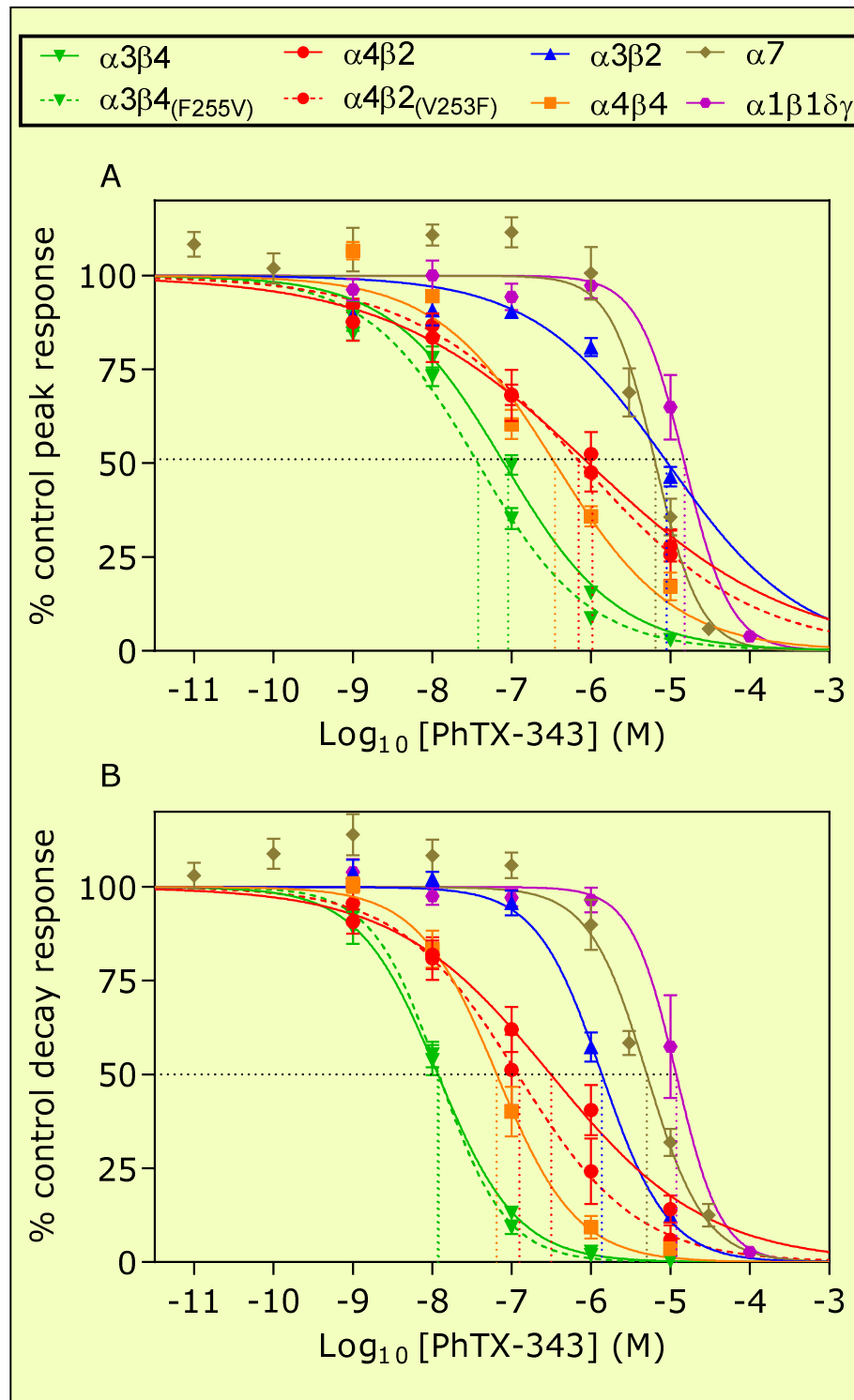


Figure 4.5. Screening PhTX-343 inhibitory effects on Peak (A) and decay (B) current of eight different subunit combinations of nAChRs expressed in *Xenopus* oocytes at a holding potential of -80 mV. Graphs are concentration-inhibition data plotted as mean % control response vs PhTX-343 concentration for peak current (top) or decay current (bottom) and curve fits are to Equation 1. Decay current for $\alpha 7$ = net charge.

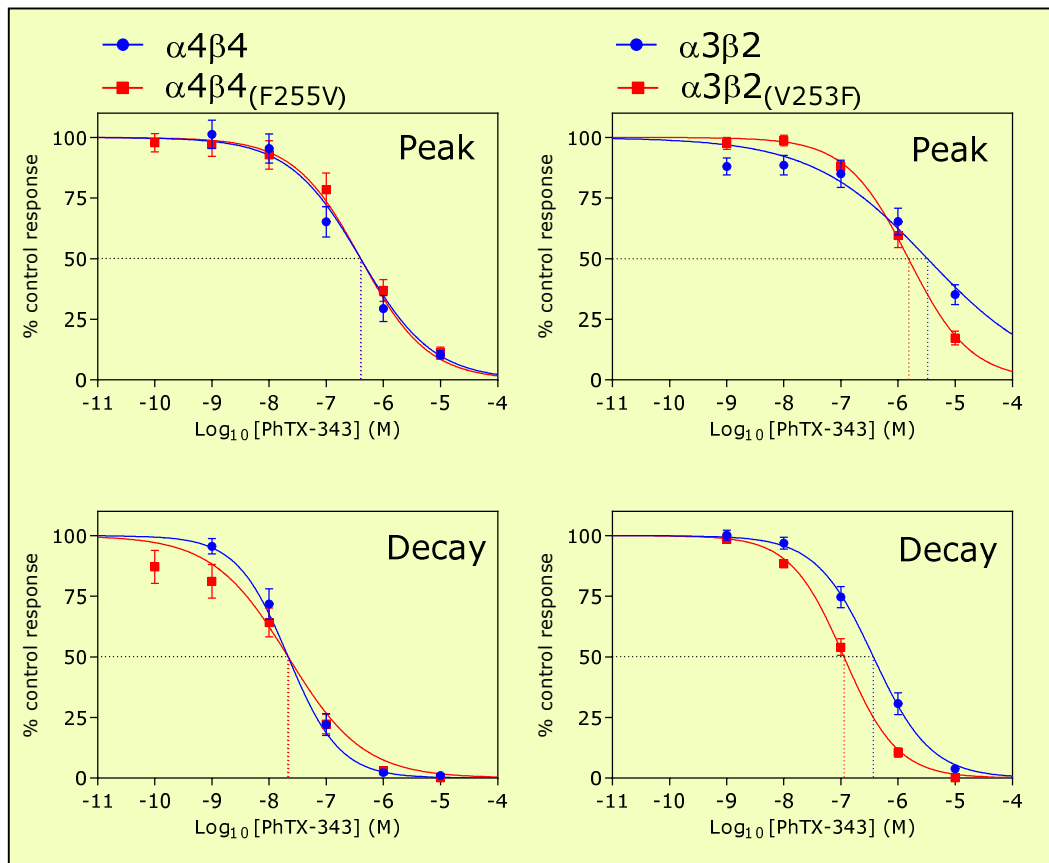


Figure 4.6. Combined rat $\alpha 4\beta 4$, $\alpha 4\beta 4_{(F255V)}$ and $\alpha 3\beta 2$, $\alpha 3\beta 2_{(V253F)}$ N-nAChRs concentration-inhibition curves for inhibition of peak and decay of EC₅₀ concentration ACh evoked response by PhTX-343 at holding potential of -100 mV. The points are mean \pm S.E.M. of *n* oocytes normalized data to the control ACh response from same cells and fits to equation 1. Peak and decay current IC₅₀ values of $\alpha 4\beta 4_{(F255V)}$ were not significantly different from the wild-type $\alpha 4\beta 4$ nAChRs, while a significant decrease in IC₅₀ values were recorded for the peak ($p=0.0114$) and decay ($p<0.0001$) current of $\alpha 3\beta 2_{(V253F)}$ compared to wild-type $\alpha 3\beta 2$ nAChRs.

4.2. Voltage-dependent and -independent inhibition of nAChRs by PhTX-343

Another approach to evaluate the mechanism of action of PhTX-343 across nAChRs is to investigate their binding site positions in relation to the membrane electric field. These experiments investigated the effect of alterations in membrane V_H on the inhibitory action of PhTX-343 for $\alpha 7$, $\alpha 4\beta 2$, $\alpha 4\beta 2_{(V253F)}$, $\alpha 4\beta 4$, $\alpha 3\beta 4$, $\alpha 3\beta 4_{(F255V)}$, $\alpha 3\beta 2$, and $\alpha 1\beta 1\delta\gamma$ subunit combinations. For each combination, concentration-inhibition curves for PhTX-343 were constructed at three different holding potentials, -60 mV, -80 mV and -100 mV. These combinations were studied to evaluate the contribution of each subunit to the binding sites and to find the optimum binding sites for PhTX-343 among these combinations (**Table 4.1**).

Voltage-dependence was observed for the inhibition of muscle-type, $\alpha 1\beta 1\delta\gamma$, nAChRs by PhTX-343 (**Figure 4.7.A**), suggesting that PhTX-343 binds to a site inside the channel pore. PhTX-343 at a concentration 1 μM or less showed roughly 10% potentiation of ACh control amplitude in oocytes clamped at -60 mV, while 100 μM inhibited approximately 90% of peak and decay current when compared to control. At $V_H = -80$ mV, peak and decay IC_{50} (95% CI) values of PhTX-343 were 15 μM (9-23 μM) and 12 μM (8-18 μM) respectively. These values increased 1.8-fold on the peak and 1.5 fold on the decay current when the membrane holding potential was increased to -60 mV, whereas shifting V_H to -100 mV reduced both IC_{50} values roughly 5-times compared to those at -80 mV.

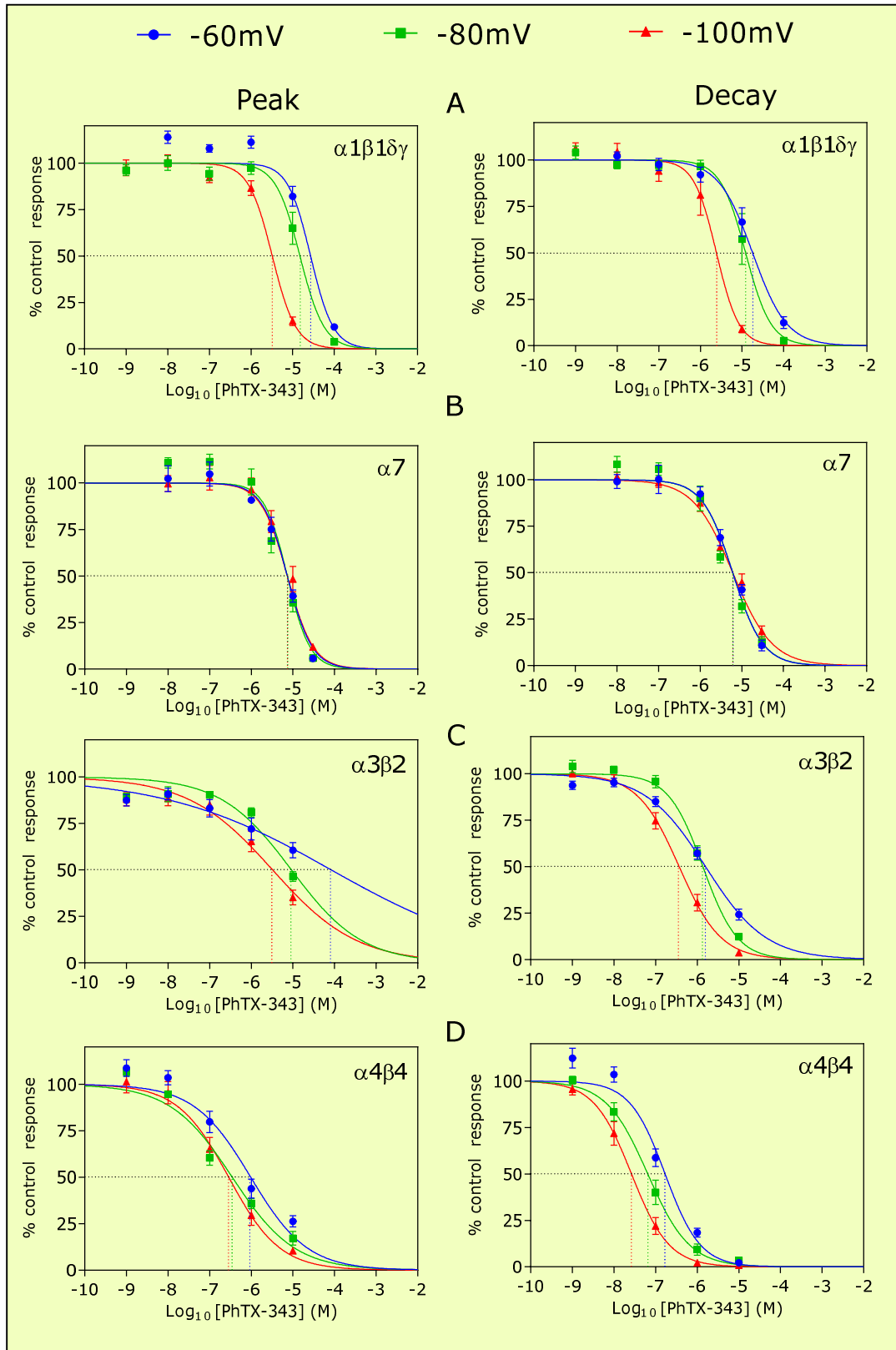
Table 4.1. Summary of PhTX-343 Peak 'P' and decay 'D' current IC₅₀ values on eight different combinations of nAChRs at three different holding potentials, -60 mV, -80 mV and -100 mV. 'D' in case of α7 = net charge. Values are presented in μM as mean IC₅₀ (95% CI) and (n) is the number of tested oocytes. Sensitivity of β4-containing nAChRs for inhibition by PhTX-343 was higher compared to β2-, β1- and non-β-containing nAChRs. Voltage-dependence was observed for all nAChR subunit combinations except homomeric α7.

nAChRs		V _H = -60 mV	V _H = -80 mV	V _H = -100 mV
α4β2	P	1.9 (1.0-3.5)	0.92 (0.41-2.09)	0.14 (0.09-0.21)
	n	(7)	(7)	(7)
	D	0.45 (0.28-0.75)	0.3 (0.17-0.45)	0.08 (0.08-0.13)
α4β2 (V253F)	P	0.6 (0.2-1.2)	0.7 (0.4-1.2)	0.1 (0.06-0.1)
	n	(14)	(10)	(8)
	D	0.06 (0.04-0.08)	0.1 (0.06-0.23)	0.01 (0.01-0.015)
α4β4	P	0.97 (0.59-1.58)	0.35 (0.24-0.50)	0.28 (0.17-0.46)
	n	(9)	(9)	(6)
	D	0.16 (0.12-0.23)	0.06 (0.04-.008)	0.02 (0.01-0.03)
α3β2	P	84 (8.59-821)	9.2 (5.8-14.5)	3.2 (1.69-6.28)
	n	(7)	(12)	(8)
	D	1.59 (1.2-2.1)	1.37 (1.1-1.6)	0.36 (0.2-0.4)
α3β4	P	0.29 (0.21-0.39)	0.08 (0.06-0.10)	0.07 (0.05-0.10)
	n	(7)	(8)	(9)
	D	0.08 (0.06-0.11)	0.01 (0.009-0.014)	0.007 (0.006-0.009)
α3β4 (F255V)	P	0.3 (0.23-0.04)	0.03 (0.02-0.04)	0.01 (0.01-0.02)
	n	(7)	(9)	(8)
	D	0.07 (0.06-0.09)	0.01 (0.010-0.014)	0.005 (0.003-0.006)
α7	P	6.7 (5.3-8.3)	6.4 (5.1-8.2)	8.7 (6.9-11)
	n	(6)	(7)	(9)
	D	6.5 (5.3-8.1)	5.0 (3.9-6.4)	6.7 (5.4-8.4)
α1β1γδ	P	27 (19-38)	15 (9-23)	3.2 (2.5-4.1)
	n	(8)	(8)	(9)
	D	18 (12-25)	12 (8-18)	2.4 (1.5-3.9)

On the other hand, inhibition of human homomeric $\alpha 7$ nAChRs by PhTX-343 was voltage-independent (**Figure 4.7.B.**). Similar to muscle type, PhTX-343 at concentrations lower than 10 nM showed slight potentiation of the ACh current response at a V_H of -80 mV. The IC_{50} calculated for peak and net charge from a plot of percentage current inhibition by PhTX-343 was 6.4 μM and 5.0 μM (n=7) respectively. There was no change observed in IC_{50} values when the standard V_H of -80 mV was increased or decreased by 20 mV.

To further investigate these divergent inhibition mechanisms by PhTX-343 between heteromeric and homomeric combinations of nAChRs, their action was compared on $\alpha 3\beta 2$ and $\alpha 4\beta 4$ nAChRs (**Figure 4.7.C. and D.**). At the highest V_H the peak inhibitory potency of PhTX-343 on $\alpha 4\beta 4$ was 0.92 μM and this decreased to 0.28 μM (3.3-fold) at the lowest V_H , while on $\alpha 3\beta 2$ this changed from 84 μM to 3.2 μM (26-fold). The results from decay current inhibition show that $\alpha 4\beta 4$ potency was roughly 10-fold and 18-fold higher than $\alpha 3\beta 2$ at -60 mV and -100 mV, respectively. These data support that inhibition of neuronal heteromeric nAChRs by PhTX-343 is dependent on the membrane holding potential but the extent of this depends on the subunits present.

Figure 4.7. (see over) Combined mouse ($\alpha 1\beta 1\delta\gamma$) (A), human ($\alpha 7$) (B), rat $\alpha 3\beta 2$ (C) and $\alpha 4\beta 4$ (D) N-nAChR concentration-inhibition curves for inhibition of ACh (10 μM for $\alpha 1\beta 1\delta\gamma$ and $\alpha 4\beta 4$, 30 μM for $\alpha 3\beta 2$ and 100 μM for $\alpha 7$) evoked peak (left) and decay (right) current by PhTX-343 at holding potentials of -100 mV, -80 mV and -60 mV. The points show mean \pm S.E.M. of n oocytes normalized against control ACh responses from the same oocyte and the curves were fitted using equation 1. For $\alpha 7$ the decay value is for net charge.



To understand the contribution of β subunits in the pharmacological action of PhTX-343 on nAChRs, we replaced β -subunits, β_2 and β_4 , in both previous combinations and generated major CNS, $\alpha_4\beta_2$, and PNS, $\alpha_3\beta_4$, nAChRs. The decay IC_{50} value of PhTX-343 on receptors containing β_2 in combination with α_4 was 0.45 μ M at -60 mV and this value was 2.8 fold higher compared to the $\alpha_4\beta_4$ combination. At holding potential -100 mV PhTX-343 potency on $\alpha_4\beta_2$ nAChRs was increased 5.6 fold (**Figure 4.8**). On the other hand, substitution of valine 253 in the β_2 -subunit by phenylalanine generates the combination $\alpha_4\beta_2(V253F)$ with decay current IC_{50} value of 0.06 μ M, 7.5 times lower than wild type $\alpha_4\beta_2$ at -60 mV holding potential. This decay IC_{50} value was not changed significantly ($p = 0.0934$) at -80 mV, while it decreased significantly ($p < 0.0001$) by 4.2-fold at -100 mV. Based on these data, PhTX-343 inhibits wild type and mutated $\alpha_4\beta_2$ nAChRs in a voltage dependent manner. This implies a critical role of the amino acid residue in the position 253 of β_2 -subunit which might participate in PhTX-343 binding sites or modulating the transduction mechanism of receptor activation or desensitization rate.

Co-expression of the β_4 -subunit with the α_3 -subunit generates a combination of nAChR, $\alpha_3\beta_4$, with the lowest decay current IC_{50} value of all wild type nAChR for PhTX-343, 7 nM at V_H -100 mV (**Figure 4.9**). This inhibitory potency was 51-fold higher compared to expression of β_2 with α_3 -subunit. This inhibition of $\alpha_3\beta_4$ nAChRs by PhTX-343 was dependent on membrane holding potential; IC_{50} values at -80 mV and -60 mV were 1.4 and 11.4 fold higher compared to that at -100 mV. Sensitivity of PhTX-343 following the replacement of phenylalanine 255 in β_4 by valine was investigated when co-expressed with α_3 -subunit ($\alpha_3\beta_4(F255V)$). This mutation in $\beta_4(F255V)$ did not produce any noticeable change in the sensitivity at -60 mV, while significantly ($P < 0.0001$) increased it at -80 mV and -100 mV compared to wild type of β_4 -subunit co-expressed with α_3 -subunit. Substitution of this residue suggests no critical role for this position in

voltage-dependent PhTX-343 binding or transduction mechanism of nAChR activation in this combination.

The IC_{50} vs voltage relationship curves for both peak and decay current inhibition by PhTX-343 were constructed based on the Woodhull model to estimate the parameter δ , the fraction of the membrane electric field penetrated by the molecule (**Figure 4.11**). PhTX-343 carries three positive charges ($z = 3$) in the polyamine chain at physiological pH (Stromgaard et al., 1999). The peak and decay current δ values calculated from IC_{50} at three different holding potentials for each combination are shown in **Figure 4.11.C**. These values were quite variable; some were positive and others were negative and in some cases the decay current value was lower than that for peak current or vice versa. For example, $\alpha 3\beta 4$ nAChRs had a δ -value higher than 0.5, which indicated a preference for the deep binding site, while in other combinations it was lower than 0.5, indicating a preference for the shallow site. Therefore, based on the predicted δ -value we concluded in general that peak and decay current inhibition of all heteromeric nAChR combinations by PhTX-34 was dependent on the membrane potential and vice versa for homomeric $\alpha 7$ nAChRs.

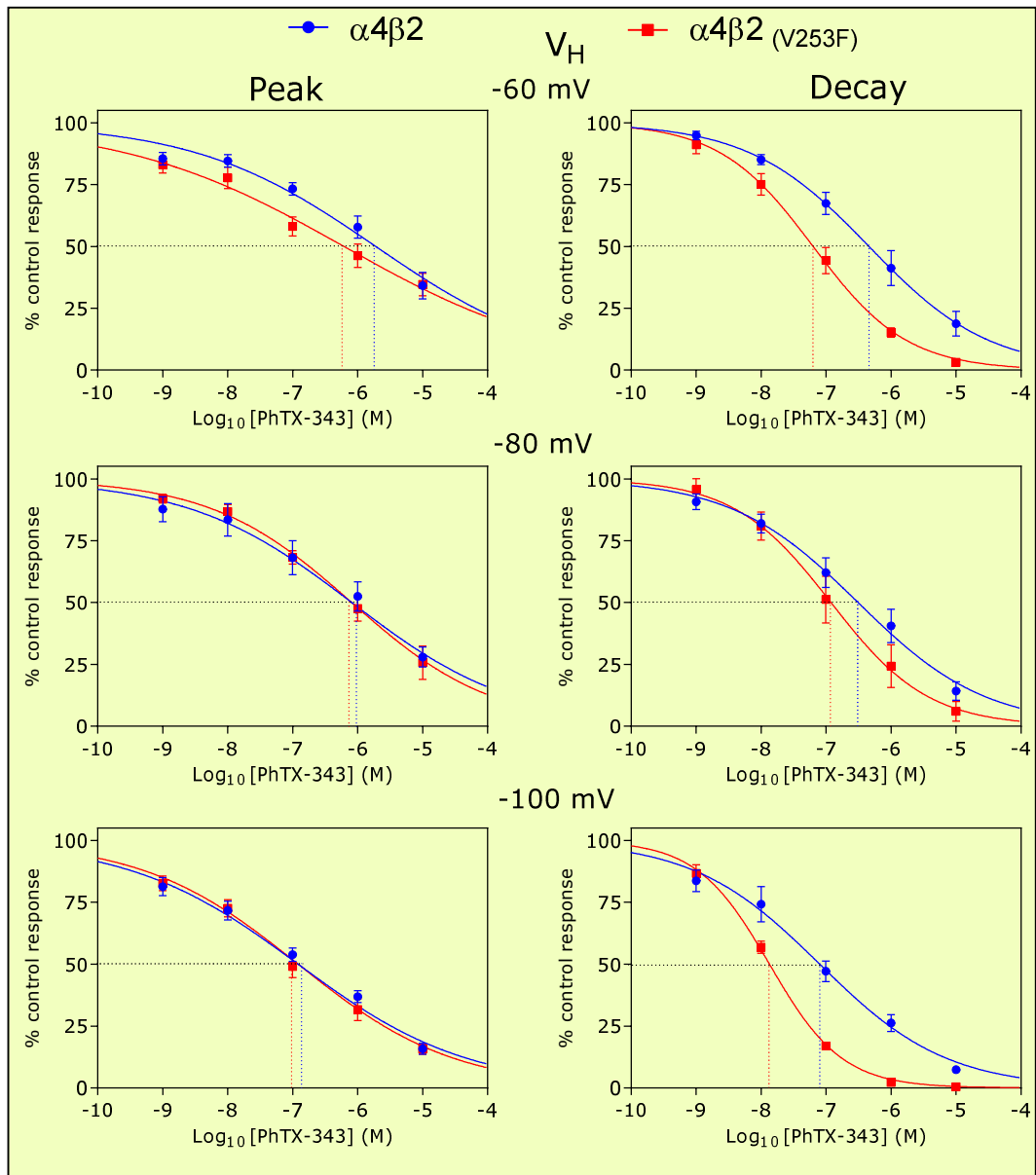


Figure 4.8. Combined rat $\alpha 4\beta 2$ and $\alpha 4\beta 2_{(v253F)}$ N-nAChR concentration-inhibition curves for inhibition of 10 μM ACh evoked peak (left) and decay (right) current by PhTX-343 at holding potentials of -100 mV, -80 mV and -60 mV. The points show mean \pm S.E.M. of n oocytes normalized to the control ACh response from same cells and curve fits are to equation 1. The IC_{50} values of $\alpha 4\beta 2_{(v253F)}$ were significantly lower than $\alpha 4\beta 2$ at all V_H for decay current but only at -60 mV for peak current.

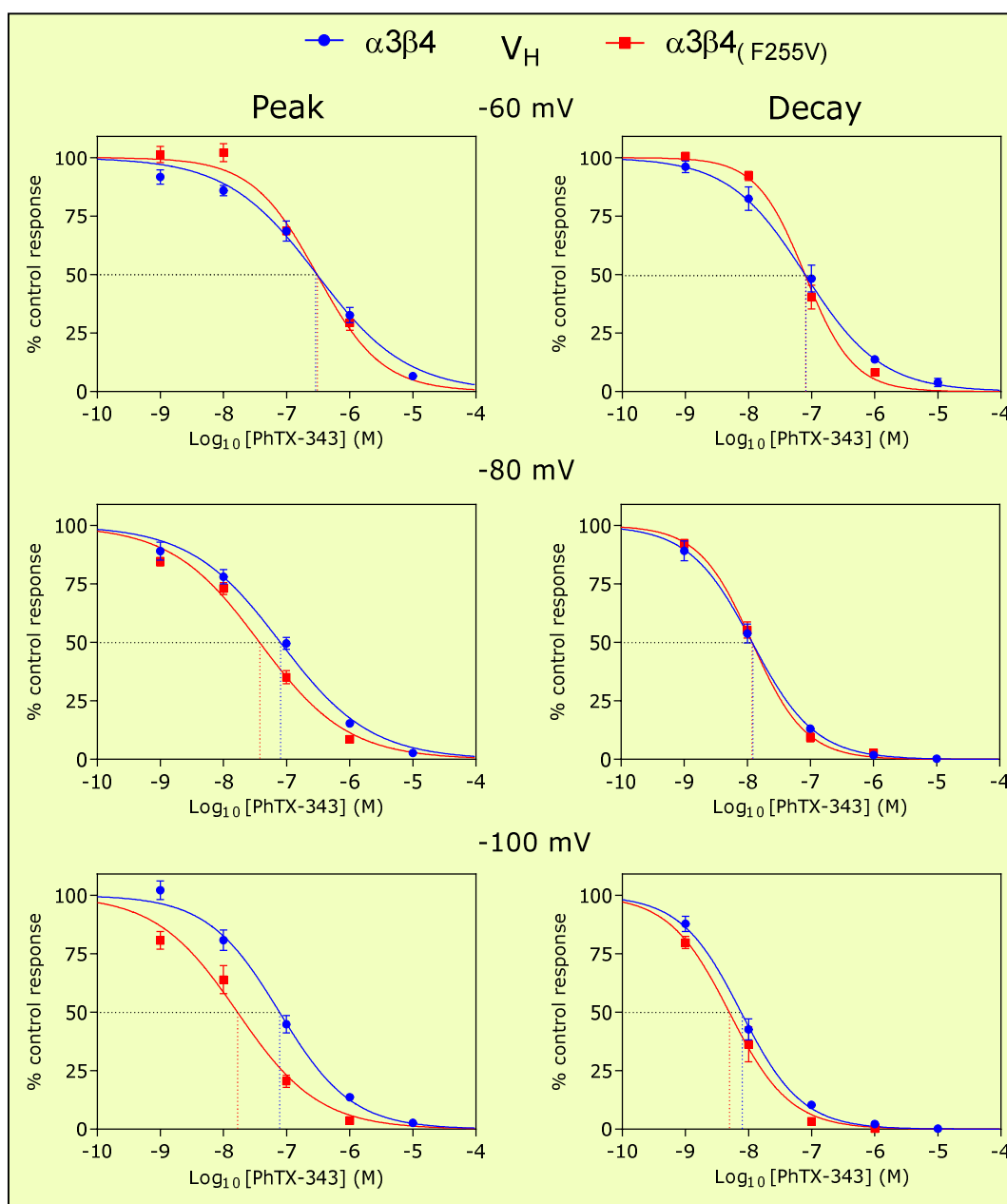


Figure 4.9. Combined rat $\alpha 3\beta 4$ and $\alpha 3\beta 4_{(F255V)}$ N-nAChR concentration-inhibition curves for inhibition of 100 μM ACh evoked peak (left) and decay (right) current by PhTX-343 at holding potentials of -100 mV, -80 mV and -60 mV. The points are mean \pm S.E.M. of n oocytes normalized to the control ACh response from same cells and curve fits are to equation 1. The IC_{50} values of $\alpha 3\beta 4_{(F255V)}$ were significantly lower than $\alpha 3\beta 4$ at -80 mV and -100 mV for peak current but only at -100 mV for decay current.

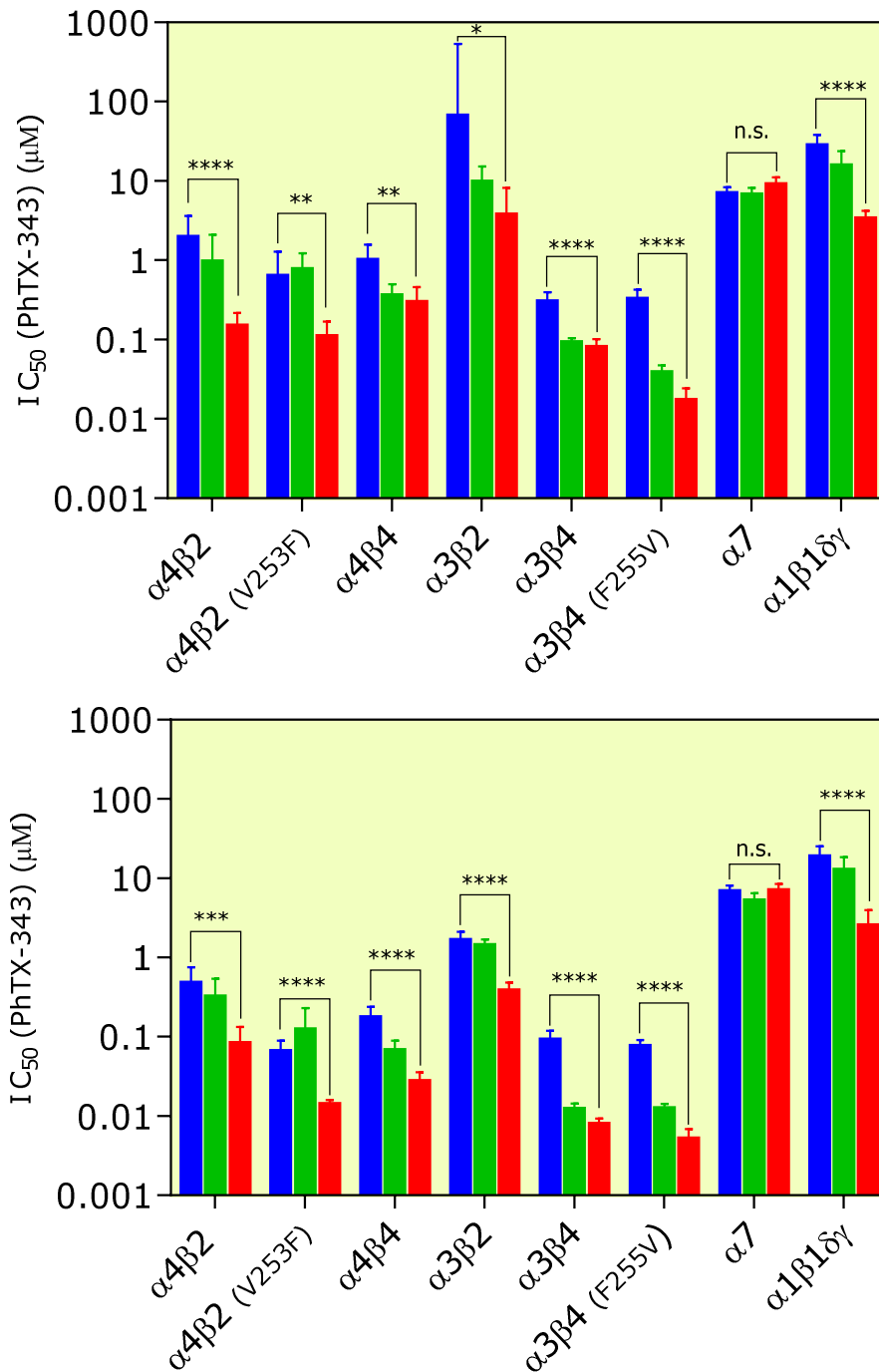


Figure 4.10. Comparison of PhTX-343 on eight different subunit combinations of nAChRs. Each bar represents the PhTX-343 IC₅₀ value (95% CI) on the particular combinations. Red, green and blue bars represent membrane holding potentials of -100 mV, -80 mV and -60 mV respectively. Peak (top) and decay (bottom) current inhibition by PhTX-343. Decay data in the case of α7 = net charge. Significance of difference between IC₅₀ at -100 mV and -60 mV is indicated by n.s. (p ≥ 0.05), * (p < 0.05), ** (p < 0.01), *** (p < 0.001) or **** (p < 0.0001).

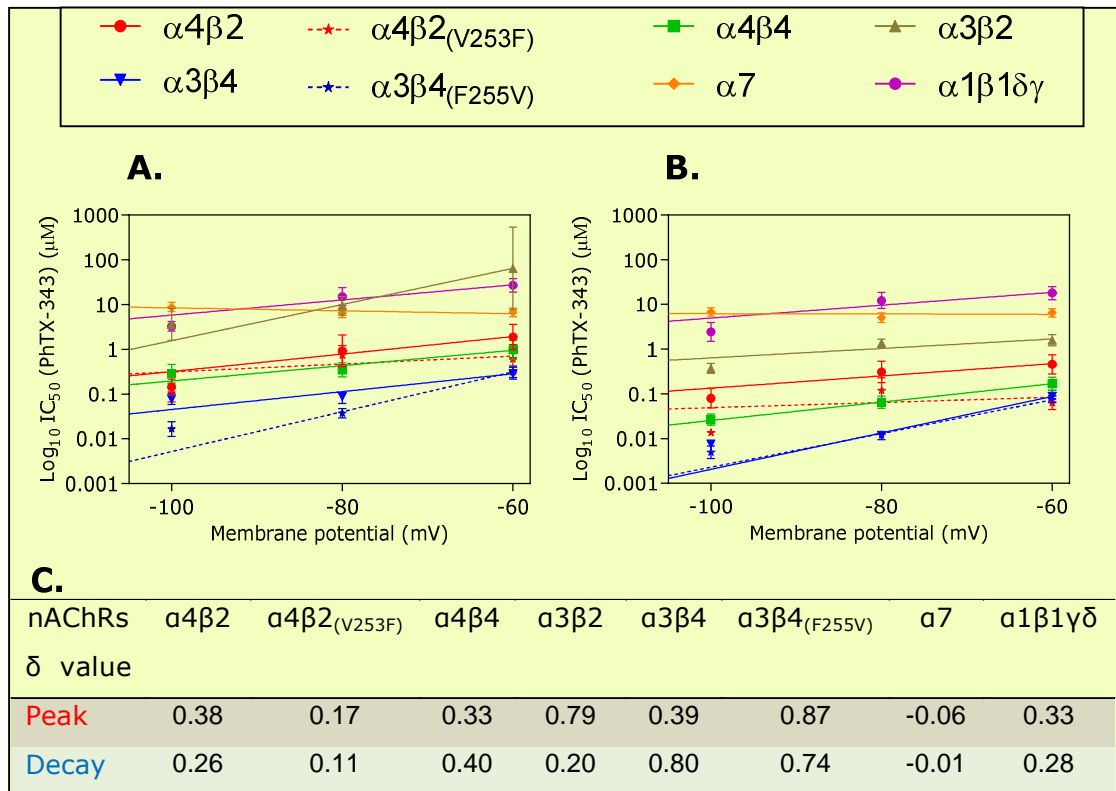


Figure 4.11. Effect of voltage on the action of PhTX-343 across eight different combinations of nAChRs. IC₅₀ values (95% CI) in µM for PhTX-343 peak (A) and decay (B) were plotted against voltage. (C) estimated δ values based on Woodhull equation when z , the number of positive charges on the molecule, equals 3.

4.3. Recovery from inhibition by PhTX-343

In this class of experiment we investigated the recovery rate of the peak and decay current of nAChRs expressed in *Xenopus* oocytes from PhTX-343. In all experiments we used approximately the ACh EC₅₀ concentration as a control and followed by co-application of ACh with increasing concentrations of PhTX-343 (10^{-10} M to 10^{-5} M) depending on combination sensitivity, with 6 minute intervals. Then, after the last co-application of PhTX-343, we continued the experiment by repeated application of control ACh concentration every 6 minutes to establish the recovery rate.

First, the recovery rate of $\alpha 3$ -containing receptors was studied. It appears that in the case of combined application of 10 μM PhTX-343 with the EC_{50} concentration of ACh for $\alpha 3\beta 4$, the size of peak and decay currents were, respectively only 3.5% and 0.1% of control. The mean value of recovery for the peak and decay current after 48 minutes was $88.2\% \pm 8.4$ and $76.7\% \pm 10.3$ respectively of control response. While $\alpha 3\beta 2$ showed lowest sensitivity to 10 μM PhTX-343 and lower recovery compared to $\alpha 3\beta 4$. Co-application of 10 μM PhTX-343 resulted in peak and decay currents of 48.4% and 12.2% of control response, respectively for $\alpha 3\beta 2$. Their mean peak and decay current recovery values were 56-57% of control response.

Secondly, we investigated the recovery rate of $\alpha 4$ -containing receptors from the inhibition of 10 μM PhTX-343. The peak and decay current of $\alpha 4\beta 2$ when exposed to 10 μM PhTX-343 was roughly 35% of control and the mean decay current recovery was 69.1%, higher than the peak value of 36.6% after 42 minutes. Co-application of 10 μM PhTX-343 resulted in peak and decay currents of 34.0% and 2.0% of control response, respectively for $\alpha 4\beta 4$. Their mean peak and decay current recovery values were 53.0% and 48.0% of control response respectively after 48 minutes.

Finally, the recovery rate of homomeric $\alpha 7$ N-nAChRs and M-nAChRs from 30 μM and 100 μM respectively was investigated. In the case of $\alpha 7$ N-nAChRs the mean recovery value obtained for the peak current was $108 \pm 5.0\%$ and for net charge movement was $111.0 \pm 6.2\%$ after 6 minutes, i.e. it was higher than the control response. Also, roughly full recovery was observed for the peak current ($99.4 \pm 3.2\%$) of M-nAChRs with slightly lower mean recovery rate for the decay current ($83.8 \pm 4.6\%$).

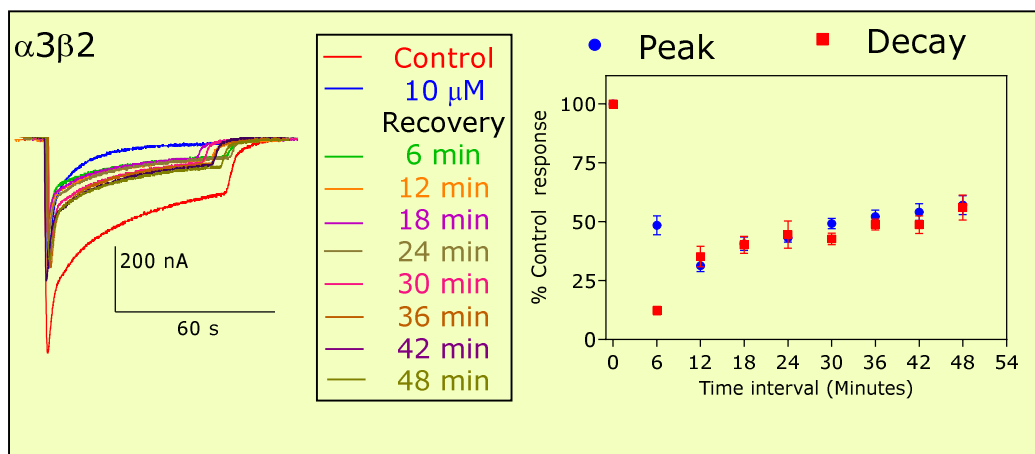
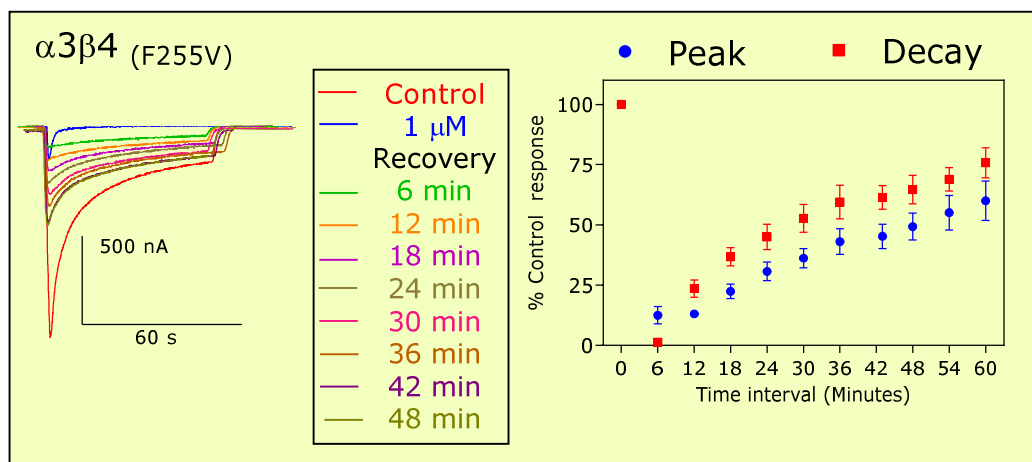
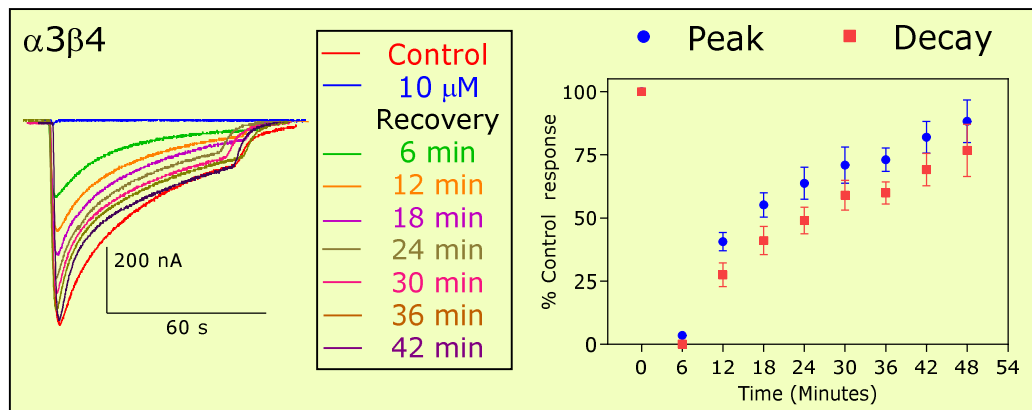


Figure 4.12. Showing recovery of $\alpha 3$ -containing nAChR responses to 30 μM $\alpha 3\beta 2$, 10 μM $\alpha 3\beta 4$ and $\alpha 3\beta 4_{(F255V)}$ ACh from inhibition by 10 μM PhTX-343 at $\alpha 3\beta 4$, $\alpha 3\beta 2$ and 10 μM PhTX-343 at $\alpha 3\beta 4_{(F255V)}$. All applications were at 6 minute intervals. In between the applications Ringer solution flowed at a rate of 3-6 ml/minute.

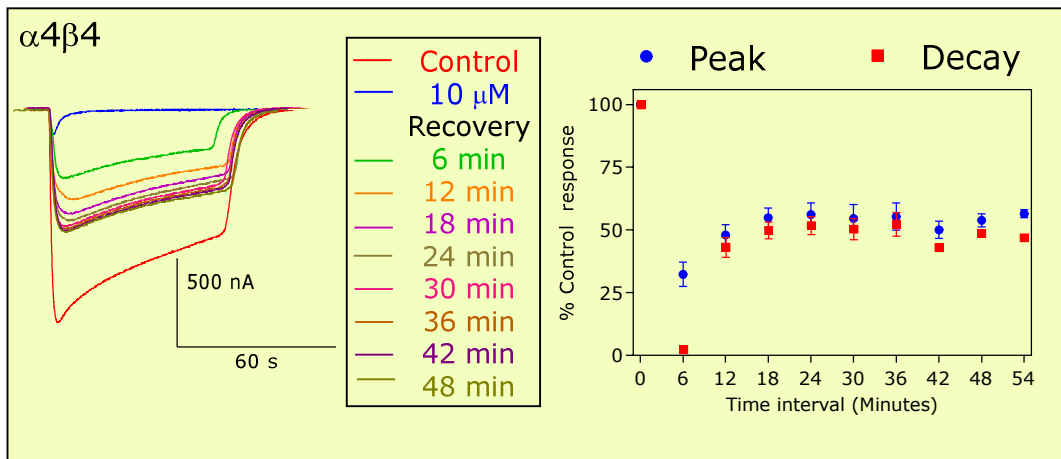
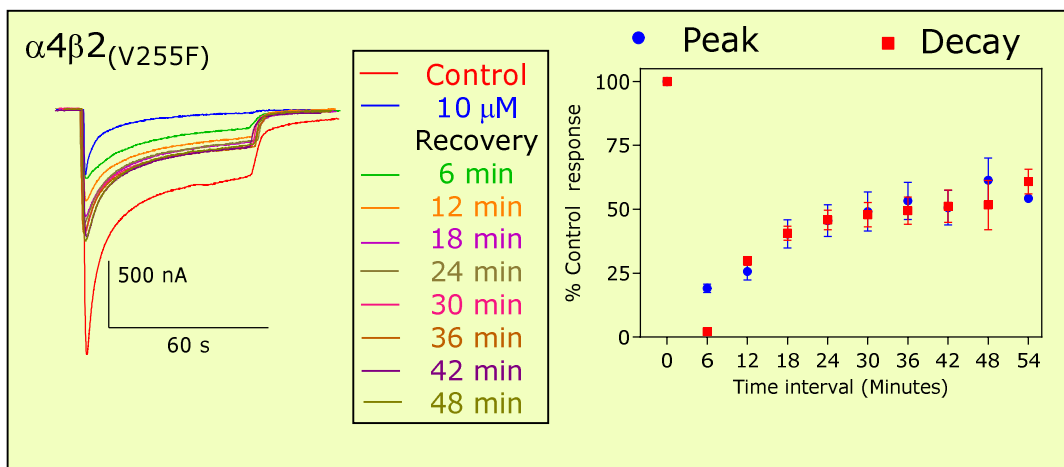
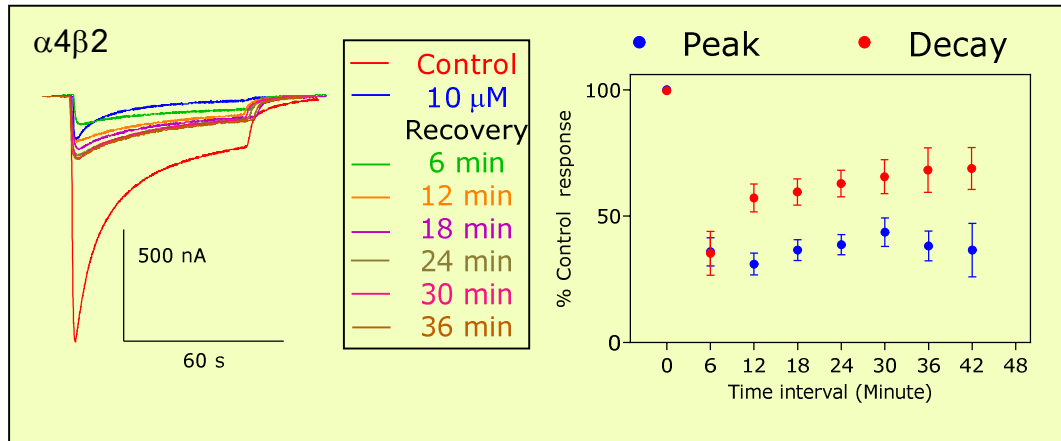


Figure 4.13. Showing recovery of $\alpha 4$ -containing nAChR responses to $10 \mu\text{M}$ ACh from inhibition by $10 \mu\text{M}$ PhTX-343. All applications were at 6 minute intervals. In between the applications Ringer solution flowed at rate of 3-6 ml/minute.

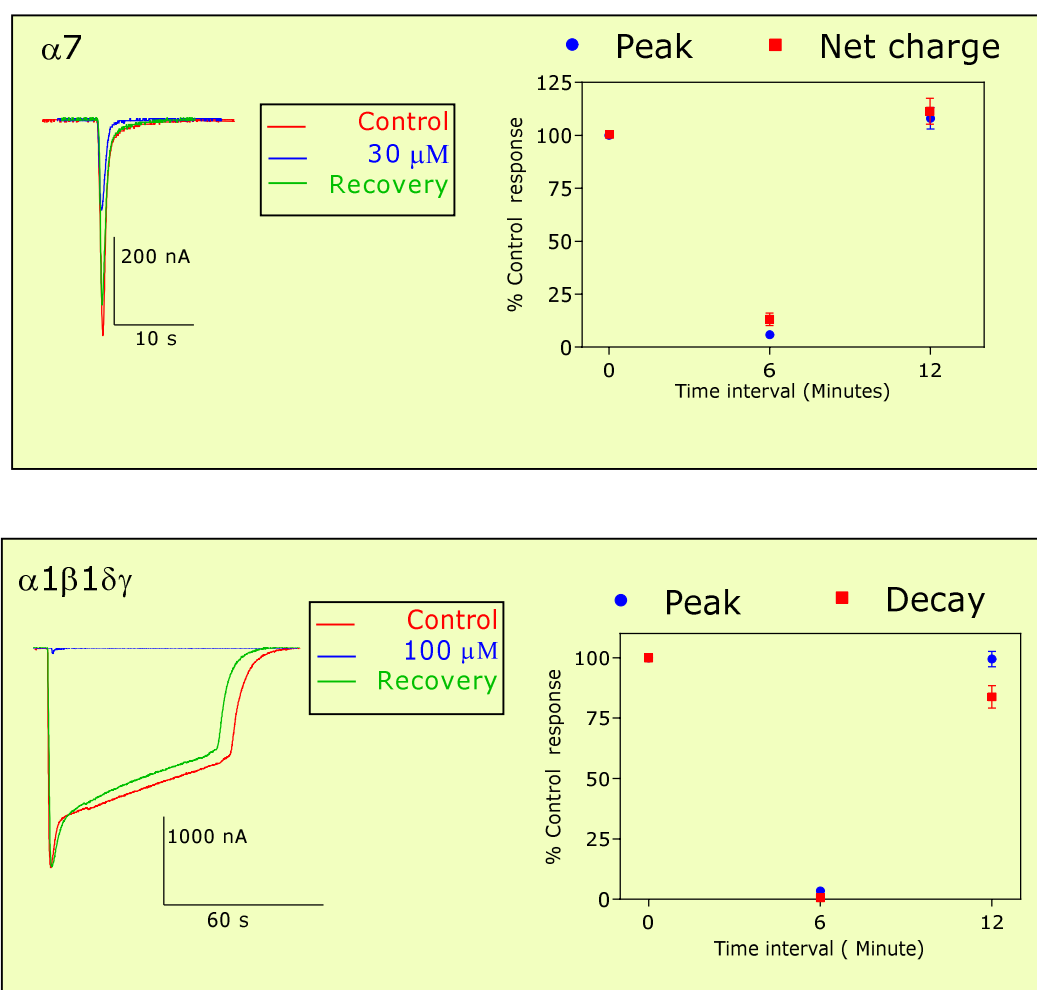


Figure 4.14. Showing recovery of $\alpha 7$ and $\alpha 1\beta 1\delta \gamma$ nAChR responses to 100 μM and 10 μM ACh from inhibition by 30 μM ($\alpha 7$) or 100 μM ($\alpha 1\beta 1\delta \gamma$) PhTX-343. All applications were at 6 minute intervals. In between the applications Ringer solution flowed at rate of 3-6 ml/minute.

4.4. Competition of PhTX-343 with ACh on nAChRs

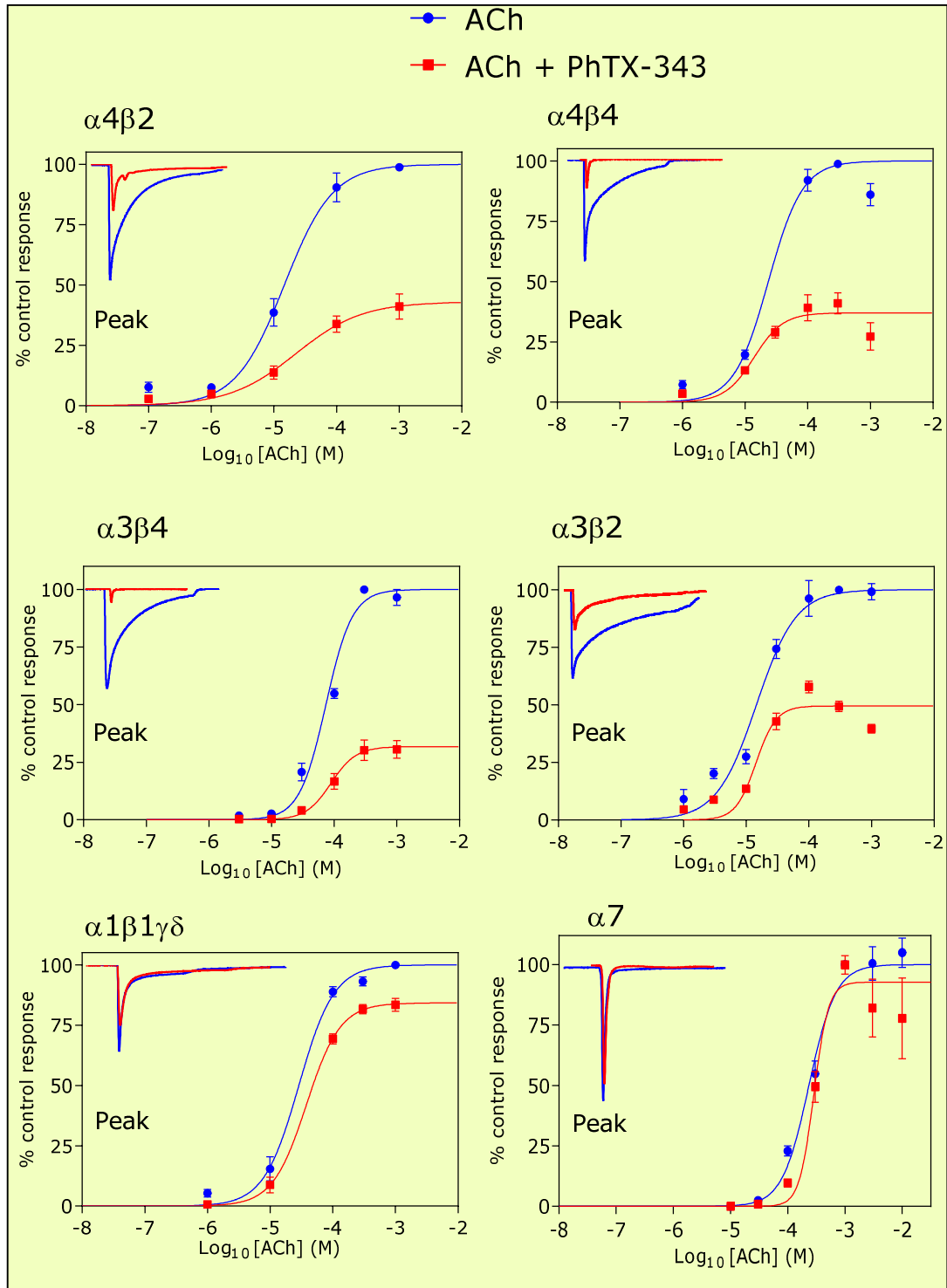
To further study the mechanism and mode of action by which PhTX-343 inhibits acetylcholine evoked inward current in oocytes expressing nAChRs, we analysed the data obtained from the effects of a single PhTX-343 concentration on inward current induced by different acetylcholine concentrations (**Figure 4.15**). Co-application of PhTX-343 with different concentrations of acetylcholine did not show any significant shift in the ACh concentration-response curve to the

right. The EC₅₀ values in the presence and absence of PhTX-343 were calculated and are presented in **Table 4.2**. Thus, the magnitude of inward current inhibition was independent of the acetylcholine concentration (n = 5-9 oocytes from different batches).

Table 4.2. The effects of PhTX-343 on nAChRs ACh concentration-response curve.

	EC ₅₀ value of nAChRs in μ M					
	α 4 β 2	α 4 β 4	α 3 β 2	α 3 β 4	α 7	α 1 β 1 γ δ
ACh	14	23	14	74	234	28
+1 μ M PhTX-343	22	13	14	89		
+10 μ M PhTX-343					288	
+30 μ M PhTX-343						38
P value EC ₅₀	0.5278	0.1941	0.9393	0.6381	0.0925	0.0875
P value						
1 mM ACh	<0.0001	<0.0001	<0.0001	<0.0001	0.09750	<0.0001
+PhTX-343						

Figure 4.15. (see over) PhTX-343 inhibits ACh mediated current responses of nAChRs in a non-competitive manner. Acetylcholine concentration-response curves in the absence (blue) or presence (red) of a constant concentration of PhTX-343 from oocytes clamped at -80 mV. ACh \pm PhTX-343 was applied for one minute at 6 minutes intervals. Traces show whole-oocyte current induced by 1000 μ M (α 4 β 2) or 300 μ M (α 4 β 4, α 3 β 4, α 3 β 2) ACh with or without 1 μ M PhTX-343, while muscle and α 7 responses were induced by 100 μ M and 1000 μ M ACh in the presence or absence of 30 μ M and 10 μ M PhTX-343, respectively. EC₅₀ values were estimated from plotted data of average current normalized as percentage of maximum current response against concentration of agonist. The ACh concentration response curve was shifted downward in the presence of PhTX-343 without any significant change in EC₅₀ values (**Table 4.2**).



CHAPTER FIVE

PHARMACOLOGICAL CHARACTERIZATION OF nAChR INHIBITION BY PhTX-12

Summary

The pharmacological actions of PhTX-12 on recombinant nAChRs expressed in *Xenopus* oocytes after micro-injection with mRNA was investigated by using TEVC. Concentration-inhibition curves for PhTX-12 were constructed for each combination of nAChR subunits at -60 mV, -80 mV and -100 mV. ACh EC₅₀ was used as a control and applied for 1 minute with 6 minutes interval either alone or co-applied with PhTX-12 at various concentrations ranging between 0.1 nM to 100 μM depending on subtype sensitivity. A four-parameter logistic equation was used to calculate the peak and decay current IC₅₀ values by plotting PhTX-12 concentration against the mean of normalised current as % of control response. It appears that both α-subunit and β-subunit are critical for PhTX-12 inhibition. PhTX-12 did not show any noticeable selectivity among investigated nAChRs with potency in the micro-molar range. It appears from IC₅₀ values at different holding potential that inhibition of nAChRs by PhTX-12 is voltage-independent or slightly voltage-dependent. These values were used in an adapted Woodhull equation to predict interaction site of PhTX-12 in the channel by calculating their δ values. PhTX-12 is a non-competitive inhibitor at α3β4 and α1β1δγ nAChRs reducing the ACh response amplitude without shifting the ACh EC₅₀ value of significantly.

5.1. PhTX-12 inhibits the ACh-induced response of wild-type and mutated nAChRs

PhTX-12 is another synthetic analogue of PhTX-433, where both secondary amino groups in the polyamine chain were replaced by methylene. Previous work showed that PhTX-12 was roughly 22-fold more potent on embryonic M-nAChRs naturally expressed in the TE671 cell line in comparison to PhTX-343 (Brier et al., 2003) while being much less active at AMPA receptors (Mellor et al., 2003). Here, we investigated the pharmacological effects of PhTX-12 on several N-nAChR subunit combinations ($\alpha 4\beta 2$, $\alpha 4\beta 2_{(V253F)}$, $\alpha 3\beta 4$, $\alpha 3\beta 4_{(F255V)}$, $\alpha 3\beta 2$, $\alpha 4\beta 4$ and $\alpha 7$) and embryonic M-nAChRs ($\alpha 1\beta 1\delta\gamma$) expressed in *Xenopus* oocytes. Concentration-inhibition curves were constructed at a standard voltage of -80 mV (**Figure 5.1, 5.2 and 5.3**) and IC_{50} values calculated for the peak current and decay current of each combination.

The decay current IC_{50} value calculated for $\alpha 1\beta 1\delta\gamma$ nAChRs at V_H -80 mV was 0.10 μM . The decay IC_{50} value obtained for $\alpha 3\beta 4$, $\alpha 3\beta 4_{(F255V)}$, $\alpha 4\beta 4$, $\alpha 4\beta 2$ and $\alpha 4\beta 2_{(V253F)}$ nAChRs were in the same range (0.10 μM - 0.28 μM) as M-nAChRs. In contrast, a 25-fold and 49-fold increase in IC_{50} value was calculated for $\alpha 3\beta 2$ and $\alpha 7$ nAChRs, respectively. The ranking order potency of nAChRs based on decay current inhibition by PhTX-12 was, $\alpha 1\beta 1\delta\gamma = \alpha 3\beta 4 > \alpha 4\beta 2 > \alpha 4\beta 4 > \alpha 4\beta 2_{(V253F)} > \alpha 3\beta 4_{(F255V)} > \alpha 3\beta 2 > \alpha 7$.

On the other hand, nAChR subunit combinations showed differences in the peak current IC_{50} value for PhTX-12. The lowest peak IC_{50} value, calculated for $\alpha 4\beta 4$ nAChRs at V_H -80 mV, was 1.64 μM . This value was increased by 3.7-fold and 6.7-fold for muscle type and homomeric $\alpha 7$ nAChRs, respectively. The peak IC_{50} value obtained for wild-type $\alpha 3\beta 4$ nAChRs was 2.7 μM , this value was not significantly ($p=0.8902$) different from mutated $\alpha 3\beta 4_{(F255V)}$ nAChRs. The peak IC_{50} value calculated for $\alpha 4\beta 2$ was 2 μM , this value doubled for mutated $\alpha 4\beta 2_{(V253F)}$ but also was not significantly ($p=0.1208$) different from wild-type.

The highest peak IC_{50} value of $60 \mu\text{M}$ was recorded for $\alpha 3\beta 2$ nAChRs. These data support that both α - and β - subunit is critical for PhTX-12 action.

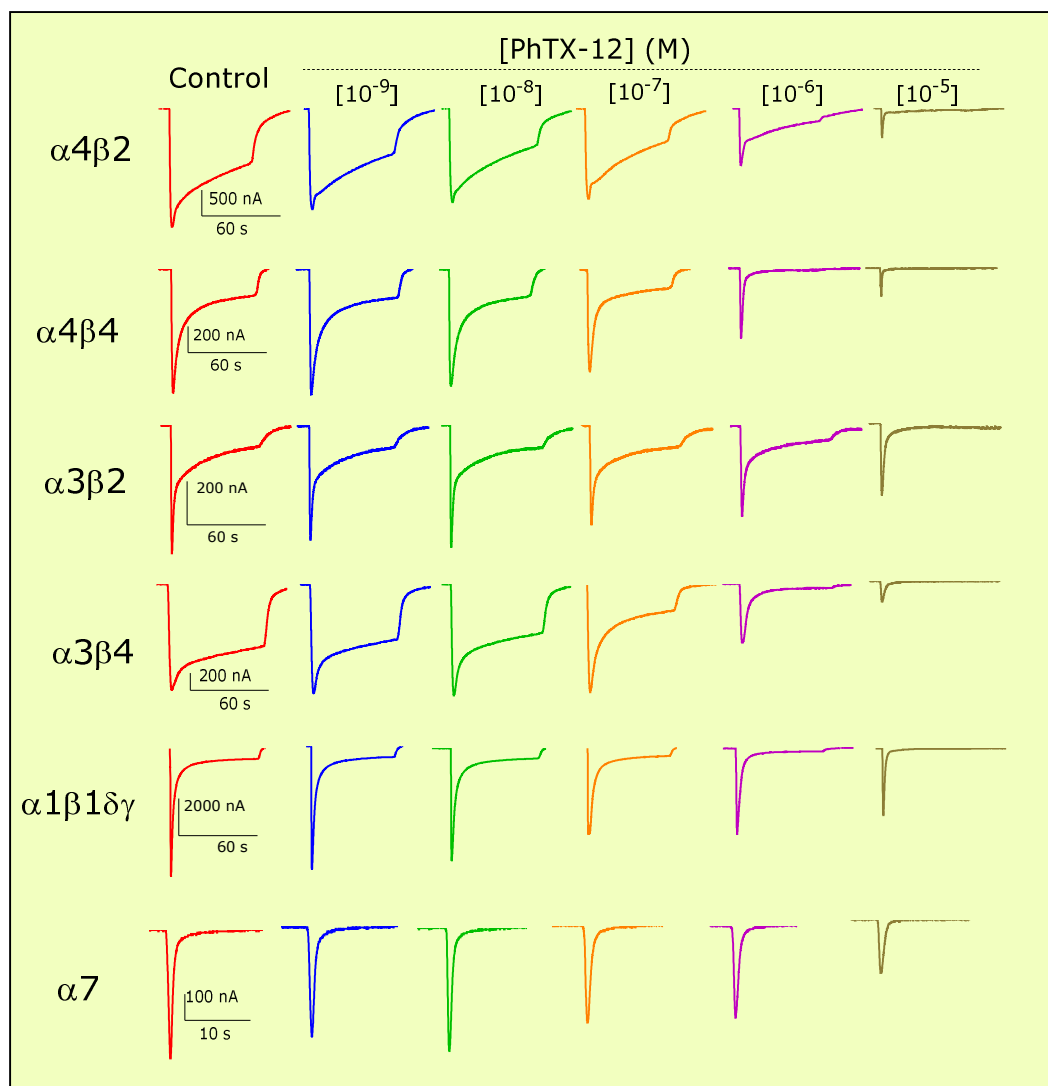


Figure 5.1. Example traces showing nAChR subtype inhibition sensitivity to PhTX-12. Approximately EC_{50} ACh concentration ($10 \mu\text{M}$ for $\alpha 4\beta 2$, $\alpha 4\beta 4$ and $\alpha 1\beta 1\delta\gamma$, $30 \mu\text{M}$ for $\alpha 3\beta 2$ and $100 \mu\text{M}$ for $\alpha 3\beta 4$ and $\alpha 7$ nAChRs) in each combination was perfused to oocytes clamped at -80 mV to generate control (Red). Then, PhTX-12 with increasing concentration (other colours) was co-perfused with ACh at six minute intervals.

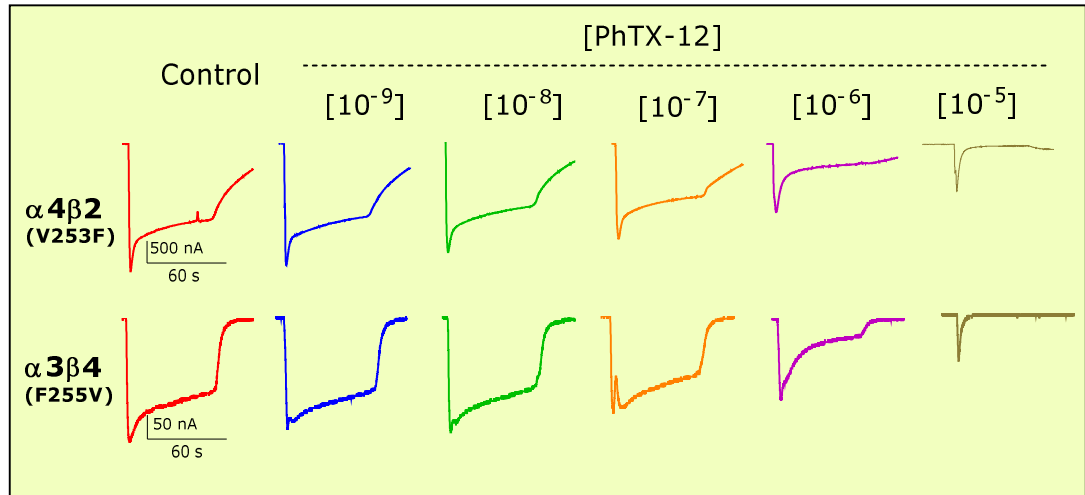


Figure 5.2. Example traces showing mutant nAChR subtype inhibition sensitivity to PhTX-12. Approximately EC_{50} ACh concentration ($10 \mu\text{M}$ for $\alpha 4\beta 2_{(V253F)}$ and $100 \mu\text{M}$ for $\alpha 3\beta 4_{(F255V)}$) in each combination was perfused over oocytes clamped at -80 mV to generate control (Red). Then, increasing concentrations of PhTX-12 (other colours) was co-perfused with ACh at 6 minute intervals.

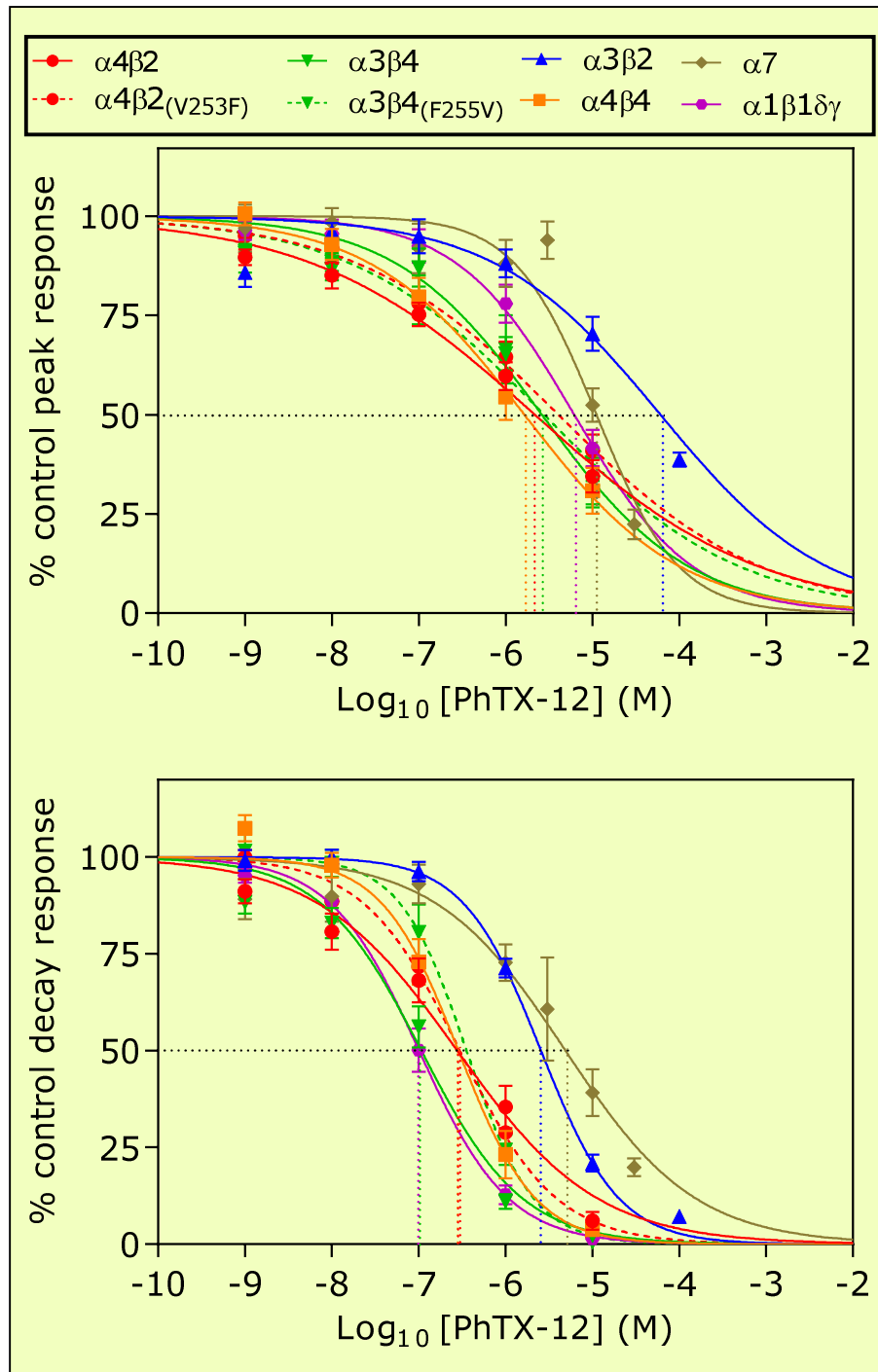


Figure 5.3. Screening PhTX-12 inhibitory effects on Peak (top) and decay (bottom) current of eight different subunit combinations of nAChRs expressed in *Xenopus* oocytes at holding potential -80 mV. Graphs are concentration-inhibition data plotted as mean % control response vs PhTX-12 concentration for peak current (top) or decay current (bottom) and curve fits are to Equation 1. Decay current of $\alpha 7$ = net charge.

5.2. Voltage effects on the inhibition of nAChRs by PhTX-12

To investigate whether alteration in the membrane holding potential affects the inhibitory actions of PhTX-12 on nAChRs, concentration-inhibition curves for PhTX-12 on $\alpha 7$, $\alpha 3\beta 2$, $\alpha 4\beta 4$, $\alpha 4\beta 2$, $\alpha 4\beta 2_{(V253F)}$, $\alpha 3\beta 4$, $\alpha 3\beta 4_{(F255V)}$ and $\alpha 1\beta 1\delta\gamma$ subunit combinations were constructed at three different V_H (-60 mV, -80 mV and -100 mV) and their IC_{50} (95% CI) values are presented in **Table 5.1**.

PhTX-12 strongly inhibited $\alpha 1\beta 1\delta\gamma$ receptors with peak and decay current IC_{50} values of 3.1 μM and 70 nM, at -60 mV (**Figure 5.4**). Neither of these values changed significantly by altering V_H to -80 mV and -100 mV; they became 6.1 μM and 5.0 μM on the peak current and 100 nM and 70 nM on the decay current, respectively. Similarly, increasing the V_H to -100 mV did not cause any noticeable change in the calculated IC_{50} values for the peak current (1.82 μM) and decay current (190 nM) of $\alpha 4\beta 4$ nAChRs (**Figure 5.4**). On the other hand, the homomeric $\alpha 7$ was the only combination that showed a significant ($p=0.026$) change in the peak current IC_{50} values calculated at -60 mV (18.7 μM) by altering membrane potential to -100 mV (**Figure 5.7.A**).

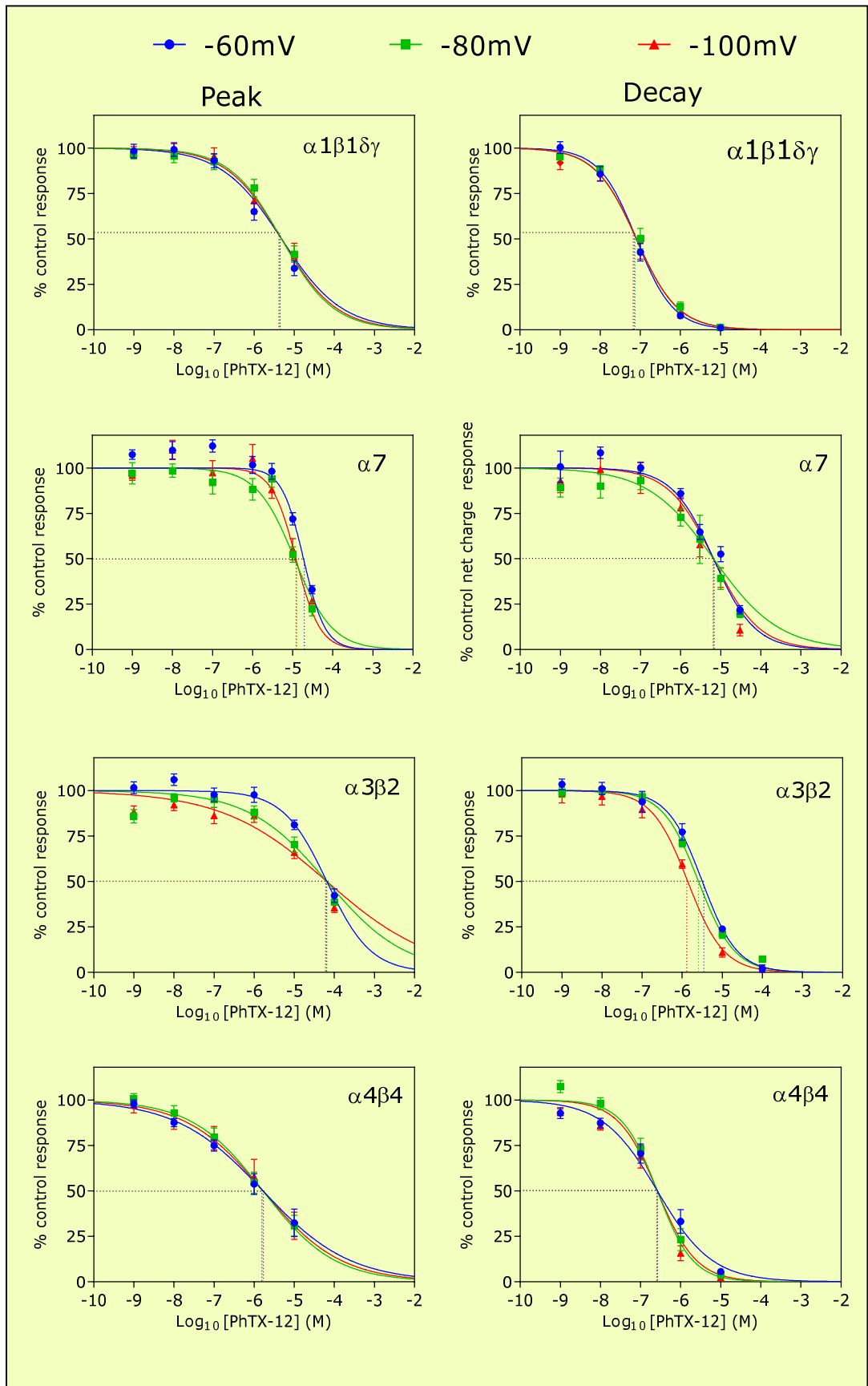
The decay current IC_{50} values of $\alpha 4\beta 2$, $\alpha 4\beta 2_{(V253F)}$, $\alpha 3\beta 4$, $\alpha 3\beta 4_{(F255V)}$, $\alpha 3\beta 2$ and $\alpha 7$ nAChRs calculated at -60 mV were significantly higher than the values at -100 mV (**Figure 5.7.B**). The decay current IC_{50} values recorded at holding potential -60 mV for $\alpha 4\beta 2$, $\alpha 3\beta 4$ and $\alpha 3\beta 4_{(F255V)}$ were 230 nM, 100 nM and 510 nM, respectively (**Figure 5.5 and 5.6**). These combinations showed strong voltage dependence between -60 mV and -100 mV ($p < 0.0001$ for all combinations). The least voltage dependent combinations ($p < 0.05$) were $\alpha 4\beta 2_{(V253F)}$ and $\alpha 7$ nAChRs by comparing their decay current IC_{50} values, 400 nM and 8900 nM respectively, calculated at $V_H = -60$ mV to that calculated at $V_H = -100$ mV. In addition, $\alpha 3\beta 2$ nAChRs were found to be moderately voltage dependent ($p < 0.001$) by comparing decay current IC_{50} calculated at -60 mV and -100 mV.

Table 5.1. Summary of PhTX-12 Peak 'P' and decay 'D' current IC₅₀ values on eight different combinations of nAChRs at three different holding potential, -60 mV, -80 mV and -100 mV. 'D' in case of α7 = net charge. Values are presented in μM as mean IC₅₀ (95% CI) and (n) is the number of tested oocytes. Similarly sensitivity for PhTX-12 was recorded for six combinations tested and lower sensitivity was recorded for α7 and α3β2 based on the decay current IC₅₀ values at -80 mV. Voltage-dependence was weak or even absent for peak current inhibition of some heteromeric combinations.

nAChRs		V _H = -60 mV	V _H = -80 mV	V _H = -100 mV
α4β2	P	3.8 (1.4-10.1)	2.1 (1.2-3.6)	1.6 (0.7-3.6)
	n	(8)	(9)	(11)
	D	0.23 (0.14-0.37)	0.27 (0.17-0.44)	0.04 (0.02-0.06)
α4β2 (V253F)	P	2.2 (1.4-3.4)	4.0 (2.2-7.3)	3.4 (1.3-8.7)
	n	(4)	(5)	(9)
	D	0.4 (0.27-0.59)	0.29 (0.25-0.34)	0.18 (0.13-0.26)
α4β4	P	1.51 (0.84-2.72)	1.64 (0.96-2.82)	1.82 (0.81-4.11)
	n	(9)	(12)	(9)
	D	0.32 (0.21-0.48)	0.28 (0.20-0.40)	0.19 (0.14-0.26)
α3β2	P	65 (35-118)	60 (21-171)	74 (21-259)
	n	(9)	(12)	(10)
	D	3.19 (2.39-4.27)	2.57 (2.16-3.06)	1.38 (1.05-1.89)
α3β4	P	3.08 (2.21-4.47)	2.61 (1.70-4.01)	2.02 (1.22-3.36)
	n	(7)	(8)	(8)
	D	0.10 (0.07-0.14)	0.10 (0.07-0.14)	0.02 (0.02-0.03)
α3β4 (F255V)	P	1.6 (0.7-3.6)	2.7 (1.1-6.8)	1.0 (0.5-2.0)
	n	(5)	(5)	(5)
	D	0.51 (0.29-0.89)	0.35 (0.25-0.49)	0.06 (0.04-0.10)
α7	P	18.7 (14-23)	11.1 (7.2-17)	12.1 (9.0-16)
	n	(12)	(12)	(10)
	D	8.9 (6.9-11)	4.9 (2.7-8.6)	5.0 (3.0-8.3)
α1β1γδ	P	3.1 (2.1-4.7)	6.1 (4.0-9.4)	5.0 (2.8-8.8)
	n	(9)	(11)	(8)
	D	0.07 (0.05-0.09)	0.10 (0.08-0.12)	0.07 (0.05-0.09)

The IC_{50} μM ($\pm 95\%$ CI) voltage relationship curves for both peak and decay current inhibition by PhTX-12 were constructed based on the Woodhull model to estimate the parameter δ , the fraction of the membrane electric field penetrated by the molecule (**Figure 5.8**). PhTX-12 carries a single positive charge ($Z = 1$) in the polyamine chain at physiological pH compared to three for PhTX-343 (Stromgaard et al., 1999). The peak and decay current δ values calculated from IC_{50} (95% CI) at three different holding potential for each combination are shown in **Figure 5.8.C**. These values were quite variable; some were positive and others were negative and in some cases the decay current value was lower than that for peak current or vice versa. Therefore, it was difficult to predict the level of voltage dependence but we predict in general that peak inhibition of all nAChR combinations by PhTX-12 was weakly dependent on the membrane potential while decay inhibition was more strongly voltage-dependent, with few exceptions.

Figure 5.4. (see over) Combined mouse ($\alpha 1\beta 1\delta\gamma$), human ($\alpha 7$), rat $\alpha 3\beta 2$ and $\alpha 4\beta 4$ concentration-inhibition curves for inhibition of 10 μM for $\alpha 1\beta 1\delta\gamma$ and $\alpha 4\beta 4$, 30 μM for $\alpha 3\beta 2$ and 100 μM for $\alpha 7$ ACh evoked peak (right) and decay (left) current by PhTX-12 at holding potentials of **-100 mV**, **-80 mV** and **-60 mV**. The shown points on curves are mean \pm S.E.M. of n oocytes normalized to the control ACh response from the same oocyte and curve fits are to equation 1. For $\alpha 7$ the decay value is for net charge.



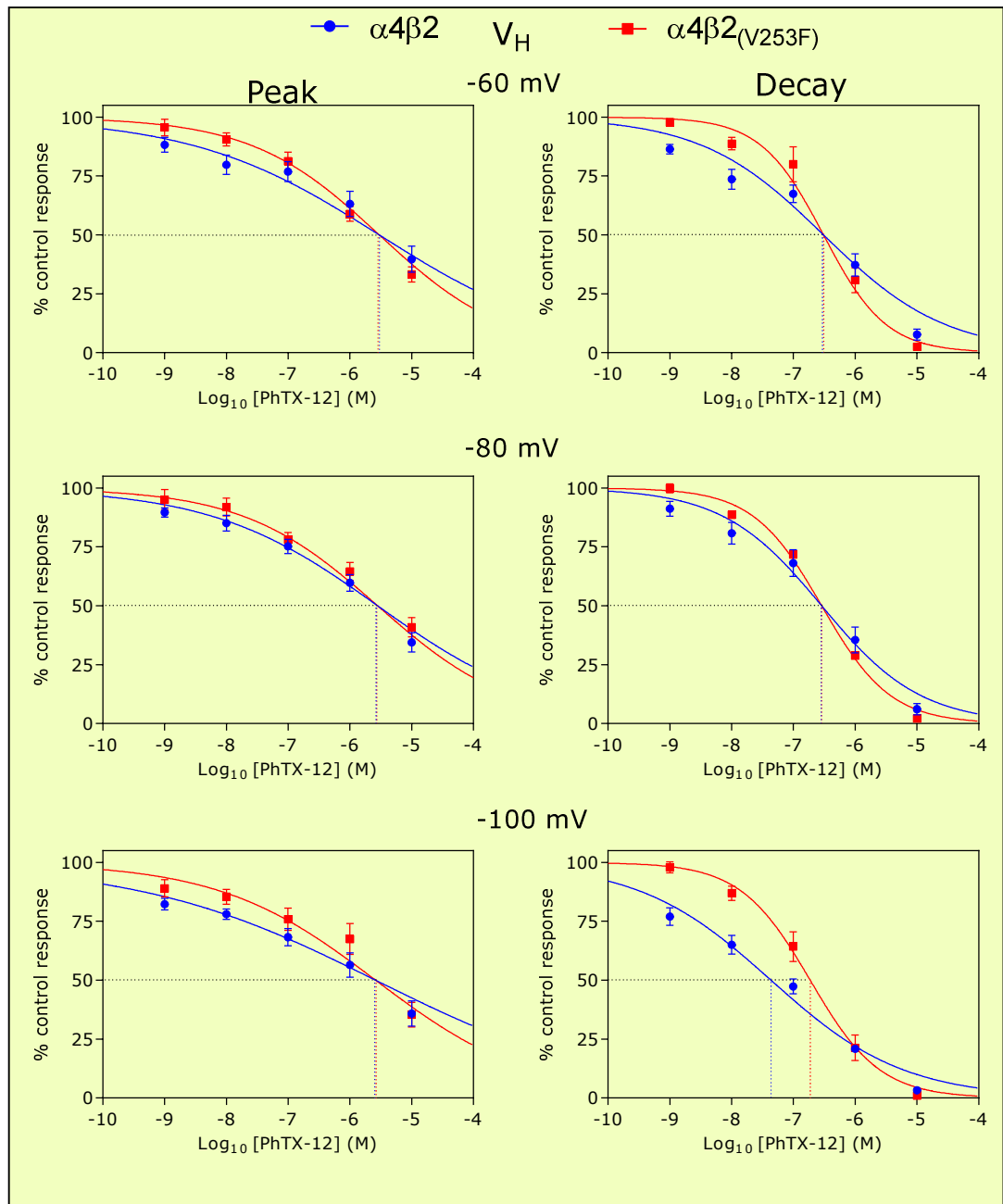


Figure 5.5. Combined rat $\alpha 4\beta 2$ and $\alpha 4\beta 2_{(V253F)}$ concentration-inhibition curves for inhibition of peak (right) and decay (left) current of $10 \mu\text{M}$ ACh evoked response by PhTX-12 at holding potentials of -100 mV (bottom), -80 mV (middle) and -60 mV (top). The shown points on curves are mean \pm S.E.M. of n oocytes normalized to the control ACh response from the same oocyte and curve fits are to equation 1. The decay current IC_{50} value of $\alpha 4\beta 2_{(V253F)}$ at -100 mV was significantly ($p < 0.0001$) higher than that of wild-type $\alpha 4\beta 2$ nAChRs otherwise there was no difference in PhTX-12 sensitivity between $\alpha 4\beta 2$ and $\alpha 4\beta 2_{(V253F)}$.

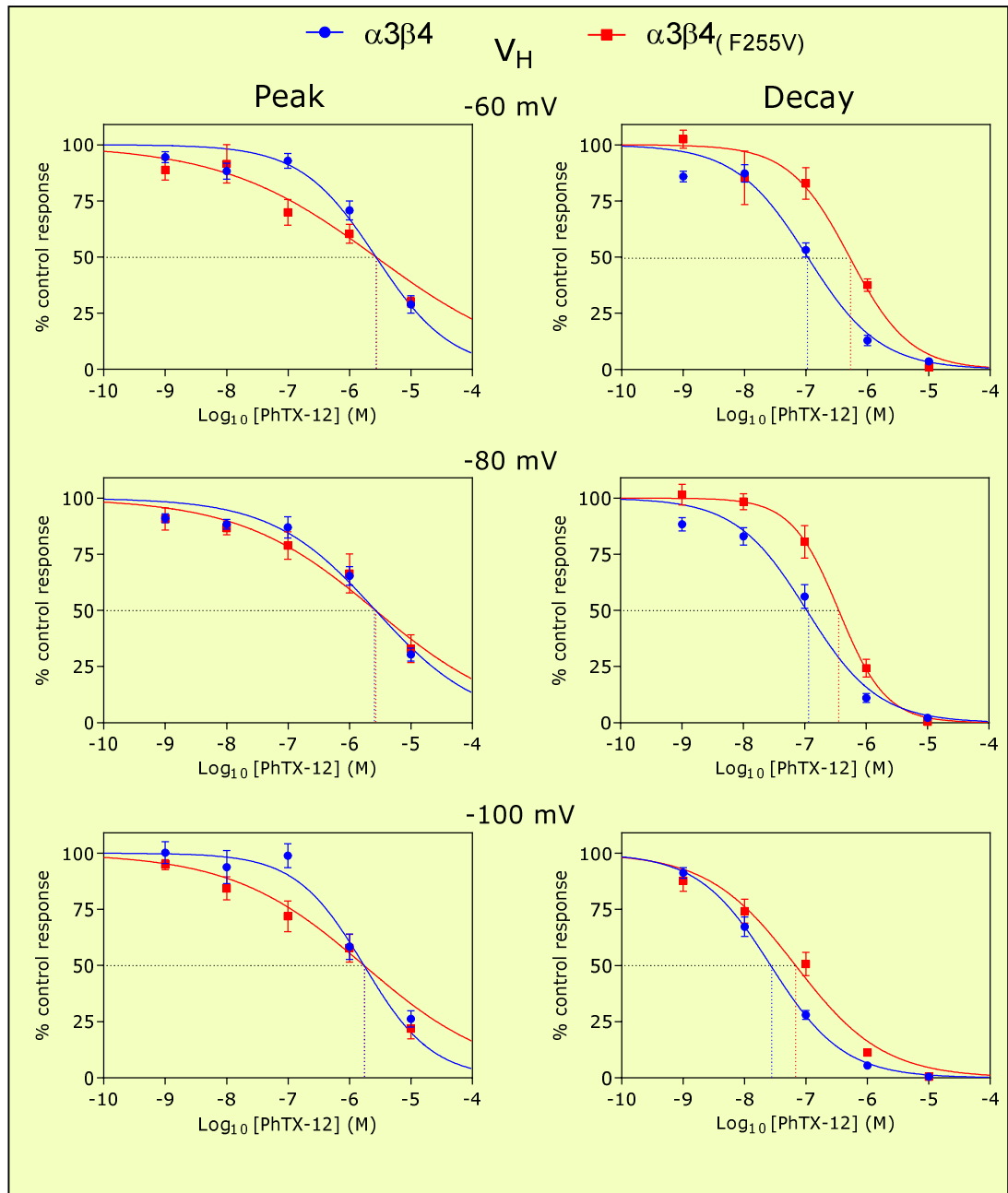


Figure 5.6. Combined rat $\alpha 3\beta 4$ and $\alpha 3\beta 4_{(F255V)}$ concentration-inhibition curves for inhibition of peak (right) and decay (left) current of 100 μM ACh evoked response by PhTX-12 at holding potentials of -100 mV (bottom), -80 mV (middle) and -60 mV (top). The shown points on curves are mean \pm S.E.M. of n oocytes normalized to the control ACh response from the same oocyte and curve fits are to equation 1. Sensitivity of $\alpha 3\beta 4_{(F255V)}$ to PhTX-12 was lower than $\alpha 3\beta 4$ at all three holding potentials for decay current inhibition ($p < 0.0001$) but there was no significant difference for peak current inhibition.

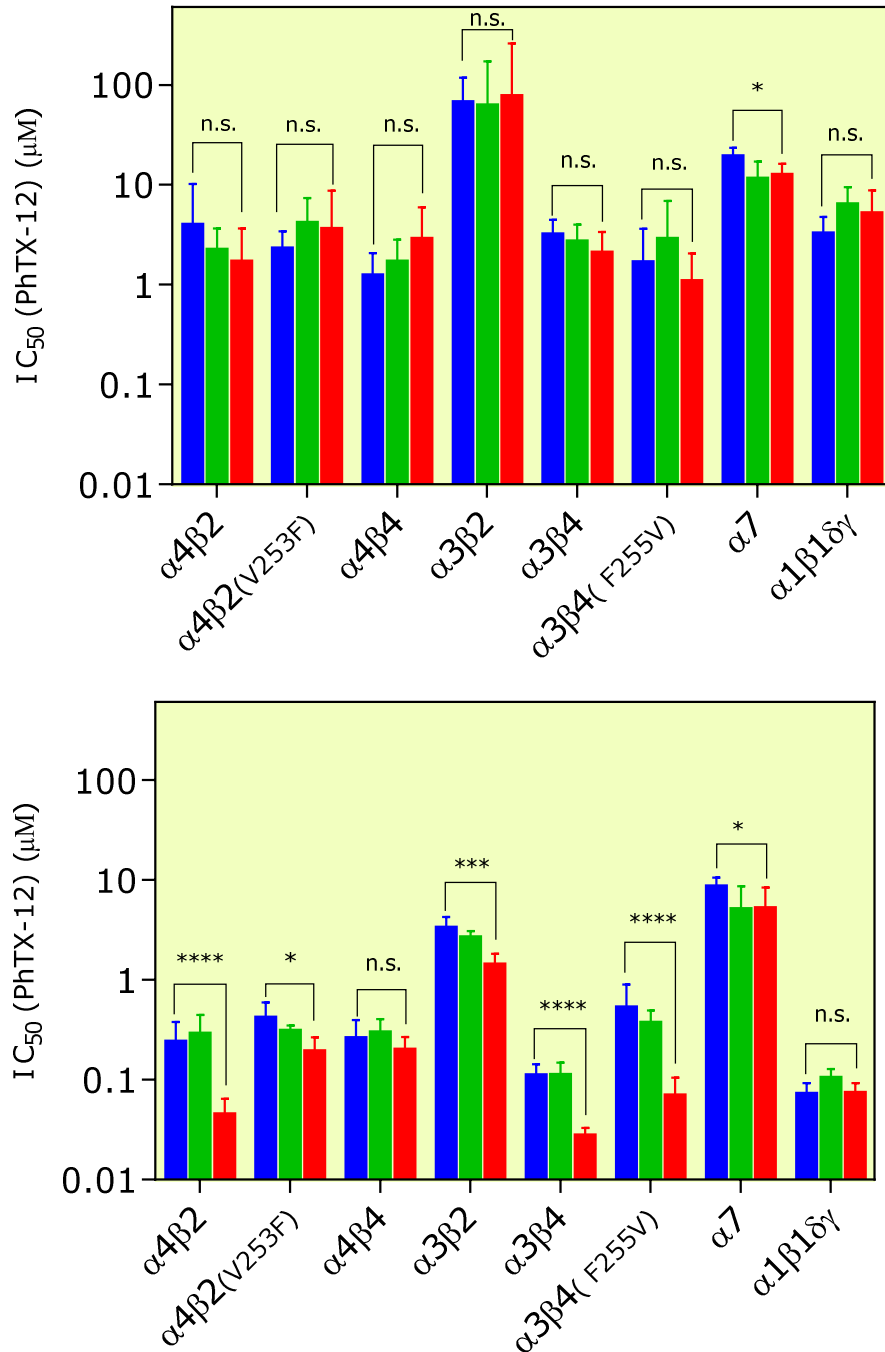


Figure 5.7. Comparison of PhTX-12 potency on eight different combinations of nAChRs. Each bar represents PhTX-12 IC₅₀ values (95% CI) on the particular combinations for peak (top) or decay (bottom) current inhibition. Red, green and blue bars represent membrane holding potentials of -100 mV, -80 mV and -60 mV respectively. Significance of difference between IC₅₀ at -100 mV and -60 mV is indicated by n.s. (p≥0.05), * (p<0.05), ** (p<0.01), *** (p<0.001) or **** (p<0.0001).

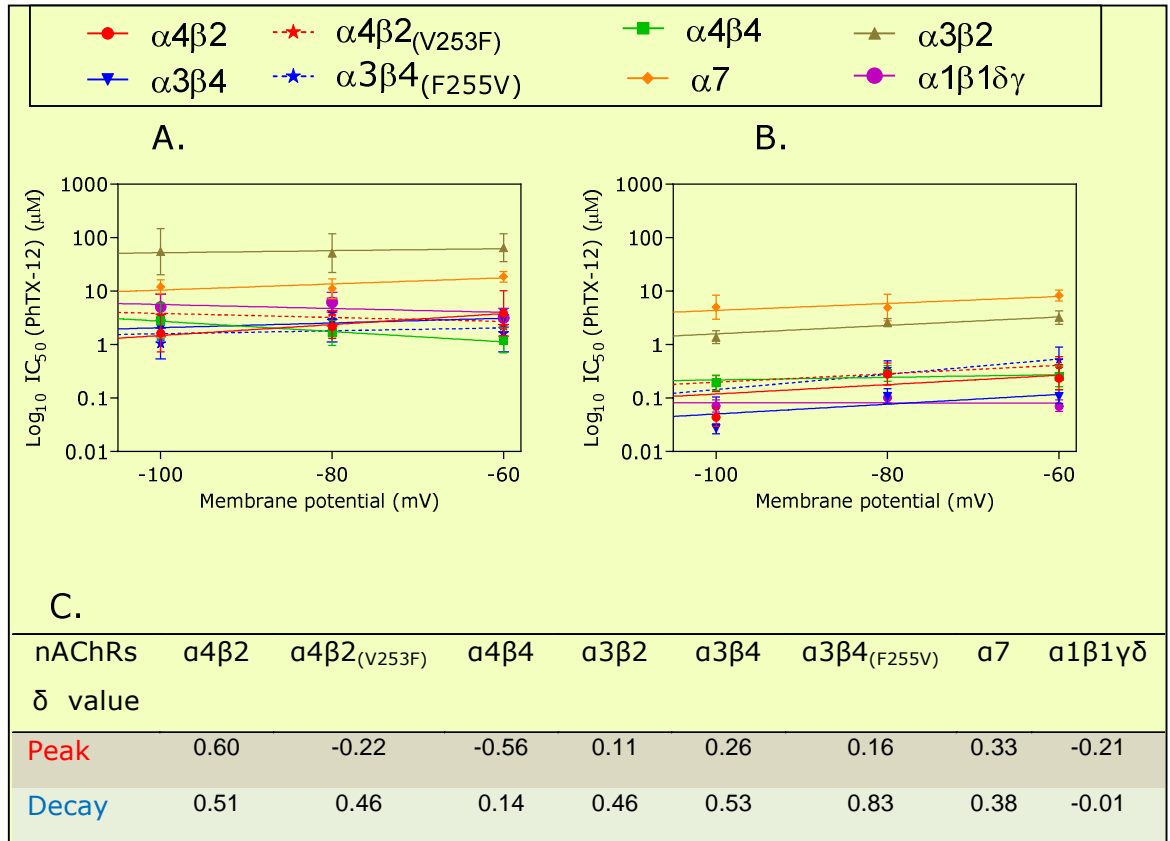


Figure 5.8. Voltage effect on action of PhTX-12 across eight different combinations of nAChR subunits. IC₅₀ values (95% CI) in µM for PhTX-12 peak (A) and decay (B) current inhibition were plotted against voltage. (C) estimated δ values based on the Woodhull equation when z, number of positive charges on molecule, equals 1.

5.3. Recovery from inhibition by PhTX-12

In this experiment nearly complete recovery of nAChRs expressed in *Xenopus* oocytes was observed 6 minutes after the previous co-application of agonist and PhTX-12 (**Figure 5.19, 5.10** and **5.11**). In the case of combined application of 10 µM PhTX-12 with EC₅₀ ACh concentration the peak amplitude of the control response of $\beta 4$ -containing receptors was reduced approximately by 70-80 %, while $\beta 2$ -, $\beta 1$ -, and non- β -containing receptors by 30-60 %. The mean value of recovery for the peak current of $\alpha 3$ -containing was roughly 90-100 %, while for $\alpha 1$ -, $\alpha 4$ - and $\alpha 7$ -containing receptors it was 80-90 %.

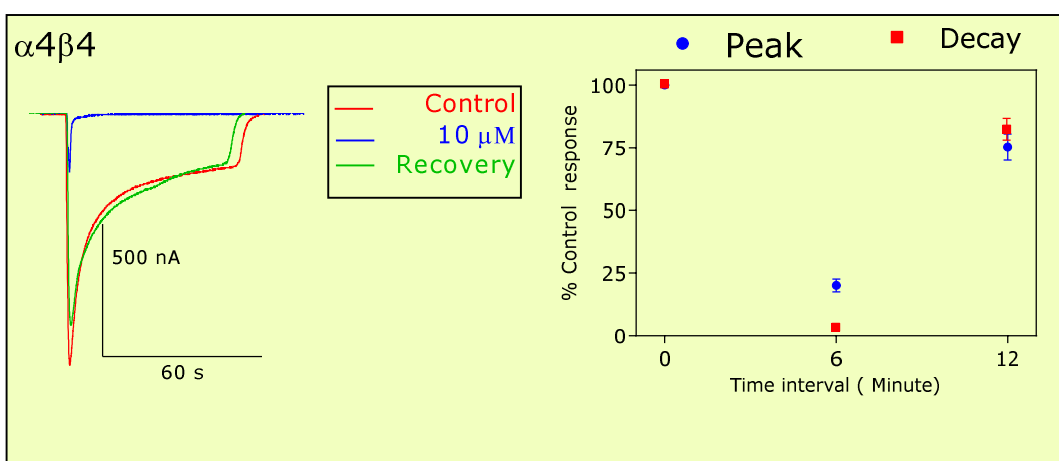
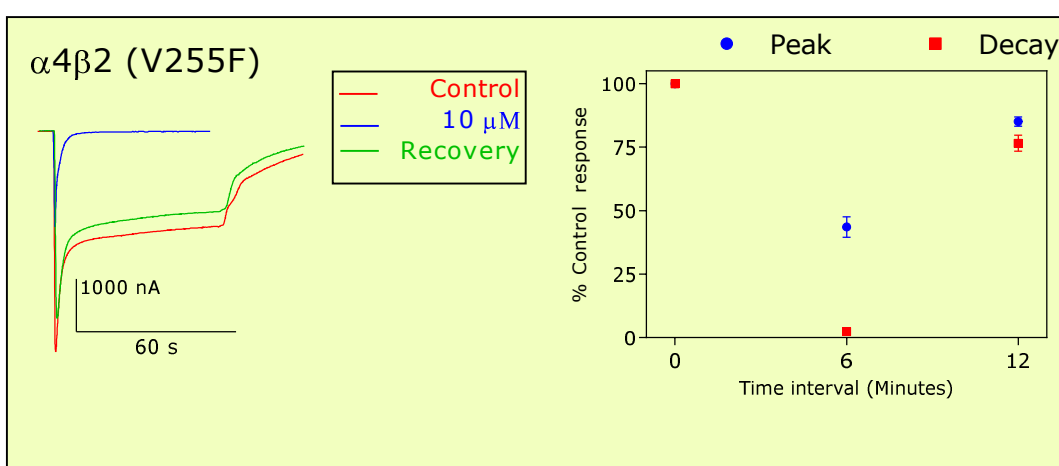
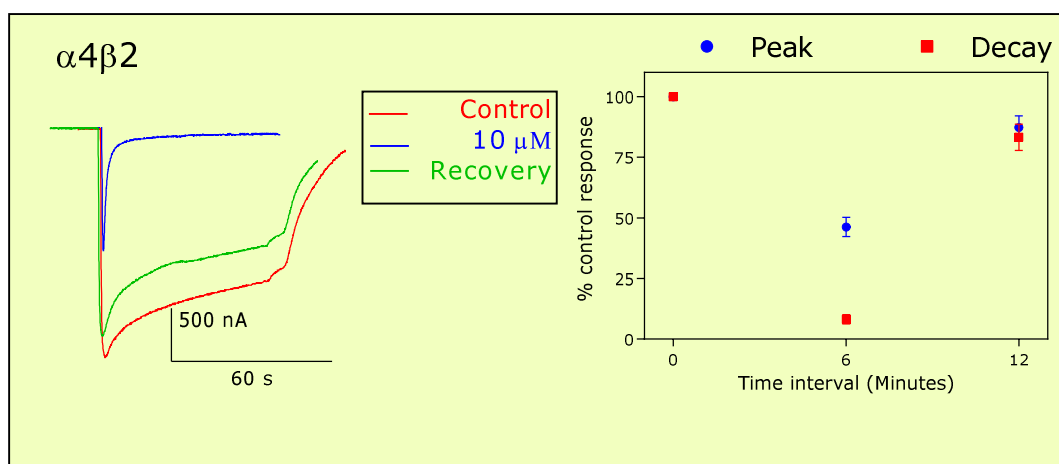


Figure 5.9. Recovery of $\alpha 4$ -containing nAChRs from antagonism by PhTX-12. Traces in each box show ACh EC_{50} concentration alone (control, recovery) or with 10 μM PhTX-12. Graphs show mean % control response for peak and decay current \pm S.E.M. before (0 min) during (6 min) and after (12 min) co-application of 10 μM PhTX-12.

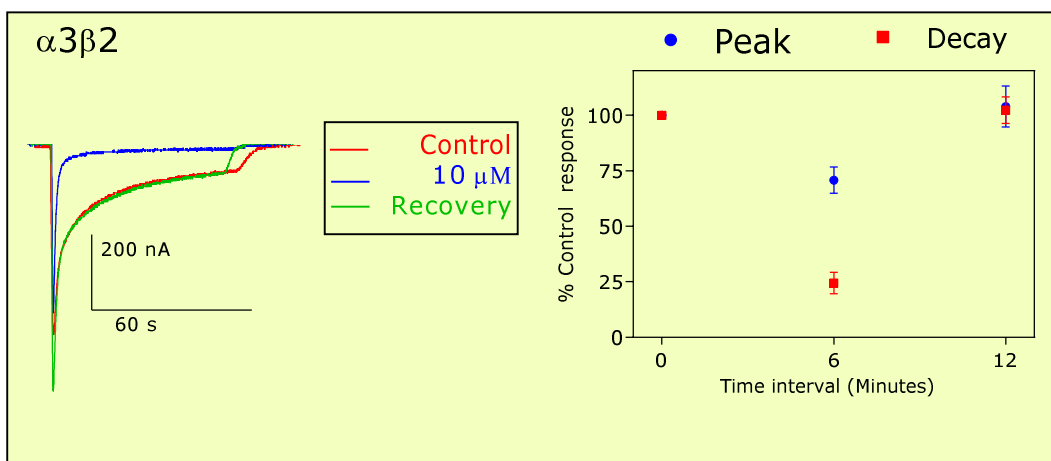
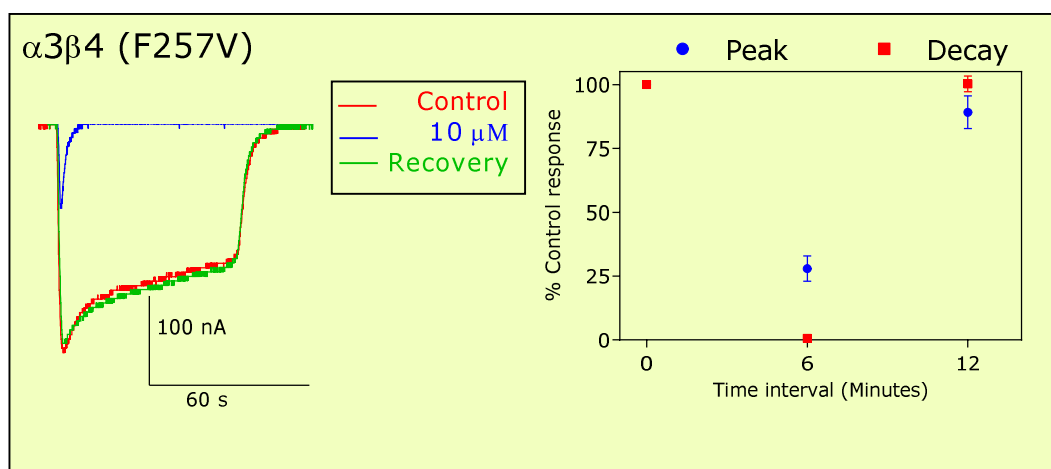
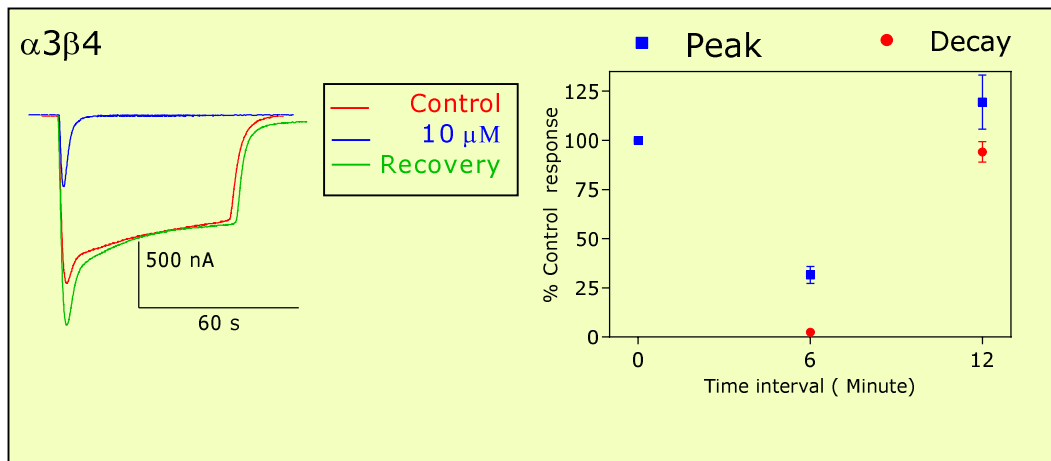


Figure 5.10. Recovery of $\alpha 3$ -containing nAChRs from antagonism by PhTX-12. Traces in each box show ACh EC_{50} concentration alone (control, recovery) or with $10\mu M$ PhTX-12. Graphs show mean % control response for peak and decay current \pm S.E.M. before (0 min) during (6 min) and after (12 min) co-application of $10\mu M$ PhTX-12.

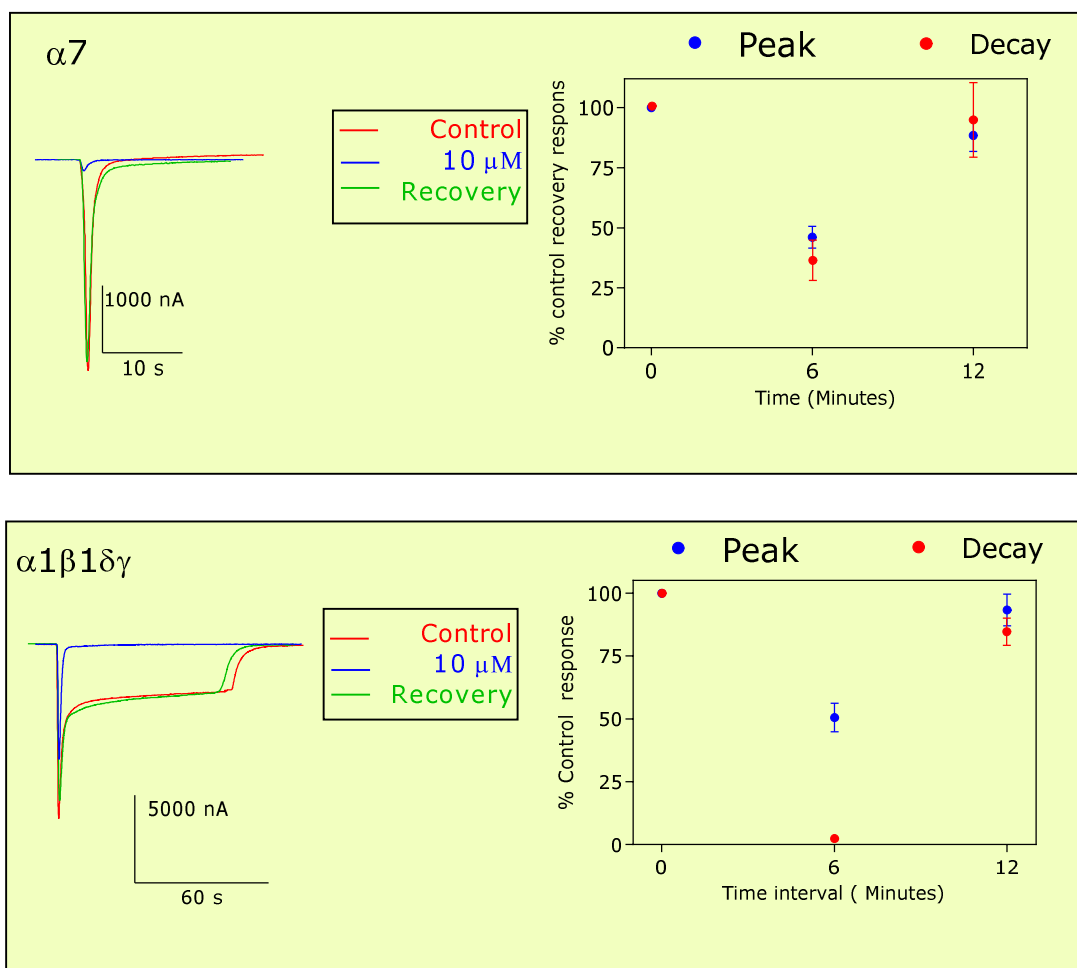


Figure 5.11. Recovery of $\alpha 7$ and $\alpha 1\beta 1\delta\gamma$ nAChRs from antagonism by PhTX-12. Traces in each box show ACh EC_{50} concentration alone (control, recovery) or with $10\mu M$ PhTX-12. Graphs show mean % control response for peak and decay current \pm S.E.M. before (0 min) during (6 min) and after (12 min) co-application of $10\mu M$ PhTX-12.

5.4. Non-competitive action of PhTX-12

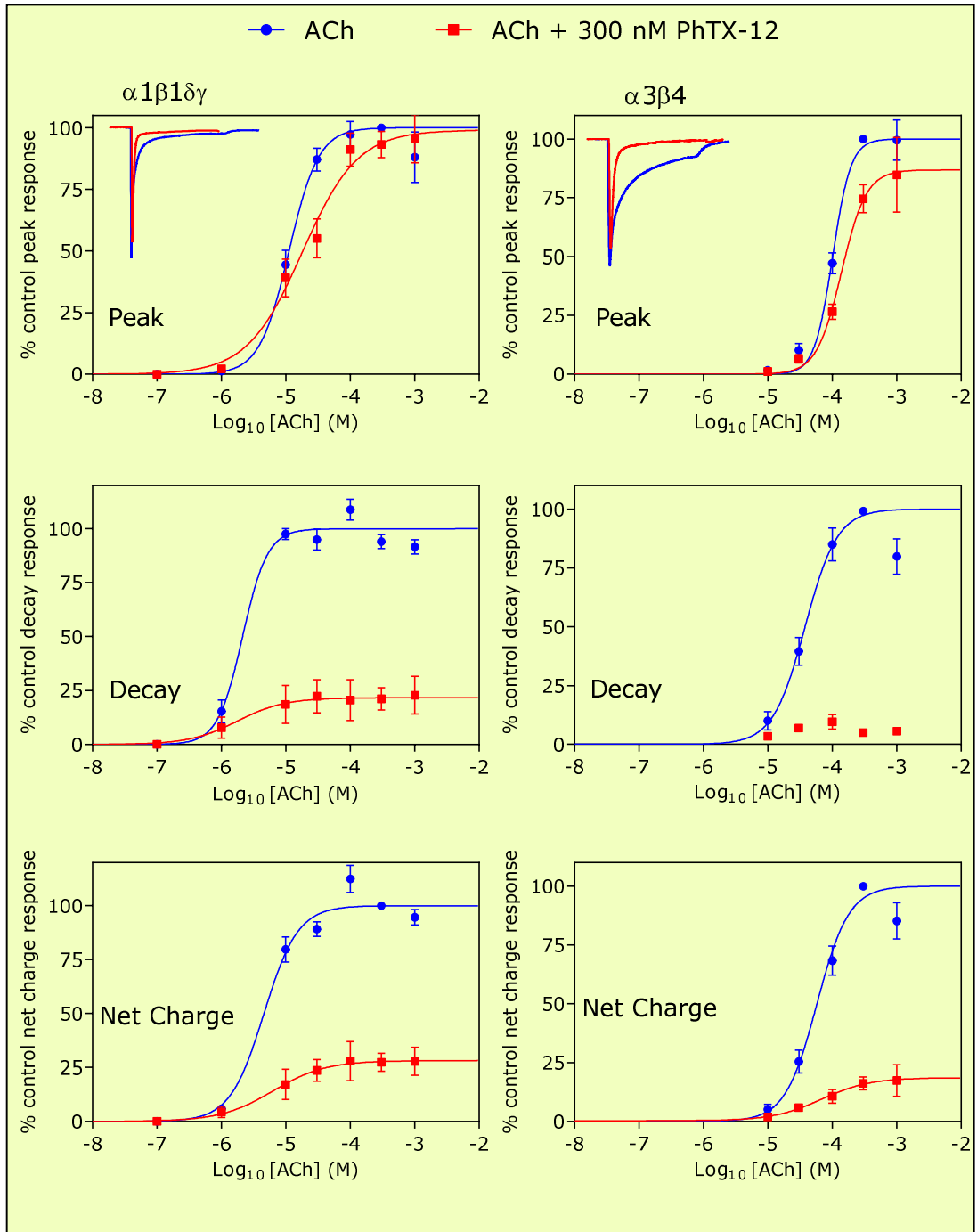
To further determine the mechanisms of inhibition by PhTX-12, ACh concentration-response curves were constructed for $\alpha 3\beta 4$ and $\alpha 1\beta 1\delta\gamma$ in the presence and absence of 300 nM PhTX-12 (**Figure 5.12**). The ACh concentration-response curves did not shift significantly to the right in the presence of 300 nM PhTX-12. The EC_{50} values for peak and decay current and net charge are presented in **Table 5.2**. Thus, in oocytes expressing $\alpha 3\beta 4$ and $\alpha 1\beta 1\delta\gamma$ nAChRs, co-treatment of 300 nM of PhTX-12 with various concentration

of ACh inhibited the magnitude of ACh inward current but this was independent on agonist concentration.

Table 5.2. The effects of 300 nM PhTX-12 on nAChR ACh concentration-response curve. N. not fitted to the equation.

nAChRs		EC ₅₀ value of nAChRs in μ M		
		Peak	Decay	Net charge
α 3 β 4	ACh	101	37	57
	+PhTX-12	139	N.	67
	P value EC ₅₀	0.1605	N.	0.8947
	P value			
	1 mM ACh +PhTX-12	0.6076	<0.0001	<0.0001
α 1 β 1 γ δ	ACh	11	2.1	4.5
	+PhTX-12	18	1.7	6.3
	P value EC ₅₀	0.1591	0.9192	0.7369
	P value			
	1 mM ACh +PhTX-12	0.4347	<0.0001	0.0002

Figure 5.12. (see over) PhTX-12 inhibits ACh mediated current response of nAChRs in a non-competitive manner. Increasing ACh concentrations were applied with or without 300 nM PhTX-12 to oocytes clamped at -80 mV as one minute application at 6 minutes intervals. Traces show whole-oocyte current induced by 300 μ M ACh with or without 300 nM PhTX-12. The EC₅₀ values were estimated from plotted data of average current normalized as percentage of maximum current response in the absence of PhTX-12 against concentration of agonist. The ACh concentration-response curve was shifted downward in the presence of PhTX-12 without any significant change in EC₅₀ values (**Table 5.2**).



CHAPTER SIX

STRUCTURE ACTIVITY RELATIONSHIP OF PhTX-343 ON $\alpha 4\beta 2$ AND $\alpha 3\beta 4$

Summary

Structure-activity studies of 21 analogues of PhTX-343, were investigated on the rat major brain $\alpha 4\beta 2$ and ganglionic $\alpha 3\beta 4$ nAChRs to improve selectivity and potency toward particular subtypes. Eleven synthetic analogues with a single region modification were used to identify the key regions responsible for toxin activity and selectivity. We showed that the difference in conformation that the PhTX polyamine tail can adopt (analogues **1**, **2** and **10**) might be a new approach for the development of new selective inhibitors of nAChRs. Also we identified that the presence of the phenyl group in the head region is critical for improving selectivity toward $\alpha 3\beta 4$ over $\alpha 4\beta 2$ nAChRs or a cyclohexane group for increasing activity. Analogues having both a cyclohexane and phenyl group show IC_{50} values in the pico-molar range and become the most potent inhibitors that have been investigated so far on nAChRs. Ten analogues with double region modification in the head region were used to investigate the role of the hydrophobicity and the bulky size. Overall, analogues show a better selectivity toward ganglion type nAChRs over the brain type with few exceptions such as analogue **7**, which lost selectivity.

6.1. Structure activity relationship (SAR)

A library of philanthotoxin analogues was developed based on the structure of PhTX-343 to identify the key regions of the toxin responsible for the inhibitory activity and selectively on $\alpha 4\beta 2$ and $\alpha 3\beta 4$ nAChRs expressed in *Xenopus* oocytes. The structure of the PhTX-343 molecule is shown in **Figure 6.1** divided into four regions (I, II, III and IV) to obtain systematic replacement in different regions. The IC_{50} values for each analogue were calculated from concentration-inhibition curves and compared to the potency of analogue **1** (PhTX-343) at a holding potential of -100 mV. The parent analogue (**1**) had peak and decay current IC_{50} s of 143 nM and 80 nM respectively for $\alpha 4\beta 2$ and 77 nM and 7 nM respectively for $\alpha 3\beta 4$, and hence 11.4-fold selectivity on the decay current of $\alpha 3\beta 4$ over $\alpha 4\beta 2$ nAChRs. Philanthotoxin derivatives were divided into two categories: single region and double region modification.

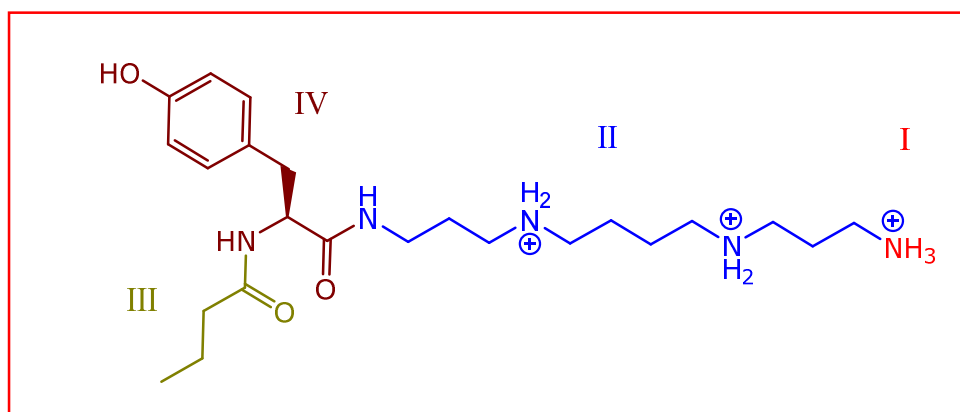


Figure 6.1. Chemical structure of PhTX-343 divided into four regions. (Red) region I= terminal ammonium group, (blue) region II= spermine, (green) region III= butyryl and (brown) region IV= tyrosine.

6.1.1. Single region modification (SRM)

The first category consisted of analogues with a single region modification. Firstly, we started to evaluate the key role of tail regions (I and II) of PhTX-343 in toxin potency by two synthetic analogues **2**, which has less positive charge in region II, and **3**, which has a more bulky group in region I, compared to analogue **1** (**Figure 6.2.** and **Table 6.1**). The potency of analogue **3**, where the terminal amino group (Region I) was replaced by a guanidinium group, on $\alpha 4\beta 2$ nAChRs was reduced approximately 8-fold on peak and 38-fold on the decay current compared to analogue **1**. Substitution of both secondary amino groups in the polyamine chain (region II) with methylene develops analogue **2** (PhTX-12; this has been extensively described in chapter 5), which lost the selectivity between $\alpha 3\beta 4$ and $\alpha 4\beta 2$ shown by **1**. This analogue showed reduced potency compared to the parental analogue **1** by roughly 26-fold on peak and 3-fold on decay current of $\alpha 3\beta 4$, likewise 11-fold reduction was observed on peak current of $\alpha 4\beta 2$ nAChRs but a 2-fold increase in potency was observed on decay current.

Secondly, the pharmacological action of three analogues (**4**, **5** and **6**) with hydrophobic head region (III and IV) modification was investigated. These analogues drastically increased potency and selectivity for $\alpha 3\beta 4$ over $\alpha 4\beta 2$ nAChRs. Extending the aliphatic chain in the region III from four carbon atoms to ten produced analogue **4**. The IC_{50} values on the peak and decay current of $\alpha 3\beta 4$ were 656 nM and 3 nM, respectively. These values were reduced 11.5 fold on peak current and increased 32-fold on decay current when tested on $\alpha 4\beta 2$ nAChRs. Removing the phenolic hydroxyl group from the aromatic nucleus of region IV of PhTX-343 produced analogue **5** with peak and decay IC_{50} value of 13 nM and 0.9 nM respectively on $\alpha 3\beta 4$. This analogue showed considerable selectivity, 16-fold on peak and 30-fold on decay, for $\alpha 3\beta 4$ over $\alpha 4\beta 2$ nAChRs (**Figure 6.3.**), compared to 1.8-fold and 11.4-fold for **1**. Analogue **6** which has a

similar chemical structure to analogue **5**, with the phenylalanyl group extended by only one methylene group, showed a decrease in peak (131 nM) and decay (20 nM) IC_{50} value on $\alpha 4\beta 2$ compared to analogue **5** and caused a reduction in selectivity by 3-fold on peak and 1.5-fold on decay compared to analogue **5**. These data suggest that modifications in head groups are important for increasing PhTX-343 potency and selectivity.

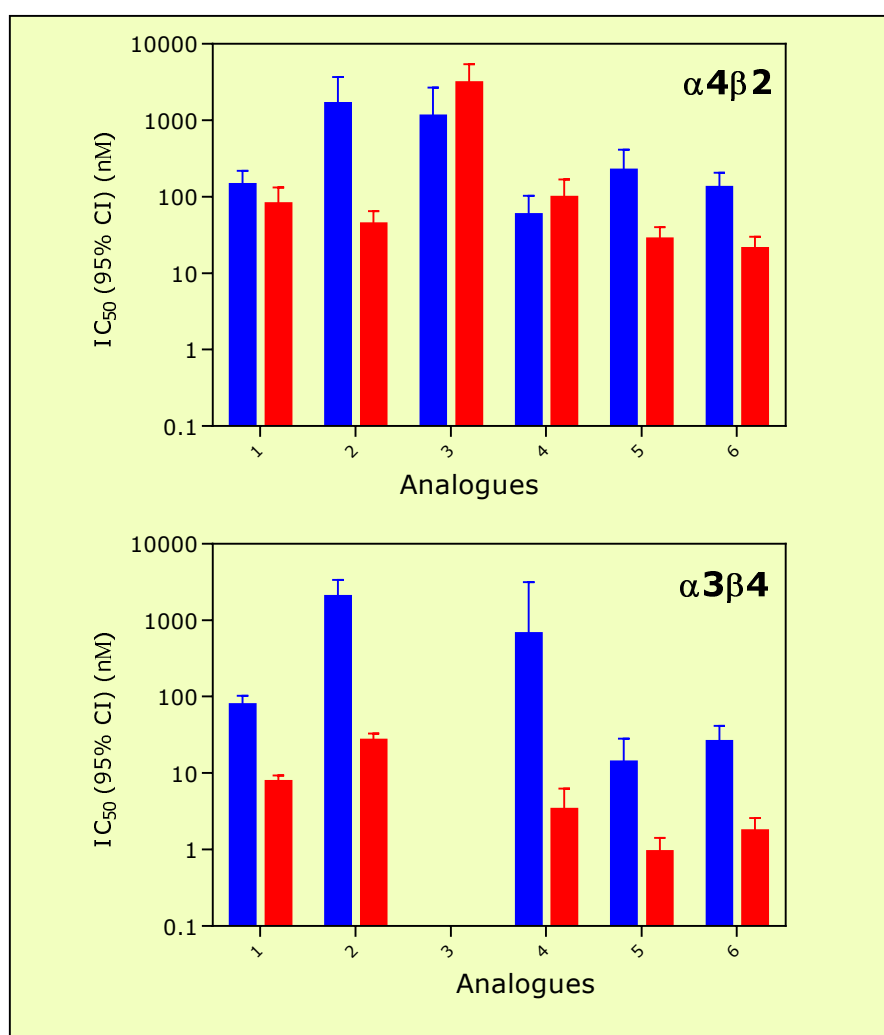


Figure 6.2. Comparison of peak (Blue bars) and decay (Red bars) current potency of PhTX-343 analogues with a single region modification on $\alpha 4\beta 2$ and $\alpha 3\beta 4$ at -100 mV. Each bar represents the analogue's IC_{50} value ($\pm 95\%$ CI) in nM.

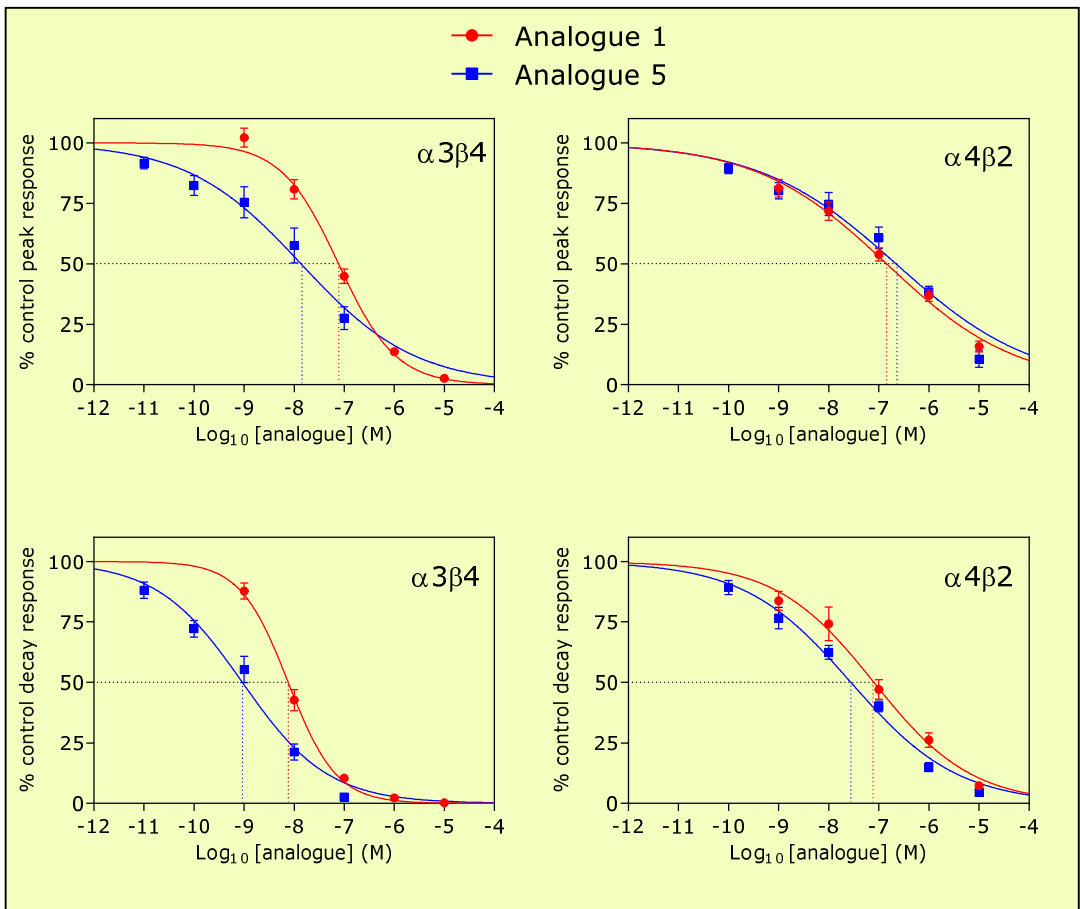
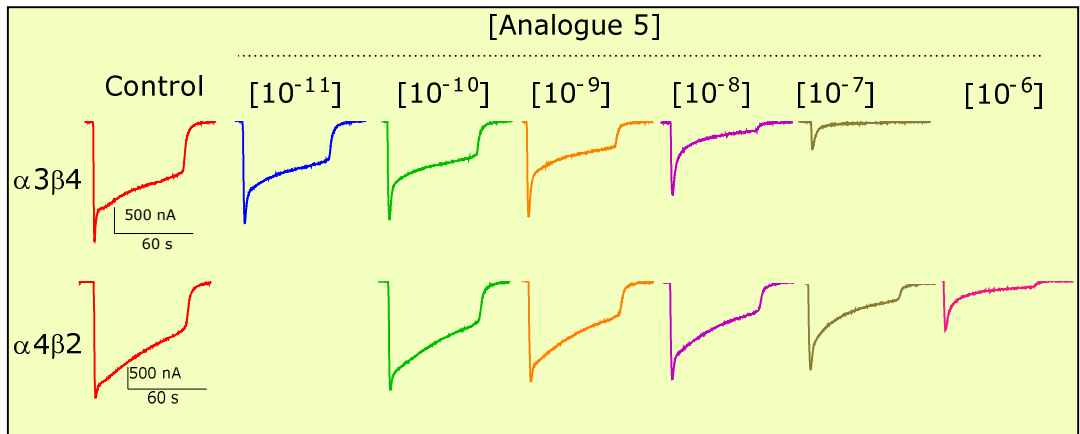
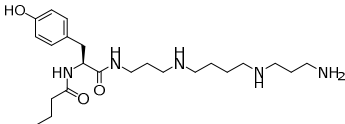
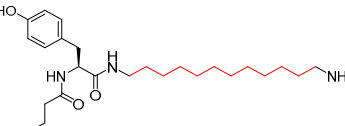
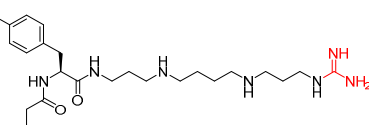
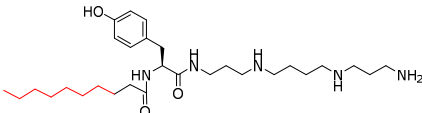
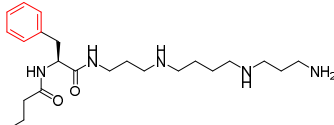
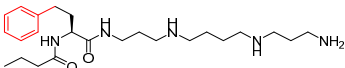


Figure 6.3. Sample traces (top) obtained by co-application of **5** with 100 μM and 10 μM ACh at -100 mV for oocytes expressing $\alpha 3\beta 4$ or $\alpha 4\beta 2$, respectively, and their corresponding concentration-inhibition curves (bottom) compared with parental analogue **1**. Analogue **5** has strong selectivity for $\alpha 3\beta 4$ over $\alpha 4\beta 2$ receptor as shown in example traces and concentration inhibition curves.

Table 6.1. Comparison of PhTX-analogue IC₅₀ values (nM) with single region modification on the major CNS and PNS hetromeric N-nAChRs

PhTX-analogues	$\alpha 4\beta 2$		$\alpha 3\beta 4$			
1. 	P	143 (94-218)	1	77 (58-102)	1	1.8
	n	(7)		(9)		
	D	80 (48-132)	1	7 (6-9)	1	11.4
2. 	P	1641 (734 - 3665)	0.08	2025 (1219-3360)	0.03	0.8
	n	(11)		(8)		
	D	43 (29-64)	1.8	26 (21-33)	0.26	1.6
3. 	P	1131 (480-2661)	0.12			
	n	(7)				
	D	3051 (1736-5362)	0.02			
4. 	P	57 (31-103)	2.5	656 (136-3159)	0.1	0.08
	n	(8)		(8)		
	D	97 (56-168)	0.8	3 (1-6)	2.3	32
5. 	P	220 (118-411)	0.6	13 (6-28)	5.9	16.9
	n	(6)		(6)		
	D	27 (19-39)	2.9	0.9 (0.6-1.4)	7.7	30
6. 	P	131 (84-205)	1.0	25 (1-41)	3	5.2
	n	(6)		(6)		
	D	20 (14-29)	4.0	1 (1-2)	7	20

Peak and decay current are represented as 'P' and 'D' respectively. IC₅₀ (95% CI) are presented in nM and (n) = number of tested oocytes. **Red** values indicate analogue's potency relative to PhTX-343 on the same receptor combination. **Blue** values represent analogue selectivity for $\alpha 3\beta 4$ over $\alpha 4\beta 2$ nAChRs.

Finally, the effect of cyclic groups on the pharmacological action of PhTX-343 was studied. It has been shown previously that substitution of the tyrosine structure with cyclohexylalanine generates the most potent and selective analogue, **7**, of PhTX-343 to have been tested on M-nAChRs expressed in TE671 cells with an IC_{50} value of 60 nM at -100 mV (Olsen et al., 2006). This analogue shows roughly similar IC_{50} for peak inhibition of $\alpha 4\beta 2$ and 2-fold lower on $\alpha 3\beta 4$ receptors, while in the case of decay current the value was in the range of 1 to 2 nM on both combinations (**Figure 6.5**). On the other hand, replacing the butyryl group by cyclohexanoyl produced analogue, **8**, one of the most potent and selective inhibitors that has ever been investigated on N-nAChRs (**Figure 6.6**). The calculated IC_{50} values on the peak and decay current of $\alpha 3\beta 4$ receptors were 2 nM and 400 pM respectively, which are 76-fold and 90-fold lower compared to $\alpha 4\beta 2$ receptors. In addition to that, analogue **9** which has cyclopentanoyl in the position of the butyryl group shows roughly 2-fold increase on peak and decrease on decay current selectivity for $\alpha 3\beta 4$ over $\alpha 4\beta 2$ receptors compared to analogue **8**. Adding cyclopropane with two different orientations, trans and cis, in the polyamine moiety (region II) generated analogues **10** and **11**. These two analogues also show 30 to 40-fold selectivity for major ganglionic type nAChRs over brain type when comparing decay current inhibition.

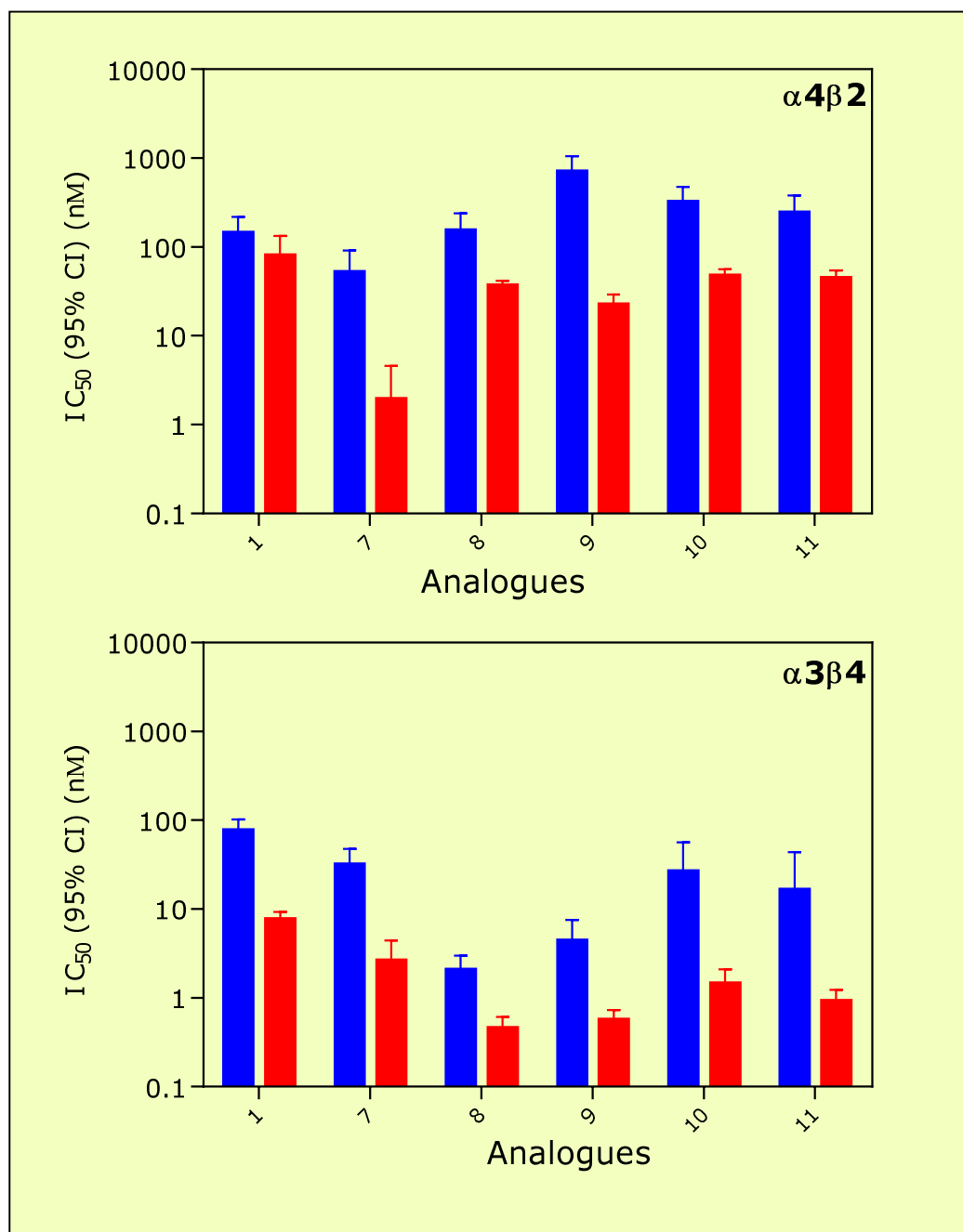


Figure 6.4. Comparison of peak (Blue bars) and decay (Red bars) current potency of PhTX-343 analogues with single region modifications incorporating cycloalkane groups on $\alpha 4\beta 2$ and $\alpha 3\beta 4$ at -100 mV. Each bar represents the analogue's IC₅₀ value ($\pm 95\%$ CI) in nM.

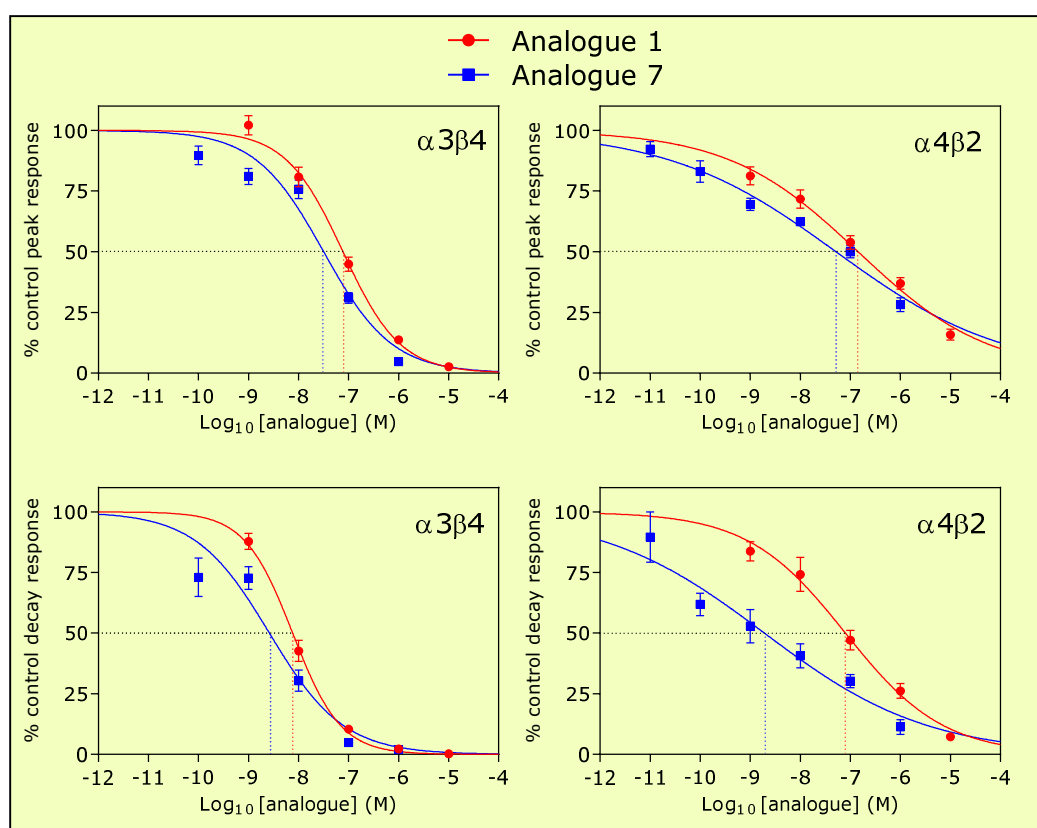
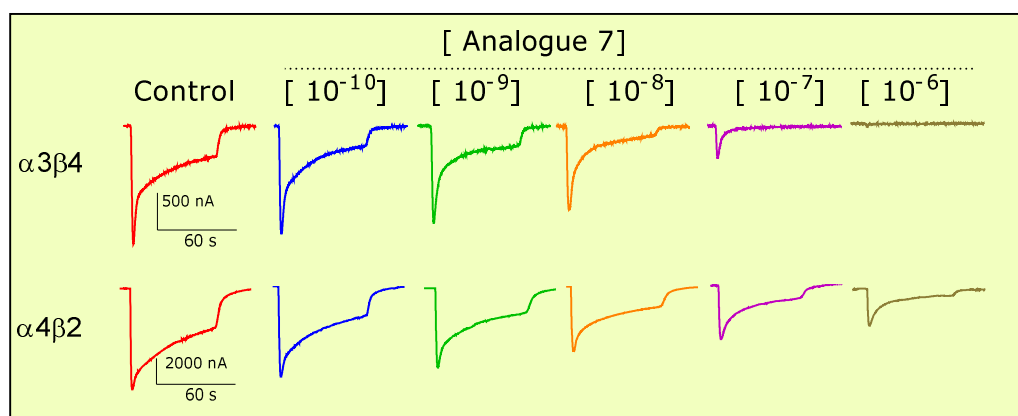
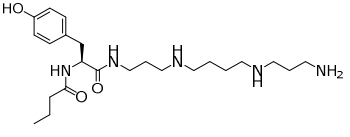
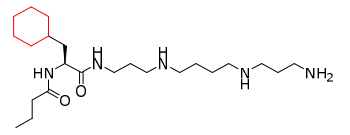
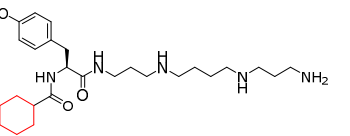
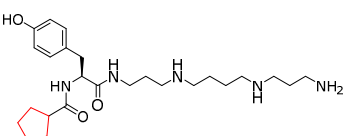
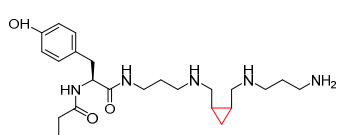
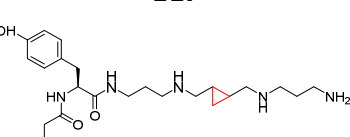


Figure 6.5. Sample traces (top) obtained by co-application of **7** with 100 μM and 10 μM ACh at -100 mV for oocytes expressing $\alpha 3\beta 4$ or $\alpha 4\beta 2$, respectively, and their corresponding concentration-inhibition curves (bottom) compared with parental analogue **1**. Analogue **7** has strong activity on $\alpha 3\beta 4$ and $\alpha 4\beta 2$ receptor but poor selectivity.

Table 6.2. Comparison of PhTX-analogues IC₅₀ values (nM) with single region modification to cyclic alkanes on the major CNS and PNS hetromeric N-nAChRs

PhTX-analogues	$\alpha 4\beta 2$		$\alpha 3\beta 4$			
1. 	P	143 (94-218)	1	77 (58-102)	1	1.8
	n	(7)		(9)		
	D	80 (48-132)	1	7 (6-9)	1	11.4
7. 	P	51 (29-90)	2.8	31 (21-47)	2.4	1.6
	n	(5)		(6)		
	D	1 (0.8-4)	80	2 (1-4)	3.5	0.5
8. 	P	153 (98-238)	0.93	2 (1-2)	38	76.5
	n	(6)		(9)		
	D	36 (28-41)	2.2	0.4 (0.3-0.6)	17.5	90
9. 	P	704 (469-1057)	0.2	4 (2-7)	19.2	176
	n	(8)		(6)		
	D	22 (17-29)	3.6	0.5 (0.4-0.7)	14	44
10. 	P	320 (215-474)	0.4	26.5 (12.5-56.2)	2.9	12
	n	(6)		(6)		
	D	47 (40-56)	1.7	1.44 (0.98-2.10)	4.8	32.6
11. 	P	243 (154-382)	0.5	16.3 (6.1-43.4)	4.7	14.9
	n	(6)		(8)		
	D	44 (36-54)	1.8	0.92 (0.68-1.23)	7.6	47.8

Peak and decay current are represented as 'P' and 'D' respectively. IC₅₀ (95% CI) are presented in nM and (n) = number of tested oocytes. **Red** values indicate analogue potency relative to PhTX-343 on the same receptor combination. **Blue** values represent analogue selectivity for $\alpha 3\beta 4$ over $\alpha 4\beta 2$ nAChRs.

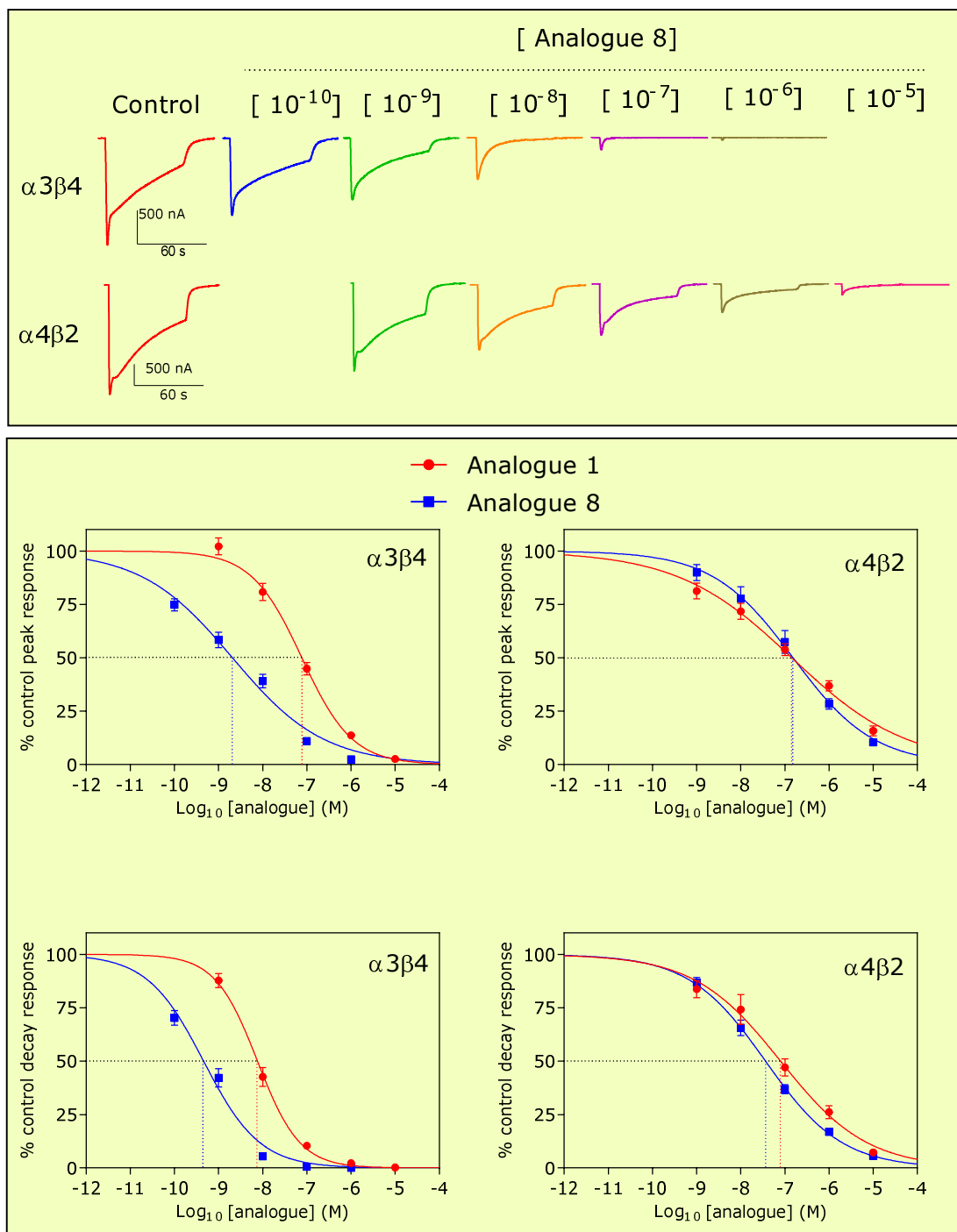


Figure 6.6. Sample traces (top) obtained by co-application of **8** with 100 μM and 10 μM ACh at -100 mV for oocytes expressing $\alpha 3\beta 4$ or $\alpha 4\beta 2$, respectively, and their corresponding concentration-inhibition curves (bottom) compared with parental analogue **1**. Analogue **8** has strong activity and selectivity on $\alpha 3\beta 4$ over $\alpha 4\beta 2$ receptor.

6.1.2. Double region modification (DRM)

The second category include analogues with double region modifications to try and further increase the activity and selectivity of PhTX-343 toward a particular subtype of receptors. Firstly, the role of cyclic group substitution in head regions (III and IV) was investigated. A range of synthetic analogues with double region modification were developed based on the structure of the highly potent compound with a single region modification, analogue **7**. Region IV substitution, tyrosine to cyclohexylalanine, was the same for all analogues **12-17** and the other cyclic group replacement was in region III (**Figure 6.7** and **Table 6.3**). Substitution of the butyryl group by cyclopropanoyl produces analogue **12**, which showed 2.6 fold higher decay current activity compared to analogue **1** on $\alpha 3\beta 4$ and 43-fold selectivity over $\alpha 4\beta 2$ nAChRs. This subtype selectivity reduced to 20, 8.3, 15.5 and 27.7-fold when region III was replaced by cyclobutanoyl **13**, cyclopentanoyl **14**, cyclohexanoyl **15** and norbornanylacetyl **17**, respectively. However, this selectivity was increased in analogue **16** which has cyclooctylacetyl in the position of the butyryl group.

Then several analogues (**18-21**) were synthesised based on the single region modification structure of the highly potent (**7**) and highly selective (**5**) analogues. These four analogues have fixed cyclohexylalanyl at region IV and variable aromatic groups in region III. Analogue **19** was the most potent and selective analogue of PhTX-343 ever tested. This analogue has a naphthalene group in place of the aliphatic chain. The peak and decay current IC_{50} values on $\alpha 3\beta 4$ nAChRs were 1 nM and 160 pM, respectively, and they were 108-fold and 87.5-fold lower compared to $\alpha 4\beta 2$. Approximately the same potency and selectivity was determined for analogue **18** with a single phenyl group in region III. On the other hand, a cinamoyl group in region III, generating analogue **20**, had a 19-fold increase in peak IC_{50} value compared to analogue **19**. Similarly, analogue **21** which has a biphenyl group caused a 55-fold and 17.5-fold

reduction in peak and decay current potency on $\alpha 3\beta 4$ nAChRs. Consequently, the latter two analogues lost selectivity for $\alpha 3\beta 4$ over $\alpha 4\beta 2$, because analogues **18-21** showed roughly the same level of activity on $\alpha 4\beta 2$.

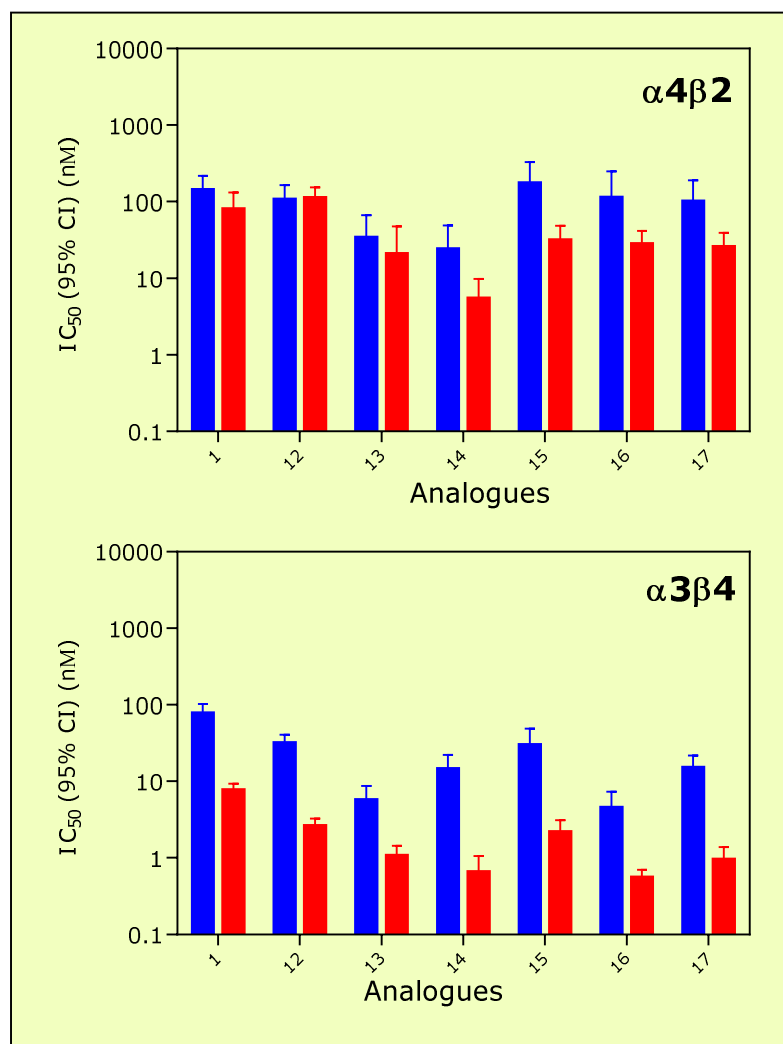
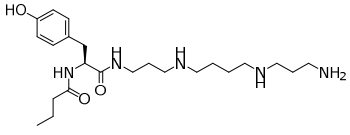
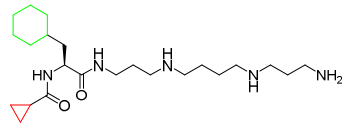
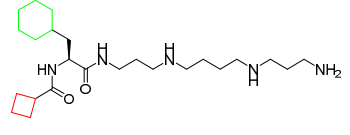
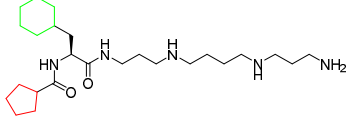
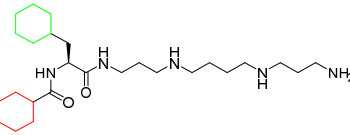
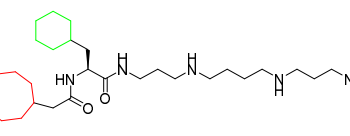
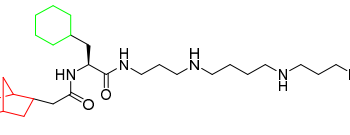


Figure 6.7. Comparison of peak (Blue bars) and decay (Red bars) current potency of PhTX-343 analogues with double region modifications on $\alpha 4\beta 2$ and $\alpha 3\beta 4$ at -100 mV. Each bar represents the analogue's IC_{50} values ($\pm 95\%$ CI) in nM.

Table 6.3. Comparison of PhTX-analogue IC₅₀ values (nM) with double region modification on the major CNS and PNS hetromeric N-nAChRs

PhTX-analogues	$\alpha 4\beta 2$		$\alpha 3\beta 4$	
1. 	P 143 (94-218)	1	77 (58-102)	1 1.8
	n (7)		(9)	
	D 80 (48-132)	1	7 (6-9)	1 11.4
12. 	P 106 (68-164)	1.3	31 (24-40)	2.4 3.4
	n (8)		(5)	
	D 112 (80-154)	0.7	2.6 (2.1-3.2)	2.6 43
13. 	P 34 (17-66)	4.2	5 (3-8)	15.4 6.8
	n (5)		(7)	
	D 20 (9-47)	4	1 (0.7-1.4)	7 20
14. 	P 23 (11-48)	6.2	14 (9-22)	5.5 1.6
	n (5)		(6)	
	D 5 (2-9)	16	0.6 (0.4-1.0)	11.6 8.3
15. 	P 174 (92-330)	0.8	29 (18-48)	2.6 6
	n (7)		(6)	
	D 31 (20-48)	2.5	2 (1-3)	3.5 15.5
16. 	P 112 (50-249)	1.2	4.5 (2.7-7.3)	17.1 24.8
	n (7)		(7)	
	D 28 (19-41)	2.8	0.5 (0.4-0.6)	14 56
17. 	P 100 (53-190)	1.4	14 (10-21)	5.5 7.1
	n (8)		(6)	
	D 25 (16-39)	3.2	0.9 (0.6-1.3)	7.7 27.7

Peak and decay current are represented as 'P' and 'D' respectively. IC₅₀ (95% CI) are presented in nM and (n) is the number of tested oocytes. Red values are indicating analogue's potency relative to PhTX-343 on the same receptor combination. Blue values represent analogue selectivity for $\alpha 3\beta 4$ over $\alpha 4\beta 2$ nAChRs.

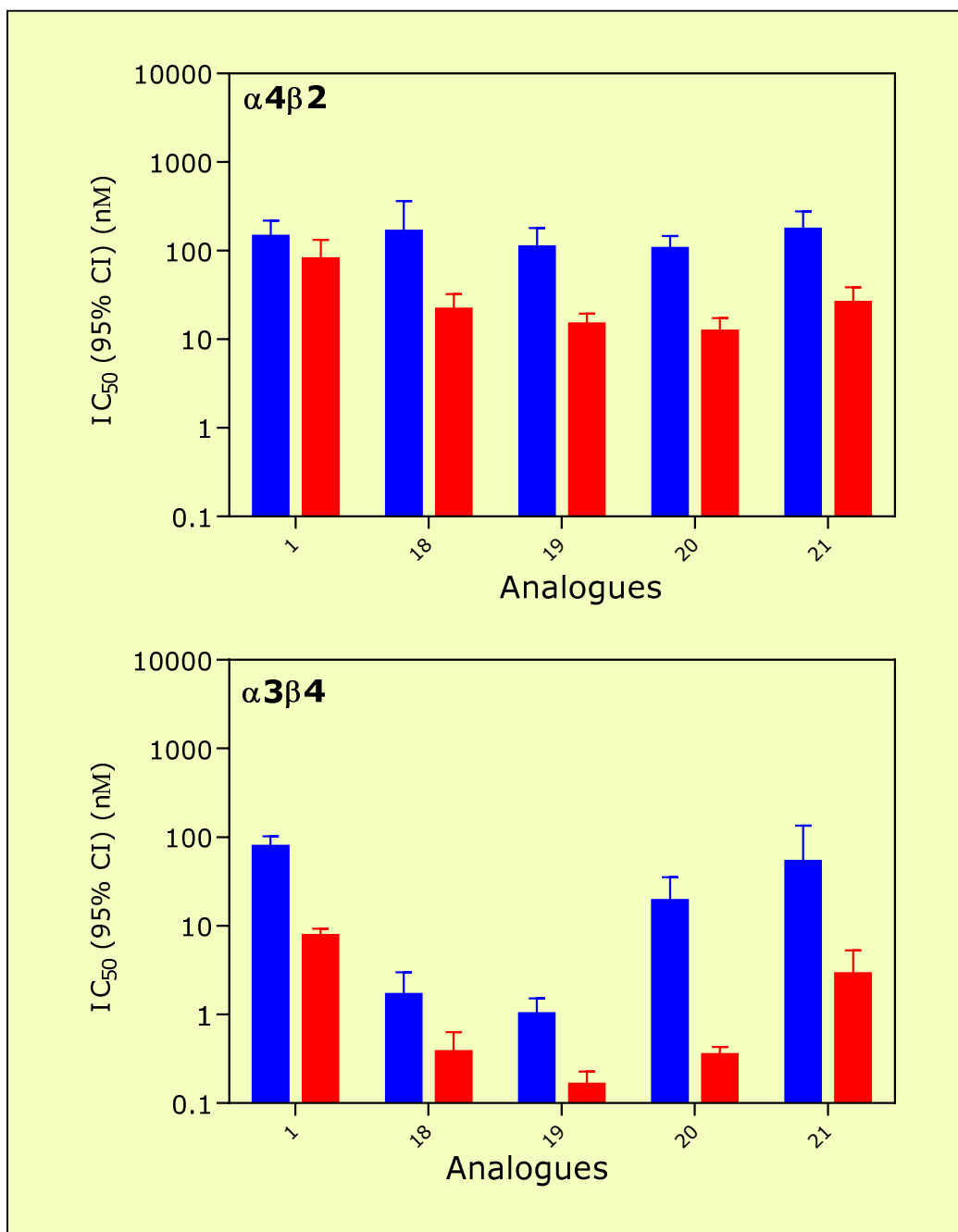
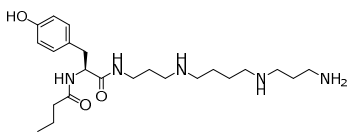
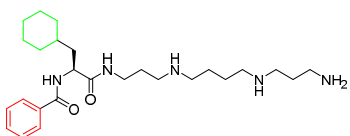
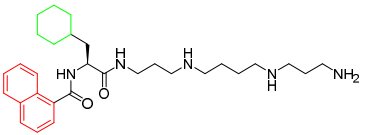
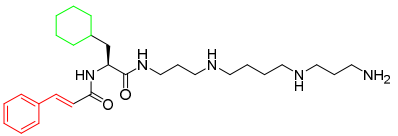
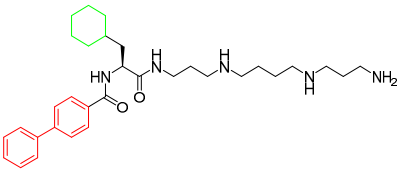


Figure 6.4. Comparison of peak (Blue bars) and decay (Red bars) current potency of PhTX-343 analogues with double region modifications on $\alpha 4\beta 2$ and $\alpha 3\beta 4$ at -100 mV. Each bar represents the analogue's IC_{50} values ($\pm 95\%$ CI) in nM.

Table 6.4. Comparison of PhTX-analogue IC₅₀ values (nM) with double region modifications on the major CNS and PNS heteromeric N-nAChRs

PhTX-analogues	$\alpha 4\beta 2$		$\alpha 3\beta 4$		
1. 	P	143 (94-218)	1	77 (58-102)	1 1.8
	n	(7)		(9)	
	D	80 (48-132)	1	7 (6-9)	1 11.4
18. 	P	163 (73-363)	0.8	1.6 (0.9-2.9)	48 101
	n	(6)		(5)	
	D	21 (14-32)	3.8	0.3 (0.2-0.6)	23.3 70
19. 	P	108 (64-180)	1.3	1.0 (0.6-1.5)	77 108
	n	(5)		(7)	
	D	14 (10-19)	5.7	0.16 (0.11-0.22)	43.7 87.5
20. 	P	104 (74-146)	1.3	19 (10-35)	4 5.4
	n	(5)		(6)	
	D	12 (8-17)	6.6	0.34 (0.27-0.43)	20.5 35.2
21. 	P	171 (105-277)	0.8	52 (20-134)	1.4 3.2
	n	(8)		(4)	
	D	25 (17-38)	3.2	2.8 (1.5-5.3)	2.5 8.9

Peak and decay current are represented as 'P' and 'D' respectively. IC₅₀ (95% CI) are presented in nM and (n) = number of tested oocytes. Red values are indicating analogue's potency relative to PhTX-343 on the same receptor combination. Blue values represent analogue selectivity for $\alpha 3\beta 4$ over $\alpha 4\beta 2$ nAChRs.

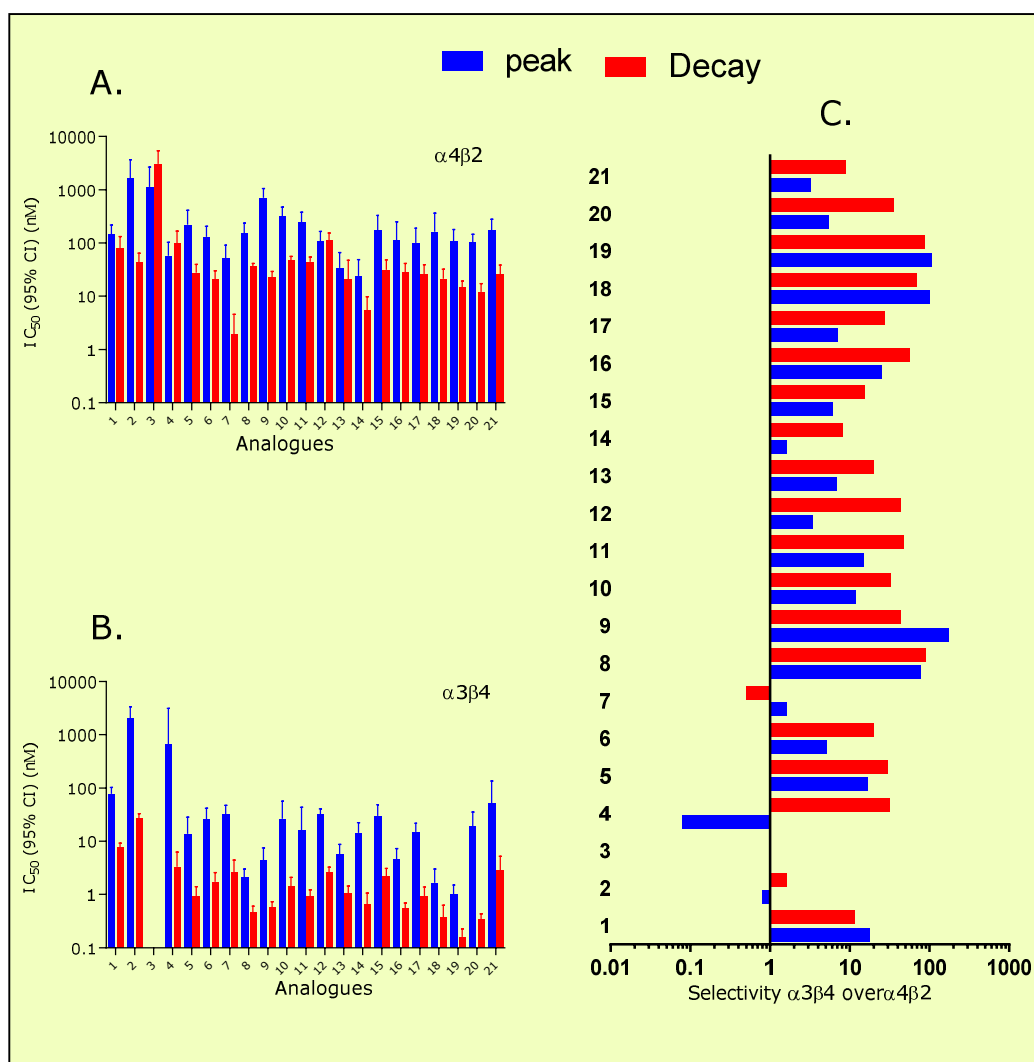


Figure 6.5. Summary of the peak and decay IC_{50} values of the 21-PhTX analogues investigated in this project. Comparison between the peak and decay current IC_{50} values on the same combination (A) $\alpha 4\beta 2$ and (B) $\alpha 3\beta 4$. (C) Showing selectivity of this group of analogues between $\alpha 3\beta 4$ and $\alpha 4\beta 2$.

6.3. Comparison of PhTX-343 potency with two LGIC antagonists

This experiment compared the difference in potency of PhTX-343 with synthetic argiotoxin-636 (ArgTX-636), a natural product from *Argiope lobata* spider (Poulsen et al., 2013) and ketamine (Yamakura et al., 2000b) on rat N-nAChRs. To investigate the role of aromatic group in the selectivity between β 2- and β 4-containing receptors. Here we show ArgTX-636 and ketamine (**Figure 6.6**) inhibit β 4-containing nAChRs with higher potency than β 2-containing, based on decay current IC_{50} value (**Figure 6.7. and Table 6.5**).

The peak current IC_{50} value calculated for ArgTX-636 on α 4 β 2 and α 3 β 4 was 50 nM, roughly the same as peak current IC_{50} value of PhTX-343 on α 3 β 4 (70 nM) but 2.8-fold lower than α 4 β 2 receptors. The decay current IC_{50} value was 80 nM on α 4 β 2 and 40-fold lower on α 3 β 4 at $V_H = -100$ mV. This high selectivity of ArgTX-636 (40-fold) for β 4 over β 2-subunits compared to 11.5 fold for PhTX-343 suggests that ArgTX-636 could serve as a lead compound for highly selective inhibitors of N-nAChRs which has been reported previously for other ionotropic receptors such as NMDAR and AMPAR (Poulsen et al., 2014; 2013).

Ketamine inhibited peak and decay currents of α 4 β 2 nAChRs with IC_{50} values of 36.8 μ M and 19.8 μ M, respectively with roughly 10-fold lower values on α 3 β 4 receptors. This data shows that the potency of ketamine was lower by 55 and 263-fold on the peak current and 271 and 240-fold on decay current of α 3 β 4 and α 4 β 2 nAChRs, respectively compared to PhTX-343. The inhibition data obtained from ArgTX-636 and ketamine further support that channel blockers containing aromatic groups block β 4-containing receptors more effectively than β 2-containing.

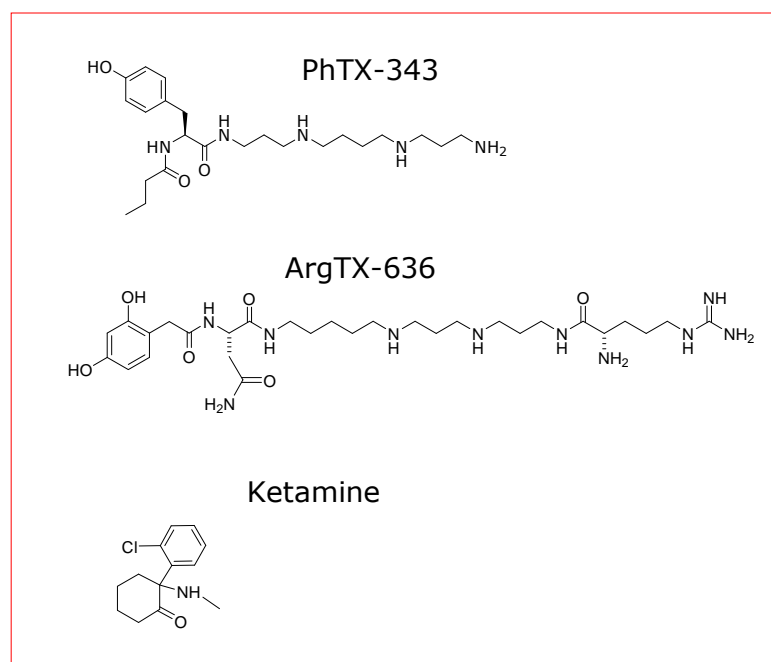


Figure 6.6. Structures of PhTX-343, ArgTX-636 and Ketamine.

Table 6.5. Comparison of PhTX-343 IC₅₀ values (μM) with two LGIC inhibitors

		α4β2		α3β4		
PhTX-343	P	0.14 (0.09-0.21)	1	0.07 (0.05-0.10)	1	2
	n	(7)		(9)		
	D	0.08 (0.08-0.13)	1	0.007 (0.006-0.009)	1	11.4
ArgTX-636	P	0.05 (0.002-0.12)	2.8	0.05 (0.01-0.27)	1.4	1
	n	(6)		(4)		
	D	0.08 (0.03-0.18)	1	0.002 (0.001-0.003)	3.5	40
Ketamine	P	36.8 (18.5-73.4)	0.003	3.4 (1.5-7.8)	0.02	10.8
	n	(5)		(5)		
	D	19.2 (10.1-36.5)	0.004	1.9 (0.63-5.9)	0.003	10.1

Peak and decay current are represented as 'P' and 'D' respectively. IC₅₀ (95% CI) are presented in μM and (n) = number of tested oocytes. Red values are indicating analogue's potency relative to PhTX-343 on the same receptor combination. Blue values represent analogue selectivity for α3β4 over α4β2 nAChRs.

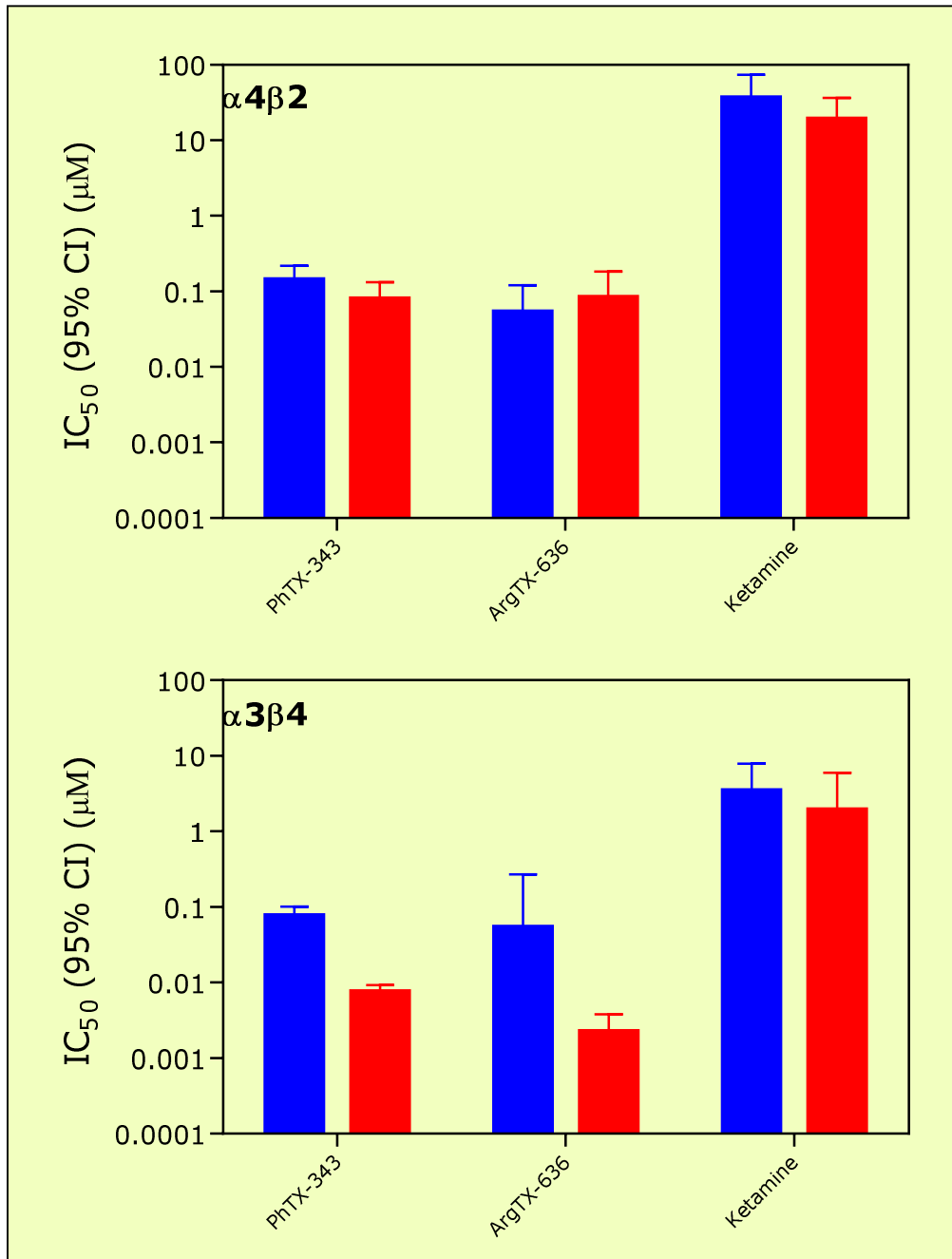


Figure 6.7. Comparison of peak (Blue bars) and decay (Red bars) current potency of PhTX-343 with two other ionotropic receptor inhibitors on $\alpha 4\beta 2$ (top) and $\alpha 3\beta 4$ (bottom) at -100 mV. Each bar represents the toxin's IC_{50} values ($\pm 95\%$ CI).

CHAPTER SEVEN

GENERAL DISCUSSION

Summary

This chapter will summarise the main findings of the study and discuss them in more detail. Firstly, we discuss why mammalian nAChRs are different in their sensitivity to ACh and desensitisation rate. We propose a model based on the size and chemical properties of different amino acids in the agonist binding site loops E and F which might explain the difference in desensitisation rate among mammalian nAChRs. Secondly, we discuss why the inhibition potency of PhTX-343 on mammalian nAChRs is strongly dependent on the β -subunit rather than the α -subunit, and why their potency on β 4-containing receptors is higher compared to β 2, β 1 and non- β -containing receptors. In contrast, the inhibition potency of PhTX-12 is mostly dependent on both the α and β -subunits. We propose a hypothesis based on the distribution of charged residues at the entrance, channel pore and exit of the channel. This hypothesis theoretically explains the reason behind the higher potency of PhTX-343 on N-nAChRs over M-nAChRs, but it does not explain the reason behind subunit-specificity among N-nAChRs. Also, it explains the basis of voltage-independence of PhTX-12 on M-nAChRs and slightly higher voltage-dependence on N-nAChRs. Finally, we discuss in more detail, the structure-activity relationship of PhTX analogues and the possible reasons behind the changes in activity and selectivity for the tested analogues on the major brain α 4 β 2 and ganglionic α 3 β 4 N-nAChRs.

7.1. Characterization of the ACh response of the nAChRs expressed in *Xenopus* oocytes

In common with previous reported studies in the literature on *Xenopus* oocytes expressing various subtypes of nAChRs (Chavez-Noriega et al., 1997; Luetje and Patrick, 1991) the whole-cell ACh response shows a fast peak current (ms) after application of ACh followed by a decaying current under prolonged exposure to the agonist with the rate depending on subunit combination. Results from our studies are in agreement with previously reported data showing that ACh at concentrations of 1 mM or higher can act as a channel blocker and reduce the maximum response and affect the desensitization rate and hence net charge movement (Luetje and Patrick, 1991; Maconochie and Knight, 1992). It appears that inhibition of $\beta 4$ -containing receptors is higher than that for $\beta 1$, $\beta 2$ and non- β -containing receptors. Receptor blocking theory by a high agonist concentration is not distinctive to nAChRs but also found in other members of the LGIC family (Jones and Westbrook, 1996).

Differences in the agonist selectivity and sensitivity profile have been reported for rat nAChRs and their human homologues (Chavez-Noriega et al., 1997). Francis et al (2000) reported an EC_{50} value of 53 μM for ACh peak current of human $\alpha 4\beta 2$ with roughly 2-fold lower value on $\alpha 4\beta 4$ N-nAChRs at $V_H = -50$ mV. Other studies calculated an EC_{50} value of 48 μM for human $\alpha 4\beta 4$ and 22-fold lower value for $\alpha 4\beta 2$ nAChRs at $V_H = -70$ mV (Yamakura et al., 2000b). Here, we reported EC_{50} values of 7.2 μM and 10 μM for rat $\alpha 4\beta 4$ and $\alpha 4\beta 2$ at $V_H = -80$ mV. The peak current EC_{50} values obtained previously from oocytes expressing rat $\alpha 4\beta 2$ nAChRs was 2 μM at -70 mV and 4-fold lower than for rat $\alpha 4\beta 4$ nAChRs (Yamakura and Harris, 2000). On the other hand the peak current EC_{50} value of rat $\alpha 3\beta 4$ was 116 μM and $\alpha 3\beta 2$ was 25 μM in this study; roughly the same ACh sensitivity variation has been reported between both $\alpha 3$ -containing nAChRs but with different potency (Yamakura et al., 2000b). EC_{50}

values of 177 μM and 12 μM have been reported for human $\alpha 7$ (Giniatullin et al., 2005) and embryonic M-nAChRs respectively. These values are in a close agreement with the EC_{50} values calculate in this project which are 150 μM for human $\alpha 7$ and 12 μM for embryonic M-nAChRs.

The rank order of decay current and net charge EC_{50} value based on the α -subunit was $\alpha 4 < \alpha 1 < \alpha 7 < \alpha 3$ -containing receptors. While based on the β -subunit the desensitization rate order were non- β -containing $> \beta 2 > \beta 4$ and $\beta 1$ -containing. We proposed a model based on the loops A-F that participate in the ACh binding pocket. This model might explain the reason behind the difference in the desensitization rate between nAChR combinations used in this study. We identified from the sequence alignment the main amino acids participating in loop A-C of the principle subunit based on the *Torpedo marmorata* $\alpha 1$ -subunit and loop D-F from the complementary subunit based on the δ - and γ -subunits of *Torpedo californica*.

The model is based on the size, number and properties of the key residues that participate in the ACh binding pocket. It appears from our model that the amino acids participating in loops A-C are identical in all principle subunits, $\alpha 1$, $\alpha 3$, $\alpha 4$ and $\alpha 7$, used in this study. Similarly, ACh binding residues in loop D of the auxiliary subunits were identical, while the main differences were observed in loops E and F. The presence of five small neutral asparagine residues in loop E of the $\alpha 7$ subunit might be the main reason behind its fast desensitization rate. In addition, reducing the number of these small neutral residues in heteromeric $\beta 2$ -containing nAChRs to two or three neutral serine residues might explain their slower desensitization compared to homomeric $\alpha 7$ receptors. On the other hand, the lowest desensitization rate between N-nAChRs was observed for $\beta 4$ -containing nAChRs; this might be due to the presence of a large and positively charged arginine in their loop E. We have shown that M-nAChRs have the lowest desensitization rate between all types of nAChRs and

this might be due to the complex interaction due to the presence of aromatic tyrosine in loop E of the δ -subunit and neutral hydrophilic serine in the γ -subunit. The presence of loop F in M-nAChRs and their absence in N-nAChRs might be the other reason that explains the low desensitization rate of M-nAChRs.

Although there is no evidence in the literature to support the idea that desensitization rates are governed by the ligand binding pocket residues, it has been shown previously that the desensitization rate of $\alpha 7$ nAChRs is decreased by substitution of threonine in ring 5 of **Table 7.1** by serine without modifying any other functional properties of the receptor (Placzek et al., 2005). Therefore, it will be worth investigating this model in the future and see if there is any relationship between agonist binding site residues and desensitization rate.

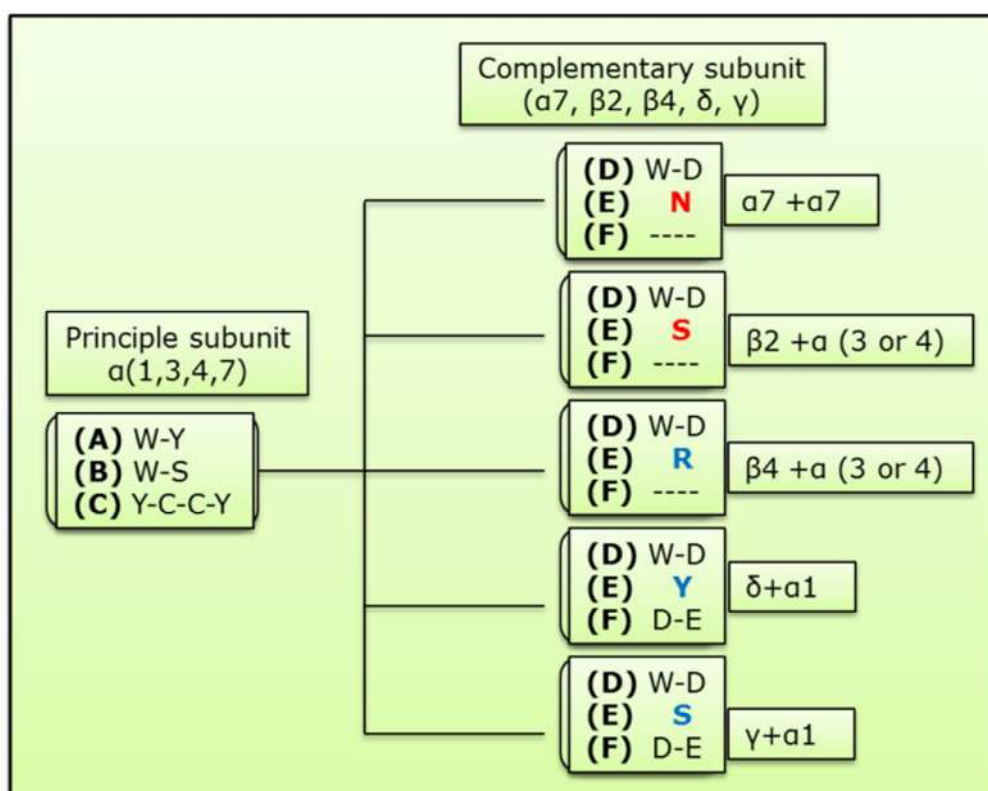


Figure 7.1. Model illustrating the key amino acids that participate in the ACh binding pocket based on the identified residues in the loops of the principle and complementary subunits of *Torpedo* species.

7.2. Screening PhTX-343 and PhTX-12 for nAChR subtype selectivity

The results presented in this investigation show that the mechanism of inhibition and recovery of vertebrate nAChRs in response to PhTX-343 is strongly influenced by their subunit combination. The β -subunit was more influential on the inhibition potency of PhTX-343 than the α -subunits. On the other hand, their inhibition and recovery by PhTX-12 did not depend strongly on any particular subunit-types. Previous work by Brier et al (2003) showed 22-fold higher activity for PhTX-12 on embryonic muscle-type nicotinic acetylcholine receptors (M-nAChR) naturally expressed in the TE671 cell line in comparison to PhTX-343. In the present study, PhTX-12 also shows higher potency over PhTX-343 on M-nAChRs expressed in *Xenopus* oocytes but does not show any considerable selectivity over N-nAChRs. On the other hand, PhTX-343 inhibits homomeric $\alpha 7$ -nAChRs with lowest potency between all investigated N-nAChRs combinations. Heteromeric $\beta 4$ -containing nAChRs were more sensitive to PhTX-343 compared to $\beta 2$ -containing receptors. The idea of $\beta 4$ -subunits having a higher sensitivity than $\beta 2$ -subunits has been investigated previously for other open channel blockers of nAChRs such as substance P (Stafford et al., 1998) and cocaine (Francis et al., 2000). However, the contrary of this idea has been confirmed for other compounds such as hexanol, pentobarbital and gaseous inhibitors such as nitric oxide (Yamakura et al., 2000a; Yamakura and Harris, 2000).

PhTX-343 tail region (I and II) amino groups become fully protonated at physiological pH (Stromgaard et al., 1999). Inhibition of ACh-induced current in nAChRs expressed in *Xenopus* oocytes by PhTX-343 was time-, subunit- and concentration-dependent. Results from our current inhibition experiments show that inhibition of peak current by PhTX-343 is less effective than on decay current and it was in agreement with Liu et al (1997). This variation in potency indicates that to interact with their binding sites and inhibit nAChRs, PhTX-343

requires time for channels to open as a consequence of signal transduction between receptor activation and gate opening (Brier et al., 2003).

Evidence from this investigation shows that PhTX-343 at a concentration of 1 nM potentiated the ACh response by $\sim 6\%$ of a few nAChR combinations such as $\alpha 7$ and $\alpha 4\beta 4$ receptors. The response potentiation might be via PhTX binding to the agonist site and might be via binding to an allosteric site which has been suggested previously for NMDA receptors (Anis et al., 1990). This finding of potentiation of the nAChR response by concentrations of 1 nM and less is in agreement with Brackley et al (1990) who found it in *Xenopus* oocytes expressing chicken N-nAChRs and Shao (1997) found it in the TE671 cell line naturally expressing M-nAChRs. Stromgaard et al (2002) reported potentiation of M-nAChRs in TE671 cells by PhTX-10. Furthermore, Shao et al (1998) observed the same phenomenon with spermine.

Our studies show that nAChRs containing $\beta 4$ -subunits had the highest affinity binding sites for PhTX-343 with the lowest IC_{50} values of all nAChRs investigated. The decay IC_{50} value for $\alpha 3\beta 4$ current inhibition by PhTX-343 calculated in this work was 80 nM at $V_H = -60$ mV and this was approximately double for $\alpha 4\beta 4$ nAChRs. These values were in the same IC_{50} value range reported previously by a patch-clamp study of the PC12 cell line, 100 nM (Liu et al., 1997). It has been shown that PC12 cells might express more than a single population of N-nAChRs but $\alpha 3\beta 4$ combinations are dominant (Rogers et al., 1992). PhTX-343 potency reduced 5.6-fold and 19.8-fold on $\alpha 4\beta 2$ and $\alpha 3\beta 2$ receptors, respectively, compared to $\alpha 3\beta 4$ nAChRs. Due to the unique regional distribution of $\beta 4$ and $\beta 2$ -subunits in the CNS and PNS (Zoli et al., 1995) and the selectivity of PhTX-343, this compound could be considered as a candidate for drug development.

It has been shown by molecular modelling and photolabile cross-linking studies that PhTX-343 enters inside the channel of nAChR (Bixel et al., 2000;

Tikhonov et al., 2004). Therefore, this variation in sensitivity between $\beta 2$ and $\beta 4$ subunit containing nAChRs might be due to a single amino acid difference between the M2 domain of $\beta 2_{(V253)}$ and $\beta 4_{(F255)}$, which is supposed to face the channel pore (Imoto et al., 1986; Oiki et al., 1988) or variation in other parts of the subunit such as the N-terminals (Stafford et al., 1998). Higher potency of PhTX-343 in $\beta 4$ -containing nAChRs might be due to stabilization of their protonated ammonium group with π -electrons of the aromatic phenylalanine which have been proposed previously for substance P (Stafford et al., 1998) or an aromatic stacking interaction (π - π electrons interaction) of the tyrosine moiety with phenylalanine. Inhibition of $\alpha 3\beta 4$ peak ($p=0.7124$) and decay ($p=0.3273$) currents were not changed significantly by phenylalanine substitution in $\beta 4$ -subunits by valine at $V_H = -60$ mV. However, replacing valine in the $\beta 2$ -subunit by phenylalanine significantly reduced the decay current IC_{50} value of $\alpha 4\beta 2$ to the level of $\alpha 3\beta 4$ ($p<0.001$) and it was significantly 2-fold lower on the peak current ($p=0.0302$). Similarly, expressing $\beta 4_{(F255V)}$ with the $\alpha 4$ -subunit did not produce any significant change in peak ($p=0.082$) and decay ($p=0.1210$) IC_{50} value at $V_H = -100$ mV compared to wild-type, whereas, $\alpha 3\beta 2_{(V253F)}$ significantly increased peak ($p=0.0114$) and decay ($p<0.001$) current potency compared to $\alpha 3\beta 2$ nAChRs. Therefore, this single amino acid residue difference in the M2 domain, between $\beta 2$ -subunit (V253) and $\beta 4$ -subunit (F255) is critical for the PhTX-343 potency on $\beta 2$ but not for $\beta 4$ -containing nAChRs. This point mutation in the M2 domain of the β -subunit has been shown to change sensitivity, at least partially, of other nAChRs to blockers such as cocaine (Francis et al., 2000), substance P (Stafford et al., 1998) and nitric oxide (Yamakura et al., 2000a).

The highest PhTX-343 decay IC_{50} value calculated for N-nAChRs was 6.5 μM for homomeric $\alpha 7$ receptors at $V_H = -60$ mV; 81-times higher than for $\alpha 3\beta 4$. As expected, M-nAChRs showed the lowest sensitivity to PhTX-343 compared to

all N-nAChRs. This difference in the sensitivity of nAChRs to PhTX-343 might be due to the difference in the distribution pattern of charged amino acid rings that 'guard' the entrance and exit of the channel pore, as shown in **Table 7.1** (Dani and Bertrand, 2007). We suggested a hypothesis based on the positions of positive and negative amino acids in the channel entrance and exit and their relationship with positive charges on PhTX-343. Theoretically, this hypothesis explains the reason behind low potency of PhTX-343 on M-nAChRs compared to heteromeric N-nAChRs but not homomeric $\alpha 7$ -nAChRs, which has unique pharmacological properties due to the absence of a β -subunit. Practically it requires further investigation by site directed mutagenesis to confirm the role of residues supposed to have a role in this hypothesis.

The hypothesis has several steps. Firstly, it is well known that nAChRs are cation selective ion channels having negatively charged residues in the loop between the M2 and M3 domains which surround the outer mouth parts of the channel to attract positively charged ions to the channel pore entrance (Dani and Bertrand, 2007; Galzi et al., 1992). In neuronal subunits negatively charged aspartate is present in the loop between M2 and M3 domain of $\beta 2_{D292}$, $\beta 4_{D311}$ and $\alpha 7_{D288}$, while in muscle subunits a glutamate is found in $\beta 1_{E300}$, γ_{E245} and ϵ_{E296} . The position and numbers of these negatively charged amino acids might be responsible for the high sensitivity of N-nAChRs for PhTX-343 over M-nAChRs. It has been shown that injection of oocytes with a different neuronal $\alpha:\beta$ subunit ratio can generate various populations of receptors that are pharmacologically different. Therefore, an injection ratio of 1:1 might generate a mixture of $2\alpha+3\beta$ or $3\alpha+2\beta$ (Zwart and Vijverberg, 1998). Heteromeric N-nAChRs consisting of $3\beta(2 \text{ or } 4)$ subunits will have three negatively charged aspartate compared to two glutamate in $\beta 1$ and γ subunits of M-nAChRs. This might conclude that M-nAChRs has lower probability than heteromeric N-nAChRs to attract a positively charged molecule like PhTX-343. This hypothesis could be further tested by

investigating the actions of PhTX-343 on the ACh-gated chloride channels. These receptors might belong to the Cys-loop LGIC superfamily because they are functionally identical to nAChRs but selective for chloride ions. They have been identified so far only in invertebrates such as the snail *Lymnaea* (van Nierop et al., 2005).

Table 7.1. Amino acid sequence of the M1-M2 loop, the M2-domain and the M2-M3 loop from the subunits used in this study from three different species r (rat), m (mouse) and h (human). Positively charged amino acids are coloured green, negatively charged orange. Blue and red amino acids are the single difference between M2 domains of $\beta 2$ and $\beta 4$ -subunits. The numbers (1-8) refer to **rings** of amino acids that line the pore from extracellular to intracellular (outer charged glutamate, leucine, valine, equatorial leucine, serine, threonine, intermediate glutamate and internal aspartate ring, respectively).

	8	7	6	5	4	3	2	1	
r- $\alpha 3$	DCG- E KVTL	CISVLL	SLTVFLL	VIT E TIP	STSLVI	PLIG			299
r- $\alpha 4$	E CG- E KVTL	CISVLL	SLTVFLL	L L IT E II	PSTSLVI	PLIG			309
r- $\beta 2$	DCG- E KMTL	CISVLL	L A LT V FLL	L L ISKIV	PPTSLD	VPLVG			297
r- $\beta 4$	DCG- E KMTL	CISVLL	L A LT F FLL	L L ISKIV	PPTSLD	IPLIG			316
m- $\alpha 1$	DSG- E KMTL	SISVLL	SLTVFLL	VIV E LIP	STSSAV	PLIG			295
m- $\beta 1$	DAG- E KMGL	SIFALL	T L TVFLL	L L ADKVP	ETSLAV	PIII			309
m- δ	DCG- E KTSV	AISVLL	AQSVFLL	L L ISKRL	PATSM	AIPLVG			313
m- γ	KAGG Q KCTV	ATNVLL	AQTVF	FLVAKK	V P ETS	QAVPLIS			254
m- ϵ	KAGG Q KCTV	SINVLL	AQTVF	FL L IA Q KIP	ETSL	SVPLLG			305
h- $\alpha 1$	DSG- E KMTL	SISVLL	SLTVFLL	VIV E LIP	STSSAV	PLIG			320
h- $\alpha 7$	DSG- E KISL	GITVLL	SLTVF	M L VA E IMP	ATSD	SVPLIA			294
h- $\beta 1$	DAG- E KMGL	SIFALL	T L TVFLL	L L ADKVP	ETSL	SVPIII			309
h- δ	DSG- E KTSV	AISVLL	AQSVFLL	L L ISKRL	PATSM	AIPLIG			310
h- γ	KAGG Q KCTV	AINVLL	AQTVF	FLVAKK	V P ETS	QAVPLIS			306
h- ϵ	QAGG Q KCTV	SINVLL	AQTVF	FL L IA Q KIP	ETSL	SVPLLG			305
h- $\alpha 5$	N E G - E KICL	CTSVLV	SLTVFLL	V I E EII	PSSSK	V I PLIG			314
h- $\alpha 9$	A S G - E KVSL	GV T ILL	AMTVF	QLMVA E IMPA	-SEN	VPLIG			300
h- $\alpha 10$	DSG- E KVSL	GV T VLL	L A LT V FQ	LL L A E SMPP	-A E S	VPLIG			229
h- $\alpha 2$	DCG- E KITL	CISVLL	SLTVFLL	L L IT E II	PSTSLVI	PLIG			329
h- $\alpha 3$	DCG- E KVTL	CISVLL	SLTVFLL	VIT E TIP	STSLVI	PLIG			305
h- $\alpha 4$	E CG- E KITL	CISVLL	SLTVFLL	L L IT E II	PSTSLVI	PLIG			309
h- $\alpha 6$	DCG- E KVTL	CISVLL	SLTVFLL	VIT E TIP	STSLV	VPLVG			304
h- $\beta 2$	DCG- E KMTL	CISVLL	L A LT V FLL	L L ISKIV	PPTSLD	VPLVG			298
h- $\beta 4$	DCG- E KMTL	CISVLL	L A LT F FLL	L L ISKIV	PPTSLD	VPLIG			296
h- $\beta 3$	D E G - E KLSL	STSVLV	SLTVFLL	V I E EII	PSSSK	V I PLIG			297

Secondly, the outer glutamate ring (1) is the first barrier that PhTX-343 faces to enter the channel from the extracellular side. The distribution ratio of positive to negatively charged residues near to the pore entrance may drastically affect the potency of PhTX-343. Heteromeric N-nAChRs will have two or maximum three positively charged amino acids in the ring 1 area depending on the number of β -subunits containing a lysine, while in the case of M-nAChRs five positively charged residues are present in this region (1 lysine from β 1, 2 lysine from γ and 1 lysine + 1 arginine from δ subunits) and none in α 7 receptors. The presence of this large number of positive charges at the external entrance of the pore in M-nAChRs compared to N-nAChRs might be the main reason that reduce the chance of fully protonated PhTX-343 polyamine tail to enter their channel (Brier et al., 2003).

Finally, there are several other charged residues further down in the channel pore which might affect the action of PhTX-343. For example ring 7, which is a negatively charged glutamate in all subunits except muscle γ and ϵ subunits, where it is a neutral glutamine. The latter two muscle subunits also have a positively charged lysine residue in ring 8 which is conversely negatively charged in all other subunits. In addition, the presence of conserved polar residues (serine, threonine or asparagine) in rings 5 and 6 of all nAChRs used in this study except the muscle β 1-subunit, which contains phenylalanine and glycine respectively, might also be responsible for the low activity of PhTX-343 on M-nAChRs. This hypothesis might explain the low sensitivity of M-nAChRs to PhTX-343 compared to N-nAChRs, but does not clarify the reason behind the subunit-specific selectivity between N-nAChRs.

This hypothesis arises from an explanation of the differences in the inward rectification phenomena and Ca^{2+} permeability among subtypes of AMPARs. Previous studies (Hollmann et al., 1991; Hume et al., 1991; Mellor, 2010; Verdoorn et al., 1991) reported that the Q/R site from M2 which is located

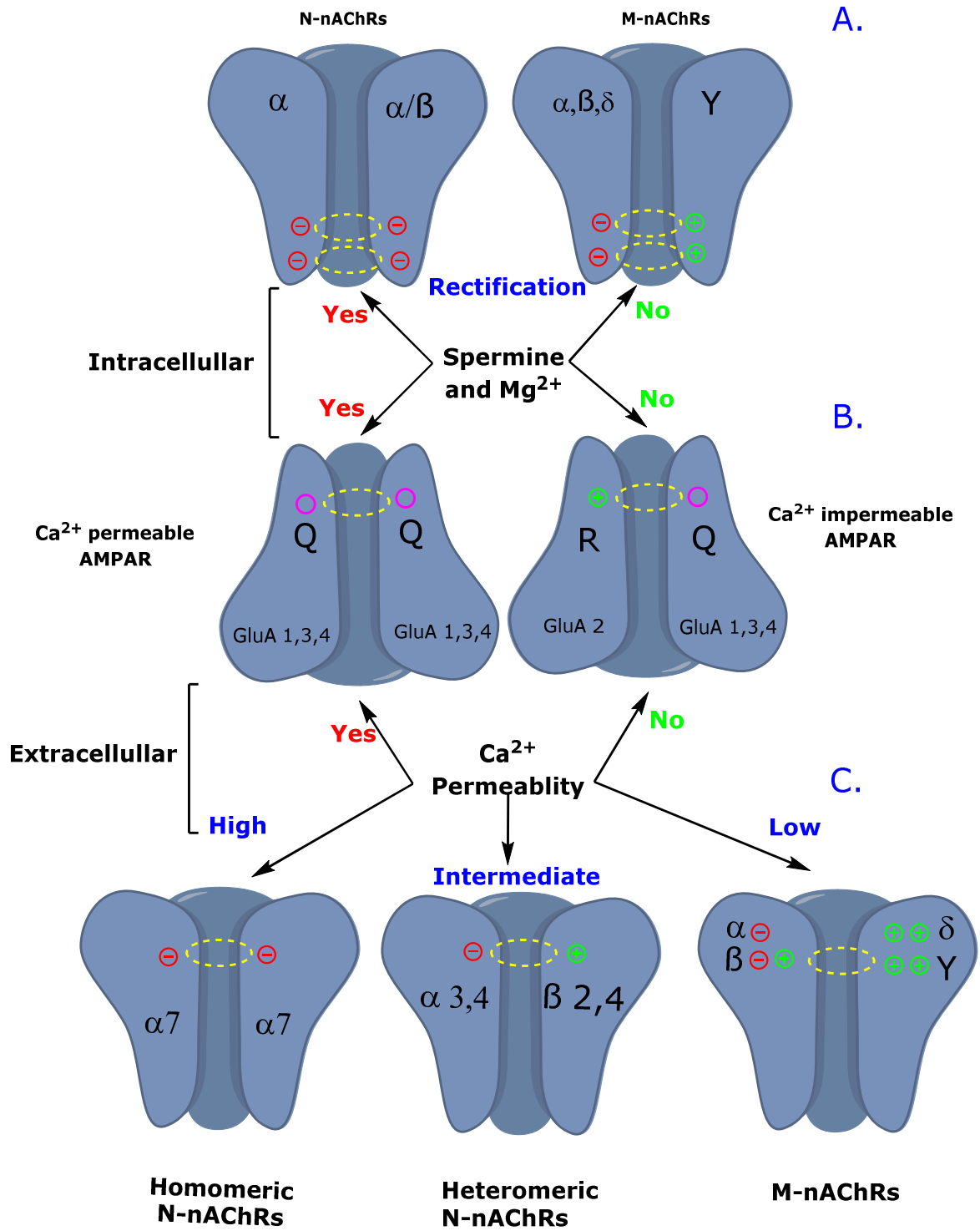
at the narrowest part of the AMPAR channel pore is critical for inward rectification and Ca^{2+} permeability properties. These studies showed a strong inward rectification for AMPARs containing GluA1, 3 and 4 subunits due to blocking by intracellular spermine permitted by the presence of only glutamine residues at the Q/R site. However, AMPARs containing a GluA2 subunit lack inward rectification due to the presence of positively charged arginine in the Q/R site which prevents entrance of spermine from the cytoplasmic side of the channel. In addition, the presence of GluA2 subunits in AMPARs drastically reduces their Ca^{2+} permeability for the same reason.

In addition to that, a difference in the pharmacological properties of GluA2-containing and lacking AMPARs has been reported particularly with regard to inhibition by extracellular application of polyamine-containing compounds of synthetic origin (Magazanik et al., 1997) or from wasps and spiders (Mellor and Usherwood, 2004; Washburn and Dingle, 1996). It has been reported earlier that a few of these natural polyamine toxins act as antagonists on native non-NMDARs of insect (Bruce et al., 1990; Kerry et al., 1988) and rats (Ashe et al., 1989). It has been shown that Arg-TX-636 (Brackley et al., 1993) and joro spider toxin (Blaschke et al., 1993) act as strong inhibitors of recombinant GluR2-lacking AMPARs and act as weak antagonists on AMPARs containing GluA2. These data further support our proposed hypothesis for the inhibition of nAChRs by PhTXs.

This hypothesis might also explain other properties such as inward rectification and high Ca^{2+} permeability in N-nAChRs compared to M-nAChRs (**Figure 7.2**) (Arneric and Brioni, 1998; Francis and Papke, 1996; Vernino et al., 1994). Previous investigations have demonstrated that the rectification of N-nAChRs might be due to positively charged intracellular molecules such as spermine and Mg^{2+} blocking the channel pore when there is a force pushing the outward passage of cations (Haghighi and Cooper, 1998; Neuhaus and Cachelin, 1990). These findings further support our hypothesis due to the fact that the presence of negatively charged residues in rings 7 and 8 of all N-nAChR subunits will

attract positively charged intracellular molecules and block outward cation current. Whereas, in the case of embryonic M-nAChRs the γ -subunit has positively charged lysine in ring 8 which acts as the main barrier preventing molecules carrying positive charge from blocking the pore and causing inward rectification. Also a neutral glutamine residue from the same subunit in ring 7 instead of glutamate might have a similar effect. In addition to that, it is important to investigate whether mammalian homomeric $\alpha 9$ or heteromeric $\alpha 9\alpha 10$ N-nAChRs will generate inward rectification or not because in the case of the $\alpha 9$ -subunit ring 8 has a neutral alanine instead of a charged residue in other α -subunits. This might suggest that N-nAChR combinations containing $\alpha 9$ will not cause inward rectification similar to M-nAChRs. It has been reported previously that nAChRs in PC12 cells appear to be less affected by changes to external Mg^{2+} concentration than to internal changes (Neuhaus and Cachelin, 1990). This data further support the critical role of ring 7 and 8 in inward rectification.

Figure 7.2. (see over) Illustrating the inward rectification and Ca^{2+} permeability properties of nAChRs and AMPAR in relation to charged residues around the pore. Pink circles represent glutamine. Green and red circles are representing positive and negative charged residue respectively. Yellow dotted circles indicate ring position in the channel. A. highlights the rings 7 and 8, and C. ring 1 of nAChRs in Table 7.1. B. shows the Q/R site in AMPAR. AMPAR idea modified from Mellor(2010).



Moreover, it has been proposed that homomeric $\alpha 7$ nAChRs has a highest Ca^{2+} permeability contributing to about 10% of the whole inward current compared to 5% for heteromeric and 2% for M-nAChRs (Vernino et al., 1992; 1994). The possible reason behind the high permeability of $\alpha 7$ to Ca^{2+} ions might be due to the absence of positively charged amino acids in ring 1 near to the external pore mouth. While in case of heteromeric N-nAChRs the presence of 2 to 3 positively charged amino acids in the same ring will reduce Ca^{2+} permeability and 5 positive residues in case of M-nAChRs will drastically diminish Ca^{2+} permeability. Incorporation of an orphan subunit in to the heteromeric $\alpha + \beta$ N-nAChRs modifies its properties (Groot-Kormelink et al., 1998). For example, insertion of the $\alpha 5$ -subunit into either $\alpha 4\beta 2$ or $\alpha 3\beta 4$ will increase Ca^{2+} permeability compared to the combinations lacking the $\alpha 5$ -subunit (Ramirez-Latorre et al., 1996). Likely, this will also happen by insertion of the $\beta 3$ -subunit. The presence of two negatively charged glutamic acid residues at the ring 1 area might be the possible reason behind increasing Ca^{2+} permeability of N-nAChRs by insertion of these orphan-subunits, although, it has been shown that replacing negatively charged glutamic acid in ring 7 of homomeric $\alpha 7$ will eliminate their permeability to Ca^{2+} without showing any effect on monovalent Na^+ and K^+ ions (Bertrand et al., 1993).

The importance of multiple positive charges on the polyamine tail of PhTX-343 for potency has been investigated previously on mammalian NMDAR, AMPAR and M-nAChRs (Mellor et al., 2003). The data from that study showed that fully protonated PhTX-343 has lower potency on M-nAChRs compared to NMDAR and AMPAR. It also showed that removing the amino group near to the head region (PhTX-83) generated a selective analogue for AMPAR, while removing both secondary ammonium groups (PhTX-12) produced a selective M-nAChR analogue. Tikhonov et al. (2004) proposed two binding modes for the middle ammonium group in the polyamine tail of PhTX-343 interacting with polar

rings inside the M-nAChR pore. The deeper binding mode shows interaction of both secondary ammonium groups with the conserved serine residue in ring 5 of all subunits used in this study except neuronal $\alpha 7$ and muscle $\beta 1$ and γ -subunits which contain polar threonine, nonpolar phenylalanine and polar asparagine, respectively. The other model suggests their binding with threonine and serine residues in ring 4. All α -subunits have a polar serine residue in this ring, while other auxiliary subunits have nonpolar alanine except muscle $\beta 1$ which has polar threonine. These two modes are in agreement with the estimated δ -values of 0.7 for $\alpha 3\beta 4$ supporting the deeper site and 0.26 for $\alpha 4\beta 2$ which supports the shallower binding site. This amino acid difference in rings 4 and 5 based on both binding modes of PhTX-343 might further clarify the reason behind greater N-nAChR inhibition compared to M-nAChRs.

It appears from our data that the presence of the secondary ammonium groups in PhTX-343 polyamine moieties are important for subtype selectivity among the investigated mammalian nAChRs expressed in *Xenopus* oocytes. However, previous research shows that the presence of this positive charge group hinders inhibition of M-nAChRs naturally expressed in TE671 cells (Brier, 2001). Other studies show their presence in the polyamine tail of natural PhTX-433 is critical for their inhibition but the molecule will lose selectivity between ionotropic glutamate and nAChRs (Stromgaard et al., 2000B). Mellor and his collaborators (2003) reported 236-fold selectivity for PhTX-83 (secondary ammonium group near to head region replaced by methylene), at AMPAR expressed in oocytes over M-nAChRs in TE671 cells. Here we show that substitution of both secondary ammonium groups by methylene to generate PhTX-12 (with decay IC_{50} value of 0.07 μM gives 34-fold selectivity over PhTX-343 on mouse M-nAChRs at $V_H = -100$ mV. Previous study on human M-nAChRs in TE671 cells recorded an 11-fold lower PhTX-12 potency and 22-fold selectivity over PhTX-343 (Brier et al., 2003). It is likely the difference in PhTX-12 activity

between the two studies is due to the recording technique and expression system. We used TEVC and mouse M-nAChRs expressed in oocytes while the other study used patch clamp of TE671 cell line naturally expressing human M-nAChRs.

PhTX-12 showed mostly the same potency level on the nAChRs investigated in this study without any noticeable subtype selectivity among them except $\alpha 7$ and $\alpha 3\beta 2$ receptors which showed a lower sensitivity to PhTX-12. Their IC_{50} values were in the low micro-molar range (1-6 μM) for peak current inhibition and in the sub-micro-molar range (0.10-0.35 μM) for decay current across all wild-type and mutated nAChRs studied except $\alpha 7$ and $\alpha 3\beta 2$ receptors which were higher at $V_H = -80$ mV. Our data on PhTX-12 are in agreement with previous investigations that absences of secondary amino groups give a folded structure to philanthotoxin as a result of chemical interaction between the terminal amino group and the head region. Consequently, they suggest a binding site at the outer part of the pore for PhTX-12 and enhancing desensitisation rate (Brier et al., 2003; Tikhonov et al., 2004). Mutation of $\beta 4_{(F255V)}$ -subunit shows increase in IC_{50} value of PhTX-12, while $\beta 2_{(V253F)}$ -subunit did not, i.e. the opposite of PhTX-343 activity. This might be due to the changes in desensitization rate. The high amino acid similarity in the proposed region for PhTX-12 binding (outer pore) might be the reason behind a lack of selectivity among nAChRs at $V_H = -80$ mV.

In the present work, the percentage of recovery from inhibition by PhTX-343 and PhTX-12 was also time and subunit dependent. Most heteromeric N-nAChRs showed only 30-70% recovery from inhibition by 10 μM PhTX-343 after 36 to 42 minutes. The only exception was $\alpha 3\beta 4$ receptors which showed 76-88% recovery, possibly because the PhTX-343 molecule can pass to the inside of the cell more easily in this combination. In contrast, M-nAChRs and homomeric $\alpha 7$ receptors show roughly full recovery after 6 minutes; this might be due to a poor

interaction between positive charges on PhTX-343 and negative residues of channel compared to the strong interaction for other combinations, which require long time for recovery. On the other hand recovery from inhibition by PhTX-12 was over 90% for $\alpha 3$ -containing nAChRs while 80-90% for $\alpha 7$, $\alpha 1$ and $\alpha 4$ -containing nAChRs. The peak current recovery of mouse M-nAChRs from PhTX-343 inhibition was lower than from PhTX-12 inhibition at -80 mV and was in accordance with previous data on M-nAChRs in TE671 cells (Brier et al., 2003).

From the present and previous studies, the exact mechanism of PhTX analogue block of nAChR inward current is still not fully clarified. One likely mode of action is that they act as open channel blockers of nAChRs. PhTX-343 induced inhibition in heteromeric nAChRs was dependent on the membrane holding potential and use dependent, which suggested an open channel blocker mechanism of action. However, voltage-independent inhibition in homomeric $\alpha 7$ did not support the open channel blocker action. It is likely that any effects of membrane voltage on the inhibition potency of PhTX-343 are related mainly with binding site on β -subunits because lack of this subunit in homomeric $\alpha 7$ receptors caused PhTX-343 inhibition to become independent on the membrane holding potential. As shown in **Figure 7.3** based on the peak current inhibition, $\beta 2$ -containing nAChRs are more affected by alteration of the membrane holding potential than $\beta 4$ -containing receptors. The idea of subunit-specific association with holding potential has been reported earlier also for cocaine (Francis et al., 2000). The voltage-dependent and independent inhibition of hetero- and homomeric nAChRs, respectively by PhTX-343 might be due the two distinct mechanisms of action. These data suggest that PhTX-343 on $\alpha 7$ binds to the same site at the outer part of the channel proposed for PhTX-12 in muscle type while in heteromeric receptors it interacts with a deeper site in the channel. It has been proposed previously that PhTX-343 has the ability to inhibit open and closed conformation of mouse M-nAChRs in BC₃H1 cells (Jayaraman et al.,

1999). This finding is not unique to PhTX-343 inhibition of nAChRs. Slater and co-workers (2002) demonstrated that the mechanism of human M-nAChR inhibition by the plant alkaloid tetrandrine is voltage-dependent while in N-nAChRs it is voltage-independent. Another study shows rat M-nAChR inhibition by strychnine is voltage-independent while it is voltage-dependent in N-nAChRs (Garcia-Colunga and Miledi, 1999).

It is well documented that the positive charges carried by molecules acting as open channel blockers, such as hexamethonium and local anesthetics, are mainly responsible for their strong voltage-dependent inhibition (Arias, 1996; Sine and Taylor, 1982). This is in agreement with strong voltage-dependent inhibition observed for wild-type and mutated heteromeric nAChRs by PhTX-343 (**Figure 7.3**). Therefore, a PhTX-343 molecule carrying three positive charges at -100 mV will have a better chance to enter the channel faster and penetrate it to reach the narrowest part of channel and consequently will strongly block the pathways of ion movement. This voltage-dependent property of PhTX-343 is in agreement with the outcomes of Liu et al (1997), who reported a strong voltage-dependent inhibition of N-nAChRs naturally expressed in the PC12 cell line. In addition, Rozental et al (1989) also reported voltage-dependent inhibition for frog end-plate current by PhTX-433.

However, PhTX-12 inhibits wild-type and mutated nAChRs in a voltage-independent or weakly-dependent manner, probably due to the presence of only a single positive charge on the tail region and fully folded conformation. These properties probably will reduce their chance to enter or deeply penetrate the membrane electric field. In M-nAChRs, voltage-independent block by PhTX-12 might be due to a shield of positive charge around ring **1** and prevent further penetration by changing membrane to a more negative voltage, while a slightly higher voltage-dependence observed in N-nAChRs might be due to less positive charges present at the same ring of the channel. The M-nAChRs voltage

dependence data is in accordance with the results of Brier et al (2003), who demonstrated weakly voltage dependent inhibition of M-nAChRs by PhTX-12 in TE671 cells. It has been proposed previously that increasing the hydrophobicity of PhTX analogues would increase their affinity toward the voltage-independent binding site in M-nAChRs of TE671 cells (Brier, 2001).

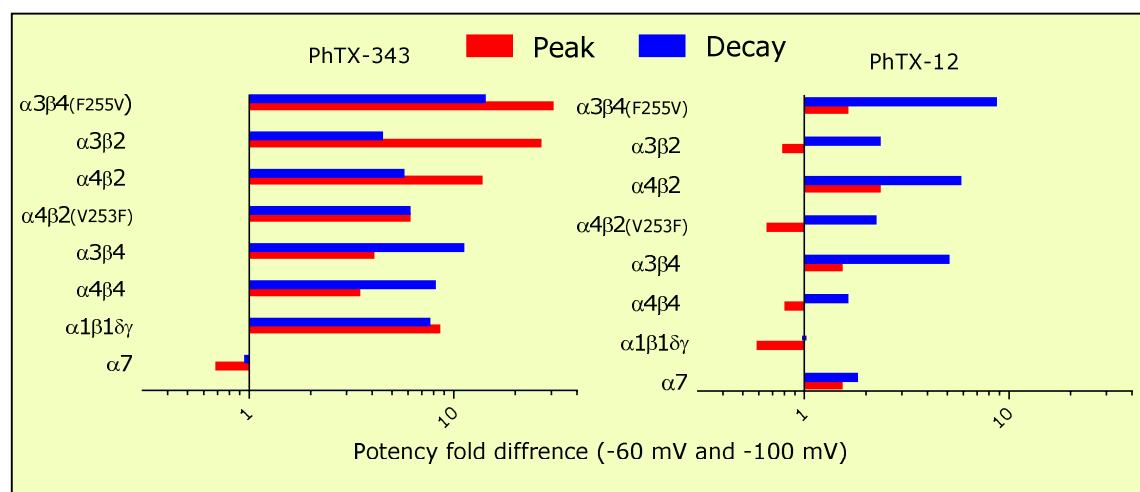


Figure 7.3. Shows peak and decay current inhibition difference between -60 mV and -100 mV of nAChRs by PhTX-343 and PhTX-12. Difference is expressed as $IC_{50}(-60\text{ mV})/IC_{50}(-100\text{ mV})$.

Another possibility is that PhTX analogues might be competitive inhibitors of nAChR inward current through their agonist binding site. It appears from the data obtained that ACh concentration-response curves of all investigated nAChR combinations in the presence of a single concentration of PhTX-343 or PhTX-12 did not show any significant change in ACh EC_{50} value. This non-competitive mode of inhibition by philanthotoxin has been observed previously by Bixel et al (2000) who showed that α -BGT has no effect on the binding affinity of N_3 -Ph-PhTX-343-Lys to nAChRs of *Torpedo californica* while a slight improvement was noticed with carbamylcholine. Also they showed (2001) that neither α -BGT nor carbamylcholine has any effect on the binding affinity of ^{125}I -MR44, a related polyamine-containing nAChR inhibitor.

It appears from decay current δ values obtained for PhTX-343 and PhTX-12 (**Figure 7.4**) that both analogues have different binding sites in different combinations based on desensitization rate. PhTX-343 showed a preference for deeper binding in receptors having lower desensitization rates like β 4-containing and M-nAChRs, while a shallower site for those with higher desensitization rates like β 2-containing and homomeric α 7 nAChRs. In contrast, PhTX-12 showed a preference for deeper sites in receptors having higher desensitization rates like β 2-containing and homomeric α 7 nAChRs and for shallow sites in combinations with lower desensitization rate like M-nAChRs and α 4 β 4, while in wild-type mutation of α 3 β 4 receptors PhTX-12 showed a preference for the deep binding site.

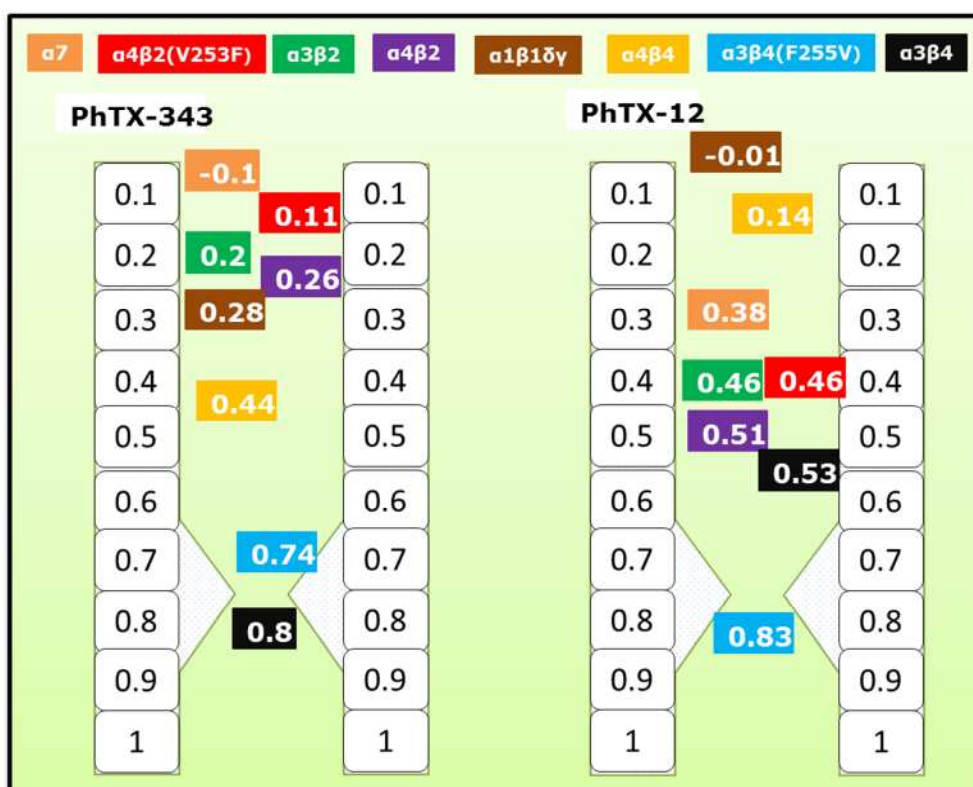


Figure 7.4. Schematic representation of the nAChR pore divided into ten similar sized sections (0.1-1). The numbers represent the penetration distance, δ value, of PhTX-343 and PhTX-12 inside channel based on the decay IC_{50} values in adapted Woodhull equation.

We determined whether the predicted distance across the membrane electric field, δ value, for PhTX-343 showed any correlation with potency and/or recovery. Based on decay current δ values, we classified the blocking of nAChRs by PhTX-343 into three categories.

The first category was nAChR combinations with a δ value greater than 0.5 and these show considerable but not complete recovery from 1 μ M or 10 μ M PhTX-343 within 42 minutes. This group include wild-type and mutated $\alpha 3\beta 4$ receptors which have δ values of 0.7 and 0.8 respectively. PhTX-343 showed highest potency on these combinations with high δ values.

The second category consisted of nAChR combinations with δ value lower than 0.5 and also comparably lower recovery from 10 μ M PhTX-343 than those in the first category. These were $\alpha 4\beta 4$, $\alpha 3\beta 2$ and $\alpha 4\beta 2$ (wild-type and mutant) which have δ values of 0.4, 0.2, 0.26 and 0.11 respectively. PhTX-343 showed intermediate potency on these combinations.

The final category consisted of nAChR combinations with δ values lower than 0.5 but can be differentiated from the second group by their high rate of recovery, showing complete recovery within 6 minutes in the case of $\alpha 7$ and near complete recovery for M-nAChR. This group includes $\alpha 7$ and M-nAChR which have δ values of 0.07 and 0.28 respectively. PhTX-343 showed the lowest potency on these receptors.

7.4. Structure-Activity Study

The results from this and previous SAR studies confirm that four regions of the philanthotoxin molecule are critical for their antagonism action (Anis et al., 1990; Nakanishi et al., 1997). A significant finding from SAR of PhTX-343 analogues in the present work was that adding a bulky group to the terminal ammonium group drastically reduced the potency, while to the head region it significantly increased the potency. Also, it appears that the presence of a

phenyl group at region III or IV is important for nAChR subtype selectivity while cyclohexane is important for activity. Therefore, the analogues that have both groups in their head region have a higher activity and strong selectivity for $\alpha 3\beta 4$ over $\alpha 4\beta 2$ nAChRs.

Modifications in the terminal ammonium group (region I) of PhTX-343 and PhTX-433 have been shown to strongly affect their antagonist potency, for example acetylation abolished activity (Benson et al., 1993) while extension increased it (Nakanishi et al., 1997). This was supported by our data that exchanging the terminal amine group of PhTX-343 for a guanidinium group (analogue **3**) caused an 8-fold and 38-fold loss of potency on peak and decay currents of $\alpha 4\beta 2$ nAChRs, respectively. ArgTX-636 which has elongation in this region showed roughly a 3-fold increase in decay current inhibition on $\alpha 3\beta 4$ compared to PhTX-343. The reason behind this increase in potency by tail extension in ArgTX-636 might be due to their ability to make stabilized H-bonds with ring 6, threonine (Nakanishi et al., 1997).

Alterations in region II, the polyamine moiety, of analogue **1** have been connected strongly with conformation and selectivity of PhTX-343 analogues across cation selective ion channels (**Figure 7.5**). A straight conformation has been proposed for the region II of analogue **1** due to the presence of three protonated amine groups, while the absence of the two secondary amine groups (analogue **2**) causes a fully-folded conformation (Tikhonov et al., 2004). Recently, Franzyk et al (2014) showed that incorporating a cis cyclopropane structure to this region of analogue **1** will cause a semi-folded conformation and this increased their activity on rat GluA1 flop subtype of AMPARs whereas the trans isomer remains linear and shows higher activity than cis. Tested here on N-nAChRs (analogues **10** and **11**), both analogues had a high selectivity for $\beta 4$ over $\beta 2$ -containing receptors; this might be due to the probability of the terminal amino groups or inserted cyclopropane group interacting with the single amino

acid difference between M2 domains of the two β -subunits as a consequence of their semi-folded conformation. This idea might become a new approach for developing selective compounds for nAChR subtypes due to the various semi-folded conformations that the PhTX molecule can adopt and consequently their interaction with different amino acids that participate in the channel pore.

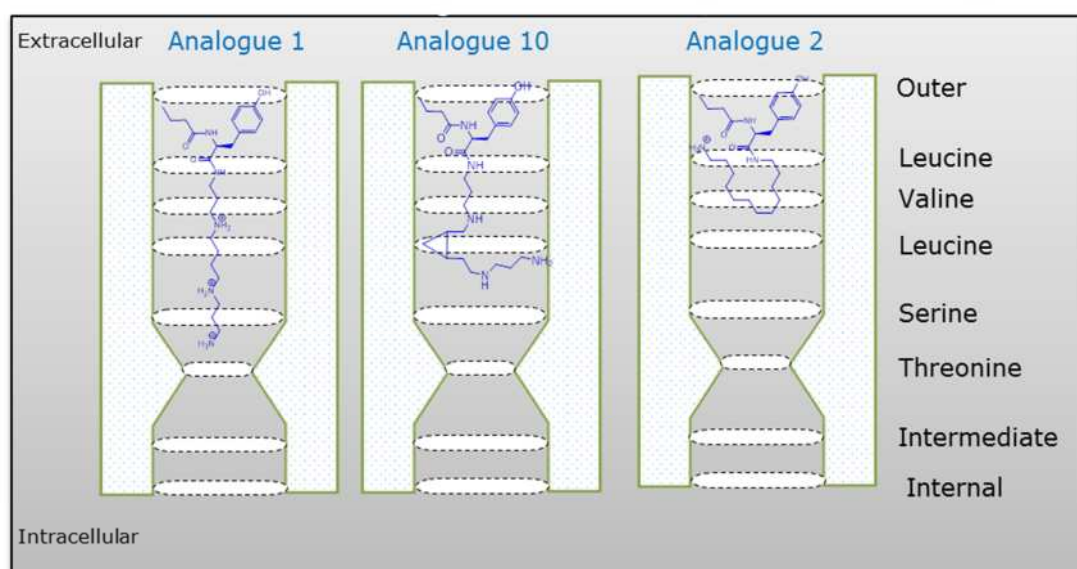


Figure 7.5. Schematic illustration of different conformations that PhTX analogues may adopt inside the channel pore based on molecular modeling data from previous studies.

It has been proposed previously that substitution in the tyrosine moiety (region IV) reduces the affinity of PhTX-343 molecules on NMDAR, while region III, butyric acid, modification increases affinity (Anis et al., 1990). It appears from the data reported here that modifications to either regions III or IV generally increase the activity and selectivity of PhTX-343 compounds to the major ganglionic $\alpha 3\beta 4$ receptors over brain $\alpha 4\beta 2$ N-nAChR combinations. For example, previous research shows that elongation in region III enhances activity on qGluR, while shortening the chain length drastically reduced the potency (Bruce et al., 1990). Analogue **4** which has a ten carbon chain in region III, here showed a slight increase in the peak current activity compared to PhTX-343 on $\alpha 4\beta 2$ but it was 10-fold reduced on $\alpha 3\beta 4$ nAChRs. On the other hand, the

decay activity increased roughly by 2-fold on $\alpha 3\beta 4$ compared to analogue **1** and reduced slightly on $\alpha 4\beta 2$. This variance in potency might be due to the difference in the channel diameter of both combinations and time required to reach their binding sites.

In addition, omission of the hydroxyl group in region IV (analogues **5** and **6**) did not cause any considerable change on the peak current activity of PhTX-343 on $\alpha 4\beta 2$ receptors, while the activity increased drastically on $\alpha 3\beta 4$ receptors. This finding suggests that the presence of a benzyl group at region IV might be critical for subtype selectivity among nAChR combinations. It also has been shown in previous studies that analogues that have hydroxyl omission show better activity on nAChRs than qGluRs (Nakanishi et al., 1994) and NMDARs (Anis et al., 1990). In insect, hydroxyl omission in PhTX-433 slightly reduced activity on neuromuscular synaptic transmission while considerably increased it on neuronal somata of *Locusta* (Benson et al., 1993; 1992).

Studies focusing on the critical roles of introduced cyclic-groups in PhTX analogues are restricted and limited to Olsen et al (2006) and more recently Franzyk et al (2014) studies. Here we have further expanded our knowledge about the profile of the different cyclic-groups in various regions of the PhTX molecule by investigating their action on N-nAChRs. These analogues show a remarkable selectivity toward $\alpha 3\beta 4$ over $\alpha 4\beta 2$ nAChRs, with a few exceptions. For instance, Olsen et al (2006) showed that the inhibitory potency of PhTX-343 was increased by 276-fold when the tyrosyl group was replaced by a cyclohexylalanine (analogue **7**). This analogue, with nano-molar IC_{50} value is the most potent known antagonist of M-nAChRs, with some similar attributes to PhTX-12, showing inhibition at +50 mV, as well as PhTX-343, showing strong voltage dependence. This demonstrates the role of cyclohexylalanine in potency and proposed their possibility to bind either to sites outside or deep inside the channel pore. This modified PhTX-343 analogue shows roughly the same activity

to M-nAChRs (60 nM) as we found on $\alpha 4\beta 2$ (51 nM) with 2-fold lower activity on the peak current of $\alpha 3\beta 4$ nAChRs. The loss of subtype selectivity between nAChRs by analogue **7** and the inhibition pattern is in contrast to our proposed hypothesis that charge distribution inside and near to the mouth of the channel pore increases their likelihood to interact with the same extracellular binding site as PhTX-12 at the entrance of the pore, rather than the deep PhTX-343 binding site. Antagonists which bind at the PhTX-12 binding site do not show selectivity because of the high amino-acid homology of all subunits in this area. The binding site of PhTX-343 shows low homology between subunits and allows for selective inhibition by different molecules.

The critical role of hydrophobicity in the head regions (III and IV) of PhTX-343 on inhibitory potency has been investigated previously. Nakanishi et al (1990) suggested that hydrophobicity is the major factor determining the inhibition potency of PhTX-343, demonstrating a critical role for the bulky group in region III. Other studies show that the potency of PhTX-343 is mainly dependent on the size of the hydrophobic head group rather than hydrophobicity; increasing the size of region III and IV leads to a marked increase in potency of PhTX-343 (Benson et al., 1992; Bixel et al., 2000). By incorporating a fixed cyclohexylalanine in region IV and increasing the size of other cyclo-substitutes in region III, cyclopropane, cyclobutane and cyclopentane, the potency of PhTX-343, as expected, increased on $\alpha 3\beta 4$ and $\alpha 4\beta 2$ nAChRs. Further increasing the hydrophobicity and size of PhTX-343 by having cyclohexyl groups in both regions III and IV caused a slight reduction in potency on $\alpha 4\beta 2$ and increase on $\alpha 3\beta 4$. This variation in potency might be due to a difference in channel diameter between $\alpha 3\beta 4$ and $\alpha 4\beta 2$ as we suggested earlier when molecules have an elongated chain in region III. It might be $\alpha 4\beta 2$ has a narrower channel compared to $\alpha 3\beta 4$ because the addition of an enormous head group to PhTX-343 reduces the potency on $\alpha 4\beta 2$, probably via preventing the

polyamine tail regions (I and II) penetrating the channel pore and interacting with the deep binding site (Tikhonov et al., 2004). The head group size was found to be a major factor in determining selectivity with several analogues of the cyclohexylalanyl (region IV) compound showing considerable selectivity for $\alpha 3\beta 4$ over $\alpha 4\beta 2$ while others did not.

Nakanishi and his co-workers (1994) proposed that adding a bulky group with modest hydrophobicity to the head regions (III and IV) of the PhTX-343 seems to be critical for the potency. By incorporating substitutions we suggested to be responsible for selectivity, phenyl group in region III, and activity, cyclohexylalanine in region IV, analogue **18** or vice versa with adding hydroxyl to phenolic group, analogue **8**, this would moderate the head region hydrophobicity. As expected, this drastically increased the potency (IC_{50} 0.3 to 2 nM) and selectivity (70 to 100-fold) on $\alpha 3\beta 4$ over $\alpha 4\beta 2$ nAChRs. Modification in analogue **8** confirmed the outcome of previous studies which show an increase in activity of PhTX-343 by 2.4-fold on locust muscle twitch contraction and 6.5-fold on *Torpedo* compared to parental analogue **1** with roughly 82-fold selectivity on NMDARs (Anis et al., 1990; Bruce et al., 1990; Nakanishi et al., 1994). Further increasing the size of the bulky group in region III of analogue **18** by replacing the phenyl group with naphthalene, lead to the most potent open channel blocker (analogue **19**) identified so far on nAChRs, with a considerable selectivity for $\alpha 3\beta 4$ over $\alpha 4\beta 2$ receptors. Based on the data reported here we concluded that the presence of a cyclohexyl and a phenyl group at the head regions, III and IV, of PhTX-343 give the molecule a most appropriate shape to fit inside their binding site in $\alpha 3\beta 4$ nAChRs with unprecedented activity and great selectivity. Modifying analogue **18** by extending the chain carrying the phenyl group in region III as in analogue **20** and **21** reduced the activity, but it was still higher than analogue **1**. This might be due to the same reason we mentioned

for earlier analogues such as compound **4** where the polyamine tail did not reach the deep binding site.

Ketamine is a synthetic anesthetic used widely in animal studies and medical practice. Previous research shows that ketamine inhibits human $\beta 4$ -containing receptors with higher potency compared to $\beta 2$ -containing receptors (Yamakura et al., 2000b). This was in agreement with what we found, with slightly higher activity on rat $\alpha 3\beta 4$ ($IC_{50} = 3.4 \mu M$) and $\alpha 4\beta 2$ ($IC_{50} = 36.8 \mu M$) compared to human nAChRs. This finding further supports the previous notion we proposed that the presence of a cyclohexyl and phenyl group in the structure of the molecule increases their affinity toward $\alpha 3\beta 4$ over $\alpha 4\beta 2$ receptors. In addition, the potency of ketamine was roughly 49-fold and 263-fold lower compared to PhTX-343 on $\alpha 3\beta 4$ and $\alpha 4\beta 2$ receptors, respectively. This might be due to the absence of the polyamine tail that is present in PhTX-343.

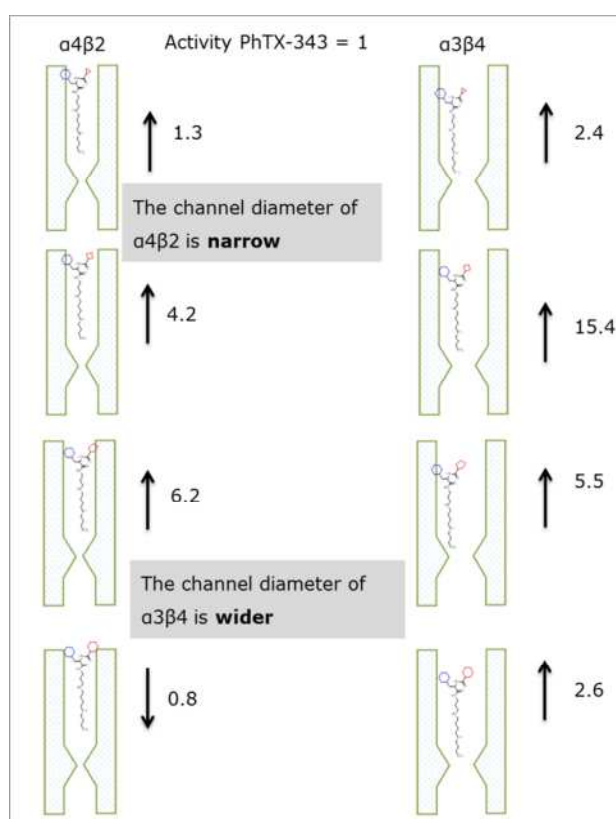


Figure 7.6. Schematic representation illustrates the channel diameter difference between $\alpha 3\beta 4$ and $\alpha 4\beta 2$ nAChRs.

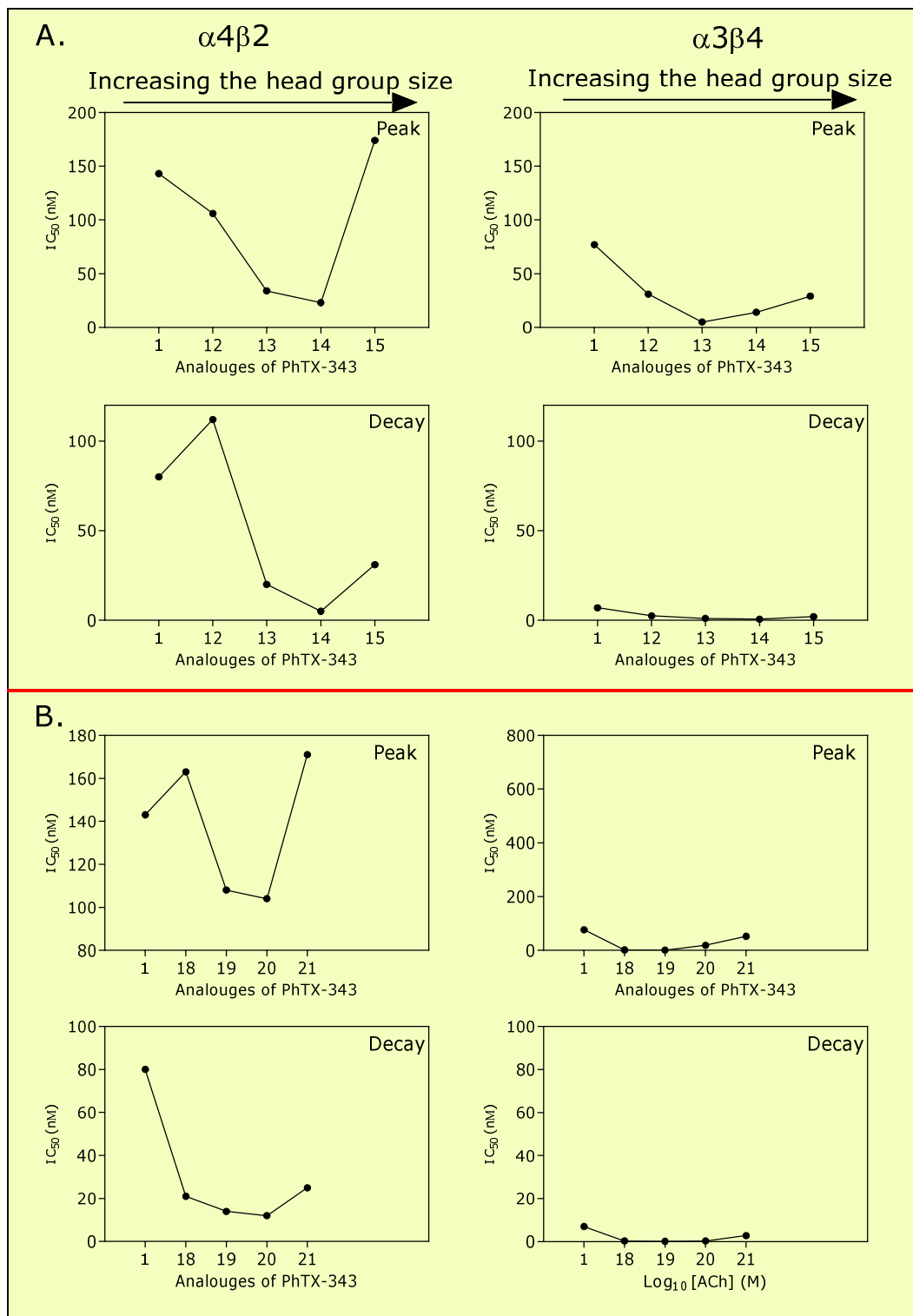


Figure 7.7. The relationship between the head group size and length in PhTX-343 analogues with their potency on $\alpha 4\beta 2$ and $\alpha 3\beta 4$ nAChRs. The numbers on x-axis refer to the analogue number. In all analogues there was a fixed cyclohexylalanyl group in region IV and the modification was in region III. (A) Shows increasing size of cyclic alkane group in region III from cyclopropane (12) to cyclohexane (15). (B) Shows increasing length and size of phenyl-containing groups. The points in the graphs are mean IC₅₀ values at V_H = -100 mV.

CONCLUSIONS

PhTX-343 inhibited nAChRs in a subunit-, time- and concentration-dependent manner, and with the exception of homomeric $\alpha 7$ receptors showed quite strong voltage dependence. Overall, PhTX-343 demonstrated strongest inhibition against $\beta 4$ -containing receptors at more negative V_H after one minute of application. This inhibition was non-competitive and proposed to be mainly due to open channels block.

On the other hand the inhibition of nAChRs by PhTX-12 was less subunit- and voltage-dependent as for PhTX-343 but like PhTX-343 it was time- and concentration-dependent. It appears that both α - and β -subunits are critical for the potency of PhTX-12. In strong contrast to PhTX-343 it showed a slight selectivity toward $\alpha 1\beta 1\delta\gamma$. Inhibition by PhTX-12, like PhTX-343, was non-competitive and thought to involve block of the pore but possibly via a shallower site than PhTX-343.

The structure-activity studies showed that adding a bulky group to the terminal ammonium drastically increased the IC_{50} value while in the head region it decreased the IC_{50} value. In addition, we identified the key head region substitutions responsible for increasing PhTX activity (cyclohexylalanine) and selectivity (phenyl group). Analogues having cyclohexylalanine and aromatic groups in the head region showed IC_{50} values in the low nano-molar and picomolar (160-400 pM) range. These data suggest that PhTXs could serve as lead compounds for highly potent and selective inhibitors of N-nAChRs.

REFEFRENCES

- Albuquerque EX, Alkondon M, Pereira EF, Castro NG, Schratzenholz A, Barbosa CT, Bonfante-Cabarcas R, Aracava Y, Eisenberg HM and Maelicke A (1997) Properties of neuronal nicotinic acetylcholine receptors: pharmacological characterization and modulation of synaptic function. *J Pharmacol Exp Ther* **280**:1117-36.
- Albuquerque EX, Pereira EF, Alkondon M and Rogers SW (2009) Mammalian nicotinic acetylcholine receptors: from structure to function. *Physiol Rev* **89**:73-120.
- Anis N, Sherby S, Goodnow R, Jr., Niwa M, Konno K, Kallimopoulos T, Bukownik R, Nakanishi K, Usherwood P and Eldefrawi A (1990) Structure-activity relationships of philanthotoxin analogs and polyamines on N-methyl-D-aspartate and nicotinic acetylcholine receptors. *J Pharmacol Exp Ther* **254**:764-73.
- Arias HR (1996) Luminal and non-luminal non-competitive inhibitor binding sites on the nicotinic acetylcholine receptor. *Mol Membr Biol* **13**:1-17.
- Arias HR (1998) Binding sites for exogenous and endogenous non-competitive inhibitors of the nicotinic acetylcholine receptor. *Biochim Biophys Acta* **1376**:173-220.
- Arias HR (2000) Localization of agonist and competitive antagonist binding sites on nicotinic acetylcholine receptors. *Neurochem Int* **36**:595-645.
- Arias HR (2012) Molecular Interactions between Ligands and Nicotinic Acetylcholine Receptors Revealed by Studies with Acetylcholine Binding Proteins. *J Thermodynam Cat* **3**:116.
- Arneric SP and Brioni JD (1998) Neuronal Nicotinic Receptors: Pharmacology and Therapeutic Opportunities. *Wiley-Liss, Inc.*:25-42.
- Arneric SP and Brioni JD (1999) *Neuronal Nicotinic Receptors Pharmacology and Therapeutic Opportunities*. John Wiley and Sons Ltd.
- Ashe JH, Cox CL and Adams ME (1989) Argitoxin-636 blocks excitatory synaptic transmission in rat hippocampal CA1 pyramidal neurons. *Brain Res* **480**:234-41.
- Ballivet M, Patrick J, Lee J and Heinemann S (1982) Molecular cloning of cDNA coding for the gamma subunit of Torpedo acetylcholine receptor. *Proc Natl Acad Sci U S A* **79**:4466-70.
- Barnard EA, Miledi R and Sumikawa K (1982) Translation of exogenous messenger RNA coding for nicotinic acetylcholine receptors produces functional receptors in *Xenopus* oocytes. *Proc R Soc Lond B Biol Sci* **215**:241-6.
- Benoit P and Changeux JP (1993) Voltage dependencies of the effects of chlorpromazine on the nicotinic receptor channel from mouse muscle cell line So18. *Neurosci Lett* **160**:81-4.
- Benson JA, L. Kaufmann, B. Huea b, M. Pelhatea b, F. Schürmann and L. Gsell TP (1993) The physiological action of analogues of philanthotoxin-4.3.3 at insect nicotinic acetylcholine receptors. *Camp. Eiochem. Physiol.* **105C**:303-310.
- Benson JA, Schurmann F, Kaufmann L, Gsell L and Piek T (1992) Inhibition of dipteran larval neuromuscular synaptic transmission by analogues of philanthotoxin-4.3.3: a structure-activity study. *Comp Biochem Physiol C* **102**:267-72.
- Bertrand D, Ballivet M, Gomez M, Bertrand S, Phannavong B and Gundelfinger ED (1994) Physiological properties of neuronal nicotinic receptors reconstituted from the vertebrate beta 2 subunit and *Drosophila* alpha subunits. *Eur J Neurosci* **6**:869-75.
- Bertrand D, Galzi JL, Devillers-Thiery A, Bertrand S and Changeux JP (1993) Mutations at two distinct sites within the channel domain M2 alter calcium permeability of neuronal alpha 7 nicotinic receptor. *Proc Natl Acad Sci U S A* **90**:6971-5.
- Bixel MG, Krauss M, Liu Y, Bolognesi ML, Rosini M, Mellor IS, Usherwood PN, Melchiorre C, Nakanishi K and Hucho F (2000) Structure-activity relationship and site of binding of

- polyamine derivatives at the nicotinic acetylcholine receptor. *Eur J Biochem* **267**:110-20.
- Bixel MG, Weise C, Bolognesi ML, Rosini M, Brierly MJ, Mellor IR, Usherwood PN, Melchiorre C and Hucho F (2001) Location of the polyamine binding site in the vestibule of the nicotinic acetylcholine receptor ion channel. *J Biol Chem* **276**:6151-60.
- Blaschke M, Keller BU, Rivosecchi R, Hollmann M, Heinemann S and Konnerth A (1993) A single amino acid determines the subunit-specific spider toxin block of alpha-amino-3-hydroxy-5-methylisoxazole-4-propionate/kainate receptor channels. *Proc Natl Acad Sci U S A* **90**:6528-32.
- Blount P and Merlie JP (1989) Molecular basis of the two nonequivalent ligand binding sites of the muscle nicotinic acetylcholine receptor. *Neuron* **3**:349-57.
- Bouzat C (2012) New insights into the structural bases of activation of Cys-loop receptors. *J Physiol Paris* **106**:23-33.
- Brackley P, Goodnow R, Jr., Nakanishi K, Sudan HL and Usherwood PN (1990) Spermine and philanthotoxin potentiate excitatory amino acid responses of *Xenopus* oocytes injected with rat and chick brain RNA. *Neurosci Lett* **114**:51-6.
- Brackley PT, Bell DR, Choi SK, Nakanishi K and Usherwood PN (1993) Selective antagonism of native and cloned kainate and NMDA receptors by polyamine-containing toxins. *J Pharmacol Exp Ther* **266**:1573-80.
- Brejč K, van Dijk WJ, Klaassen RV, Schuurmans M, van Der Oost J, Smit AB and Sixma TK (2001) Crystal structure of an ACh-binding protein reveals the ligand-binding domain of nicotinic receptors. *Nature* **411**:269-76.
- Brier TJ (2001) The interaction of polyamine-amides with the nicotinic acetylcholine receptors of the TE671 cell line Nottingham.
- Brier TJ, Mellor IR, Tikhonov DB, Neagoe I, Shao Z, Brierley MJ, Stromgaard K, Jaroszewski JW, Krosgaard-Larsen P and Usherwood PN (2003) Contrasting actions of philanthotoxin-343 and philanthotoxin-(12) on human muscle nicotinic acetylcholine receptors. *Mol Pharmacol* **64**:954-64.
- Broadbent S, Groot-Kormelink PJ, Krashia PA, Harkness PC, Millar NS, Beato M and Sivilotti LG (2006) Incorporation of the beta3 subunit has a dominant-negative effect on the function of recombinant central-type neuronal nicotinic receptors. *Mol Pharmacol* **70**:1350-7.
- Bruce M, Bukownik R, Eldefrawi AT, Eldefrawi ME, Goodnow R, Jr., Kallimopoulos T, Konno K, Nakanishi K, Niwa M and Usherwood PN (1990) Structure-activity relationships of analogues of the wasp toxin philanthotoxin: non-competitive antagonists of quisqualate receptors. *Toxicon* **28**:1333-46.
- Changeux JP (2012) The nicotinic acetylcholine receptor: the founding father of the pentameric ligand-gated ion channel superfamily. *J Biol Chem* **287**:40207-15.
- Changeux JP, Devillers-Thiery A and Chemouilli P (1984) Acetylcholine receptor: an allosteric protein. *Science* **225**:1335-45.
- Changeux JP, Kasai M and Lee CY (1970) Use of a snake venom toxin to characterize the cholinergic receptor protein. *Proc Natl Acad Sci U S A* **67**:1241-7.
- Chavez-Noriega LE, Crona JH, Washburn MS, Urrutia A, Elliott KJ and Johnson EC (1997) Pharmacological Characterization of Recombinant Human Neuronal Nicotinic Acetylcholine Receptors $\alpha 2\beta 2$, $\alpha 2\beta 4$, $\alpha 3\beta 2$, $\alpha 3\beta 4$, $\alpha 4\beta 2$, $\alpha 4\beta 4$ and $\alpha 7$ Expressed in *Xenopus* Oocytes. *Journal of Pharmacology and Experimental Therapeutics* **280**:346-356.
- Chiara DC, Middleton RE and Cohen JB (1998) Identification of tryptophan 55 as the primary site of [3H]nicotine photoincorporation in the gamma-subunit of the Torpedo nicotinic acetylcholine receptor. *FEBS Lett* **423**:223-6.

- Chiara DC, Xie Y and Cohen JB (1999) Structure of the agonist-binding sites of the Torpedo nicotinic acetylcholine receptor: affinity-labeling and mutational analyses identify gamma Tyr-111/delta Arg-113 as antagonist affinity determinants. *Biochemistry* **38**:6689-98.
- Choi SK, Kalivretanos AG, Usherwood PN and Nakanishi K (1995) Labeling studies of photolabile philanthotoxins with nicotinic acetylcholine receptors: mode of interaction between toxin and receptor. *Chem Biol* **2**:23-32.
- Clarke PB, Schwartz RD, Paul SM, Pert CB and Pert A (1985) Nicotinic binding in rat brain: autoradiographic comparison of [3H]acetylcholine, [3H]nicotine, and [125I]-alpha-bungarotoxin. *J Neurosci* **5**:1307-15.
- Conroy WG and Berg DK (1995) Neurons can maintain multiple classes of nicotinic acetylcholine receptors distinguished by different subunit compositions. *J Biol Chem* **270**:4424-31.
- Corringer PJ, Baaden M, Bocquet N, Delarue M, Dufresne V, Nury H, Prevost M and Van Renterghem C (2010) Atomic structure and dynamics of pentameric ligand-gated ion channels: new insight from bacterial homologues. *J Physiol* **588**:565-72.
- Corringer PJ, Bertrand S, Galzi JL, Devillers-Thierry A, Changeux JP and Bertrand D (1999) Mutational analysis of the charge selectivity filter of the alpha7 nicotinic acetylcholine receptor. *Neuron* **22**:831-43.
- Corringer PJ, Le Novere N and Changeux JP (2000) Nicotinic receptors at the amino acid level. *Annu Rev Pharmacol Toxicol* **40**:431-58.
- Couturier S, Bertrand D, Matter JM, Hernandez MC, Bertrand S, Millar N, Valera S, Barkas T and Ballivet M (1990) A neuronal nicotinic acetylcholine receptor subunit (alpha 7) is developmentally regulated and forms a homo-oligomeric channel blocked by alpha-BTX. *Neuron* **5**:847-56.
- Czajkowski C and Karlin A (1995) Structure of the nicotinic receptor acetylcholine-binding site. Identification of acidic residues in the delta subunit within 0.9 nm of the 5 alpha subunit-binding. *J Biol Chem* **270**:3160-4.
- Dani JA and Bertrand D (2007) Nicotinic acetylcholine receptors and nicotinic cholinergic mechanisms of the central nervous system. *Annu Rev Pharmacol Toxicol* **47**:699-729.
- Dascal N (1987) The use of *Xenopus* oocytes for the study of ion channels. *CRC Crit Rev Biochem* **22**:317-87.
- Deneris ES, Boulter J, Swanson LW, Patrick J and Heinemann S (1989) Beta 3: a new member of nicotinic acetylcholine receptor gene family is expressed in brain. *J Biol Chem* **264**:6268-72.
- Dennis M, Giraudat J, Kotzyba-Hibert F, Goeldner M, Hirth C, Chang JY, Lazure C, Chretien M and Changeux JP (1988) Amino acids of the Torpedo marmorata acetylcholine receptor alpha subunit labeled by a photoaffinity ligand for the acetylcholine binding site. *Biochemistry* **27**:2346-57.
- Dineley-Miller K and Patrick J (1992) Gene transcripts for the nicotinic acetylcholine receptor subunit, beta4, are distributed in multiple areas of the rat central nervous system. *Brain Res Mol Brain Res* **16**:339-44.
- Drenan RM, Grady SR, Whiteaker P, McClure-Begley T, McKinney S, Miwa JM, Bupp S, Heintz N, McIntosh JM, Bencherif M, Marks MJ and Lester HA (2008) In vivo activation of midbrain dopamine neurons via sensitized, high-affinity alpha 6 nicotinic acetylcholine receptors. *Neuron* **60**:123-36.
- Duret G, Van Renterghem C, Weng Y, Prevost M, Moraga-Cid G, Huon C, Sonner JM and Corringer PJ (2011) Functional prokaryotic-eukaryotic chimera from the pentameric ligand-gated ion channel family. *Proc Natl Acad Sci U S A* **108**:12143-8.

- Dutton JL and Craik DJ (2001) alpha-Conotoxins: nicotinic acetylcholine receptor antagonists as pharmacological tools and potential drug leads. *Curr Med Chem* **8**:327-44.
- Duvoisin RM, Deneris ES, Patrick J and Heinemann S (1989) The functional diversity of the neuronal nicotinic acetylcholine receptors is increased by a novel subunit: beta 4. *Neuron* **3**:487-96.
- Eldefrawi A.T EM, Konno K, Mansour NA, Nakanishi K, Oltz E and Usherwood PN. (1988) Structure and synthesis of a potent glutamate receptors antagonist in wasp venome. *Proc. Natl. Acad. Sci. U.S.A.* **85**:4910-4913.
- Elgoyhen AB, Johnson DS, Boulter J, Vetter DE and Heinemann S (1994) Alpha 9: an acetylcholine receptor with novel pharmacological properties expressed in rat cochlear hair cells. *Cell* **79**:705-15.
- Elgoyhen AB, Vetter DE, Katz E, Rothlin CV, Heinemann SF and Boulter J (2001) alpha10: a determinant of nicotinic cholinergic receptor function in mammalian vestibular and cochlear mechanosensory hair cells. *Proc Natl Acad Sci U S A* **98**:3501-6.
- Fleming JT, Squire MD, Barnes TM, Tornoe C, Matsuda K, Ahnn J, Fire A, Sulston JE, Barnard EA, Sattelle DB and Lewis JA (1997) Caenorhabditis elegans levamisole resistance genes lev-1, unc-29, and unc-38 encode functional nicotinic acetylcholine receptor subunits. *J Neurosci* **17**:5843-57.
- Francis MM and Papke RL (1996) Muscle-type nicotinic acetylcholine receptor delta subunit determines sensitivity to noncompetitive inhibitors, while gamma subunit regulates divalent permeability. *Neuropharmacology* **35**:1547-56.
- Francis MM, Vazquez RW, Papke RL and Oswald RE (2000) Subtype-selective inhibition of neuronal nicotinic acetylcholine receptors by cocaine is determined by the alpha4 and beta4 subunits. *Mol Pharmacol* **58**:109-19.
- Franzyk H, Grzeskowiak JW, Tikhonov DB, Jaroszewski JW and Mellor IR (2014) The Effects of Conformational Constraints in the Polyamine Moiety of Philanthotoxins on AMPAR Inhibition. *Chemmedchem* **9**:1725-1731.
- Gaimarri A, Moretti M, Riganti L, Zanardi A, Clementi F and Gotti C (2007) Regulation of neuronal nicotinic receptor traffic and expression. *Brain Res Rev* **55**:134-43.
- Galzi JL, Devillers-Thiery A, Hussy N, Bertrand S, Changeux JP and Bertrand D (1992) Mutations in the channel domain of a neuronal nicotinic receptor convert ion selectivity from cationic to anionic. *Nature* **359**:500-5.
- Galzi JL, Revah F, Black D, Goeldner M, Hirth C and Changeux JP (1990) Identification of a novel amino acid alpha-tyrosine 93 within the cholinergic ligands-binding sites of the acetylcholine receptor by photoaffinity labeling. Additional evidence for a three-loop model of the cholinergic ligands-binding sites. *J Biol Chem* **265**:10430-7.
- Gao M, Wang Y and Wu j (2014) The Roles of a5-Containing nAChRs in the Brain. *Biochemistry & Pharmacology*:3.
- Garcia-Colunga J and Miledi R (1999) Modulation of nicotinic acetylcholine receptors by strychnine. *Proc Natl Acad Sci U S A* **96**:4113-8.
- Giniatullin R, Nistri A and Yakel JL (2005) Desensitization of nicotinic ACh receptors: shaping cholinergic signaling. *Trends Neurosci* **28**:371-8.
- Giraudat J, Gali J, Revah F, Changeux J, Haumont P and Lederer F (1989) The noncompetitive blocker [(3)H]chlorpromazine labels segment M2 but not segment M1 of the nicotinic acetylcholine receptor alpha-subunit. *FEBS Lett* **253**:190-8.
- Glushakov AV, Voytenko LP, Skok MV and Skok V (2004) Distribution of neuronal nicotinic acetylcholine receptors containing different alpha-subunits in the submucosal plexus of the guinea-pig. *Auton Neurosci* **110**:19-26.
- Gotti C and Clementi F (2004) Neuronal nicotinic receptors: from structure to pathology. *Prog Neurobiol* **74**:363-96.

- Gotti C, Fornasari D and Clementi F (1997) Human neuronal nicotinic receptors. *Prog Neurobiol* **53**:199-237.
- Gotti C, Hanke W, Maury K, Moretti M, Ballivet M, Clementi F and Bertrand D (1994) Pharmacology and biophysical properties of alpha 7 and alpha 7-alpha 8 alpha-bungarotoxin receptor subtypes immunopurified from the chick optic lobe. *Eur J Neurosci* **6**:1281-91.
- Grady SR, Salminen O, McIntosh JM, Marks MJ and Collins AC (2010) Mouse striatal dopamine nerve terminals express alpha4alpha5beta2 and two stoichiometric forms of alpha4beta2*-nicotinic acetylcholine receptors. *J Mol Neurosci* **40**:91-5.
- Grando SA, Horton RM, Pereira EF, Diethelm-Okita BM, George PM, Albuquerque EX and Conti-Fine BM (1995) A nicotinic acetylcholine receptor regulating cell adhesion and motility is expressed in human keratinocytes. *J Invest Dermatol* **105**:774-81.
- Groot-Kormelink PJ, Luyten WH, Colquhoun D and Sivilotti LG (1998) A reporter mutation approach shows incorporation of the "orphan" subunit beta3 into a functional nicotinic receptor. *J Biol Chem* **273**:15317-20.
- Gurdon JB, Lane CD, Woodland HR and Marbaix G (1971) Use of frog eggs and oocytes for the study of messenger RNA and its translation in living cells. *Nature* **233**:177-82.
- Haghighi AP and Cooper E (1998) Neuronal nicotinic acetylcholine receptors are blocked by intracellular spermine in a voltage-dependent manner. *J Neurosci* **18**:4050-62.
- Herrero CJ, Garcia-Palomero E, Pintado AJ, Garcia AG and Montiel C (1999) Differential blockade of rat alpha3beta4 and alpha7 neuronal nicotinic receptors by omega-conotoxin MVIIC, omega-conotoxin GVIA and diltiazem. *Br J Pharmacol* **127**:1375-87.
- Herz JM, Johnson DA and Taylor P (1989) Distance between the agonist and noncompetitive inhibitor sites on the nicotinic acetylcholine receptor. *J Biol Chem* **264**:12439-48.
- Hollmann M, Hartley M and Heinemann S (1991) Ca²⁺ permeability of KA-AMPA-gated glutamate receptor channels depends on subunit composition. *Science* **252**:851-3.
- Huang LY, Catterall WA and Ehrenstein G (1978) Selectivity of cations and nonelectrolytes for acetylcholine-activated channels in cultured muscle cells. *J Gen Physiol* **71**:397-410.
- Hucho F, Tsetlin VI and Machold J (1996) The emerging three-dimensional structure of a receptor. The nicotinic acetylcholine receptor. *Eur J Biochem* **239**:539-57.
- Hume RI, Dingledine R and Heinemann SF (1991) Identification of a site in glutamate receptor subunits that controls calcium permeability. *Science* **253**:1028-31.
- Imoto K, Konno T, Nakai J, Wang F, Mishina M and Numa S (1991) A ring of uncharged polar amino acids as a component of channel constriction in the nicotinic acetylcholine receptor. *FEBS Lett* **289**:193-200.
- Imoto K, Methfessel C, Sakmann B, Mishina M, Mori Y, Konno T, Fukuda K, Kurasaki M, Bujo H, Fujita Y and et al. (1986) Location of a delta-subunit region determining ion transport through the acetylcholine receptor channel. *Nature* **324**:670-4.
- Itier V and Bertrand D (2001) Neuronal nicotinic receptors: from protein structure to function. *FEBS Lett* **504**:118-25.
- Jaroszewski JW, Matzen L, Frolund B and Krogsgaard-Larsen P (1996) Neuroactive polyamine wasp toxins: nuclear magnetic resonance spectroscopic analysis of the protolytic properties of philanthotoxin-343. *J Med Chem* **39**:515-21.
- Jayaraman V, Usherwood PN and Hess GP (1999) Inhibition of nicotinic acetylcholine receptor by philanthotoxin-343: kinetic investigations in the microsecond time region using a laser-pulse photolysis technique. *Biochemistry* **38**:11406-14.
- Jensen AA, Frolund B, Liljefors T and Krogsgaard-Larsen P (2005) Neuronal nicotinic acetylcholine receptors: structural revelations, target identifications, and therapeutic inspirations. *J Med Chem* **48**:4705-45.

- Jones AK, Raymond-Delpech V, Thany SH, Gauthier M and Sattelle DB (2006) The nicotinic acetylcholine receptor gene family of the honey bee, *Apis mellifera*. *Genome Res* **16**:1422-30.
- Jones AK and Sattelle DB (2003) Functional genomics of the nicotinic acetylcholine receptor gene family of the nematode, *Caenorhabditis elegans*. *BioEssays* **26**:39-49.
- Jones MV and Westbrook GL (1996) The impact of receptor desensitization on fast synaptic transmission. *Trends Neurosci* **19**:96-101.
- Jones S, Sudweeks S and Yakel JL (1999) Nicotinic receptors in the brain: correlating physiology with function. *Trends Neurosci* **22**:555-61.
- Kao PN, Dwork AJ, Kaldany RR, Silver ML, Wideman J, Stein S and Karlin A (1984) Identification of the alpha subunit half-cystine specifically labeled by an affinity reagent for the acetylcholine receptor binding site. *J Biol Chem* **259**:11662-5.
- Karlin A (1967) On the application of "a plausible model" of allosteric proteins to the receptor for acetylcholine. *J Theor Biol* **16**:306-20.
- Kerry CJ, Ramsey RL, Sansom MS and Usherwood PN (1988) Single channel studies of non-competitive antagonism of a quisqualate-sensitive glutamate receptor by argiotoxin636--a fraction isolated from orb-web spider venom. *Brain Res* **459**:312-27.
- Khiroug SS, Harkness PC, Lamb PW, Sudweeks SN, Khiroug L, Millar NS and Yakel JL (2002) Rat nicotinic ACh receptor alpha7 and beta2 subunits co-assemble to form functional heteromeric nicotinic receptor channels. *J Physiol* **540**:425-34.
- Kuo Y, Lucero L, Michaels J, DeLuca D and Lukas RJ (2002) Differential expression of nicotinic acetylcholine receptor subunits in fetal and neonatal mouse thymus. *J Neuroimmunol* **130**:140-54.
- Kuryatov A, Onksen J and Lindstrom J (2008) Roles of accessory subunits in alpha4beta2(*) nicotinic receptors. *Mol Pharmacol* **74**:132-43.
- Lansdell SJ and Millar NS (2004) Molecular characterization of Dalpha6 and Dalpha7 nicotinic acetylcholine receptor subunits from *Drosophila*: formation of a high-affinity alpha-bungarotoxin binding site revealed by expression of subunit chimeras. *J Neurochem* **90**:479-89.
- Lansdell SJ, Schmitt B, Betz H, Sattelle DB and Millar NS (1997) Temperature-sensitive expression of *Drosophila* neuronal nicotinic acetylcholine receptors. *J Neurochem* **68**:1812-9.
- Le Novere N, Corringer PJ and Changeux JP (2002) The diversity of subunit composition in nAChRs: evolutionary origins, physiologic and pharmacologic consequences. *J Neurobiol* **53**:447-56.
- Lee C (2003) Conformation, action, and mechanism of action of neuromuscular blocking muscle relaxants. *Pharmacol Ther* **98**:143-69.
- Li-Smerin Y, Levitan ES and Johnson JW (2001) Free intracellular Mg(2+) concentration and inhibition of NMDA responses in cultured rat neurons. *J Physiol* **533**:729-43.
- Li L, Zhong W, Zacharias N, Gibbs C, Lester HA and Dougherty DA (2001) The tethered agonist approach to mapping ion channel proteins--toward a structural model for the agonist binding site of the nicotinic acetylcholine receptor. *Chem Biol* **8**:47-58.
- Lindstrom J (2010) Nicotinic Acetylcholine Receptors. In: *Encyclopedia of Life Science (ELS)*. John Wiley and Sons, Ltd: Chichester.
- Lindstrom J, Anand R, Peng X, Gerzanich V, Wang F and Li Y (1995) Neuronal nicotinic receptor subtypes. *Ann N Y Acad Sci* **757**:100-16.
- Lindstrom j and Patrick j (1974) purification of acetylcholine receptors by affinity chromatography.
- Lindstrom JM (2000) Acetylcholine receptors and myasthenia. *Muscle Nerve* **23**:453-77.

- Lipovsek M, Fierro A, Perez EG, Boffi JC, Millar NS, Fuchs PA, Katz E and Elgoyhen AB (2014) Tracking the Molecular Evolution of Calcium Permeability in a Nicotinic Acetylcholine Receptor. *Mol Biol Evol.*
- Liu M, Nakazawa K, Inoue K and Ohno Y (1997) Potent and voltage-dependent block by philanthotoxin-343 of neuronal nicotinic receptor/channels in PC12 cells. *Br J Pharmacol* **122**:379-85.
- Lloyd GK and Williams M (2000) Neuronal nicotinic acetylcholine receptors as novel drug targets. *J Pharmacol Exp Ther* **292**:461-7.
- Luetje CW and Patrick J (1991) Both alpha- and beta-subunits contribute to the agonist sensitivity of neuronal nicotinic acetylcholine receptors. *J Neurosci* **11**:837-45.
- MacDermott AB, Role LW and Siegelbaum SA (1999) Presynaptic ionotropic receptors and the control of transmitter release. *Annu Rev Neurosci* **22**:443-85.
- Maconochie DJ and Knight DE (1992) A study of the bovine adrenal chromaffin nicotinic receptor using patch clamp and concentration-jump techniques. *J Physiol* **454**:129-53.
- Magazanik LG, Buldakova SL, Samoilova MV, Gmiro VE, Mellor IR and Usherwood PN (1997) Block of open channels of recombinant AMPA receptors and native AMPA/kainate receptors by adamantane derivatives. *J Physiol* **505 (Pt 3)**:655-63.
- Mao D, Perry DC, Yasuda RP, Wolfe BB and Kellar KJ (2008) The alpha4beta2alpha5 nicotinic cholinergic receptor in rat brain is resistant to up-regulation by nicotine in vivo. *J Neurochem* **104**:446-56.
- Martin RJ (1997) Modes of action of anthelmintic drugs. *Vet J* **154**:11-34.
- Marubio LM, del Mar Arroyo-Jimenez M, Cordero-Erausquin M, Lena C, Le Novere N, de Kerchove d'Exaerde A, Huchet M, Damaj MI and Changeux JP (1999) Reduced antinociception in mice lacking neuronal nicotinic receptor subunits. *Nature* **398**:805-10.
- Matsuda K, Buckingham SD, Kleier D, Rauh JJ, Grauso M and Sattelle DB (2001) Neonicotinoids: insecticides acting on insect nicotinic acetylcholine receptors. *Trends Pharmacol Sci* **22**:573-80.
- McGehee DS and Role LW (1995) Physiological diversity of nicotinic acetylcholine receptors expressed by vertebrate neurons. *Annu Rev Physiol* **57**:521-46.
- Mellor IR (2010) The AMPA receptor as a therapeutic target: current perspectives and emerging possibilities. *Future Med Chem* **2**:877-91.
- Mellor IR, Brier TJ, Pluteanu F, Stromgaard K, Saghyan A, Eldursi N, Brierley MJ, Andersen K, Jaroszewski JW, Krogsgaard-Larsen P and Usherwood PN (2003) Modification of the philanthotoxin-343 polyamine moiety results in different structure-activity profiles at muscle nicotinic ACh, NMDA and AMPA receptors. *Neuropharmacology* **44**:70-80.
- Mellor IR and Usherwood PNR (2004) Targeting ionotropic receptors with polyamine-containing toxins. *Toxicon* **43**:493-508.
- Mertz JE and Gurdon JB (1977) Purified DNAs are transcribed after microinjection into *Xenopus* oocytes. *Proc Natl Acad Sci U S A* **74**:1502-6.
- Mihalak KB, Carroll FI and Luetje CW (2006) Varenicline is a partial agonist at alpha4beta2 and a full agonist at alpha7 neuronal nicotinic receptors. *Mol Pharmacol* **70**:801-5.
- Millar NS (1999) Heterologous expression of mammalian and insect neuronal nicotinic acetylcholine receptors in cultured cell lines. *Biochem Soc Trans* **27**:944-50.
- Millar NS (2003) Assembly and subunit diversity of nicotinic acetylcholine receptors. *Biochem Soc Trans* **31**:869-74.
- Millar NS and Denholm I (2007) Nicotinic acetylcholine receptors: targets for commercially important insecticides. *Invert Neurosci* **7**:53-66.
- Millar NS and Gotti C (2009) Diversity of vertebrate nicotinic acetylcholine receptors. *Neuropharmacology* **56**:237-46.

- Millar NS and Harkness PC (2008) Assembly and trafficking of nicotinic acetylcholine receptors (Review). *Mol Membr Biol* **25**:279-92.
- Miller PS and Aricescu AR (2014) Crystal structure of a human GABAA receptor. *Nature* **512**:270-5.
- Miyazawa A, Fujiyoshi Y and Unwin N (2003) Structure and gating mechanism of the acetylcholine receptor pore. *Nature* **423**:949-55.
- Moeller HB and Fenton RA (2010) Can one Bad Egg' really spoil the batch? *J Physiol* **588**:2283-4.
- Moroni M and Bermudez I (2006) Stoichiometry and pharmacology of two human alpha4beta2 nicotinic receptor types. *J Mol Neurosci* **30**:95-6.
- Nakanishi K, Goodnow R, Konno K, Niwa M, Bukownik R, Kallimopoulos TA, Usherwood P, Eldefraw AT and E1defrawi ME (1990) Philanthotoxin-433 (PhTX-433), a non-competitive glutamate receptor inhibitor. *Pure & Appl. Chem.* **62**:1223-1 230.
- Nakanishi K, Huang X, Jiang H, Liu Y, Fang K, Huang D, Choi SK, Katz E and Eldefrawi M (1997) Structure-binding relation of philanthotoxins from nicotinic acetylcholine receptor binding assay. *Bioorg Med Chem* **5**:1969-88.
- Nakanishi K, Seok-ki Choi, Danwen Hwang, Keith Ierro, Mario Orlando, Aristotle G. Kalivretenos, Amira Eldefrawi, Mohyee Eldefrawi and Usherwood PNR (1994) Bioorganic studies of transmitter receptors with philanthotoxin analogs. *Pure & Appl. Chem.* **66**:671-678.
- Neher E and Steinbach JH (1978) Local anaesthetics transiently block currents through single acetylcholine-receptor channels. *J Physiol* **277**:153-76.
- Neuhaus R and Cachelin AB (1990) Changes in the conductance of the neuronal nicotinic acetylcholine receptor channel induced by magnesium. *Proc Biol Sci* **241**:78-84.
- Nicke A, Wonnacott S and Lewis RJ (2004) Alpha-conotoxins as tools for the elucidation of structure and function of neuronal nicotinic acetylcholine receptor subtypes. *Eur J Biochem* **271**:2305-19.
- Oiki S, Danho W, Madison V and Montal M (1988) M2 delta, a candidate for the structure lining the ionic channel of the nicotinic cholinergic receptor. *Proc Natl Acad Sci U S A* **85**:8703-7.
- Olsen CA, Mellor IR, Wellendorph P, Usherwood PN, Witt M, Franzyk H and Jaroszewski JW (2006) Tuning wasp toxin structure for nicotinic receptor antagonism: cyclohexylalanine-containing analogues as potent and voltage-dependent blockers. *ChemMedChem* **1**:303-5.
- Osman AA, Schrader AD, Hawkes AJ, Akil O, Bergeron A, Lustig LR and Simmons DD (2008) Muscle-like nicotinic receptor accessory molecules in sensory hair cells of the inner ear. *Mol Cell Neurosci* **38**:153-69.
- Papke RL and Heinemann SF (1991) The role of the beta 4-subunit in determining the kinetic properties of rat neuronal nicotinic acetylcholine alpha 3-receptors. *J Physiol* **440**:95-112.
- Paterson D and Nordberg A (2000) Neuronal nicotinic receptors in the human brain. *Prog Neurobiol* **61**:75-111.
- Placzek AN, Grassi F, Meyer EM and Papke RL (2005) An alpha7 nicotinic acetylcholine receptor gain-of-function mutant that retains pharmacological fidelity. *Mol Pharmacol* **68**:1863-76.
- Plazas PV, Katz E, Gomez-Casati ME, Bouzat C and Elgoyhen AB (2005) Stoichiometry of the alpha9alpha10 nicotinic cholinergic receptor. *J Neurosci* **25**:10905-12.
- Pohanka M (2012) Alpha7 nicotinic acetylcholine receptor is a target in pharmacology and toxicology. *Int J Mol Sci* **13**:2219-38.
- Poulsen MH, Andersen J, Christensen R, Hansen KB, Traynelis SF, Stromgaard K and Kristensen AS (2014) Binding of ArgTX-636 in the NMDA Receptor Ion Channel. *J Mol Biol.*

- Poulsen MH, Lucas S, Bach TB, Barslund AF, Wenzler C, Jensen CB, Kristensen AS and Stromgaard K (2013) Structure-activity relationship studies of argiotoxins: selective and potent inhibitors of ionotropic glutamate receptors. *J Med Chem* **56**:1171-81.
- Prado WA and Segalla DK (2004) Antinociceptive effects of bethanechol or dimethylphenylpiperazinium in models of phasic or incisional pain in rats. *Brain Res* **1018**:272-82.
- Quick MW and Lester RA (2002) Desensitization of neuronal nicotinic receptors. *J Neurobiol* **53**:457-78.
- Raftery MA, Hunkapiller MW, Strader CD and Hood LE (1980) Acetylcholine receptor: complex of homologous subunits. *Science* **208**:1454-6.
- Ramirez-Latorre J, Yu CR, Qu X, Perin F, Karlin A and Role L (1996) Functional contributions of alpha5 subunit to neuronal acetylcholine receptor channels. *Nature* **380**:347-51.
- Rasmussen AH, Strobaek D, Dyhring T, Jensen ML, Peters D, Grunnet M, Timmermann DB and Ahring PK (2014) Biophysical and pharmacological characterization of alpha6-containing nicotinic acetylcholine receptors expressed in HEK293 cells. *Brain Res* **1542**:1-11.
- Revah F, Galzi JL, Giraudat J, Haumont PY, Lederer F and Changeux JP (1990) The noncompetitive blocker [3H]chlorpromazine labels three amino acids of the acetylcholine receptor gamma subunit: implications for the alpha-helical organization of regions MII and for the structure of the ion channel. *Proc Natl Acad Sci U S A* **87**:4675-9.
- Reynolds JA and Karlin A (1978) Molecular weight in detergent solution of acetylcholine receptor from *Torpedo californica*. *Biochemistry* **17**:2035-8.
- Rogers SW, Mandelzys A, Deneris ES, Cooper E and Heinemann S (1992) The expression of nicotinic acetylcholine receptors by PC12 cells treated with NGF. *J Neurosci* **12**:4611-23.
- Role LW and Berg DK (1996) Nicotinic receptors in the development and modulation of CNS synapses. *Neuron* **16**:1077-85.
- Romanelli MN, Gratteri P, Guandalini L, Martini E, Bonaccini C and Gualtieri F (2007) Central nicotinic receptors: structure, function, ligands, and therapeutic potential. *ChemMedChem* **2**:746-67.
- Romanelli MN and Gualtieri F (2003) Cholinergic nicotinic receptors: competitive ligands, allosteric modulators, and their potential applications. *Med Res Rev* **23**:393-426.
- Rozental R, Scoble GT, Albuquerque EX, Idriss M, Sherby S, Sattelle DB, Nakanishi K, Konno K, Eldefrawi AT and Eldefrawi ME (1989) Allosteric inhibition of nicotinic acetylcholine receptors of vertebrates and insects by philanthotoxin. *J Pharmacol Exp Ther* **249**:123-30.
- Sargent PB (1993) The diversity of neuronal nicotinic acetylcholine receptors. *Annu Rev Neurosci* **16**:403-43.
- Sattelle DB (1980) Acetylcholine receptors of insects. *Adv Insect Physiol*:15.
- Shao Z (1997) The effect of polyamine amide toxins and polyamines on nicotinic acetylcholine receptors of the TE671 cell line, Nottingham.
- Shao Z, Mellor IR, Brierley MJ, Harris J and Usherwood PN (1998) Potentiation and inhibition of nicotinic acetylcholine receptors by spermine in the TE671 human muscle cell line. *J Pharmacol Exp Ther* **286**:1269-76.
- Sigel E (2010) Microinjection into *Xenopus* Oocytes. *Encyclopedia of Life Science*. www.els.net (last accessd July 2012). Nature Publishing group.
- Sine SM (1993) Molecular dissection of subunit interfaces in the acetylcholine receptor: identification of residues that determine curare selectivity. *Proc Natl Acad Sci U S A* **90**:9436-40.

- Sine SM, Claudio T and Sigworth FJ (1990) Activation of Torpedo acetylcholine receptors expressed in mouse fibroblasts. Single channel current kinetics reveal distinct agonist binding affinities. *J Gen Physiol* **96**:395-437.
- Sine SM, Kreienkamp HJ, Bren N, Maeda R and Taylor P (1995) Molecular dissection of subunit interfaces in the acetylcholine receptor: identification of determinants of alpha-conotoxin M1 selectivity. *Neuron* **15**:205-11.
- Sine SM and Taylor P (1982) Local anesthetics and histrionicotoxin are allosteric inhibitors of the acetylcholine receptor. Studies of clonal muscle cells. *J Biol Chem* **257**:8106-104.
- Skok M, Lykhmus E, Bobrovnik S, Tzartos S, Tsouloufis T, Vanderesse R, Coutrot F, Thong Cung M, Marraud M, Krikorian D and Sakarellos-Daitsiotis M (2001) Structure of epitopes recognized by the antibodies to alpha(181-192) peptides of neuronal nicotinic acetylcholine receptors: extrapolation to the structure of acetylcholine-binding domain. *J Neuroimmunol* **121**:59-66.
- Skok MV, Kalashnik EN, Koval LN, Tsetlin VI, Utkin YN, Changeux JP and Grailhe R (2003) Functional nicotinic acetylcholine receptors are expressed in B lymphocyte-derived cell lines. *Mol Pharmacol* **64**:885-9.
- Slater Y, Houlihan LM, Cassels BK, Lukas RJ and Bermudez I (2002) Effects of the plant alkaloid tetrandrine on human nicotinic acetylcholine receptors. *Eur J Pharmacol* **450**:213-21.
- Stafford GA, Oswald RE, Figl A, Cohen BN and Weiland GA (1998) Two domains of the beta subunit of neuronal nicotinic acetylcholine receptors contribute to the affinity of substance P. *J Pharmacol Exp Ther* **286**:619-26.
- Steinlein OK and Bertrand D (2008) Neuronal nicotinic acetylcholine receptors: from the genetic analysis to neurological diseases. *Biochem Pharmacol* **76**:1175-83.
- Stromgaard K, Bjornsdottir I, Andersen K, Brierley MJ, Rizoli S, Eldursi N, Mellor IR, Usherwood PN, Hansen SH, Krogsgaard-Larsen P and Jaroszewski JW (2000A) Solid phase synthesis and biological evaluation of enantiomerically pure wasp toxin analogues PhTX-343 and PhTX-12. *Chirality* **12**:93-102.
- Stromgaard K, Brier TJ, Andersen K, Mellor IR, Saghyan A, Tikhonov D, Usherwood PN, Krogsgaard-Larsen P and Jaroszewski JW (2000B) Solid-phase synthesis and biological evaluation of a combinatorial library of philanthotoxin analogues. *J Med Chem* **43**:4526-33.
- Stromgaard K, Brierley MJ, Andersen K, Slok FA, Mellor IR, Usherwood PN, Krogsgaard-Larsen P and Jaroszewski JW (1999) Analogues of neuroactive polyamine wasp toxins that lack inner basic sites exhibit enhanced antagonism toward a muscle-type mammalian nicotinic acetylcholine receptor. *J Med Chem* **42**:5224-34.
- Stromgaard K, Jensen LS and Vogensen SB (2005) Polyamine toxins: development of selective ligands for ionotropic receptors. *Toxicon* **45**:249-54.
- Stromgaard K, Mellor IR, Andersen K, Neagoe I, Pluteanu F, Usherwood PN, Krogsgaard-Larsen P and Jaroszewski JW (2002) Solid-phase synthesis and pharmacological evaluation of analogues of PhTX-12-A potent and selective nicotinic acetylcholine receptor antagonist. *Bioorg Med Chem Lett* **12**:1159-62.
- Stuhmer W (1998) Electrophysiologic recordings from *Xenopus* oocytes. *Methods Enzymol* **293**:280-300.
- Sumikawa K, Houghton M, Emtage JS, Richards BM and Barnard EA (1981) Active multi-subunit ACh receptor assembled by translation of heterologous mRNA in *Xenopus* oocytes. *Nature* **292**:862-4.
- Taly A, Corringer PJ, Guedin D, Lestage P and Changeux JP (2009) Nicotinic receptors: allosteric transitions and therapeutic targets in the nervous system. *Nat Rev Drug Discov* **8**:733-50.

- Tasneem A, Iyer LM, Jakobsson E and Aravind L (2005) Identification of the prokaryotic ligand-gated ion channels and their implications for the mechanisms and origins of animal Cys-loop ion channels. *Genome Biol* **6**:R4.
- Tikhonov DB, Mellor IR and Usherwood PN (2004) Modeling noncompetitive antagonism of a nicotinic acetylcholine receptor. *Biophys J* **87**:159-70.
- Tomizawa M and Casida JE (2001) Structure and diversity of insect nicotinic acetylcholine receptors. *Pest Manag Sci* **57**:914-22.
- Unwin N (2005) Refined structure of the nicotinic acetylcholine receptor at 4Å resolution. *J Mol Biol* **346**:967-89.
- Unwin N (2013) Nicotinic acetylcholine receptor and the structural basis of neuromuscular transmission: insights from Torpedo postsynaptic membranes. *Q Rev Biophys* **46**:283-322.
- van Duijn CM, Havekes LM, Van Broeckhoven C, de Knijff P and Hofman A (1995) Apolipoprotein E genotype and association between smoking and early onset Alzheimer's disease. *BMJ* **310**:627-31.
- van Nierop P, Keramidas A, Bertrand S, van Minnen J, Gouwenberg Y, Bertrand D and Smit AB (2005) Identification of molluscan nicotinic acetylcholine receptor (nAChR) subunits involved in formation of cation- and anion-selective nAChRs. *J Neurosci* **25**:10617-26.
- Verdoorn TA, Burnashev N, Monyer H, Seeburg PH and Sakmann B (1991) Structural determinants of ion flow through recombinant glutamate receptor channels. *Science* **252**:1715-8.
- Vernino S, Amador M, Luetje CW, Patrick J and Dani JA (1992) Calcium Modulation and High Calcium Permeability of Neuronal Nicotinic Acetylcholine Receptors. *Neuron* **8**:127-134.
- Vernino S, Hopkins S and Wang Z (2009) Autonomic ganglia, acetylcholine receptor antibodies, and autoimmune ganglionopathy. *Auton Neurosci* **146**:3-7.
- Vernino S, Rogers M, Radcliffe KA and Dani JA (1994) Quantitative measurement of calcium flux through muscle and neuronal nicotinic acetylcholine receptors. *J Neurosci* **14**:5514-24.
- Vetter DE, Katz E, Maison SF, Taranda J, Turcan S, Ballesteros J, Liberman MC, Elgoyhen AB and Boulter J (2007) The alpha10 nicotinic acetylcholine receptor subunit is required for normal synaptic function and integrity of the olivocochlear system. *Proc Natl Acad Sci U S A* **104**:20594-9.
- Wada E, McKinnon D, Heinemann S, Patrick J and Swanson LW (1990) The distribution of mRNA encoded by a new member of the neuronal nicotinic acetylcholine receptor gene family (alpha 5) in the rat central nervous system. *Brain Res* **526**:45-53.
- Wada E, Wada K, Boulter J, Deneris E, Heinemann S, Patrick J and Swanson LW (1989) Distribution of alpha 2, alpha 3, alpha 4, and beta 2 neuronal nicotinic receptor subunit mRNAs in the central nervous system: a hybridization histochemical study in the rat. *J Comp Neurol* **284**:314-35.
- Wang F, Gerzanich V, Wells GB, Anand R, Peng X, Keyser K and Lindstrom J (1996) Assembly of human neuronal nicotinic receptor alpha5 subunits with alpha3, beta2, and beta4 subunits. *J Biol Chem* **271**:17656-65.
- Wang H and Sun X (2005) Desensitized nicotinic receptors in brain. *Brain Res Brain Res Rev* **48**:420-37.
- Washburn MS and Dingledine R (1996) Block of alpha-amino-3-hydroxy-5-methyl-4-isoxazolepropionic acid (AMPA) receptors by polyamines and polyamine toxins. *J Pharmacol Exp Ther* **278**:669-78.
- Wilson G and Karlin A (2001) Acetylcholine receptor channel structure in the resting, open, and desensitized states probed with the substituted-cysteine-accessibility method. *Proc Natl Acad Sci U S A* **98**:1241-8.

- Wilson GG and Karlin A (1998) The location of the gate in the acetylcholine receptor channel. *Neuron* **20**:1269-81.
- Woodhull AM (1973) Ionic blockage of sodium channels in nerve. *J Gen Physiol* **61**:687-708.
- Xu W, Gelber S, Orr-Urtreger A, Armstrong D, Lewis RA, Ou CN, Patrick J, Role L, De Biasi M and Beaudet AL (1999) Megacystis, mydriasis, and ion channel defect in mice lacking the alpha3 neuronal nicotinic acetylcholine receptor. *Proc Natl Acad Sci U S A* **96**:5746-51.
- Yamakura T, Borghese C and Harris RA (2000a) A transmembrane site determines sensitivity of neuronal nicotinic acetylcholine receptors to general anesthetics. *J Biol Chem* **275**:40879-86.
- Yamakura T, Chavez-Noriega LE and Harris RA (2000b) Subunit-dependent inhibition of human neuronal nicotinic acetylcholine receptors and other ligand-gated ion channels by dissociative anesthetics ketamine and dizocilpine. *Anesthesiology* **92**:1144-53.
- Yamakura T and Harris RA (2000) Effects of gaseous anesthetics nitrous oxide and xenon on ligand-gated ion channels. Comparison with isoflurane and ethanol. *Anesthesiology* **93**:1095-101.
- Zoli M, Le Novere N, Hill JA, Jr. and Changeux JP (1995) Developmental regulation of nicotinic ACh receptor subunit mRNAs in the rat central and peripheral nervous systems. *J Neurosci* **15**:1912-39.
- Zwart R and Vijverberg HP (1998) Four pharmacologically distinct subtypes of alpha4beta2 nicotinic acetylcholine receptor expressed in *Xenopus laevis* oocytes. *Mol Pharmacol* **54**:1124-31.

APPENDIX

Parts of this work have been published separately as abstracts in conference proceedings and journals as detailed below:

***British Pharmacological Society annual meeting, London, 18th to 20th December 2012.**

The actions of philanthotoxin-343 on rat $\alpha 4\beta 2$ neuronal nicotinic acetylcholine receptors

It is useful to understand the pharmacological and functional properties of the major hetero-oligomeric neuronal nicotinic acetylcholine receptor (N-nAChR), $\alpha 4\beta 2$, in the mammalian central nervous system. Here, we studied the actions of philanthotoxin-343 (PhTX-343), a synthetic analogue of philanthotoxin-433, the active component of the Egyptian solitary digger wasp, *Philanthus triangulum*, venom, on rat $\alpha 4\beta 2$ N-nAChR expressed in *Xenopus* oocytes. Whole-cell current elicited by application of ACh was measured electrophysiologically by using two-electrode voltage clamp at three different holding potentials ($V_H = -60$ mV, -80 mV and -100 mV). PhTX-343 concentration-inhibition curves were constructed and IC_{50} values estimated for each holding potential. The IC_{50} value for PhTX-343 inhibition of peak $\alpha 4\beta 2$ current at -100 mV was $0.18 \mu\text{M}$ and this significantly increased to $1.41 \mu\text{M}$ ($p < 0.0001$) and $1.87 \mu\text{M}$ ($p < 0.0001$) at -80 mV and -60 mV, respectively. It is important to note that toxin potency was augmented by holding the cell at more negative V_H indicating its voltage-dependent manner of action. This property supports the open channel blocker mechanism of N-nAChRs by PhTX-343 that requires gate opening first and then inhibition of ion flow through the nAChR channel. The IC_{50} s were significantly lower than those obtained previously for muscle type nAChR. We conclude that PhTX-343 works as a potent open channel blocker of the $\alpha 4\beta 2$ mammalian N-nAChR.

*** The RSC/SCI Symposium on Ion Channels as Therapeutic Targets,
Cambridge, 18th to 19th March 2013**

***The First International Scientific Conference for Kurdistan Students,
Nottingham, 16th September, 2013**

**Potent Inhibition of $\alpha 4\beta 2$ and $\alpha 3\beta 4$ Neuronal Nicotinic Acetylcholine
Receptors by Philanthotoxin-343**

Philanthotoxin-343 (PhTX-343) is a synthetic analogue of philanthotoxin-433, the active component of the Egyptian solitary digger wasp, *Philanthus triangulum*, venom. Previous research has shown that this toxin is an open channel blocker of muscle-type nicotinic acetylcholine receptors (M-nAChR) with moderate potency. In this study, we investigate the pharmacological action of PhTX-343 on the major mammalian hetero-oligomeric neuronal nicotinic acetylcholine receptors (N-nAChR), $\alpha 4\beta 2$ and $\alpha 3\beta 4$, expressed in *Xenopus* oocytes. Whole-cell currents in response to application of acetylcholine alone or co-applied with PhTX-343 were studied electrophysiologically using two-electrode voltage-clamp at three different membrane holding potentials ($V_H = -60$ mV, -80 mV and -100 mV). PhTX-343 concentration-inhibition curves were constructed and IC_{50} values estimated for each holding potential. The IC_{50} value for PhTX-343 inhibition of peak current at -100 mV was 180 nM and 62 nM for $\alpha 4\beta 2$ and $\alpha 3\beta 4$, respectively. The toxin potency was augmented by holding the cell at more negative V_H indicating its voltage-dependent manner of action. It is important to note that PhTX-343 activity is not influenced by increasing the ACh concentration which indicates non-competitive antagonist action. These properties support the open channel blocker mechanism of N-nAChRs by PhTX-343 that requires gate opening first. The IC_{50} s were significantly lower than those obtained previously for muscle type nAChR. This variation in potency may be related to amino acids from the β subunit lining the ion channel. Therefore, we conclude that PhTX-343 works as a potent open channel blocker of the major heteromeric mammalian N-nAChR.

***British Pharmacological Society annual meeting, London, 17th to 19th December 2013**

Inhibition of Neuronal Nicotinic Acetylcholine Receptors by Philanthotoxins is Strongly Influenced by Subunit Composition

Philanthotoxin-343 (PhTX-343) and Philanthotoxin-12 (PhTX-12) are synthetic analogues of philanthotoxin-433, the active component of the Egyptian solitary digger wasp, *Philanthus triangulum*, venom. They have shown a different inhibitory mode of action on embryonic muscle-type nicotinic acetylcholine receptors (M-nAChR) naturally expressed in the TE671 cell line with moderate potency. To try and confirm predictions of potential binding sites from this earlier work, we investigated the pharmacological action of both analogues on different mammalian hetero-oligomeric neuronal nicotinic acetylcholine receptor (N-nAChR) subunit combinations expressed in *Xenopus* oocytes. Whole-cell currents in response to application of acetylcholine alone or co-applied with PhTX-analogue were studied electrophysiologically using two-electrode voltage-clamp at three different membrane holding potentials ($V_H = -60$ mV, -80 mV and -100 mV). Concentration-inhibition curves were constructed and IC_{50} values estimated for each holding potential. The IC_{50} values for PhTX-343 inhibition of $\alpha 3\beta 4$, $\alpha 3\beta 2$ and $\alpha 4\beta 2$ peak currents at -100 mV were 0.077 μ M ($n=9$), 3.20 μ M ($n=8$) and 0.170 μ M ($n=7$) respectively; for PhTX-12 they were 2.03 μ M ($n=8$), 36.0 μ M ($n=10$) and 0.430 μ M ($n=7$) respectively. The potency of PhTX-343 was strongly augmented by holding the cell at more negative V_H while this was not the case for PhTX-12 where weak voltage-dependence was observed. Inhibition by PhTX-343 was not influenced by increasing the ACh concentration which indicates a non-competitive antagonist action. These properties support the open channel block mechanism of N-nAChRs by PhTX-343 that requires gate opening first. The variation in potency is most likely due to a single amino acid change in the $\beta 2/4$ subunit pore lining region. Therefore, we strengthen our conclusion that PhTX-343 works as a potent open channel blocker of the mammalian heteromeric N-nAChR and has binding site deep in the channel while the PhTX-12 site is near to the outside of channel. These distinct binding sites in the nAChR pore could be exploited to develop subtype selective therapeutics.

***American Biophysics Society 58th annual meeting, San Francisco, California, 15th-19th February 2014**

Subunit-Dependent Inhibition of Neuronal Nicotinic Acetylcholine Receptors by Philanthotoxins

Philanthotoxin-433 (PhTX-433) is the active component of the Egyptian solitary digger wasp, *Philanthus triangulum*, venom which non-selectively inhibits several excitatory ion channels. To improve selectivity two synthetic analogues, Philanthotoxin-343 (PhTX-343) and Philanthotoxin-12 (PhTX-12), were developed. Previous work showed a 22-fold selectivity for PhTX-12 on embryonic muscle-type nicotinic acetylcholine receptors (M-nAChR) naturally expressed in the TE671 cell line in comparison to PhTX-343. In this study, we investigated the pharmacological action of both analogues on different mammalian hetero-oligomeric neuronal nicotinic acetylcholine receptor (N-nAChR) subunit combinations expressed in *Xenopus* oocytes. Whole-cell currents in response to application of acetylcholine alone or co-applied with PhTX-analogue were studied electrophysiologically using two-electrode voltage-clamp at three different membrane holding potentials ($V_H = -60$ mV, -80 mV and -100 mV). Concentration-inhibition curves were constructed and IC_{50} values estimated for each holding potential. The IC_{50} values for PhTX-343 inhibition of $\alpha 3\beta 4$, $\alpha 3\beta 2$, $\alpha 4\beta 2$ and $\alpha 4\beta 4$ peak currents at -100 mV were 0.077 μ MM ($n=9$), 3.20 μ MM ($n=8$), 0.170 μ MM ($n=7$) and 0.28 μ MM ($n=6$) respectively; for PhTX-12 they were 2.03 μ MM ($n=8$), 36.0 μ MM ($n=10$), 0.430 μ MM ($n=7$) and 1.82 μ MM ($n=9$) respectively; i.e. in contrast to M-nAChR, PhTX-343 was more potent than PhTX-12 in all cases. The potency of PhTX-343 was strongly augmented by holding the cell at more negative V_H while this was not the case for PhTX-12 where weak voltage-dependence was observed. The variation in potency is most likely due to a single amino acid change in the $\beta 2/4$ subunit pore lining region. Therefore, we conclude that PhTX-343 works as a potent open channel blocker of the mammalian heteromeric N-nAChR and has binding site deep in the channel while the PhTX-12 site is near to the outside of channel.

***Nicotinic Acetylcholine Receptors, 23-26 July 2014, Churchill College, Cambridge, UK.**

***American Society for Neuroscience annual meeting, Washington DC, 15th to 19th November 2014.**

Inhibition of nicotinic acetylcholine receptors by philanthotoxins is strongly influenced by subunit composition

Philanthotoxin-433 (PhTX-433) is active component of the Egyptian solitary digger wasp, *Philanthus triangulum*, venom which non-selectively inhibits several excitatory ion channels. To improve selectivity two synthetic analogues, Philanthotoxin-343 (PhTX-343) and Philanthotoxin-12 (PhTX-12), were developed. Previous work by Brier et al. (2003) showed a 22-fold better selectivity for PhTX-12 on embryonic muscle-type nicotinic acetylcholine receptors (M-nAChR) naturally expressed in the TE671 cell line in comparison to PhTX-343. In this study, we investigated the pharmacological action of both analogues on mammalian hetero- and homooligomeric neuronal nicotinic acetylcholine receptor (N-nAChR) subunit combinations expressed in *Xenopus* oocytes. Whole-cell currents in response to application of acetylcholine alone or co-applied with PhTX-analogue were studied electrophysiologically using two-electrode voltage-clamp at three different membrane holding potentials ($V_H = -60$ mV, -80 mV and -100 mV). Concentration-inhibition curves were constructed and IC_{50} values estimated for each holding potential. The IC_{50} values for PhTX-343 inhibition of $\alpha 3\beta 4$, $\alpha 3\beta 2$, $\alpha 4\beta 2$, $\alpha 4\beta 4$ and $\alpha 7$ peak currents at -100 mV were $0.077 \mu\text{M}$ ($n=9$), $3.20 \mu\text{M}$ ($n=8$), $0.170 \mu\text{M}$ ($n=7$), $0.28 \mu\text{M}$ ($n=6$) and $8.7 \mu\text{M}$ ($n=9$) respectively; for PhTX-12 they were $2.03 \mu\text{M}$ ($n=8$), $36.0 \mu\text{M}$ ($n=10$), $0.430 \mu\text{M}$ ($n=7$), $2.7 \mu\text{M}$ ($n=8$) and $12.1 \mu\text{M}$ ($n=10$) respectively; i.e. in contrast to M-nAChR, PhTX-343 was more potent than PhTX-12 in all cases. The variation in potency is most likely due to a single amino acid change in the $\beta 2/4$ subunit pore lining region. For inhibition of heteromeric N-nAChRs, the potency of PhTX-343 was strongly augmented by holding the cell at more negative V_H while this was not the case for PhTX-12 where only weak voltage-dependence was observed. The inhibition of homomeric $\alpha 7$ receptors by both toxins was voltage-independent. Therefore, we conclude that PhTX-343 works as a potent open channel blocker of the mammalian heteromeric N-nAChR and has binding site deep in the channel while the PhTX-12 site is near to the outside of channel. In contrast, inhibition of homomeric $\alpha 7$ receptors may be through interaction at an alternative site outside the channel pore.

***British Pharmacological Society annual meeting, London, 16th to 18th December 2014**

Pharmacological actions of philanthotoxin analogues on $\alpha 4\beta 2$ and $\alpha 3\beta 4$ nicotinic acetylcholine receptors

Neuronal nicotinic acetylcholine receptors (nAChRs) are excitatory ion channels, which have wide subtype diversity due to the many possible subunit combinations, some heteromeric, others homomeric. Each subunit is composed of a large N-terminal segment containing the ACh binding site and four membrane-spanning segments named M1-M4. The pore lumen is lined mainly by the second of these membrane segments, M2. nAChRs play a critical role in many physiological and pathophysiological processes, thus, neuronal nAChRs have become targets for drug discovery and research.

The venom of the Egyptian digger wasp contains a toxin, philanthotoxin-433 (PhTX-433), that works as a strong non-competitive inhibitor of ionotropic glutamate receptors and nAChRs in their target prey. PhTX-433 has a polyamine tail and aromatic head group. The main obstacle facing the use of the natural toxin (PhTX-433) as a candidate for drug development and understanding pharmacological characteristics of ionotropic receptors is the lack of subtype selectivity. The present study aims to investigate the activity and selectivity of twenty one synthetic analogues on rat neuronal $\alpha 4\beta 2$ and $\alpha 3\beta 4$ nAChRs. We showed that the presence of positive charge in the polyamine tail of PhTX compounds is essential for nAChR subtype selectivity and their removal makes the molecule lose its selectivity. Also, it appears that adding a bulky group to the terminal ammonium drastically reduced the activity while in the head region it increased their potency. In addition, we identified the key regions and substitutions responsible for increasing PhTX activity, cyclohexylalanine, and selectivity, phenolic group. Analogues having cyclohexylalanine and a phenolic group in the head region showed IC_{50} values in the low nano-molar and pico-molar (160-400 pM) range. These data suggest that PhTXs could serve as lead compounds for highly potent and selective inhibitors of N-nAChRs.

***6th International Conference on Natural Toxins, Suez Canal University, Ismailia, Egypt 15th to 16th December 2014**

**MODIFICATION OF THE POLYAMINE MOIETY OF PHILANTHOTOXIN
ALTERS INHIBITION OF IONOTROPIC GLUTAMATE AND NICOTINIC
ACETYLCHOLINE RECEPTORS AND THEIR SUBTYPES**

Philanthotoxin-433 (PhTX) derived from the venom of the solitary wasp *Philanthus triangulum*, and its synthetic derivative PhTX-343, is a potent inhibitor of ionotropic glutamate and nicotinic acetylcholine receptors (nAChR). PhTX is formed of a modular butyryl-tyrosyl-thermospermine structure which forms a head-tail type configuration. We performed a series of structural modifications to the tail region of PhTX looking to increase potency at, and selectivity between, the aforementioned ionotropic receptors and their subtypes. These properties were assessed by two electrode voltage clamp assays of *Xenopus* oocytes expressing GluA1 flop α -amino-3-hydroxy-5-methyl-4-isoxazolepropionic acid receptors (AMPA), or $\alpha 4\beta 2$ or $\alpha 3\beta 4$ nAChRs. Addition of a cyclopropane moiety to the polyamine tail of PhTX-343 increased the potency at $\alpha 4\beta 2$ and $\alpha 3\beta 4$ nAChRs and AMPARs relative to PhTX-343. At nAChRs, both cis and trans-cyclopropyl-PhTX-343 show half maximal inhibitory concentration (IC₅₀) values in the low nanomolar range, with 32.6- and 47.8-fold selectivity for $\alpha 3\beta 4$ over $\alpha 4\beta 2$, respectively. The same compounds were less potent at GluA1 flop AMPARs, than nAChRs, with IC₅₀ values of 1.79 μ M and 240 nM for cis and trans-cyclopropyl-PhTX-343, respectively. These data suggest that PhTX and its analogues are useful/interesting compounds that are not only selective for nAChRs but also for sub-types within the nAChR population.